WORKSHOP ON

THE MARTIAN SURFACE AND ATMOSPHERE THROUGH TIME

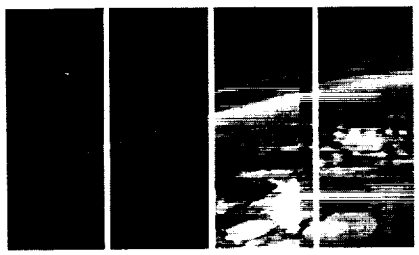

MSATT

Mars Surface and Atmosphere Through Time

LPI Technical Report Number 92-02

LUNAR AND PLANETARY INSTITUTE 3600 BAY AREA BOULEVARD HOUSTON TX 77058-1113

LPI/TR--92-02

WORKSHOP ON
THE MARTIAN SURFACE AND ATMOSPHERE THROUGH TIME

Conveners
Robert M. Haberle
Bruce M. Jakosky

Held at
Boulder, Colorado
September 23–25, 1991

Sponsored by
Lunar and Planetary Institute
NASA MSATT Study Project
Laboratory for Atmospheric and Space Physics (LASP), University of Colorado, Boulder

Lunar and Planetary Institute 3600 Bay Area Boulevard Houston TX 77058-1113

LPI Technical Report Number 92-02
LPI/TR--92-02

Compiled in 1992 by
LUNAR AND PLANETARY INSTITUTE

The Institute is operated by Universities Space Research Association under Contract NASW-4574 with the National Aeronautics and Space Administration.

This report may be cited as:
Haberle R. M. et al., eds. (1992) *Workshop on the Martian Surface and Atmosphere Through Time*. LPI Tech. Rpt. 92-02, Lunar and Planetary Institute, Houston. 182 pp.

Papers in this report may be cited as:
Author A. A. (1992) Title of paper (abstract). In *Workshop on the Martian Surface and Atmosphere Through Time* (R. M. Haberle et al., eds.), pp. xx-yy. LPI Tech. Rpt. 92-02, Lunar and Planetary Institute, Houston.

This report is distributed by:

ORDER DEPARTMENT
Lunar and Planetary Institute
3600 Bay Area Boulevard
Houston TX 77058-1113

Mail order requestors will be invoiced for the cost of shipping and handling.

Preface

This report contains abstracts of papers presented at the "kick-off" workshop for MSATT (Mars Surface and Atmosphere Through Time). The workshop was sponsored by the Lunar and Planetary Institute (LPI), the Laboratory for Atmospheric and Space Physics (LASP) at the University of Colorado, and the MSATT Study Group. It was hosted by LASP and held on September 23–25, 1991, at the Conference area of the Coors Events Center on the Boulder campus of the University of Colorado. Program committee members were Bob Haberle, Bruce Jakosky, Ken Tanaka, Ben Schuraytz, and Amos Banin. The workshop was convened by Bob Haberle and Bruce Jakosky, and coordinated by Ben Schuraytz, with assistance from the staff of the Program Services Department and Publications Services Department at the LPI.

The purpose of the workshop was to bring together the MSATT community and interested researchers to begin to explore the interdisciplinary nature of, and to determine the relationships between, various aspects of Mars science that involve the geological and chemical evolution of its surface, the structure and dynamics of its atmosphere, interactions between the surface and atmosphere, and the present and past states of its volatile endowment and climate system. It was the intention of the workshop organizers to involve a broad spectrum of Mars researchers in order to foster interdisciplinary collaborations. The format was chosen to allow maximum time for discussion and interaction. Over 100 people attended and judged the workshop to be highly successful.

Plans are now being formulated to hold focused workshops that will pursue in greater detail the various issues raised in Boulder. At the end of the three-year study project, a final "wrap-up" workshop will be held that will bring the community together once again to assess the accomplishments of the program and to help increase the science return from the Mars Observer.

Robert M. Haberle, Chairman
MSATT Steering Committee

Program

Monday Morning, September 23, 1991

B. Haberle, B. Jakosky - Welcoming Address

SESSION I: CURRENT NATURE OF THE SURFACE
INVITED PRESENTATIONS

Greeley R.
Current Geological Processes

Lee S. W.
Current Surface Properties

SESSION I: POSTER PRESENTATIONS
A. PHYSICAL PROPERTIES

Sullivan R. J.
Characterization of Martian Near-Subsurface Materials by Determination of Cohesion and Angle of Internal Friction

Xu P. Greeley R.
Comparison of Drift Potential Derived from Mars GCM with Rock Abundance from IRTM

Betts B. H. Murray B. C.
Thermally Distinct Ejecta Blankets from Martian Craters

Ruff S. W.
Dorsa Argentea Type Sinuous Ridges, Mars: Linear Dune Hypothesis

Harmon J. K. Slade M. A. Hudson R. S.
Mars: Wavelength-Dependent Dual Polarization Global Scattering

Strickland E. L. III
Physical Interpretation of Thermal and Reflected Data on Martian Surface Units

PRESENTED BY TITLE ONLY

Strickland E. L. III
Physical Properties of Deucalionis, Eos, and Xanthe-Type Units in the Central Equatorial Region of Mars

Strickland E. L. III
Physical Properties of Meridiani Sinus-Type Units in the Central Equatorial Region of Mars

Strickland E. L. III
Physical Properties of Oxia/Lunae Planum and Arabia-Type Units in the Central Equatorial Region of Mars

Strickland E. L. III
Surface Photometric Properties and Albedo Changes in the Central Equatorial Region of Mars

B. PHOTOMETRIC OBSERVATIONS AND INTERPRETATIONS

Erard S. Bibring J.-P. Drossart P.
Infrared Photometric Behavior and Opposition Effect of Mars

McEwen A. S.
Temporal Variability of the Surface and Atmosphere of Mars: Viking Orbiter Color Observations

James P. B. Clancy R. T. Lee S. W. Kahn R. Zurek R. Martin L. Singer R.
Observations of Mars Using Hubble Space Telescope

Herkenhoff K. E.
Dark Material in the Polar Layered Deposits on Mars

PRESENTED BY TITLE ONLY

Lee S. W. Clancy R. T.
Mars: Correcting Surface Albedo Observations for Effects of Atmospheric Dust Loading

DISCUSSION

Monday Afternoon, September 23, 1991

SESSION II: HISTORY OF GEOLOGICAL PROCESSES
INVITED PRESENTATIONS

Tanaka K.
Long-term Geological Processes

Baker V.
Oceans and Ice-related Geological Evolution

SESSION II: POSTER PRESENTATIONS
A. WATER AND ICE-RELATED GEOMORPHOLOGY

Clifford S. M. Carr M. H.
The Subsurface Hydrologic Response of Mars to the Thermal Evolution of its Early Crust

Cave J. A.
Ice in the Northern Lowlands and Southern Highlands of Mars and its Enrichment Beneath the Elysium Lavas

Rotto S. L. Tanaka K. L.
Chryse Planitia Region, Mars: Channeling History, Flood-Volume Estimates, and Scenarios for Bodies of Water in the Northern Plains

Scott D. H. Rice J. W. Jr. Dohm J. M. Chapman M. G.
Amazonis and Utopia Planitiae: Martian Lacustrine Basins

Parker T. J. Gorsline D. S.
Distribution of Coastal Morphology in the Martian Northern Lowlands

PRESENTED BY TITLE ONLY

B. IMPACT CRATERS AND PROCESSES

PRESENTED BY TITLE ONLY

C. VOLCANIC PROPERTIES AND PROCESSES

Tuesday Morning, September 24, 1991

SESSION III: GEOCHEMISTRY AND MINERALOGY OF THE MARTIAN SURFACE

SESSION III: POSTER PRESENTATIONS
A. COMPOSITIONAL AND SPECTROSCOPIC STUDIES

PRESENTED BY TITLE ONLY

B. GEOCHEMISTRY AND WEATHERING PROCESSES

PRESENTED BY TITLE ONLY

Jones J. H.
Distribution of Water on Mars: Implications from SNC Meteorites

Wright I. P. Grady M. M. Pillinger C. T.
On the Isotopic Composition of Magmatic Carbon in SNC Meteorites

B. ATMOSPHERIC EVOLUTION PROCESSES

Fox J. L.
Nitrogen Escape from Mars

Mahaffy P. Mauersberger K.
Volatile Tracers of Martian Atmospheric Evolution: Present Measurement Status and Requirements for Future Investigations

Zhang M. H. G. Luhmann J. G. Nagy A. F. Bougher S. W.
The Ancient Oxygen Exosphere of Mars: Implications for Atmosphere Evolution

DISCUSSION

Wednesday Afternoon, September 25, 1991

SESSION VI: CLIMATE HISTORY AND VOLATILE CYCLES
INVITED PRESENTATIONS

Pollack J.
Short- and Long-Term Climate Change

Zent A.
Surface-Atmosphere Interactions—Volatiles

SESSION VI: POSTER PRESENTATIONS
A. NATURE OF EARLY CLIMATE AND CLIMATE EVOLUTION

Postawko S. Fanale F.
Influence of Heat Flow on Early Martian Climate

Kasting J. F. Brown L. L. Acord J. M. Pollack J. B.
Was Early Mars Warmed by Ammonia?

Stephens S. K. Stevenson D. J.
Carbonate Formation on Mars: History of the CO_2 Atmosphere from Models of Diffusion-Limited Growth in Non-Aqueous Environments

Plescia J. Crisp J.
Recent Elysium Volcanism—Effects on the Martian Atmosphere

Contents

Summary of Technical Sessions

SESSION I: CURRENT NATURE OF THE SURFACE

Summarized by R. Greeley and S. Lee

An assessment of the current state of Mars includes consideration of geological activity and the nature of its surface. R. Greeley reviewed possible geological activity and noted that terrestrial planets are potentially subjected to impact cratering, volcanism, tectonic deformation, and surface modification by such agents as wind and downslope movement of debris. Although data for Mars are too limited to make definitive statements about the current activity of most of these processes, approximate assessments can be made. Volcanism and tectonism both result from heat generated in planetary interiors. Although geologic mapping shows that some areas of Mars are surfaced with "young" lava flows, there is no direct evidence that volcanism is currently active. Similarly, there is nothing to suggest current crustal deformation and, until a seismometer network is established, there are no means to assess tectonic processes. Impact cratering is inferred to occur on Mars, but, by extrapolation from the Moon and Earth, impacts occur infrequently. Consequently, gradation (surface weathering, erosion, and deposition) appears to be the primary geologic process active on Mars. Chemical and physical weathering of rocks undoubtedly occur, but in the cold, dry atmosphere of Mars, rates of weathering are probably low in comparison to Earth. In the absence of water, weathered debris will be transported primarily by wind and gravity (mass movements); for example, the small "landslide" observed at Viking Lander Site 1 shows that mass movements occur, at least on a small scale. Frequent dust storms attest to active aeolian processes, which appear to be the primary agents of surface modification today.

Despite more than two decades of study, many of the fundamental aspects of dust storms, such as the mechanisms for entraining the very fine (micrometer-sized) particles that constitute the dust clouds, are poorly known. However, analysis of Viking data and Earth-based telescopic observations provide insight into the timing and sources of dust storms and potential deposition sites of dust on Mars. Recently obtained Hubble Space Telescope images of Mars show the potential for extending the database for observation of Mars over a longer time period than currently available.

The present distribution of surficial deposits (i.e., unconsolidated sediments) is known only indirectly from models using Viking IRTM and Soviet Phobos Thermoscan data, inferences from photogeologic studies, and (limited) radar observations. Maps derived primarily from the Viking IRTM data have been generated to show particle distributions on Mars, and some correlations have been made with features such as wind streaks and areas of dust storm origin. In addition, results from the NASA Ames General Circulation Model (GCM) that predict when and where winds might occur as a function of season on Mars have been correlated with wind streaks and models of "block" distributions. Results from these correlations also suggest sites of wind deflation and deposition.

In summary, numerous areas on Mars have been identified where additional information, as can be obtained from the Mars Observer and Mars 94/96 missions, could provide insight into the current state of geological activity and the distribution of particulate material on the surface.

SESSION II: HISTORY OF GEOLOGICAL PROCESSES

Summarized by K. Tanaka and V. Baker

This session considered some of the remarkable geological evidence for water-related processes throughout the history of Mars, including the possibility for ancient, short-lived oceans and polar glaciers on Mars.

Most important of the science issues are questions of water amounts, reservoirs, transfers, and cycling through time. The geological problems that generated most discussion were various interpretations of timing rates and mechanisms of large-scale planetary water transfer. Nevertheless, as summarized in the overview presentations, there are important points of consensus among geologists, as follows: (1) Abundant landforms indicate massive amounts of water stored for much of martian history as ice and ground water in the martian crust. (2) During the first billion years or so of martian history (the Noachian Epoch), considerable water flowed on the surface, forming the valley networks that are widely distributed on the heavily cratered southern uplands of the planet. (3) During post-Noachian Mars history immense floods emanated from local areas, mostly east and west of the great Tharsis bulge. (4) The floods debouched onto the northern plains of Mars where ponded water temporarily accumulated.

K. Tanaka's presentation demonstrated that volcanic, tectonic, and impact processes on Mars define the hydrologic properties of the crust and that large-scale thermal events caused by such processes correlated with geomorphologic history. Such events include cessation of widespread valley network formation at the end of the Noachian Period, postulated development of the cryosphere during the Early Hesperian, and outflow channel and possible polar cap formation during the Late Hesperian and Amazonian. Major uncertainties remaining in the geologic record (and hence

their effect on the hydrologic/climate history) include the volume of volcanic materials erupted during the Noachian Period and whether or not the northern lowlands may have been lowered by a tectonic event at the end of the Noachian.

V. Baker's talk presented a model for the formation of a temporary ocean in the northern plains of Mars and consequent effects on the planet's water cycle. Along with proposed paleoshorelines in the northern plains and the huge outflow channels that debouch into the plains, landforms near the south pole (interpreted by J. Kargel to be glacially derived) were offered as evidence to support the ocean/hydrologic cycle model.

One set of unresolved issues involves the actual causes for the Noachian surface-water flow. A warm, wet atmosphere capable of appreciable precipitation is one possible way of recharging the aquifers that discharged to valley heads. Hydrothermal processes (as described by V. Gulick) provide an alternative means to recycle water from downstream areas back to basin headwaters. In many cases, simple drainage of an initially high water table without continuing, long-term recharge seems to require improbable physics for valley formation.

Conditions leading to the post-Noachian cataclysmic floods include the lowering of the northern plains and the adjacent rise of the Tharsis bulge. S. Clifford hypothesized that deep ground-water reservoirs supplied water for upward movement in the crust by long-term thermal diffusion. Perched aquifers beneath an ice-rich cryosphere are interpreted as sources for the cataclysmic outflow of water. According to Baker, the largest floods, dated to the late Hesperian by S. Rotto and Tanaka, are associated with the bulging and volcanism of the Tharsis uplift. Immense discharges were conveyed along the radial system of fractures created by the bulge.

Ponding of the flood water on the northern plains has been interpreted by D. Scott and colleagues. T. Parker and D. Gorsline envision extensive inundation of the entire northern plains, citing features that seem to be older than those mapped by the Scott group. A possibly related observation is the new interpretation by Kargel and R. Strom of relatively young (Amazonian) glaciation on Mars. The spatial and temporal associations of these various phenomena have been explained in a conceptual scheme presented by Baker. Relying upon numerous studies by other investigators, this preliminary model involves episodic, short-term periods of planetwide water cycling between a northern plains sea or ocean and the southern hemisphere active glaciation. The model provides an interesting basis for future studies of Mars in that either its confirmation or refutation would seem to provide fascinating new information about Mars processes.

The many facets of the ocean model stimulated lively controversy during the ensuing discussion period. Some thought that the proposed glacial landforms could be interpreted differently. The crater-retention age offered for the period of glaciation appeared to conflict with other workers' results. Some felt that freezing of the ocean surface would occur quickly and might hamper the ocean's ability to affect the water cycle or produce shoreline features. Another question was whether sufficient water could be made available from the martian crust, particularly if much of the water was frozen, to produce a sizable ocean.

The 14 poster presentations and 3 additional abstracts submitted show that many planetary geologists are actively addressing geologic issues related to the hydrologic and climatic histories of Mars, and that various promising avenues of research in these areas are yet available through spacecraft, Earth-based data sets, and SNC meteorites.

SESSION III: GEOCHEMISTRY AND MINERALOGY OF THE MARTIAN SURFACE

Summarized by R. Singer and B. Clark

The surface composition of Mars, its geochemistry and mineralogy, were discussed in two review papers and 14 poster papers. Topics covered included the use of remote sensing data at various spectral ranges for mineral identification on Mars, simulation studies with various analog minerals, in-depth characterization of these analogs (palagonites, iron-rich clays), and chemical reactivity of the Mars soil and suggested weathering pathways for its formation.

What emerged from the presentations and lively discussions in the workshop was the fact that the search for Mars soil analogs goes on, without any conclusive evidence being presented for any of the suggested compositions. It has become increasingly evident that the existing data suggest the possibility that much of the silicon- and iron-containing phases in the martian soil are short-range-ordered, or "amorphous," i.e., do not have well-developed crystallinity. Among the several questions that arise if this is true are (1) What is the mechanism of formation that led to the production and enrichment of these phases in the soil? (2) Why didn't the secondary silicate and iron oxides in the martian soil "ripen" and develop into well-crystallized mineral grains, despite the long period of time since the putative aqueous weathering of the basaltic rocks that took place on the face of a wetter and warmer Mars?

More direct data on the mineral nature of the martian soil and better understanding of the planet's climatic history are required in order to begin to resolve these enigmas.

SESSION IV: PRESENT ATMOSPHERE

Summarized by R. Zurek and Y. Yung

This session focused on several issues relevant to MSATT goals: the general circulation and climate of Mars and the photochemistry of its atmosphere.

R. Zurek began by reviewing what the Viking and Mariner 9 missions have told us about the general circulation and climate of Mars. Although the coverage in space and time is not complete, we now have a good first-order understanding of the thermal structure and inferred wind systems on Mars. Of necessity, this understanding comes in part from modeling studies that have been used to help "fill in" the data gaps. While this is a useful approach, Zurek cautioned that the models have not been generally validated, and that perhaps we have become too confident of their predictions. Mars Observer may very well surprise us in this regard.

The outstanding issues for martian meteorology center on the general circulation, dust storms, and volatile transport. The general circulation—at least as far as we currently understand it—consists of a zonal mean circulation similar to, but more prominent than, Earth's Hadley circulation, traveling extratropical wave disturbances that are vigorous during winter and almost nonexistent during summer, stationary planetary waves associated with large-scale topography and perhaps the thermophysical properties of the soil, thermal tides, and condensation flow. However, the full three-dimensional structure of these various components, how they vary with season, and the factors responsible for driving them are not well known.

Planetary-scale dust storms are unique to Mars and must greatly perturb the general circulation. Yet the mechanisms responsible for their growth and decay, as well as their curious interannual variability, are still uncertain. Zurek reviewed some ideas about these storms, and emphasized the fact that they do not occur every martian year as was previously suggested. Evidence for this interannual variability was found during the Viking mission, and subsequent reexamination of the telescopic record (all the way back to Lowell's time) suggests it may be episodic, though the coverage is not complete enough to be convincing.

Y. Yung then presented our current understanding of photochemical processes on Mars. He noted that photochemical reactions occur throughout the martian atmosphere and that much of the research in this area has focused on explaining the stability of CO_2 against photodissociation into CO and O. Though it has not been confirmed by direct measurements, it is now believed that catalytic cycles involving odd H are the main reason for the stability of CO_2. Several theories were reviewed that differ in the way CO is oxidized by the hydroxyl radical (OH). While it is not possible to distinguish between these theories with the available data, the importance of odd H in catalyzing the recombination is demonstrated by the observed (low) abundances of CO and O_2, and the anticorrelation of water with O_3.

During the discussion part of this session there was some debate about the requirement of photochemical models for relatively large values of the vertical eddy diffusion coefficient ($>10^8$ cm^2 s^{-1}) and the ability of the atmosphere to provide such intense mixing. Although the breaking of vertically propagating tidal motions has been theoretically predicted, estimates of the subsequent mixing yield smaller eddy coefficients. Zurek pointed out that at the breaking level only a fraction of the wave will actually break since a half-wavelength away the perturbation temperature field set up by the tide will tend to stabilize, rather than drive, convective mixing. This touched off a more general discussion on the use of eddy mixing coefficients to represent transport. Strong gradients do not necessarily imply strong transport, and transport can actually occur against the gradient in some instances. No consensus was reached on this issue. However, there is a definite requirement for the exchange of mass across the 30-km level; how that occurs globally is not yet known.

SESSION V: LONG-TERM VOLATILE EVOLUTION

Summarized by B. Fegley and J. Luhmann

The session on evolutionary considerations was separated into two distinct presentations and discussion periods, loss to the surface and escape to space, but it was evident throughout that progress on the matter of evolution demands a combined approach. For example, while there is nothing to prevent the ongoing loss of O related to photochemical processes in the primarily CO_2 atmosphere and O_2^+ ionosphere, the consequences of this escape depend on interactions with the surface that determine the atmospheric oxidation state. In turn, the surface-atmosphere interactions depend on the degree of atmosphere oxidations. Meanwhile, processes in the atmosphere and surface resulting from the surface temperature are closely coupled to the evolution of the solar radiation spectrum. Some escape processes also depend on evolving solar wind conditions. It was clear that even the term "original inventory" is ambiguous since it is used to refer to both nebular or cosmic abundances and to the era following heavy bombardment.

The key issues that need to be resolved include the following. First, we need to know the composition and abun-

dance of volatiles outgassed on early Mars. This issue involves four main questions: (1) What volatiles were outgassed during planetary accretion and what was their molecular speciation? (2) What fraction of these different gases was retained by the planet and what fraction was lost to space during the accretion process? (3) For the fraction that was retained, which volatiles remained in the early martian atmosphere and which ones were trapped in the planetary interior (e.g., by dissolving in an early magma ocean or in magma lakes that later solidified)? (4) What is the abundance and molecular speciation of volatiles later outgassed during the early history of Mars? Many of these same questions are also relevant to the Earth, and also need to be investigated for our own planet.

A second key issue is quantifying the rates of important gas-solid reactions (e.g., carbonate formation) that act as volatile sinks. The specific reactions that are generally believed to be important reactions of CO_2 with common minerals found in igneous rocks are

$$MgSiO_3 + CO_2 \rightarrow MgCO_3 + SiO_2 \quad (1)$$

$$Mg_2SiO_4 + 2CO_2 \rightarrow 2MgCO_3 + SiO_2 \quad (2)$$

$$CaAl_2Si_2O_8 + CO_2 \rightarrow CaCO_3 + Al_2SiO_5 + SiO_2 \quad (3)$$

At present, no kinetic data are available for the relevant reactions under the appropriate conditions, which are from room temperature (or slightly above) down to present martian temperatures, and CO_2 pressures of a few bars down to the present pressures of a few millibars.

A third issue is determining how efficiently the surface sinks competed with atmospheric escape processes for depleting water. Processes such as subsurface ground ice and permafrost formation are probably efficient sinks for water loss from the martian atmosphere and surface. Intuitively, one also expects that the formation of Fe_2O_3 from magnetite (Fe_3O_4)—essentially rusting—should be fairly rapid, but that formation of Fe_2O_3 from FeO-bearing silicates may be more sluggish. Again, no kinetic data are available under the conditions of interest. At the same time, there is no way to avoid escape to space of O as long as the atmosphere is dominated by CO_2. The consequences of this simultaneous escape must be evaluated.

Finally, a fourth key issue is determining the efficiency as a function of time for the surface sinks (for volatiles) as conditions evolved toward those on present-day Mars (low temperature, low surface pressure) and for the parallel escape processes. The surface sinks issue could be addressed using the kinetic data obtained from laboratory studies designed to address the second and third issues above. For escape, we need to determine how the evolving Sun modified the rates of contemporary escape processes. We can in principle learn from the similarly escaping N isotope abundances, but the cross sections for some of the pertinent reactions are so poorly known that interpretation of that isotopic signature is currently very difficult. We also do not, except for rare-element isotopes perhaps, have a clear picture of the importance of early hydrodynamic escape processes.

At the planned focused workshop on atmospheric evolution in June 1992 we hope to bring together expertise on the various essential aspects of the highly interdisciplinary evolution problem. Our task will be to further constrain the scenarios for evolution based on current knowledge and to determine what we need to do in the laboratory and through remote and *in situ* experiments to make significant progress in this area.

SESSION VI: CLIMATE HISTORY AND VOLATILE CYCLES

Summarized by J. Pollack and A. Zent

J. Pollack discussed the theory of short- and long-term climate change on Mars, reviewed the three volatile cycles, CO_2, H_2O, and dust, and also discussed the controversy regarding the question of whether early Mars was wet and warm. In reviewing arguments for and against the latter question he discussed the occurrence of valley networks in the ancient cratered terrain of Mars. Recent evidence has suggested that the total amount of water required to carve the networks was greater than could be stored within the apparent drainage basin, necessitating some kind of recycling mechanism. He also mentioned that there was geologic evidence of enhanced erosion rates early in Mars' history. As evidence against the possibility of an early wet and warm Mars, the recent modeling results of J. Kasting were discussed, which predict that CO_2 condensation would preclude adequate warming to produce globally averaged surface temperatures of 273 K.

A. Zent discussed the physics of volatile-surface exchange. He mentioned that the exchange of water between the atmosphere and subsurface is not well understood. He discussed limits of the diurnal exchange of water, and outlined the uncertainties in boundary layer physics that obscure the issue. Such issues include the role of the radiative properties of fogs and the relative role of vertical exchange and horizontal transport in establishing the H_2O column abundance. There have also been a number of recent advances in understanding the physics of the annual CO_2 cap balance, including the effects of conducted heat in establishing the mass balance, the role of atmospheric dust, and ice emissivity. Finally, he touched on the possible role of water in displacing CO_2 from adsorption sites, an effect known as coadsorption. The possible implications for the total inventory of adsorbed CO_2 and quasiperiodic climate

change are profound if the regolith is unable to hold more than a few additional millibars of CO_2.

During the discussion, Kasting went into greater detail on his CO_2 greenhouse calculations. He said that up to 86% of the current solar flux was necessary with a few bars of CO_2 to get up to 273 K, and that this level of radiation was not achieved until about 2 Ga, long after network formation. The case for a wet, warm early Mars is still undecided, although additional issues are continually being developed.

Abstracts

51-91
55970

N92-28989 p.2 9

IRON MÖSSBAUER SPECTROSCOPY: SUPERPARAMAGNETISM IN HYDROTHERMAL VENTS AND THE SEARCH FOR EVIDENCE OF PAST LIFE ON MARS; David G. Agresti and Thomas J. Wdowiak, Physics Department, University of Alabama at Birmingham, Birmingham, AL 35294.

AM 538 929

Iron Mössbauer spectroscopy (FeMS) is a nuclear resonance technique that provides direct information on the distribution of iron among its oxidation states and the several mineralogical phases present in a sample of interest. The geochemical cycle of iron is strongly coupled to the chemistry of the abundant biogenic elements hydrogen, carbon, oxygen, and sulfur. The study by FeMS of extraterrestrial samples of various ages thus provides insight into certain aspects of prebiotic chemistry and the origin of life. During condensation of the solar nebula, it is believed that Fe^{2+} was incorporated into Mg-silicates (pyroxenes and olivines) at temperatures between 500 and 1000K, while Fe^{3+} appeared only below about 400K, being found in magnetite and in the hydrosilicates (clay-like compounds) [1]. Oxidation to Fe^{3+} may also have taken place later, as on the surface of Mars, but not the moon, leading to distinct planetary mineralogy. Each resulting phase can be readily distinguished by FeMS.

FeMS can also provide evidence for the existence of iron in a form not previously suspected. In 1984, we reported [2] that the Orgueil meteorite, a carbonaceous chondrite of interest due to its primitive nature and the inclusion of amino acids and other organics, contains an appreciable fraction of its iron in a superparamagnetic (sp) phase. We suggested that this nanocrystalline phase (<30-nm grain size) was formed during an aqueous period in the history of the parent body and that the sp component may have served as a catalyst for formation of the organic component. Although the precise nature of this phase is still unresolved, other primitive meteorites (e.g. Murchison [3]) are now known to contain a sp fraction as well. Since nanophase material appears amorphous to x-ray diffraction (XRD), the existence of extraterrestrial superparamagnetism was unknown before our application of FeMS to Orgueil.

We have also applied FeMS to laboratory analogues whose reflectance spectra match those from the Martian bright regions and have established that the surface of Mars may contain iron in a superparamagnetic phase, specifically nanophase hematite (α-Fe_2O_3) [4].

In view of the demonstrated value of FeMS in the study of extraterrestrial iron and the fact that, after silicon and oxygen, iron is the most abundant element on the surface of Mars, we proposed [5], and have under development [6,7], a backscatter Mössbauer spectrometer with x-ray fluorescence capability (BaMS/XRF) for use on Mars as a geophysical prospecting instrument. Specifically, we have proposed [8] BaMS/XRF as part of the geochemistry instrumention on NASA's Mars Environmental Survey (MESUR) mission. BaMS/XRF will have applications in: a) the study of past environments through the examination of sedimentary materials; b) the study of the contemporary Martian environment; and c) the study of iron-containing minerals of possible biogenic origin. Development of a reference library from a geophysical point of view for putative Martian surface materials (laboratory and terrestrial analogues and SNC meteorites) at appropriate temperatures is now underway.

Based on the increasing evidence of liquid water during an early Martian epoch, on the discovery of sp iron in Orgueil and possibly Mars, and in anticipation of a Mars BaMS, we have carried out preliminary optical reflectance and FeMS measurements on mineral products (iron oxyhydroxides) of deep-sea hydrothermal activity [9]. These measurements demonstrate that such material, which is associated with microbial organisms found in the area of "deep-sea smokers," has distinguishing spectral characteristics. Similarities, as well as differences, to

Martian reflectance spectra are observed. In general, optical, FeMS, and XRD results correlate well. Material from an inactive vent shows the clear FeMS signature of superparamagnetism, while that from an active vent does not. It appears that amorphous biogenic matter is eventually converted to a crystalline form which includes a sp fraction. The discovery of nanophase hematite or other sp material in deposits on Mars could indicate an archaic hydrothermal site of potential exopaleontological interest.

Additional samples from deep-sea smokers, thermal springs, and subglacial volcanism should be investigated. For the purpose of interpreting future space-craft data, a file of optical (uv, vis, ir), FeMS, XRD, and magnetic susceptibility measurements would be helpful. Products of volcanism in aqueous environments will likely be distinct from those created by other processes. Minerals (especially sp precipitates) produced during hydrothermal activity with and without the aid of biologic processes may show distinct characteristics. Other terrestrial bacterial samples exhibiting superparamagnetism include: magnetotactic bacteria (small magnetite inclusions); sulfur-metabolizing bacteria; and sp magnetite grains used to infer a primitive bacterial ecosystem four miles underground [10]. Observable "aging" effects may include dessication, cycling between temperature extremes, exposure to uv radiation, and other laboratory simulations of the extraterrestrial environment.

If there has been archaic biotic activity on Mars analogous to that found in terrestrial deep-sea smokers, it is very likely that iron was involved and that sp iron would be a tracer. In the terrestrial marine situation, there appears to be a correlation between the distribution of iron-rich sediments and the location of hydrothermal vents [11]. As space-craft data are developed, a file on hydrothermal products will provide a database for interpreting physical evidence on the aqueous (and possibly biogenic) history of Mars and a means to determine its extent. For example, ancient hot springs located on the fringes of impact areas [12] and recent volcanism in Valles Marineris [13] have been suggested. The improvement in spatial resolution of Martian reflectance spectra expected from Mars Observer (1992), when correlated with FeMS and other physical measurements on hydrothermal products, should help correlate Martian aqueous history with present geologic features. Similar, but more mineralogically definitive, results may be expected from the BaMS/XRF instrument proposed for MESUR, (1998?) which involves a number of small landers distributed over the surface of Mars.

[1] Knudsen J.M. (1989) Hyperfine Interactions 47, p. 3-31.
[2] Wdowiak T.J. and Agresti D.G. (1984) Nature 311, p. 140.
[3] Madsen M.B. *et al.* (1988) Hyperfine Interactions 41, p. 827-830.
[4] Morris R.V., Agresti D.G., *et al.* (1989) J. Geophys. Res. 94, p. 2760-2778.
[5] Morris R.V., Agresti D.G., Shelfer T.D., and Wdowiak T.J. (1989) Lunar Planet. Sci. 20, p. 721-722.
[6] Agresti D.G. *et al.* (1990) Lunar Planet. Sci. 21, p. 5-6.
[7] Shelfer T.D. *et al.* (1991) Lunar Planet. Sci. 22, p. 1229-1230.
[8] NASA Planetary Instrument Definition and Development Program (1991).
[9] Collected from the area of the East Pacific Rise and supplied to us by Jeffrey C. Alt.
[10] Gold T. (1991), reported in Discover, Feb. 1991, p. 12.
[11] Coale K.H. *et al.* (1991) Nature 352, p. 325-328.
[12] Brakenridge G.R.*et al.* (1985) Geology 13, p. 859-862.
[13] Lucchitta B.K. (1987) Science 235, p. 565-567.

THE NANOPHASE IRON MINERAL(S) IN MARS SOIL; A. Banin[1,2], T. Ben-Shlomo[1], L. Margulies[1], D.F. Blake[2] and A. U. Gehring[3] ([1]The Hebrew University, Rehovot, Israel; [2]NASA Ames Research Center, Moffett Field, CA 94035; [3]University of California, Berkeley CA 94720)

Introduction. Iron-enriched smectites have been suggested as important mineral compounds of the Mars soil. They were shown to comply with the chemical analysis of the Martian soil (1), to simulate many of the findings of the Viking Labeled Release experiments on Mars (2,3) and to have spectral reflectance in the VIS-NIR strongly resembling the bright regions on Mars. The analogy with Mars soil is based, in a number of aspects, on the nature and behavior of the iron oxides and oxyhydroxides deposited on the surface of the clay particles. We wish to summarize our knowledge of the properties of these iron phases, present some recent findings on them, and discuss their potential relevance to Mars surface processes.

Formation and solubility. The iron phases in the Mars soil analog clays are deposited on the surface of the clay in a laboratory process (4,5) which generally simulates, but considerably enhances, the natural reaction sequences of hydrolysis-precipitation-oxidation or oxidation-hydrolysis-precipitation occurring during the oxidative weathering of iron-containing primary silicate rocks on Earth. The process involves slow titration of acidic clay with a solution of Fe(II) salt while the pH is controlled by the presence of OH-ion exchange resin. The later stages of the process, during which most of the iron is deposited, occur within a narrow range of pH, in a slightly acidic to slightly basic environment (pH 6.6-7.4), and at practically constant redox (pe + pH = 11.5-12.0). The double hydroxy salt of iron, ferrosic oxide ($Fe(II)Fe(III)_2(OH)_8$), appears to form at this stage (6). Upon aging in suspension, continued oxidation of the iron causes slow transformation into thermodynamically more stable mineral form(s) which are less soluble than $Fe(OH)_3$(amorp.) and more soluble than lepidocrocite (γ-FeOOH) and maghemite (γ-Fe_2O_3) (6). This is typical for many natural environments on Earth in which ferrous iron in solution is oxidized and forms insoluble "green-rust" (a double hydroxy-iron phase) which then, upon further oxidation, may transform to either goethite (α-Fe_2O_3), lepidocrocite, maghemite or ferrihydrite ($Fe_5O_7(OH).4H_2O$) (7). Such processes may have taken place on Mars during acidic-oxidative weathering of rocks (8).

Mineral identification. Powder x-ray diffractograms of the iron enriched clays do not show any of the characteristic diffraction patterns of the known crystalline iron oxides or oxyhydroxides (9). It appears as if the iron phases are completely amorphous. However, a recent study using selected area electron diffraction and microanalytical techniques have detected some crystallization and identified lepidocrocite (γ-FeOOH) as the mineral present (6). The mineral appears to crystallize only after a relatively high load of iron was added to the clay (5-6 times the cation exchange capacity; 10-13% Fe_2O_3 added). Even then, powder ring diffraction patterns are obtained and not single spot patterns of well developed single crystals.

Microscopic Observations. Electron microscopy shows no discrete particles of iron oxide-oxyhydroxides forming until added iron reached 3-4% Fe_2O_3 but the clay particles became somewhat more electron dense indicating fine coating with the added iron (6). Small, electron-dense, discrete and isodiametrical particles appeared at added iron contents above 8-9% Fe_2O_3. The iron oxide-oxyhydroxide particles are <10 nm, smaller than typically found in synthesis studies of iron oxides (10). They appear to preferentially bind at the edges of the clay particles.

Optical properties. The reflectance spectra of Mars-soil-analog iron enriched clays in the visible range strongly resemble the reflectance curves of the bright regions on Mars (11-13). Both the Mars and the analog's spectra do not show any pronounced typical and well defined absorption features of the crystalline iron oxides in the visible range. (Recent telescopic observations of Mars did document weak absorption features at .62-.72μm and .81-.94μm (12). The spectra are characterized by almost monotonous but significant decrease in reflectance from the NIR towards the UV (14,15). This spectral behavior has been generally attributed to nanophase iron oxides, and was recently specifically attributed to superparamagnetic nanophase hematite (16-18,12). This

assignment does not appear to be unique and singular since we find that amorphous iron oxides and nanophase lepidocrocite also agree quite well with the Martian spectra in the VIS-NIR range.

The chemical reactivity of the iron-enriched clays strongly resembles, and offers a plausible mechanism for the somewhat puzzling observations of the Viking Biology experiments (19). The analogs decomposed ^{14}C formate, the most labile organic component in the media used in the Labeled Release experiment, at a rate and to the extent measured on Mars (2,3) and simulated the sorption ("peak 1") and synthesis ("peak 2") activities of the Mars soil measured during the Pyrolytic Release experiments (20). These unique chemical reactivities are attributed to the combined catalytic effects of the iron oxide-oxyhydroxide and silicate phase surfaces (2,3).

Magnetic properties. We have recently found, and report here for the first time, that heating of the iron-enriched clays, in which lepidocrocite has been identified, to 300°C, renders them magnetic to the extent that they readily adhere to a weak hand-held magnet. This is in agreement with the observations that the Mars soil as a whole adhered to inserted magnets (21). The heat treatment converted the antiferromagnetic lepidocrocite to the strongly ferrimagnetic maghemite - a well known conversion. Hargraves et al. (21) have originally suggested maghemite as the magnetic mineral in a qualified manner since a formation scenario on Mars could not be offered at the time. Our present findings suggest that the magnetic properties of the Mars soil can be attributed to partial conversion of lepidocrocite to maghemite by relatively brief heating to 300°C such as by meteoritic impacts or shallow magmatic intrusions.

Summary. The evidence at hand suggests that iron enriched clays, containing nanophase lepidocrocite, which crystallizes from more amorphous ferrous and ferric iron hydroxides and double hydroxy phases on the extensive microscopic surfaces of phyllosilicate (smectite clays) minerals, bears strong resemblances to many of the known properties of the Martian soil. These analogs are produced under conditions that may be geologically and chemically realistic on Mars. While much of the oxidized iron in the system remains amorphous, part of it crystallizes as lepidocrocite, an oxyhydroxy iron mineral typically formed on Earth as the result of reoxidation of ferrous iron. Although iron in lepidocrocite is fully oxidized, the formation of this oxyhydroxy mineral is preferred were conditions of limited aeration (low redox) prevail and were ferrous iron is slowly undergoing oxidation (7,10). The reflectance spectra and chemical reactivity of iron-enriched clays, mimic quite faithfully those of the Martian soil. Mild heat treatment converts the lepidocrocite to maghemite and imparts enough magnetism to cause adherence of the powders to a weak magnet, as was observed for the Martian soil. It should be emphasized that we do not consider the identification of lepidocrocite, on the basis of the existing set of Mars observations and measurements, to be singular. Other iron oxide minerals, particularly superparamagnetic hematite have been also shown (16-18) to have a similar assemblage of properties. Further and more detailed data on the mineral nature of the Mars soil are necessary, therefore, to establish unambiguously the identity of the iron oxide mineral(s) present in it. Such data may be forthcoming in the near future from the Mars Observer and other missions to Mars.

References: 1.Toulmin, P., III et al. (1977) JGR 82, 4625-4634. 2.Banin, A. and Rishpon, J. (1979) J. Mol. Evol. 14, 133-152. 3.Banin, et al. (1988) Origins of Life 18, 239-265. 4.Banin, A. (1971) "Quantitative ion exchange process for clay". U.S. Patent No. 3,725,528. 5.Gerstl, Z. and Banin, A. (1980) Clays Clay Min. 28, 335-345. 6.Banin, A., et al. (1991) LPSC XXII, 49-50. 7.Taylor, R. M. (1987) in Chemistry of Clays and Clay Minerals (Newman, A.C.D., Ed.; Wiley-Interscience) 129-201. 8.Burns, R.G. and Fisher, D.S. (1990) JGR 95, 14,415-14,421. 9.Ben-Shlomo, T. and Banin, A. (1989) LPSC XX, 65-66. 10.Schwertmann, U. (1987) in Iron in Soils and Clay Minerals (Stucki,J.W.,Goodman,B.A. and Schwertmann,U. eds.; Reidel) 207-211. 11.McCord, T.B. et al. (1982) JGR 87, 3021-3032. 12.Bell, J.F.III, et al. (1991) JGR 95 14,447-14,461. 13.Banin, et al. (1985) JGR 90, C771-C774. 14.Singer, R.B. (1982) JGR 87, 10,159-10,168. 15.Singer, R.B. (1985) Adv. Space Res. 5, 59-66. 16.Morris, R.V., et al. (1989) JGR 94, 2760-2778. 17.Morris, R.V. and Lauer, H.V.Jr. (1990) JGR 95, 5101-5109. 18.Morris, R.V., et al. (1990) JGR 95, 14,427-14,434. 19.Klein, H.P. (1979) Rev. Geophys. Space Phys. 17, 1655-1667. 20.Hubbard, J.S. (1979) J. Mol. Evol. 14, 211-222. 21.Hargraves, R.B., et al. (1977) JGR 82, 4547-4558. 22.The work reported here was supported in part by the NASA Exobiology Research Program and by grants from the National Research Council Washington D.C., and the Hebrew University Israel.

MARTIAN IMPACT CRATER DEGRADATION STUDIES: IMPLICATIONS FOR LOCALIZED OBLITERATION EPISODES. N. G. Barlow, SN21, NASA/Johnson Space Center, Houston, TX 77058.

Early spacecraft missions to Mars revealed that impact craters display a range of degradational states, but full appreciation of the range of preservational characteristics was not revealed until the Mariner 9 and Viking missions in the 1970's. Many studies have described the spatial and temporal distribution of obliteration episodes based on qualitative descriptions of crater degradation (1, 2, 3). Recent advances in photoclinometric techniques have led to improved estimates of crater morphometric characteristics. The present study is using photoclinometry to determine crater profiles and is comparing these results with the crater geometry expected for pristine craters of identical size. The result is an estimate of the degree of degradation suffered by martian impact craters in selected regions of the planet. Size-frequency distribution analyses of craters displaying similar degrees of degradation within localized regions of the planet may provide information about the timing of obliteration episodes in these regions.

Initial analysis is concentrating on craters within an area 5° latitude by 5° longitude centered on the proposed Mars landing sites within ±40° of the equator (4). Viking Orbiter images of approximately 40 m/px resolution have been selected for these areas and crater diameter, depth, and rim height are obtained using the photoclinometry program of Davis and Soderblom (5). Comparison of crater depth values using photoclinometry and shadow estimates indicates the two values are identical within 5%. The results are compared to estimated crater depth and rim height values for fresh craters of identical size using relationships derived by Pike and Davis (6). The ratio of measured value to expected pristine value gives an estimate of the percentage change which the crater depth and rim height have undergone.

Five landing sites have been analyzed to date--site 61 in Arabia (30°N 327°W), and sites 21 (18.95°N 53.5°W), 24 (17.9°N 53.8°W), 25 (17.65°N 54.2-54.3°W), and 26 (18.2°N 57°W) in Maja Valles. Rim height values are not correlated with crater depth values and in fact vary widely across the regions. Crater depth values, however, vary in a more systematic manner at all five sites and are believed to represent actual variations in crater degradation state.

Figures 1a and b show the regional degradation variations indicated by the crater depth analysis. The distinction between areas of degradation is much finer than that determined by studies using qualitative descriptions of preservational classes. Three of the five landing sites (sites 61, 25, and 26) are located in areas where the surrounding craters are highly degraded (measured crater depth less than 25% of expected pristine crater depth). This suggests that surface materials found near these landing sites will be very weathered. The other two sites (21 and 24) are found in areas with moderate amounts of crater degradation, but near boundaries with highly degraded regions. Thus, fresh materials are expected to be rare to non-existent at these five sites.

No correlation between areas of high, medium, or low degradation with the stratigraphic geologic units (7, 8, 9) is found. This finding supports previous studies which argue against a constant obliteration rate throughout martian history. Sufficient numbers of craters will soon be available for the Maja Valles sites for crater statistical analyses to be performed. The results of these analyses for regions of low, medium, and high degradation

will provide information on the relative ages of these regions and will provide constraints on the timing of the obliterative episode(s) responsible for the degradation seen in these areas (10).

REFERENCES: (1) Hartmann W.K. (1973) *J. Geophys. Res.*, **78**, 4096-4116. (2) Soderblom L.A. et al. (1974) *Icarus*, **22**, 239-263. (3) Chapman C.R. and Jones K.L. (1977) *Ann. Rev. Earth Planet. Sci.*, **5**, 515-540. (4) Greeley R. (1990) *NASA Ref. Public. 1238*. (5) Davis P.A. and Soderblom L.A. (1984) *J. Geophys. Res.*, **89**, 9449-9457. (6) Pike R.J. and Davis P.A. (1984) *Lunar Planet. Sci. XV*, 645-646. (7) Scott D.A. and Tanaka K.L. (1986) *Misc. Invest. Ser. Map I-1802-A*. (8) Greeley R. and Guest J.A. (1987) *Misc. Invest. Ser. Map I-1802-B*. (9) Tanaka K.L. (1986) *J. Geophys. Res.*, **91**, E139-E158. (10) Barlow N.G. (1988) *Icarus*, **75**, 285-305.

Figure 1. Degradation maps of (a) Arabia and (b) Maja Valles. "High" indicates measured to pristine crater depth ratios in the range of 0 to .25, "Medium" indicates ratios between .25 and .55, and "Low" refers to ratios in the range .55 to 1.00. Scale bar is 100 km for Arabia and 50 km for Maja Valles. Dark circles are locations of proposed landing sites.

MIDLATITUDE WEATHER SYSTEMS ON MARS: IS THERE A HEMISPHERIC ASYMMETRY? J.R. Barnes, Department of Atmospheric Sciences, StAg Hall 326, Oregon State University, Corvallis, OR 97331

The Viking Lander meteorology observations confirmed that midlatitude weather systems are present in the northern hemisphere of Mars during the autumn, winter, and early spring seasons. These systems have properties consistent with a development through baroclinic instability of the wintertime zonal-mean circulation (1,2). It is known that the weather systems must be of importance for the zonal-mean circulation by virtue of their heat and momentum transports (3). Observations show that they are associated with dust raising (4), and they must be involved in the transport of dust; the weather systems almost certainly must act to produce significant water transports as well (5). Recent simulations with the NASA-Ames Mars General Circulation Model (GCM) show that the heat transports by the weather systems (and by the zonal-mean circulation) during northern winter can be very substantial - large enough to significantly reduce the CO_2 condensation at polar latitudes (6). This could be largely responsible for the observed early spring halt in the north polar cap recession and for the presence of westerly winds near the cap edge during this season (7).

Whether midlatitude weather systems like those in the north are present in the southern hemisphere during (southern) autumn, winter, and spring is not known - the available observations do not allow this question to be answered. Their existence is certainly to be expected on basic theoretical grounds, since the southern winter circulation should be highly unstable baroclinically (though probably somewhat less so than that in northern winter because of the eccentricity of Mars' orbit, and possibly also because of lower dust loadings). Previous Mars GCM simulations have exhibited vigorous midlatitude weather systems in southern winter (3). Recent GCM simulations, however, show weather systems of greatly reduced strength (in comparison to those in northern winter) in southern winter (8). The primary cause of this appears to be the zonally symmetric (longitudinally averaged) component of the Mars GCM topography in the southern hemisphere, as a result of dynamical effects largely anticipated by earlier modeling studies (2). GCM simulations with flat topography exhibit strong weather systems in southern winter.

If strong weather systems are indeed absent during southern winter, this would constitute yet another striking hemispheric asymmetry on Mars (as for that in the residual polar caps, the polar hoods, the polar cap albedoes, atmospheric water abundance, etc.). The presence of relatively weak weather disturbances in southern winter could be of significance for the residual polar cap asymmetry, because of reduced poleward heat transports in the south.

The topography incorporated in the current set of Mars GCM simulations is derived from the Mars Consortium topography, which is based upon Mariner 9 data. The zonally symmetric component of this topography slopes sharply downwards towards the pole in southern middle and high

latitudes, the polar region being relatively low. Somewhat similar topographic slopes are actually present in the northern hemisphere as well, but these do not act to suppress baroclinic instability nearly as strongly - though they do appear to have very significant effects on the northern weather systems in the current GCM simulations. A new Mars topography has been generated using Viking data (and Earth-based radar data) as well as the Mariner 9 data, the Mars Digital Terrain Model (DTM). This topography is extremely different from the older topography in southern middle and high latitudes: in particular, its zonally symmetric component is not characterized by steep slopes, as middle and high latitudes are uniformly - except for Hellas - very elevated (~ 3-5 km). The observational origins of these striking differences in the two topographies are not entirely clear, though Viking IRTM data are consistent with an elevated south polar region. An absence of steep downward slopes in high latitudes probably means that the southern weather systems would not be strongly suppressed (though there could be other aspects of the topography that might inhibit weather activity) - a Mars GCM simulation with the DTM topography is being pursued to see if this is indeed the case.

Mars Observer will make observations that will determine whether or not strong weather systems are present in southern winter. It will also determine the global topography to a very high accuracy. Until then, it would seem that the question of the existence of southern hemisphere weather activity must remain an open one - given the uncertainties in the available topographic data and the possible strong influences of large topography on the Mars weather systems.

REFERENCES

(1) Barnes, J.R. (1980) *J. Atmos. Sci.*, **37**, 2002-2015.
(2) Barnes, J.R. (1984) *J. Atmos. Sci.*, **41**, 1536-1550.
(3) Pollack, J.B., C.B. Leovy, P.W. Greiman, and Y. Mintz (1981) *J. Atmos. Sci.*, **38**, 3-29.
(4) Briggs, G.A. and C.B. Leovy (1974) *Bull. Amer. Met. Soc.*, **55**, 278-296.
(5) Haberle, R.M. and B.M. Jakosky (1990) *J. Geophys. Res.*, **95**, 1423-1437.
(6) Pollack, J.B., R.M. Haberle, J. Schaeffer, and H. Lee (1990) *J. Geophys Res.*, **95**, 1447-1474.
(7) Kahn, R. (1984) *J. Geophys. Res.*, **89**, 6671-6688.
(8) Barnes, J.R., R.W. Zurek, J.B. Pollack, and R.M. Haberle (1989) *EOS, Trans. Amer. Geophys. U.*, **70**, 1180.

MARS: COMPOSITIONAL VARIABILITY OF FERRIC/FERROUS MINERALS AND POLAR VOLATILES FROM GROUNDBASED IMAGING SPECTROSCOPY: James F. Bell III (Planetary Geosciences Division, University of Hawaii, 2525 Correa Rd., Honolulu 96822 and Remote Sensing Lab, University of Washington, AJ-20, Seattle 98195. e-mail: jimbo@ruth.pgd.hawaii.edu)

Background: Our current understanding of the composition of the martian surface and atmosphere is derived from over a century of focused ground-based and airborne telescopic measurements as well as data returned from the Mariner, Viking, and Phobos spacecraft missions. These observations have yielded a wealth of data on surface geomorphology and atmospheric composition, but have provided surprisingly little unambiguous information on the specific mineralogy of the surface soils, rocks, and æolian dust. This situation exists because of the paucity of high-quality spacecraft spectroscopic measurements of the surface, the difficulty in obtaining absolutely-calibrated spectrophotometric data of Mars from ground-based telescopes and spacecraft, and the relatively poor spatial resolution (100s of km) that can be obtained from ground-based data. Despite these limitations, there are several things about the ferric and ferrous mineralogy of Mars that we know for certain: (1) The martian spectrum in the visible is dominated by strong ferric oxide charge-transfer and electronic transition absorptions. Previous observers have ascribed these features to "field minerals" like limonite [*e.g.* Sharanov 1961; Sagan *et al.* 1965] and palagonite [*e.g.* Soderblom and Wenner 1978; Singer 1982]. Much recent work has been done, however, to attempt to define the ferric mineralogy beyond these broad limits. Morris *et al.* [1989] have re-analyzed spectra obtained in the 1970s and have found evidence for both bulk crystalline and nanophase hematite, an interpretation verified by more recent observational data [Bell *et al.* 1990a]. Grain size is an important but poorly understood variable that drastically effects quantitative determinations of mineral abundances from these data. Also, little is known of the spectral properties of nanophase ferric oxides other than hematite [Morris and Lauer, 1990]. (2) Many regions of the martian surface exhibit rather weak absorption band(s) in the 1.0 μm region that are due to ferrous minerals. Considerable analysis of these features [*e.g.* Singer *et al.* 1979; Singer and Roush, 1985] has shown them to be primarily caused by high-Fe, low-Ca clinopyroxenes. As well, more recent observations have provided tantalizing preliminary evidence of pyroxene mineralogy variations on the surface [Singer *et al.* 1990; Bell *et al.* 1990b].

In an attempt to constrain further the ferric and ferrous mineralogy of Mars, Bell *et al.* [1989; 1990b] obtained high resolution imaging spectroscopic data of much of the martian surface in the visible and near-infrared (0.4-1.1 μm) during the 1988 opposition. Preliminary analysis of these data showed further evidence of crystalline hematite absorption features at 0.8-0.9 μm and 0.6-0.7 μm. Additionally, the 0.6-0.7 μm Fe(III) band was shown to vary across the surface, with a substantial correlation with albedo (higher albedo => deeper band) in the region studied. Calibration of this 1988 data set (along with a similar data set obtained during the 1990 opposition) has been ongoing, and this abstract reports some of the most recent results of the analysis of these data using linear spectral mixture modeling.

Mixing Model Approach: The spectral mixing model approach used here is based on the linear image-oriented model recently developed at the University of Washington [Adams *et al.* 1986, 1989; Possolo *et al.*, unpublished manuscript]. Instead of using laboratory mineral spectra as mixture endmembers, "image endmembers" are chosen directly from the data. In this way, additional effects caused by instrument artifacts and lighting geometry variations can be effectively separated from possible compositional variations. Image endmembers are chosen so as to minimize the total residual error ε for each pixel in the areal mixing equation [Adams *et al.* 1989]:

$$DN_c = \left[\sum_{i=1}^{n} F_i DN_{i,c}\right] + E_c \quad \text{where} \quad \sum_{i=1}^{n} F_i = 1 \qquad (1)$$

where DN_c is the data value of each pixel in channel c, F_i is the fraction of each of the n endmembers within each pixel, $DN_{i,c}$ is the data value of endmember i in channel c, E_c is the residual (error) of the fit in channel c, and where the total (rms) residual error for each pixel in all M bands is defined as:

$$\varepsilon = \left[M^{-1}\sum_{c=1}^{M} E_c^2\right]^{0.5} \qquad (2)$$

The calculated values of F_i, E_c, and ε are displayed as images, and an iterative approach is used to determine the best choice of n and $DN_{i,c}$. Care is also taken to examine the actual values of F_i within the fraction image cube, since superpositive (> 1) and supernegative (< 0) values are not strictly prohibited in equations (1), yet such values may occur if the endmember spectra have not been properly chosen [Possolo *et al.*, unpublished manuscript].

Results: Mars imaging spectroscopic data in the 0.4-0.8 μm wavelength region have been modeled using equations (1). The original data have been spectrally subsampled by 10 (M=15). Several different models have been combined to define 6 units (cf. Fig. 1): (1) a red, high albedo unit with a deep near-UV charge transfer edge, distinct crystalline absorption band at 0.6-0.7 μm, and flat or positive near-IR spectral slope (type region: Arabia); (2) a red, low albedo unit with a shallow ferric charge transfer band, no indication of crystalline iron oxide bands, and a negative spectral slope in the near-IR (type region: Western Syrtis Major); (3) a white, high albedo south polar cap unit; (4) a blue, moderate albedo unit that occurs along the morning limb and surrounding the north polar region; (5) a red, low albedo unit with a deeper near-UV ferric absorption feature than unit (2) and with a negative near-IR slope (type regions: Eastern Syrtis Major, Hellas); and (6) a very low flux and slightly red "sky" unit corresponding to scattered Mars light. As will be seen below, these 6 units are not necessarily all spectrally independent.

Modeling of the surface as a mixture between units 1 and 2 only (Model A: bright and dark) accounts for nearly 95% of the spectral variance in the data. Examination of the ε and E_c residual images (equation 2) from such a model allows the other 4 units to be characterized. For example, analysis of residual images in Model A in the 0.6-0.7 μm region revealed a spatially coherent boundary between eastern and western Syrtis Major Planitia, with the western half of Syrtis looking spectrally similar to unit 2 and the eastern half having a distinctly more ferric character, corresponding to unit 5. This boundary has also been observed in other ground-based and Phobos-2 ISM data sets [Pinet and Chevrel 1990; Erard *et al.* 1991]. Residual analysis was crucial in the identification of unit 5, since except for the weak band between 0.6-0.7 μm, unit 5 appears to be a linear mixture of 80-90% unit 2 and 10-20% unit 1.

Residuals from Model A are also used to reveal the volatile units, 3 and 4. The south polar cap is known to be predominantly CO_2 ice, however its spectrum has a substantial ferric component [*e.g.* Bell *et al.* 1990]. Thus, using the cap as an image endmember does not allow the contributions of ice vs. dust to be unmixed. In a preliminary attempt at determining the ice/dust ratio for the polar cap region, a "reference endmember" spectrum [Adams *et al.* 1986, 1989] of CO_2 snow [Warren *et al.* 1990] has been added to Model A. Analysis of the "CO_2 ice" fraction images from this model (Model B) show a bimodal distribution of volatile species. The whitest and brightest materials with the highest volatile fractions correspond to the south polar cap (unit 3). A substantially lower but still discrete fraction corresponds to bright morning limb clouds and the north polar hood (unit 4). An important difference between units 3 and 4 besides this fractional abundance difference is that unit 4 appears mixed with both bright and dark surface units (depending on its geographic location) while unit 3 is always best fit by mixing with bright unit 1 materials. It is important to note that accurate fractional abundances of CO_2 ice vs. ferric dust in the polar cap (or the polar hoods) cannot be uniquely determined using these scaled data since grain size produces large variations in visible to near-IR ice reflectance [Warren *et al.* 1990]. Additionally, H_2O ice cannot be uniquely discriminated from CO_2 ice in the visible and near-IR without additional albedo and grain size information. Modeling of these parameters is continuing using this data set as well as other near-IR imaging spectral data obtained during the 1990 opposition [Bell and Crisp 1991a,b].

References: Adams J.B. *et al.* (1986) *JGR, 91,* 8098-8112. Adams J.B. *et al.* (1989) *Proc. IGARSS 12th, vol I,* 16-21. Bell J.F. III *et al.* (1989) *EOS, 70,* 50. Bell J.F. III *et al.* (1990a) *JGR, 95,* 14447-14461. Bell J.F. III *et al.* (1990b) *PLPSC 20th,* 479-486. Bell J.F. III and D. Crisp (1991a) *LPSC XXII,* 73-74. Bell J.F. III and D. Crisp (1991b) submitted to *Icarus.* Erard S. *et al.* (1991) *PLPSC 21st,* 437-455. Morris R.V. *et al.* (1989) *JGR, 94,* 2760-2778. Morris R.V. and H.V. Lauer (1990) *JGR, 95,* 5101-5109. Pinet P. and S. Chevrel (1990) *JGR, 95,* 14435-14446. Sagan C. *et al.* (1965) *Icarus, 4,* 43-61. Sharanov V.V. (1961) *Sov. Astron. AJ, 5,* 199-202. Singer R.B. *et al.* (1979) *JGR, 84,* 8415-8426. Singer R.B. (1982) *JGR, 87,* 10159-10168. Singer R.B. and T.L. Roush (1985) *BAAS, 17,* 737. Singer R.B. *et al.* (1990) *BAAS, 22,* 1061. Soderblom L.A. and D.B. Wenner (1978) *Icarus, 34,* 622-637. Warren S.G. *et al.* (1990) *JGR, 95,* 14717-14742.

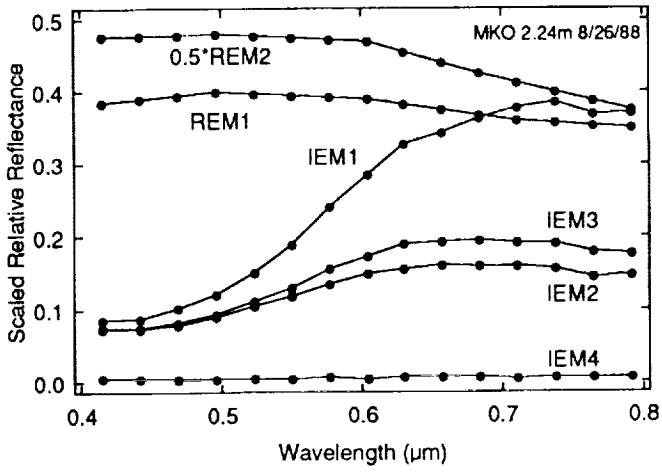

FIGURE 1: Image endmembers (IEM) and reference endmembers (REM) used in this Mars linear mixing analysis. IEM1 = Arabia; IEM2 = W. Syrtis; IEM3 = E. Syrtis; IEM4 = Sky; REM1 = CO_2 snow (2000 μm); REM2 = H_2O snow (1000 μm). REM data from Warren *et al.* (1990).

THERMALLY DISTINCT EJECTA BLANKETS FROM MARTIAN CRATERS; B. H. Betts and B. C. Murray, California Institute of Technology

The study of ejecta blankets on Mars gives information about the martian surface, subsurface, geologic history, atmospheric history, and impact processes. In February and March, 1989, the Termoskan instrument on board the Phobos '88 spacecraft of the USSR acquired the highest spatial resolution thermal data ever obtained for Mars, ranging in resolution from 300 meters to 3 km per pixel [1]. Termoskan simultaneously obtained broad band visible channel data. The data covers a large portion of the equatorial region from 30°S latitude to 6°N latitude. Utilizing the Termoskan data set we have discovered tens of craters with Thermal Infrared Distinct Ejecta (TIDE) in the equatorial regions of Mars (Figure 1). The lower resolution Viking IRTM thermal data were unable to distinguish TIDEs [2].

Virtually all of the 100 plus TIDEs seen in the Termoskan data are located on the plains near Valles Marineris. There cannot be a uniform blanket of depth greater than a very few centimeters on the plains where TIDEs occur, otherwise they would not be thermally distinct. There is a startlingly clear correlation of TIDE existence with terrains of Hesperian age, implying some kind of spatial or temporal dependence on Hesperian terrains. TIDEs are present on all the Hesperian aged units (as defined by [3,4]) observed by Termoskan. No TIDEs are associated with any of the thousands of craters within the data set that occur on the older Noachian units, with the exception of 5 craters clustered near a high contrast albedo boundary in Sinus Meridiani. TIDEs do not appear on the portions of the younger Tharsis Amazonian units seen in the data, though the low crater density of the Amazonian units in general makes drawing solid conclusions about these units difficult. The Hesperian terrain dependence can be explained by neither atmospheric nor impactor variations, because Noachian terrains should have experienced the same Hesperian atmospheric and impactor conditions. We suggest that the almost exclusive Hesperian dependency may be due to either relatively thin layering of differing materials versus more homogeneous Noachian units and/or a lack of material available for redeposition relative to more regolith-like or erosion product rich Noachian terrains.

On the Hesperian units where TIDEs are present, profiles across different ejecta blankets vary greatly in both the thermal and visible channels [5,6]. Some of the blankets appear warmer than their surroundings, some appear cooler, and some do not show up at all. Some thermally distinct ejecta blankets appear distinct in the visible channel as well, implying compositional differences relative to the surroundings. Others however do not, implying textural differences. Of the TIDEs that are associated with discernible lobate ejecta blankets, the boundaries of the thermally distinct areas often follow closely the termini of the lobate ejecta blankets, even when the ejecta blankets show a high degree of sinuosity. This implies that the thermally distinct nature of TIDEs must be due to the primary ejecta formation process; either directly, from either compositional or textural effects of the ejecta material itself; or indirectly, for example through preferential deposition of certain sized particles on the blankets due to increased roughness of the blankets relative to the surroundings. Note that not all discernible lobate ejecta blankets are thermally distinct. Some TIDEs occur near similar craters that do not show thermally distinct ejecta blankets, thus arguing against wind patterns or locally available aeolian material providing a single overall explanation for the observed variations.

In order to look for correlations within the data, we have compiled a database which currently consists of 110 craters [6] in an area rich in TIDEs and geologic unit variations. For each crater we include morphologic information from [7] in addition to geographic, geologic, and physical information and Termoskan thermal infrared and visible data. There are no correlations between temperature difference (ejecta temperature - surrounding area temperature), time of day corrected temperature, or thermal freshness, with any of the following: crater diameter, ejecta morphology, interior morphology, existence of central pits, ratio of ejecta diameter to crater diameter (a measure of degree of fluidization), or surrounding area temperature.

Results of our analyses so far indicate that no one simple process is responsible for TIDE variations seen on Hesperian units. However, excavation of an underlying layer (perhaps megaregolith) causing different ejecta or differently textured ejecta blankets could cause the variations observed if combined with one or more circumstances such as availibility of aeolian material, degradational state of ejecta, atmospheric variations over time, or wind patterns. Observations using the 3 km per pixel resolution Thermal Emission Spectrometer on Mars Observer will greatly expand the seasonal, diurnal, and geographic coverage of TIDEs and enable us to constrain this new, interesting phenomenon. In addition, observations by MOC and MOLA on Mars Observer and Termoskan 2 and the camera on Mars 94 will be extremely useful for adding a variety of new information relevant to our understanding of the TIDE phenomenon.

REFERENCES: (1) Murray, B.C., M.K. Naraeva, A.S. Selivanov, B.H. Betts, T. Svitek, V.D. Kharlamov, M.L. Santee, Y.M. Gektin, D.A. Fomin, D.A. Paige, A.S. Panfilov, D. Crisp, J.W. Head, S.L. Murchie, and T.Z. Martin, 1991, *Planetary and Space Science*, Vol. 39, No. 1/2, pp. 237-265.; (2) Christensen, P. R., personal communication (1991); (3) Witbeck, N.E., K.L. Tanaka, and D.H. Scott, (1988) (preliminary version). U.S. Geological Survey Miscellaneous Investigations, scale 1:2,000,000, to be published; (4) Scott, D.H. and Tanaka, K.L. (1986). U.S. Geological Survey Miscellaneous Investigations Series Map I-1802A; (5) Betts, B.H. and B.C. Murray (1991). In *Lunar and Planetary Science XXII, pp.* 97-98; (6) Betts, B. H. and B. C. Murray (1991). Article in preparation; (7) Barlow, N. G. (1987). *Catalog of Large Martian Impact Craters*, submitted as a NASA contractor report.

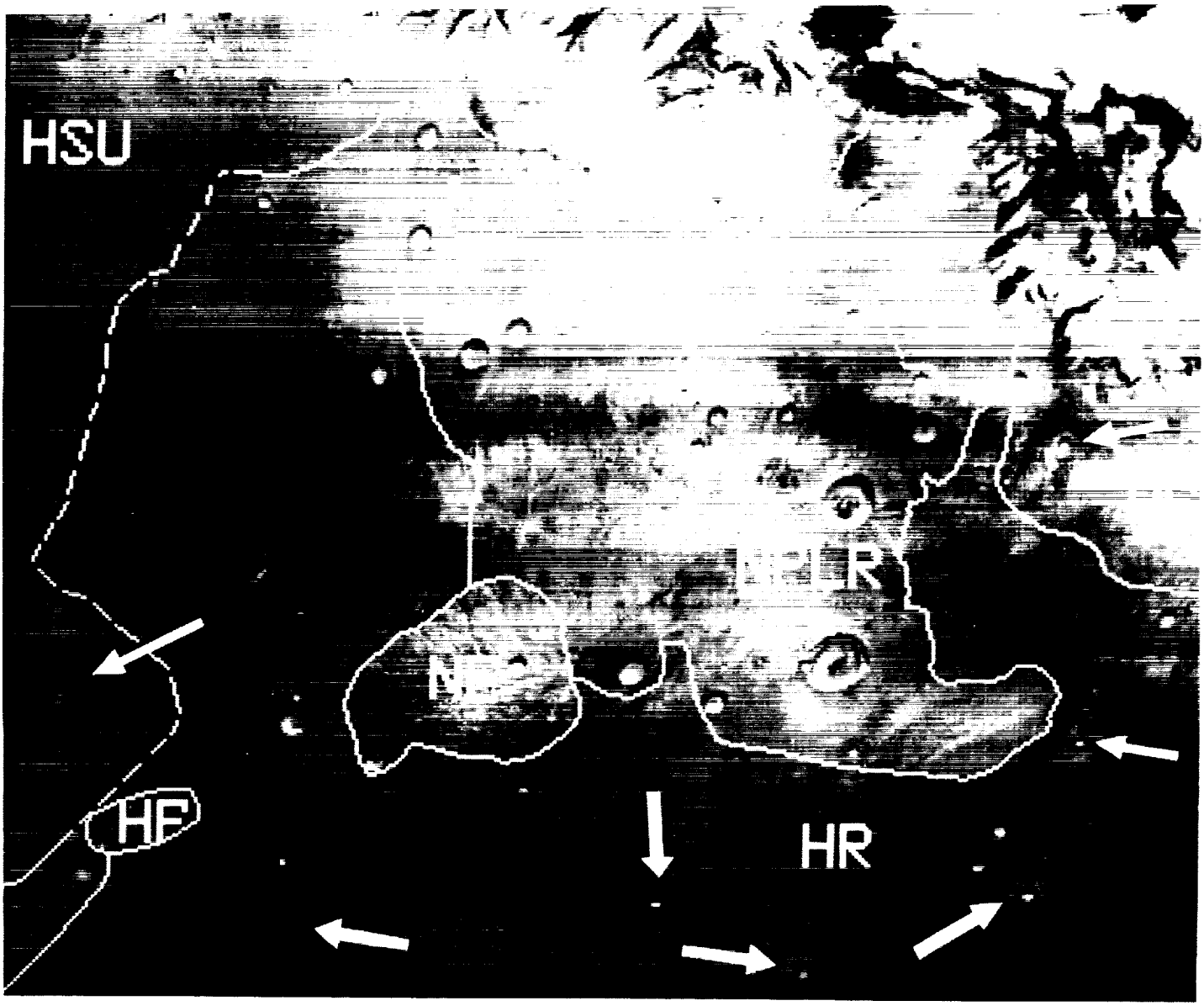

Figure 1: THERMALLY DISTINCT EJECTA DEPOSITS. In this Termoskan infrared image of region just south of Valles Marineris, the darker regions are cooler, lighter are warmer. Time of day is near local noon. North is top. Phase angle is approximately zero for all points. The dark East-West band is the thermal signature of the passage of the shadow of Phobos.

Note the thermally distinct ejecta deposits denoted in the image seen as bright rings surrounding craters. These deposits are 2 K to 5 K warmer than their surroundings. Other craters exhibit distinct ejecta deposits cooler than surroundings. Where lobate ejecta blankets appear as thermally distinct, the thermally distinct outline in the Termoskan data closely matches the actual boundary of the lobate ejecta blanket.

White lines indicate geologic map unit boundaries. Geologic units shown are from Witbeck *et al.* (1988) and Scott and Tanaka (1986) with some interpolation between the two. Units shown, from oldest are: Nplr = Noachian plateau ridged unit; Nf = Noachian fractured unit; HF = Hesperian fractured unit; Hr = Hesperian ridged plains material; Hsu = Hesperian Syria Planum formation. Thermally distinct ejecta blankets occur frequently on various Hesperian units in this region (e.g. Hr, Hsu, and Hf), but not on the older Noachian units (e.g. Nplr, Nf). This relationship implies that the thermally distinct nature of ejecta is target material dependent. This dependency could either be due to rock type variation (e.g. through some type of layering) or through variability in the amount of material available on different terrain units for local redeposition and blanketing.

JJ5744458

N92-28995

21

INFRARED IMAGING OF MARS FOR VOLATILE DISTRIBUTION AND SEASONAL VARIABILITY BETWEEN 2.4 and 5.1 μm. Diana L. Blaney, MS 183-501, Jet Propulsion Laboratory, California Institute of Technology, 4800 Oak Grove Drive, Pasadena, CA, 91109.

Recent advances in ground-based infrared imaging now allow for sub-arc second spectral imaging. The data discussed here was collected at the NASA Infrared Telescope Facility using protocam, a 62x58 InSb array camera with a circular variable filter and a plate scale 0.2 arc-seconds / pixel. These images are a first attempt at extended seasonal infrared coverage of Mars to look for seasonal variations. Currently, data collected in June, 1990 at Ls=241 (southern spring) and in January, 1991 Ls=360 (late southern summer) is being reduced and analyzed.

The 3 micron bound water band is the strongest surface absorption feature on Mars in the infrared. Infrared spectroscopy can also be useful in the detection of ice and frost deposits, especially in the polar regions. While imaging and spectroscopy at visible wavelengths allows for the detection of condensates, infrared information is needed to distinguish between water and carbon dioxide ice/frost deposits.

In the June (southern hemisphere spring) images, the south polar cap totally disappears in the 3.4 micron CO2 frost band and is bright in the 3.1 micron water ice band, indicating that water ice is not a detectable component of the south polar cap at this season. Further investigations are currently under way to look for residual water ice after the disappearance of the seasonal south polar cap in the January images (late southern hemisphere summer).

The June images that have been focussed on had a sub-earth point located at 184 longitude, and 23.8 S latitude which put the center of the disk in the southern highland region between Elysium and Amazonis. Examination of the June images show that there are four surface units identifiable: a CO2 frost deposit, a northern plains unit, an equatorial unit, and a southern highland unit. At this resolution there does not appear to be any latitudinal variations in the 3 micron band that is independent of the 2.4 micron albedo features. The northern planes unit and the southern highland unit have very similar "color" in the three micron band as demonstrated by the rise out of the band, but different brightness levels. The equatorial unit has a distinct three micron color implying a compositional difference. The albedo features at 2.4 microns have decreased contrast at longer wavelengths, till they are unrecognizable at 4 microns.

INFLUENCE OF AERODYNAMIC ROUGHNESS LENGTH ON AEOLIAN PROCESSES: EARTH, MARS, VENUS, Dan G. Blumberg and Ronald Greeley, *Department of Geology, Arizona State University, Tempe, AZ. 85287-1404.*

The aerodynamic roughness length (z_0) is the height at which a wind profile assumes a zero velocity. The lower part of the atmospheric boundary layer will be impeded by friction with the surface. An increase in surface roughness will also increase the shear stress required to initiate particle entrainment by the wind. Bagnold (1941) estimated z_0 as being 1/30 of the mean particle size. In Nature, surface roughness is composed of non erodible elements as well as sand-size erodible particles. To assess z_0 values as a function of terrain, field experiments were conducted to obtain wind profiles monitored over natural surfaces at 15 sites in the Mojave Desert, Death Valley, and Nye County, Nevada. These sites span a variety of arid-land terrains, including smooth playas, alluvial fans, and lava flows; z_0 values ranged from 0.0001 cm to 1 cm. These values were incorporated in a threshold model (Greeley et al., 1974) and a flux model (White, 1979) to assess transport efficiency over such terrains in three planetary environments (Venus, Mars, and Earth), and for particle sizes ranging from 60μm to 500μm. Threshold and flux are a function of planetary environment, particle density and size (Dp), and z_0, and the shear velocity. Results show that threshold (U_{*_t}) on Mars is 95 cm/s to 550 cm/s, Earth = 15 cm/s to 120 cm/s, and Venus = 2 cm/s to 16 cm/s. The potential flux (q) was calculated by applying a shear velocity of 1.2 x U_{*_t} (for Dp=250μm and z_0=0.84 cm). Results show that flux on Mars is ~14 g $cm^{-1}s^{-1}$, on Earth it is ~3 g $cm^{-1}s^{-1}$, and on Venus 0.5 g $cm^{-1}s^{-1}$. Under all planetary environments, the results also show a dramatic decrease in the flux for particles >200μm when z_0 increases above 0.0085 cm. (corresponding to sites consisting of alluvium). When z_0 approaches 0.03 cm (corresponding to a mantled pahoehoe lava), the flux diminishes.

References Cited

Bagnold R.A., 1941, p. 265.

Greeley R. and J.D. Iversen and J.B. Pollack and N. Udovich and B. White, 1974, *Proc. R. Soc.*, p. 331-360.

White B., 1979, *J.G.R.*, p. 4643-4651.

23

DUST STORM DRIVEN VARIATIONS OF THE MARS THERMOSPHERE AND EXOSPHERE: COUPLING OF ATMOSPHERIC REGIONS;
S W Bougher (LPL, U. of Arizona, Tucson, AZ 85721), C G Fesen (Dartmouth College, Hanover, NH 03755), and R W Zurek (JPL, Pasadena, CA 91109).

The National Center for Atmospheric Research (NCAR) thermospheric general circulation model (TGCM) for the Earth has been modified to examine the three-dimensional structure and circulation of the upper atmosphere of Mars (MTGCM). The solar, orbital, and seasonal responses of the Mars thermosphere above 100 km have been examined for various combination of input parameters [1]. Calculations driven by this changing in-situ solar forcing are generally successful in explaining existing Mars data. However, Mariner 9 UVS airglow measurements taken during a global dust storm provide evidence of large temperature variations uncorrelated with solar activity, and local time variations of 130.4 nm emission (O mixing ratios) contrary to in-situ driven winds [2]. We expect significant forcing of the thermosphere from below as a result of upward propagating gravity waves or tides generated by solar heating of airborne dust.

The effects of upward propagating tides are introduced into the MTGCM by appropriately specifying its lower boundary condition according to classical tidal theory. We first adapt the terrestrial scheme used by Fesen *et al.*, [3] to a Mars model appropriate to Mariner 9 conditions. This observational period occurred during near solar minimum fluxes. Estimates for amplitudes and phases of the likely dominant semi-diurnal (2,2) mode at the mesopause ($\sim$100 km) are specified for a range of possible lower atmosphere dust conditions. Selected simulations of solar plus tidally driven MTGCM temperature and oxygen mixing ratios are contrasted with corresponding Mariner 9 inferred values [4]. Subsequent calculations are made for the Mars thermosphere during solar maximum conditions. The changing thermospheric response and the depth of penetration of these semi-diurnal tides into the thermosphere are noted over the solar cycle.

Finally, the time varying response by the globally averaged exospheric temperatures and the neutral densities is presented, with possible implications for escape to space of light atoms. Our work suggests that dust storm driven tides (generated in the dust laden lower atmosphere near Ls=270) can provide a strong episodic forcing that effects the entire upper atmosphere. Future observations are needed to further confirm this coupling, and to establish the typical magnitude and periodicity of these tidal effects.

[1] Bougher, S. W., Roble, R. G., Ridley, E. C., and Dickinson, R. E., (1990) J. Geophys. Res., 95, 14811-14827.

[2] Stewart, A. I. F., Alexander, M. J., Meier, R. R., Paxton, L. J., Bougher, S. W., and Fesen, C. G., (1991) J. Geophys. Res., 96, in press.

[3] Fesen, C. G., Dickinson, R. E., and Roble, R. G., (1986) J. Geophys. Res., 91, 4471-4489.

[4] Bougher, S. W., Fesen, C. G., and Zurek, R. W., (1991) EOS Trans. AGU, 72, 17, 170.

SIMULATIONS OF SURFACE WINDS AT THE VIKING LANDER SITES USING A ONE-LEVEL MODEL. Alison F.C. Bridger, Dept. Meteorology, San Jose State University, San Jose, CA 95192, and Robert M. Haberle, NASA/Ames Research Center, 245-3, Moffett Field, CA 94035-1000.

The one-level model developed by Mass and Dempsey (1) for use in predicting surface flows in regions of complex terrain has been adapted to simulate surface flows at the Viking lander sites on Mars. In the one-level model, prediction equations for surface winds and temperatures are formulated and solved. Surface temperatures change with time in response to diabatic heating, horizontal advection, adiabatic heating and cooling effects, and horizontal diffusion. Surface winds can change in response to horizontal advection, pressure gradient forces, Coriolis forces, surface drag, and horizontal diffusion. Surface pressures are determined by integration of the hydrostatic equation from the surface to some reference level. The model has successfully simulated surface flows under a variety of conditions in complex-terrain regions on Earth (1,2).

It is assumed in the model that terrain influences the flow through a "layer of topographic influence", which we take to be 7km deep in this study. At this level, temperatures are calculated initially, and then remain fixed in time. Entry data are used to specify temperatures (and, if desired, winds) at some reference level above the surface (2 km in this study). A lapse rate of 2.5 deg C/km is assumed.

From a quiescent initial state (dawn or dusk), an integration forward in time simulates the diurnal cycle as diabatic heating is imposed. The form of the heating is as in (1), except that a sin-squared profile produces a time variation of surface temperature that better simulates those observed at both VL1 and VL2. The amplitude of the heating function is adjusted until the diurnal temperature trace approximately matches the observed. The flow is subject to surface drag, which is parameterized via a simple drag law formulation. As in (1), we enhance the drag by a factor of 2.8, and allow values to change from day-to-night.

We examine two scenarios with the aim of studying thermally-induced slope flows on Mars. In the first we study flows induced up or down a hypothetical slope (aligned east-west) which is subject to heating or cooling. The terrain is similar to that used in (3), i.e., plain-slope-plateau. The equations are solved on a 40 x 40 grid with a resolution of 10 km in both directions. In a 36-hour simulation, surface temperatures at a point in the center of the domain (i.e., mid-slope) increased from 190K at dawn to 240K in 12-15 hours, and then cooled to 190K after 24 hours. The warming in the model lags the observed warming by about 2 hours. An upslope flow begins to develop as the heating progresses, eventually reaching peak speeds of O(8 m/s) after 12-15 hours. Speeds are reduced after dusk, and eventually a downslope flow is established. Surface winds veer during the diurnal cycle. Results are also presented for cases in which a prevailing flow aloft is assumed in the model. This upper-level flow could, for example, be representative of a slope-induced flow parallel to the terrain contours. In these cases, winds may both veer and back with time during the diurnal cycle.

In the second scenario, Mars Digital Terrain Model topography data at 1/8 deg resolution are used to conduct a simulation of thermally-induced surface flows in the region of VL1.The equations are solved on a 63 x 63 grid at a resolution of approximately 7.5 km. Results are reported from simulations with and without a prevailing flow aloft.

SIMULATIONS OF SURFACE WINDS AT THE VIKING LANDER SITES. Bridger and Haberle.

If the model proves successful in reproducing observed surface winds at the lander sites, a simple dust package will be added to examine the interactions between dust and local circulations. Dust will be picked up when wind speeds exceed a critical value. A column dust loading profile will be assumed, and will be allowed to modify the diabatic heating. The resulting changes to surface flows will then be examined.

References. (1) Mass, C.F. and D.P. Dempsey, 1985: A One-Level Mesoscale Model for Diagnosing Surface Winds in Mountainous and Coastal Regions. *Mon. Wea. Rev.*, **113**, 1211-1227. (2) Alpert, P. and B. Getenio, 1988: One-Level Diagnostic Modeling of Mesoscale Surface Winds in Complex Terrain. Part I: Comparison with Three-Dimensional Modeling in Israel. *Mon. Wea. Rev.*, **116**, 2025-2046. (3) Ye, Z.J., M. Segal and R.A. Pielke, 1990: A Comparative Study of Daytime Thermally Induced Upslope Flow on Mars and Earth. *J. Atmos. Sci.*, **47**, 612-628.

RATES OF OXIDATIVE WEATHERING ON THE SURFACE OF MARS

Roger G. Burns, Department of Earth, Atmospheric and Planetary Sciences, Massachusetts Institute of Technology, Cambridge, MA 02139.

Preface. Implicit in the mnemonic "MSATT" is that **rates** of surface processes on Mars through time should be investigated, including studies of the kinetics and mechanism of oxidative weathering reactions occurring in the martian regolith. Such measurements are described here.

Introduction. Two major elements analysed in the Viking Lander XRF experiment that are most vulnerable to atmospheric oxidation are iron and sulfur. Originally, they occurred as Fe^{2+}-bearing silicate and sulfide minerals in basaltic rocks on the surface of Mars. However, chemical weathering reactions through time have produced ferric- and sulfate-bearing assemblages now visible in the martian regolith. Such observations raise several questions: (1) when did the oxidative weathering reactions take place on Mars? (2) Is the oxidized regolith a fossilized remnant of past weathering processes and, if so, can chemical interactions of the ancient martian atmosphere with its surface be deduced from surviving phases? (3) Are the weathering reactions still occurring in the frozen regolith and, if so, are they seasonal? (4) What are the kinetics and mechanism of past and present-day oxidative weathering reactions on Mars. These questions may be addressed experimentally by studying reaction rates of dissolution and oxidation of basaltic minerals, and by identifying reaction products forming on the mineral surfaces. Reported here are results for the oxidation of pyrrhotite and dissolved ferrous iron.

Background. Since iron-rich komatiitic basalts are generally believed to be primary rocks on the surface of Mars, their constituent silicate (olivine, pyroxenes) and sulfide (pyrrhotite, pentlandite) minerals are cogent substrates for studying chemical weathering processes that produced the oxidized martian regolith. Terrestrial komatiites associated with sulfide mineralization are commonly weathered to surficial gossan deposits consisting of poorly crystalline ferric-bearing oxide, oxyhydroxide, sulfate and clay silicate phases resulting from the dissolution, mobilization and oxidation of the primary minerals. Chemical weathering reactions for sulfide-bearing basaltic assemblages derived from field relationships, petrographic analyses and experimental studies of gossans include **{1,2}**:

[1] $Fe_7S_{8(s)}$ (pyrrhotite) + $^3/_2\,O_{2(aq)}$ + $6\,H^+$ => $4\,FeS_{2(s)}$ (pyrite) + $3\,Fe^{2+}$ + $3H_2O$

[2] $FeS_{2(s)}$ + $^7/_2\,O_{2(aq)}$ + H_2O => Fe^{2+} + $2\,SO_4^{2-}$ + $2\,H^+$

[3] Fe^{2+} + $^1/_4\,O_{2((aq)}$ + H^+ => Fe^{3+} + $^1/_2\,H_2O$

[4] Fe^{3+} + $2\,H_2O$ => $FeOOH_{(s)}$ (ferrihydrite) + $3\,H^+$

[5] $(Mg,Fe)_2SiO_4$ (olivine) => Mg^{2+} + Fe^{2+} + SiO_2 => clay silicates + FeOOH

Traces of dissolved Fe^{3+} and oxygen (formed by primoidal photolysis of water vapor exhaled from erupting basaltic magma) in percolating groundwater initiated abiotic deep-weathering reactions beneath the water table. Supergene alteration of pyrrhotite to pyrite occurred, followed by dissolution of the iron sulphides, which generated strongly acidic (pH 1 to 5) and sulfate-rich (10^{-2} M) solutions. Such acidic groundwater decomposed the ferromagnesian silicates, liberating dissolved Mg^{2+}, Fe^{2+}, silica, etc. Subsequently, ferrolysis occurred when Fe^{2+} ions were oxidized to Fe^{3+} and eventually hydrolysed to ferric oxide (hematite) or oxyhydroxide (ferrihydrite, goethite) phases. This chemical weathering model forms the basis for experimental determinations of reaction rates applicable to surface-atmosphere interactions on Mars.

Measurements of Pyrrhotite Oxidation. To verify reactions [1] and [2], sterilized pyrrhotite was reacted in stoppered flasks in the temperature range 40-60 °C with various inorganic acids saturated with dissolved oxygen at initial pH values of 2, 3 and 4 for time periods ranging from 1 to 56 days. Reaction products were measured by Mössbauer spectroscopy at 4.2 K **{3}** to characterize the x-ray amorphous phases, and solutions were analysed for dissolved Fe and sulfate ions. In reactions commenced at pH 2, the pH increased to 3.2-3.5 and concentrations of dissolved Fe exceeded 8,500 μM. In the Mössbauer spectra, doublets attributed to FeS_2 (pyrite) appeared, the intensity of which increased relative to the pyrrhotite magnetic hyperfine spectrum after longer reaction time intervals. Reactions in solutions initally at pH 3 and 4 rose to above pH 5.5 and

produced much lower concentrations of dissolved Fe (<400 μM). The Mössbauer spectra now showed magnetic sextets originating from nanophase goethite and hydronium jarosite, in addition to the FeS_2 doublets. The FeS_2 and FeOOH peak intensities all increased with time relative to the pyrrhotite peaks, except in the presence of 0.6M NaCl which appeared to initially inhibit pyrite formation. In the pH 2 reactions, 50% conversion of Fe_7S_8 to FeS_2 occurred within 2 months. However, the rate of pyrite production decreased at lower temperatures and with rising pH. Extrapolation to 0 °C indicated that <5% convertion of pyrrhotite to pyrite would occur in 1 year. In solutions exceeding pH 3, the Fe(III) phases attained steady-state concentrations of about 5-10 percent of the reaction products during the first 50% of the reaction of pyrrhotite to pyrite.

Deductions from Ferrolysis Reactions. Reaction rates for the oxidation of dissolved Fe^{2+} ions, released by the oxidation of pyrite and chemical weathering of ferromagnesian silicates, are strongly pH dependent and are very slow below pH 6. The rate equation for pH ≥ 5.5 is given by

$$-d[Fe^{2+}]/dt = k_1 [Fe^{2+}] [O_{2\,(aq)}] / [H^+]^2$$

where $k_1 = 8\ (\pm 2.5) \times 10^{-15}$ liter^2 mole^{-2} atm^{-1} min^{-1} **{4,5}**. This equation indicates that there is a 100-fold decrease in the rate of oxidation for each unit decrease of pH. At ambient conditions on Earth (T = 295 K, P_{O2} = 0.2 atm), with pH = 6 and dissolved Fe^{2+} = 5.5 ppm (10^{-4} M), the rate of oxidation of Fe^{2+} would be about 0.4 wt.% Fe per year. There is a ten-fold decrease in reaction rate for each temperature-interval decrease of 15 °C **{4,5}**. Rates also decrease with increasing ionic strength, and are slower in SO_4^{2-} than Cl^--bearing solutions. Thus, in brine eutectics proposed for Mars **{6}** (which are themselves slightly acidic due to hydrolysis reactions) that have equilibrated with oxygen ($P_{O2} = 10^{-5}$ atm) in the martian atmosphere, rates of oxidation of dissolved Fe^{2+} could be 10^6 to 10^8 times slower than those in laboratory experiments performed at 20 °C.

In more acidic solutions (pH < 5), the rate of oxidation becomes independent of pH, so that

$$-d[Fe^{2+}]/dt = k_2 [Fe^{2+}] [O_{2\,(aq)}]$$

Thus, the rate of reaction [3] is extremely slow at low pH; for example, at ambient temperature (20 °C) and atmospheric pressure (P_{O2} = 0.2 atm), oxidation of Fe^{2+} reached only 5% completion after 150 days **{4,5}**. The reaction is catalysed, however, by high surface areas of product FeOOH phases formed in reaction [4] and by light, reflecting the influence of photochemical processes.

Applications to Mars.. On Mars where present-day ambient temperatures and oxygen partial pressures are much lower than those on Earth, the rate of oxidation of any dissolved Fe^{2+} ions there now should be considerably slower, particularly in frozen acidic regolith, so that dissolved Fe^{2+} ions may persist, except at the surface where exposure to ultraviolet radiation may catalyse their oxidation. On the present-day outermost surface of Mars, hydroxyl-bearing minerals such as clay silicates, goethite and jarosite are predicted to be thermodynamically unstable **{7}**, but may persist there metastably if the kinetics of dehydration reactions are sufficiently slow at low temperatures.

The question arises whether reaction rates were higher in the past on Mars. Surface features on Mars testify to the flow of water during its early history, and hence higher temperatures, which would have accelerated the rate of oxidation of Fe^{2+} ions. Moreover, a wet, warm climate on early Mars would have stabilized goethite relative to hematite. However, acid-buffering by wall-rock alteration reactions have probably been minimal on Mars due to the absence of spreading centers, subduction zones and negligible recycling of the crust by plate tectonics. Therefore, the acidity of groundwater (now permafrost) may have been maintained during the chemical evolution of the martian surface, thereby aiding the stability, solubility and transport of Fe^{2+}, silica, etc. The CO_2-dominated atmosphere on Mars may be the result of, or have contributed to, acidic groundwater (now permafrost) that may exist on Mars. Models suggesting that CO_2 partial pressures of the martian atmosphere in the past might have been higher than present-day values would result in increased acidity of the groundwater, further stabilizing dissolved Fe^{2+} ions. **{8}**

References. {1} C.F.Blain & R.L.Andrews, *Min. Sci. Engng.* 9, 119 (1977); {2} R.G.Burns, *Proc. 18th LPSC*, 713 (1988); {3} R.G.Burns & D.S.Fisher, *JGR*, 95, 14415 & 14169 (1990); {4} P.C.Singer & W.Stumm, *Science*, 167, 1121 (1970); {5} W.Stumm & J.J.Morgan, *Aquatic Chemistry* (1970); {6} G.W.Brass, *Icarus*, 42, 20 (1980); {7} J.L.Gooding, *Icarus*, 33, 483 (1978); {8} Research supported by NASA grant no. NAGW-2220.

MARTIAN CHANNEL NETWORKS : A REVISED STRAHLER APPROACH FOR QUANTITATIVE MORPHOMETRY, N.A. Cabrol(1,2) and E.A. Grin (1).

(1) Laboratoire de Physique du Système Solaire, Observatoire de Paris, 92195 Meudon Cedex, France.
(2) Laboratoire de Géographie Physique, URA DO141 CNRS, 92195 Meudon, France

To characterize the martian channel tributary networks, empirical rules of Strahler are applied in this study [1]. The proposed statistical analysis is based upon the relationship between the number of network tributaries (branches) and the network order (N).
When 2 branches *i* and *j* join, the new branch order is i+1 if i=j, and i if i>j, or j if j>i. The network oder corresponds to the terminal branch order. This method avoids climatologic and stream discharge speculations.
In terrestrial hydrology, the network order N is generally included between 3 and 4. The Strahler hierarchical network order is defined by : n_1 = total number of order 1 branches, n_2 = total number of order 2 branches and, n_n = total number of order n branches. The mean value between the branch number of ratios n_1/n_2, n_2/n_3 and, n_n/n_{n+1} is 3. Therefore, the graphical representation of this relationship is a straight line [Fig.A] and its gradient *k* characterizes a fluvial network.
From a statistical survey of thousands terrestrial rivers, Strahler deduced the probability areas in which the river lines occur [Fig.B]. The example of Fig.B displays the Strahler principle for terrestrial rivers between order 2 and 5 : 50% of the rivers are represented in area 1, 90% in area 2, and 100% in area 3. Therefore, a terrestrial fluvial network is physiographically built according to hydrologic rules if its representative line is included in one of these areas.
This technique is directly applied in this study to martian channel networks. The aim is to assess if martian fluvial-like features could be considered as hydrologic constructs and to define their respective areas of representativity.
The following statistics is based upon a survey of 2208 martian channels among those 200 well-preserved networks were selected. 70% appear to be of order 3, 11% of order 4, and the rest either 2 and 5. These characters are significantly similar to terrestrial fluvial constructs. The branch organizations of order 3 martian networks are represented in [Fig.C]. Fig.D is the deduced probability areas of apparition for these networks. Their branch organization occurences are summarized in table 1.
Basic properties can be deduced from the charts of Figs.C and D and from the table :
1 - Martian networks behave as hydrogeological constructs with recurrent organization.
2 - The abascus shows that 2 lines with respective gradients (k_1 and k_2) are necessary to characterize a martian network. The angle of junction of these 2 lines characterizes a lack of order 2 branches. This observation is valid for any order of networks. This lack has an important genetic implication. The network survey shows that a large amount of order 1 tributaries join directly the main branch without connecting other branches . This deficiency in order 2 branches could be related to a lateral sapping processes of underground water on Mars.

3 - Deduced from the previous remarks, martian networks are not true binary systems, as are usually drainage basins feeded by rainfalls.

In addition, the order of martian network is not related to its drainage area. This character is divergent from terrestrial hydrology [2]. The width of branches (included always between 1-2 km) is not in ratio with the branch order. This result is in conflict with terrestrial features but in accordance with the sapping process.

References [1] Strahler, A., 1952 : Hypsometric analysis of erosional topology. Bulletin of the Geological Society of America. [2] Cabrol, N., 1990: Physiographic characteristics of martian drainage basins. LPI Technical Report 9006, pp. 93-94.

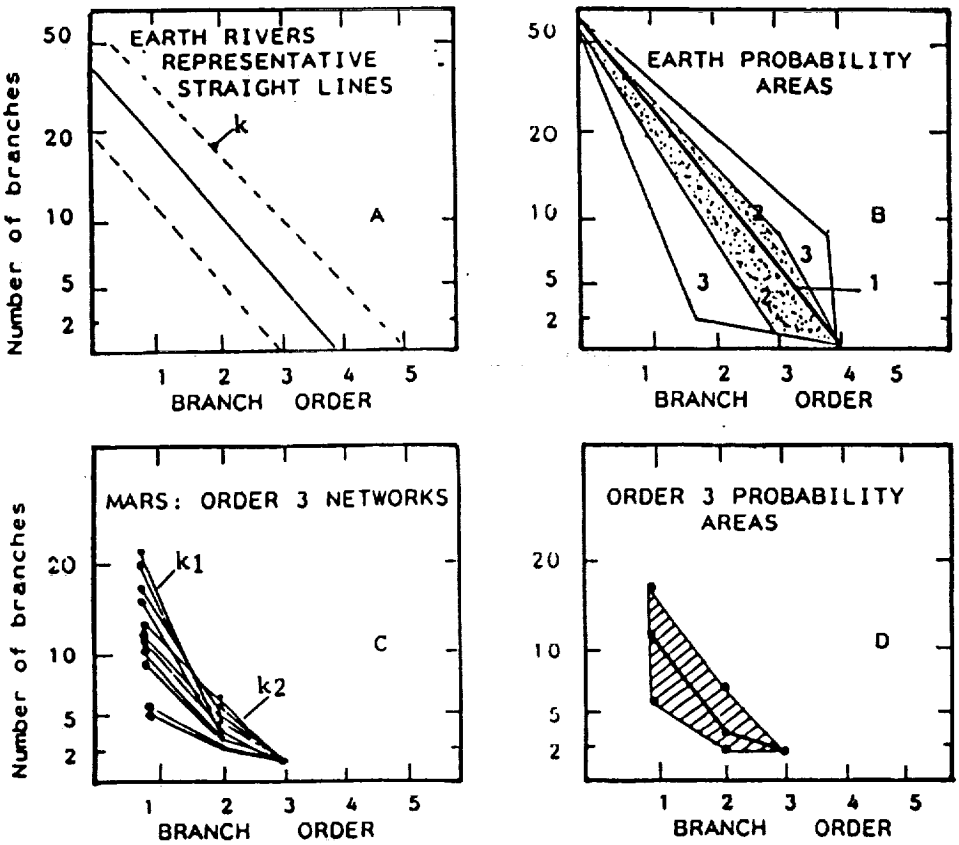

Table 1 : order 3 networks

Branch order	Number of branches	Occurences (%)
1	11	50
	18	25
	6	25
2	5	33
	3	42
	2	25
3	1	100

Drainage basins included between 2400 and 92000 km²

S13-91
85082
P.2 30

4 1396000

N92-29001

ICE IN THE NORTHERN LOWLANDS AND SOUTHERN HIGHLANDS OF MARS AND ITS ENRICHMENT BENEATH THE ELYSIUM LAVAS

Julie A. Cave, University College London, U.L.O. Planetary Image Centre, 33–35 Daws Lane, Mill Hill, London NW7 4SD.

A comprehensive study of the Elysium region (1) has revealed evidence of widespread ground-ice, whose concentration and depth has varied considerably. Ejecta mobility (2,3,4) and crater morphology analyses of a database of 7289 craters (5) have been used to investigate the distribution of ice between longitudes 245°–155° and latitudes 20°S–45° N, an area incorporating all of the Elysium Quadrangle and large portions of Amenthes, Amazonis, Mare Tyrrhenum, Aeolis, Memnonia, Cebrenia and Diacria Quadrangles. The analysis of these data has concentrated on the variation of the ejecta mobility and the distribution of various morphologies with crater diameter, latitude, altitude and geological unit (6,7). In the case of the ejecta mobility, the gradients of ejecta versus crater diameter graphs (henceforth EvsΦ) of sub-divisions of the data, and the positions of apparent gradient discontinuities were obtained (8). These are presumed to reflect the relative proportion of volatiles incorporated into the ejecta and the depth to the volatile-rich material respectively. The data subsets were then further divided into craters larger and smaller than the calculated break-point diameters so that the properties of the upper and deeper layers of Mars can be examined separately. The onset diameters of features thought to indicate the involvement of sub-surface ice, such as distal ramparts, jagged-edged ejecta, central pits or partial extra layers of ejecta are, in places, smaller than the calculated break-point diameters: the proportion of these features is, however, clearly greater in the larger than the smaller crater populations, reinforcing the interpretation that the larger craters are in general more mobile than the smaller craters owing to the excavation of ice at depth.

The simultaneous examination of ejecta mobility, crater morphology and surface features has enabled several conclusions to be drawn regarding the location of sub-surface ice in the region. The ice-distribution is shown to be highly dependent upon latitude and geological situation; in particular pronounced differences in the distribution between the Highlands and Lowlands are seen, and concentrations of ice have been detected beneath the Elysium lavas.

The Highlands–Lowlands distribution of ice:

There are several striking differences between the EvsΦ graphs of Lowland and Highland craters (see figure). Amongst the Lowland craters there is significant scatter in the data, at all diameters, and the ejecta have a wide range of mobilities. For Highland craters however, although there is some scatter present in the data for large craters, there is a far better defined relationship between the plotted parameters, reflecting a stronger control on the possible ejecta range. This difference is also evident in the relevant χ^2_ν's. This may be due to the diversity of terrain types in the Northern Lowlands, and the range of latitudes as compared with the more uniform Highland terrain sampled in this study. Both graphs exhibit a clear general rise in the ratio with increasing crater diameter, but the break-point in the gradient occurs at a significantly large crater diameter for the Highland craters (8.75±0.40 km) than it does for the Lowland ones (6.99±0.60 km). This indicates that the ice was present at greater depths in the Highlands, than it was in the Lowlands, in agreement with (3,4,9).

Few rampart craters, or other fluidized ejecta morphologies occur within small Highland craters. The unit Npld is particularly lacking in fluid crater features, down to considerable depths (1), which may be a consequence of the release of water during the formation of the pervasive valley networks of this unit. In the Lowlands, however, the distribution of ice-related features indicates that the ice is closer to the surface, and that it shows a strong latitudinal dependence, as noted previously from a study of the ejecta mobility (8). A higher proportion of Lowland craters exhibit fluidized features (1,3); the ice is nearer to the surface in the north, so proportionally more craters are affected by its presence. Conversely, the most strongly fluidized craters are in fact found in the Highlands, in very large craters (1). This suggests that, though the ice in the Lowlands is nearer the surface, the greatest concentrations of ice (and perhaps liquid water) were present *at depth* in the Southern Highlands. The reservoirs of the Highlands probably provided significant proportions of the later Lowland ground-ice, by the redistribution of water in channeling episodes, and by the gradual dessication of the surface layers, and atmospheric transport of water vapour to the north. If the linear decrease of break-point diameter (and hence depth to the ice) with increasing latitude (8) is extrapolated northwards, it predicts that all craters potentially excavated ice at latitudes of 58±10° N and that all craters in the database (i.e., > 1.8 km diameter) will have done so at 48±9° N.

This result correlates with the proliferation of highly fluidized pedestal craters at these latitudes (which occur at very small diameters), and theoretical predictions of ice stability (10). The highly modified surfaces in these northern regions are also suggestive of quantities of ice very near to the surface, probably incorporated in extensive sedimentary deposits.

Ice in the Elysium volcanic region

A pronounced concentration of ice beneath the Elysium lavas is indicated by the high proportion of large craters with central pits, double ejecta, partial extra ejecta lobes, jagged edges and high average ejecta mobility on this unit (Ael_1) as compared with all other geological units (1). These features generally occur only in large craters (of over 9.4 km in diameter) and the upper layers of the unit appear relatively dry; in particular, radial ejecta craters and a low average ejecta mobility are found for Elysium Mons and areas immediately surrounding the construct (11). A smaller concentration of ice is indicated to the east, largely corresponding with the ridged plains (unit Hr), but the pronounced clustering of fluidized features and the high mobility ejecta associated with materials at depth below the Elysium lavas indicates that substantial amounts of ice were present here. Further evidence of an ice-rich layer capped by the lavas is provided by the chaotic breakup of the surface to the west and north of Elysium Mons, and the concentration of outflow channels to the northwest. In addition, the deposits associated with these channels have been shown to be rich in ice (11), and to have morphologies consistent with their emplacement as lahars (12). The results of the crater study imply that not only was the presence of an enhanced volcanic heat flux responsible for the generation of channels and chaotic terrain in the area, but more importantly, that the volcano itself appears *responsible* for the localised enrichment of sub-surface ice. It is therefore suggested that a substantial proportion of the enhanced ice deposit under the lavas originated from the emplacement of juvenile water from the underlying magma body. The emplacement mechanism is unknown: early water-rich deposits may have been covered by later effusive activity, or, perhaps more credibly, water rising from the magma was trapped by the relatively impermeable surface lavas. Several authors have noted the apparent association of volcanic and channel features on Mars (e.g., 13) and a juvenile water origin has been proposed to explain the distribution of the various martian channels (14). Within the region studied here, with the exception of Hebrus Valles, the channels with Lowland sources are closely associated with Elysium Mons. This work has provided further evidence that this association is not coincidental, and strongly suggests that, in the case of *this* volcanic province, juvenile water has contributed to the formation of a substantial sub-surface ice reservoir. References: (1) Cave J.A., Ph.D. Thesis, 1991. (2) Mouginis-Mark

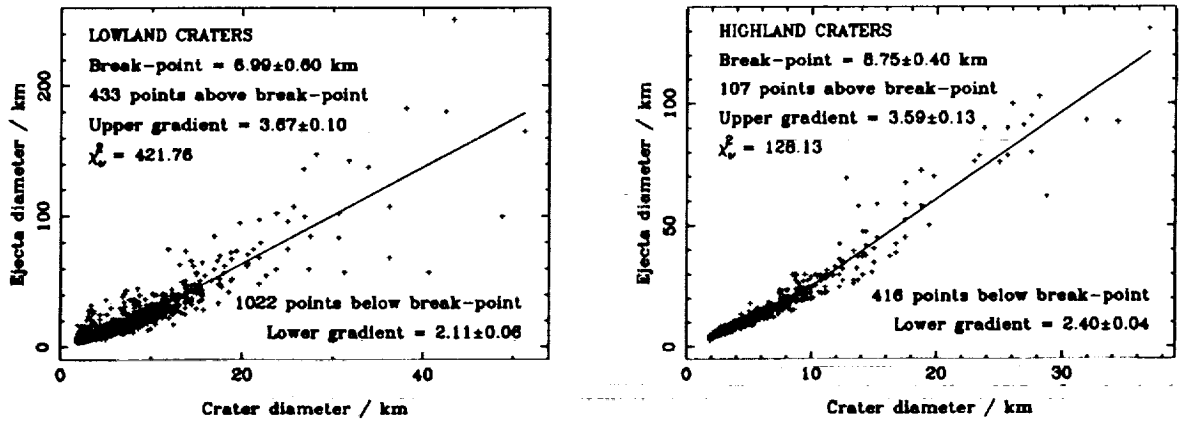

P.J., J.G.R. **84** 8011–8022, 1979.

(3) Costard F.M., Earth, Moon, and Planets, **45** 265–290, 1989. (4) Kuzmin R.O., Bobina N.N., Zabalueva E.V., and Shashkina V.P., L.P.S.C. **XIX** 655–657, 1988. (5) Cave J.A., L.P.S.C. **XXI** 179, 1990. (6) Scott D.H. and Tanaka K.L., Map I-1802-A, U.S.G.S., 1986. (7) Greeley R. and Guest J.E., Map I-1802-B, U.S.G.S., 1987. (8) Cave J.A., L.P.S.C. **XXII** 187–188, 1991. (9) Rossbacher L.A., and Judson, S., Icarus **45** 25–38, 1981. (10) Fanale F.P., Icarus **28** 179–202, 1976. (11) Cave J.A., L.P.S.C. **XXII** 189–190, 1991. (12) Christiansen E.H., Geology **17** 203–206, 1989. (13) Greeley R., Science **236**, 1653–1654, 1987. (14) Robinson C., Ph.D. Thesis, 1991.

MARSNET SURFACE AND ATMOSPHERE INVESTIGATIONS

A.F. Chicarro, Space Science Department, ESA/ESTEC, 2200 AG Noordwijk, The Netherlands.

Following an ESA preliminary study on the possible areas of European participation in the future international exploration of Mars (1), and a recent ESA in-depth scientific and technical assessment study (2), MARSNET was selected for further Phase-A studies as a potential European contribution to such exploration. The MARSNET mission consist of a network of small stations to be landed on the surface of Mars. All surface stations will have identical design and payload, and will be located several thousand km apart from each other. The required operational lifetime on the surface of Mars for all landers is one Martian year (687 days) to carry out long-term meteorological and seismological measurements. The availability of a data relay orbiter at low altitude is assumed. The instruments are mounted on a platform under the semi-hard lander solar array, as shown in **Figure 1**. The main scientific goals of the mission during the atmospheric descent and on the surface are outlined below.

Internal structure and activity: The seismological experiment, consisting of three-axes type seismometers on-board each of the stations, will look for evidence of seismic activity of Mars and determine its origin, give the position of the seismic sources, and determine the internal structure of Mars. Seismic data are also needed to understand the surface hemispheric asymmetry of Mars.
Magnetic field: A fluxgate magnetometer will carry out measurements in order to firmly establish if the planet has an intrinsic magnetic dipole today, study the fluctuations of the magnetic field at the surface of Mars, and determine the natural waves induced by the interaction of the solar wind with the planetary environment.
Site geology: A panoramic surface television camera and a descent imager will provide information on regional and local geology of the landing sites, including grain size distribution of sediments and texture of rocks and weathering products, nature and composition of minerals and rocks, presence or absence of biological structures, structural and stratigraphic features giving clues to the geological evolution of the landing site area.
Geochemistry and mineralogy: The history of surface materials through volcanic, metamorphic, sedimentary, impact and weathering processes can only be inferred from a detailed study of its minerals and texture, its major and trace element chemistry and isotopic composition. A combination of an α-backscatter and an XRF-spectrometer will allow to determine all major as well as the most important minor elements like P, S, Cl, K, Cr, Mn, Ni. A neutron detector will yield data on the concentration of hydrogen (in form of bound water or ice). A γ-ray spectrometer will determine the elements H, O, Mg, Al, Si, S, Cl, Ca, and Fe, in addition to K, Th and U.
Magnetic properties of minerals: A Mössbauer spectrometer will provide information on the magnetic properties, and possible paleomagnetic signatures, of the Martian surface rocks (igneous and sedimentary), and will identify the strongly magnetic phase existing in the Martian soil.
Meteorology: The key objectives for local and global meteorological investigations are the determination of diurnal, semi-diurnal and seasonal P, T and wind cycles in the planetary boundary layer for the various sites, as well as their dependence on altitude, latitude, and local topography; global and local dust storms; role of water and CO_2 cycles; planetary waves and fronts, cyclones, thermal tides; atmospheric global circulation. The meteorological package will include dedicated sensors for pressure, temperature, relative humidity, and wind velocity. The panoramic camera will be used for measuring the optical thickness, cloudiness, fog and frost.
Atmospheric structure: The atmospheric structure study during the aerodynamical entry and the parachute descent of the network surface stations will focus on temperature, pressure and atmospheric density vertical profiles, including accelerometry measurements.
Surface properties and surface-atmosphere interactions: A thermal array probe will determine the variations with time of surface temperatures and the thermal properties of the Martian soil down to a depth of 2 m. A permittivity meter will determine the subsurface moisture content. It will provide essential information on the soil structure, including small-scale discontinuities such as fractures, cavities, boulders and sedimentary changes.
Exobiology: More data on Martian geology and climate, both past and present, are required to assess the likelihood of life having appeared and evolved on Mars. In particular, the occurrence of water, distribution and cycle of biogenic elements and their compounds, variations in atmospheric pressure, temperature and solar irradiance will be studied. A solar-UV radiation dosimeter will perform in-situ measurements of the intensity of the solar spectrum, and its seasonal and latitudinal variations at different sites.

MARSNET will provide a global scientific perspective of Mars, and will be one of the robotic precursor missions to future *Sample Return* and *Manned Exploration* missions. NASA is also actively studying a network mission to Mars called MESUR. An existing understanding of future cooperation between the two agencies could develop into a joint ESA/NASA global *Mars Network* mission, where ESA could provide three surface stations (MARSNET) and NASA a number of additional ones (MESUR), complementing each other in terms of locations and investigations.

References: (1) Chicarro A.F., Scoon G.E.N. and Coradini M., *Mission to Mars: Report of the Mars Exploration Study Team*, ESA SP-1117, ESA, 140 pp, 1989. (2) Chicarro A.F., Coradini M. et al., *MARSNET: Report on the Assessment Phase Study*, ESA SCI(91)6, ESA, 111 pp., 1991.

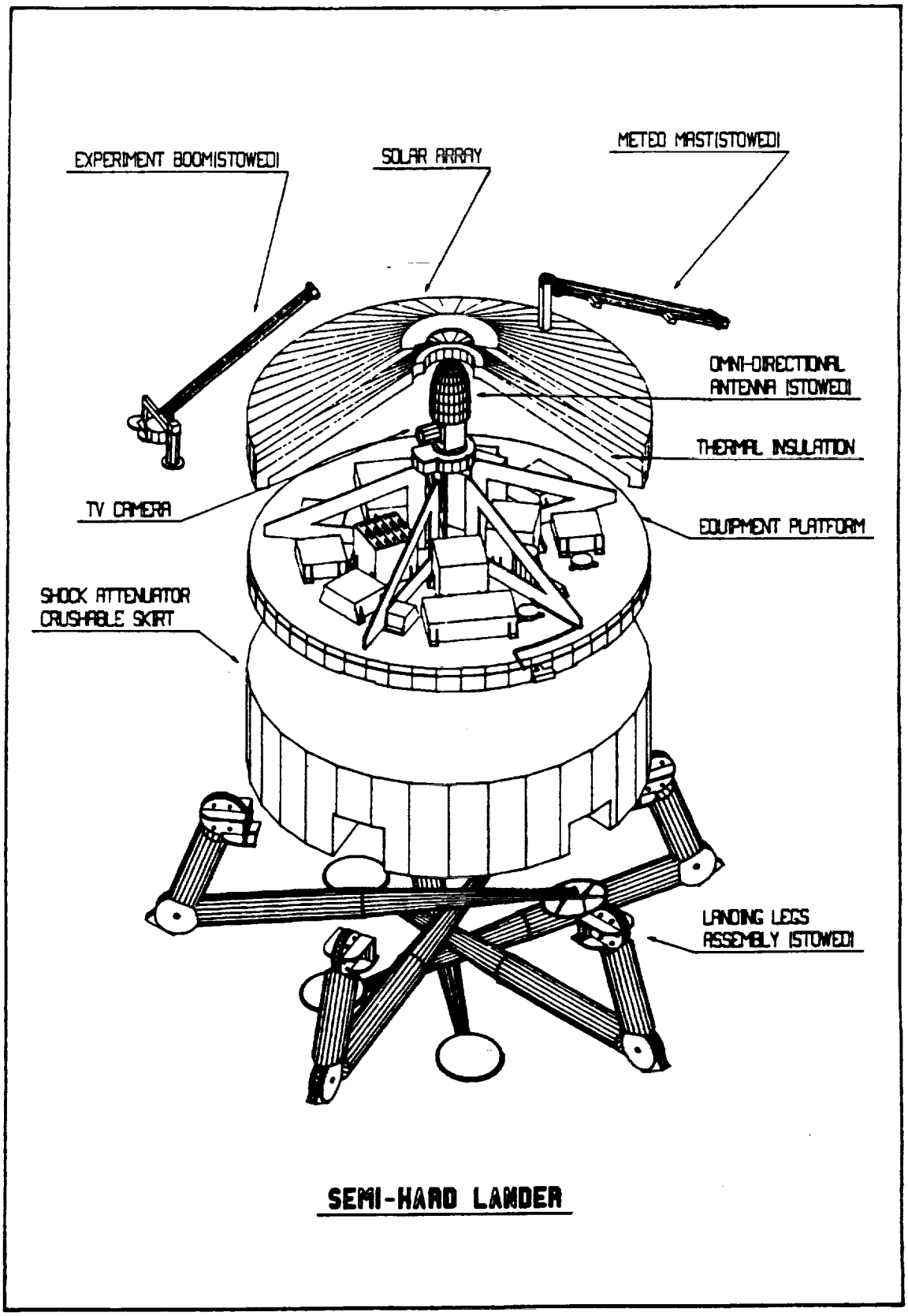

Figure 1: *MARSNET semi-hard lander exploded view.*

34

MARS DUST AND CLOUD OPACITIES AND SCATTERING PROPERTIES: R.T. Clancy and S.W. Lee, Laboratory for Atmospheric and Space Physics, U. of Colorado

We have recently completed an analysis of the visible emission-phase-function (EPF) sequences obtained with the solar-band channel of the IRTM instrument on-board the two Viking orbiters (1). Roughly 100 of these EPF sequences were gathered during the 1977-1980 period, in which the total broad-band (.3-3.0 microns) reflectances of the atmosphere/surface above specific locations on Mars were measured versus emission angle as the spacecraft passed overhead. A multiple scattering radiative transfer program (2) was employed to model the EPF observations in terms of the optical depths of dust/clouds, their single scattering albedos and phase functions, and the Lambert albedos and phase coefficient of the underlying surfaces. Due to the predominance of atmospheric scattering at large atmospheric pathlengths and/or large dust opacities, we were able to obtain strong constraints on the scattering properties of dust/clouds and their opacities for a wide range of latitudes, longitudes, and seasons on Mars.

The temporal dependence of derived dust opacities is similar to that inferred from the Viking lander observations (3), in that maximum opacities of 2-3 were observed at various locations to accompany the two global dust storms of 1977. The opacities of clouds observed at north polar latitudes in spring (L_S=36-43°), and fall mid-latitudes in the northern and southern hemispheres were typically 0.5. The dust single scattering phase function (for scattering angles of 50-170°) is found to agree with that derived from Viking lander sky brightness observations (3), although the single scattering asymmetry factor is much smaller (0.56) than was originally reported (0.79) by Pollack et al. (3). We also obtain a dust single scattering albedo (0.92) which is significantly higher than that derived from the Viking lander analysis (0.86).

We present arguments, independent of the EPF analysis, to the effect that dust particle sizes may be 5-10 smaller than the 2.0 micron cross-section weighted average radius suggested by Pollack et al. (3) and Toon et al. (4). The observed ratio of visible to infrared dust opacities is much more consistent with smaller particle sizes, and current observations do not measure the 10° forward diffraction lobe of dust adequately to define the dust particle sizes on the basis of visible scattering observations. The uncertain particle sizes of dust, and the discrepancy in dust single scattering albedos and asymmetry parameters we outline above have very important implications for the radiative effects of dust heating/cooling for the atmosphere of Mars.

(1) Clancy R.T. and Lee S.W. (1991), *Icarus*, in press; (2) Stamnes K., Tsay S.-C., Wiscombe W. and K. Jayaweera (1988), *Appl. Op.*, **27**, 2502-2509.; (3) Pollack J., Colburn D., Flasar F.M., Kahn R., Carlston C. and Pidek D. (1979), *J. Geophys. Res.*, **84**, 2929-2945. (4) Toon O.B., Pollack J.B. and Sagan C. (1977), *Icarus*, **30**, 663-696.

VLA MAPPING OF 1.35 CM WATER EMISSION FROM THE MARS ATMOSPHERIC LIMB; R.T. Clancy, LASP, U. of Colorado; A.W. Grossman, Dept. Astronomy, U. of Maryland; and D.O. Muhleman, Div. Geol. and Planetary Sci., Caltech.

We report preliminary results of 1.35 cm spectral line observations, in which we employed the NRAO Very Large Array (VLA) interferometer to map the horizontal and vertical distributions of water vapor around the Mars atmospheric limb in early December of 1990. The increased atmospheric pathlengths presented near the limb of Mars and the high angular resolution afforded by the VLA at centimeter wavelengths lead to a remarkably sensitive, remote measurement of water in the atmosphere of Mars. We achieved ~300 km horizontal resolution (~1" angular resolution) on Mars, operating in the C configuration of the VLA, when Mars was 17.3" in diameter. This allows us to resolve the latitudinal and diurnal variations (morning vs. evening limb) in atmospheric water emission around the limb of Mars. We derive the vertical distribution of atmospheric water from observed pressure-broadening in the spectrally resolved lineshapes (1). These observations, which consist of two eight-hour integrations obtained on Dec 3-4 and Dec 6-7, correspond to late winter in the northern hemisphere of Mars (L_S=344°).

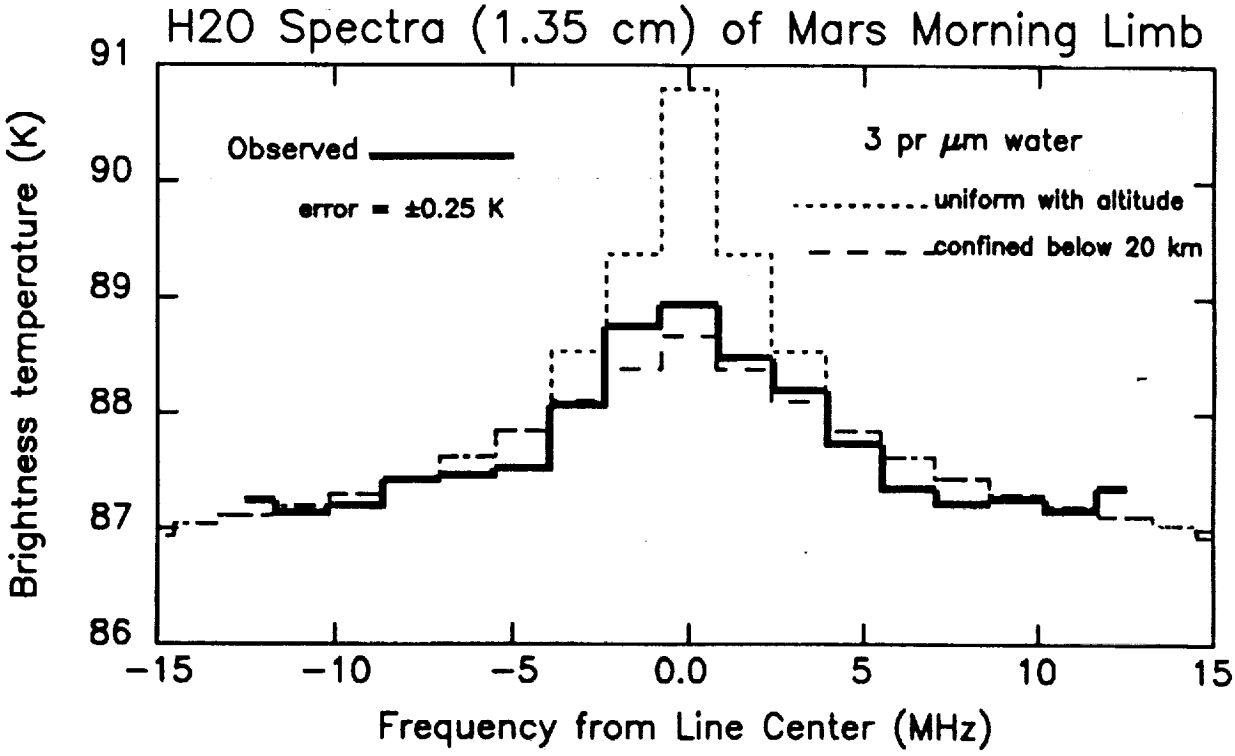

Figure 1. VLA spectrum of 1.35 cm water line emission averaged over the morning limb of Mars on Dec 3-4, 1990 (L_S=344°). Synthetic spectra correspond to 3 pr microns of water vertically well mixed (dotted) or frozen out above 20 km altitude (dashed).

MARS ATMOSPHERIC WATER: Clancy, R.T., A.W. Grossman, D.O. Muhleman.

In figure 1, we indicate the Dec 3-4 spectrum averaged over the morning limb of Mars. Two synthetic spectra indicate the expected line emission for 3 precipitable microns of water with a uniform vertical distribution (dotted) and a vertical distribution in which water decreases rapidly above 20 km altitude (dashed). Two initial conclusions are that the global atmospheric water abundance for Mars was very small at the time of our observations; and that the water mixing ratio decreased rapidly above 20 km altitude, possibly due to saturation. The saturation vapor pressure of water occurs at 20 km altitude if Mars atmospheric temperatures are ~20 K cooler than implied by the Viking IRTM and lander descent observations. Such cooler atmospheric temperatures have been argued on the basis of ground-based microwave observations of Mars atmospheric CO (1). Our 3 pr micron column abundance for water can be compared to the global value of ~6 pr microns, observed for the same season with the Viking MAWD experiment in 1977 (2).

We will investigate the latitudinal and diurnal variations when the data corresponding to the second day of observations are reduced. We also plan to compare these VLA water observations with a very complementary set of Hubble Space Telescope ozone observations. R.T. Clancy obtained ultraviolet (220-330 nm) spectra and images of Mars on Dec 13, 1990 as part of a general Mars observing program with the Hubble Space Telescope, led by Phil James at the U. of Toledo.

(1) Clancy, R.T., D.O. Muhleman, and G.L. Berge (1990) *J. Geophys. Res.*, **95**, p. 14543-14554. (2) Jakosky, B.M. and C.B. Farmer (1982) *J. Geophys. Res.*, **87**, p.2999-3019.

THE SUBSURFACE HYDROLOGIC RESPONSE OF MARS TO THE THERMAL EVOLUTION OF ITS EARLY CRUST. S. M. Clifford* and M. H. Carr**, *Lunar and Planetary Institute, 3303 NASA Rd. 1, Houston, TX 77058, **U.S. Geological Survey, 345 Middlefield Rd., Menlo Park, CA 94025.

The martian valley networks and outflow channels provide persuasive evidence that large bodies of groundwater were present on Mars throughout much of its early geologic history [*Baker*, 1982; *Carr*, 1986]. However, little attention has been focussed on how these volatile reservoirs may have responded to the thermal evolution of the early martian crust. In this regard, one process that has likely been of critical importance to the subsurface hydrologic evolution of Mars is thermal vapor diffusion.

When a temperature gradient is present in a moist porous medium it gives rise to a corresponding vapor pressure gradient. As a result of this pressure difference, water vapor will diffuse from the higher temperature (higher vapor pressure) region to the lower temperature (lower vapor pressure) region, transferring both moisture and latent heat through the soil. By this process, the martian geothermal gradient may have driven the vertical transport of a considerable volume of H_2O vapor from the comparatively warm reservoirs of groundwater present at depth to the colder near-surface regolith.

It has been known for over 75 years that vapor transport in excess of that predicted by Fick's law will occur in a moist porous medium under the influence of a temperature gradient [*Bouyoucos*, 1915]. More recently, *Philip and deVries* [1957] and *Cary* [1963] have proposed two different but widely used models for calculating the magnitude of this type of thermally driven vapor transfer. Despite the differences in approach, it has been shown that the final form of the flux equations for both models are identical [*Taylor and Cary*, 1964; *Jury and Letey*, 1979]. After *Cary* [1966], the thermally driven vapor flux is given by

$$J_{H_2O} = - \frac{\beta D_{eff} P_{H_2O} L_v}{R_v^2 T^3} \frac{dT}{dz} \qquad (1)$$

where D_{eff} is the effective diffusion coefficient of H_2O in CO_2, P_{H_2O} is the saturated vapor pressure of H_2O at a temperature T, L_v is latent heat of vaporization, R_v is the gas constant for water vapor, and β is a dimensionless factor whose value (typically around 1.83, *Jury and Letey*, 1979) depends on regolith temperature, porosity, and water content.

For a geothermal gradient of 15 K km^{-1}, and a regolith pore size of 1-10 μm, equation (1) predicts that the flux of water vapor to the freezing front at the base of the martian cryosphere will be ~ 8.3×10^{-5} - 2.8×10^{-4} m H_2O yr^{-1} (where the cryosphere is defined as that region of the crust where the temperature remains continuously below the freezing point of water [*Fanale*, 1976; *Rossbacher and Judson*, 1981]). This flux is equivalent to the vertical transport of 1 km of water every 10^6 - 10^7 years, or roughly 10^2 - 10^3 km of water over the course of martian geologic history. Indeed, there is reason to believe that this flux rate was even greater in the past. Models of the thermal history of Mars suggest that 4 billion years ago the planet's internal heat flow was ~ 3 - 5 times larger than it is today [e.g., *Davies and Arvidson*, 1981, *Schubert and Spohn*, 1990]. Since the vapor flux rate predicted by equation (1) is directly proportional to the temperature gradient, this implies a similar increase in the volume of water cycled through the early crust.

Inspection of equation (1) and reveals that the flux of H_2O leaving the groundwater table will exceed that which finally reaches the freezing front at the base of the cryosphere. This difference is due to the sensitive dependence of P_{H_2O} on temperature. As shown by *Jackson et al.* [1965], once a closed system has been established (*i.e.*, the pore volume of the cryosphere has been saturated with ice), a dynamic balance of opposing fluxes is achieved. As water vapor rises from the warmer depths to the colder regolith above, it will condense, creating a circulation system of rising vapor and descending liquid condensate.

The process of thermal vapor diffusion, and the development of a low-temperature hydrothermal circulation system within the crust, likely had a profound effect on the growth of the martian cryosphere and the geomorphic evolution of the planet's surface. For example, if the dissection of the martian cratered highlands by integrated networks of small valleys is truly the result of rainfall or snow melt from a warmer, wetter early climate, then Mars must have once possessed near-surface groundwater flow systems similar to those now found on Earth --

where, as a consequence of atmospheric recharge, the water table conformed to the shape of the local terrain. However, with both the transition to a colder climate and the decline in Mars' internal heat flow, a freezing front eventually developed in the regolith that propagated downward with time -- creating a thermodynamic sink for any H_2O within crust. Initially, water may have entered this developing region of frozen ground from both the atmosphere and underlying groundwater. However, as ice condensed within the near-surface pores, the deeper regolith was ultimately sealed off from any further atmospheric supply. From that point on, the only source of water for the thickening cryosphere must have been the thermally-driven upward flux of vapor from the underlying reservoirs of groundwater.

With the elimination of atmospheric recharge, the elevated water tables that once followed the local topography eventually decayed. The continuity of pore space provided by sediments, breccia, and interbasin faults and fractures should have then allowed the water table to hydrostatically readjust until it ultimately conformed to a surface of constant geopotential. This conclusion is supported by investigations of areally-extensive groundwater systems on Earth that experience little or no precipitation (*e.g.*, *Mifflin and Hess*, 1979; *Cathles*, 1990).

Once the pore volume of the martian cryosphere was saturated with ice, the thermally-driven vapor flux from the groundwater below could have led to the formation and maintenance of near-surface perched aquifers, fed by the downward percolation of condensed vapor from the higher and cooler regions of the crust. Eventually the hydrostatic pressure exerted by the accumulated water may have been sufficient to disrupt the overlying ground ice, allowing the stored volume to discharge onto the surface. Such a scenario may have been repeated hundreds of times during the first half-billion years of martian geologic history, possibly explaining how some valley networks may have evolved in the absence of atmospheric precipitation [*Pieri*, 1980; *Carr*, 1983]. However, as the internal heat flow of the planet continued to decline, the thickness of the cryosphere may have grown to the point where it could no longer be disrupted by the limited hydrostatic pressure that could develop in a perched aquifer, thus drawing an end to the period of valley network formation.

The convective cycling of 10^2 - 10^3 kilometers of water between the water table and the base of the martian cryosphere should have also had a considerable effect on the geochemical evolution of the crust. Groundwater that resides within crustal rocks for hundreds of millions of years generally evolves into a highly mineralized brine consisting of a saturated mixture of chlorides, carbonates, sulfates, silica, and a variety of other dissolved species [*White*, 1957]. On Mars, the geochemistry of the groundwater is likely to have also been strongly influenced by the influx of minerals leached from crustal rocks by hydrothermal circulation. This process will deplete the crust between the water table and base of the cryosphere of any easily dissolved substances, concentrating many of them in the underlying groundwater to levels far in excess of their respective saturation points. The resulting precipitation of these minerals beneath the water table should have lead to the development of a distinct geochemical horizon within the crust (similar to that proposed by *Soderblom and Wenner* [1978]). Where exposed by subsequent faulting or erosion, this horizon should appear as a relatively competent layer whose upper boundary conforms to a surface of constant geopotential. Although not diagnostically unique, such an observation is consistent with mineral deposition in an unconfined aquifer in hydrostatic equilibrium.

The calculations presented here suggest that a geothermal gradient as small as 15 K km^{-1} could drive the vertical transport of 1 km of water vapor to the freezing front at the base of the cryosphere every 10^6 - 10^7 years. The magnitude of this flux suggests that the process of geothermally-induced vapor diffusion may have played a critical role in the initial emplacement of martian ground ice and the subsequent geomorphic and geochemical evolution of the planet's crust.

References: Baker, V. R., The Channels of Mars, Univ. of Texas Press, Austin, 198 pp., 1982; Bouyoucos, G. J., J. Agr. Res., 5, 141-172, 1915; Carr, M. H., Icarus, 68, 187-216, 1986; Carr, M. H., Icarus, 56, 476-495, 1983; Cary, J. W., Soil Sci. Soc. Amer. Proc., 30, 428-433, 1966; Cary, J. W., J. Phys. Chem., 67, 126-129, 1963; Cathles, L.M., Science, 248, 323-329, 1990; Davies, G. F. and R. E. Arvidson, Icarus, 45, 216-230, 1981; Fanale, F. P., Icarus, 28, 179-202, 1976; Jackson, R. D., D. A. Rose, and H. L. Penman, Nature, 205, 314-316, 1965; Jury, W. A. and J. Letey, Jr., Soil Sci. Soc. Amer. J., 43, 823-827, 1979; Milfflin, M.D. and J.W. Hess, J. Hydrology, 43, 217-237, 1979; Philip, J. R. and D. A. de Vries, Trans. Amer. Geophys. Union, 38, 222-228, 1957; Pieri, D., Science, 210, 895-897, 1980; Rossbacher, L. A. and S. Judson, Icarus, 45, 39-59, 1981; Schubert, G. and T. Spohn, J. Geophys. Res., 95, 14095-14104, 1990; Soderblom, L. A., and D. B. Wenner, Icarus, 34, 622-637, 1978; Taylor, S. T. and J. W. Cary, Soil Sci. Soc. Proc., 167-172, 1964; White, D. E., Bull. Geol. Soc. Amer., 68, 1659-1682, 1957.

ANALYSIS OF MARTIAN ATMOSPHERIC AND SURFACE OPTICAL PROPERTIES BETWEEN 4.4 AND 5.1 μm: Dave Crisp and Diana L. Blaney, MS 169-237, Jet Propulsion Laboratory, 4800 Oak Grove Drive, Pasadena, CA, 91109.

Spectra of Mars taken at wavelengths between 4.4 and 5.1 μm provide constraints on the temperatures and optical properties of the surface and the atmosphere because they include similar contributions from reflected sunlight and thermal emission. The combined effects of reflection and thermal emission act to reduce surface spectral contrasts, but these spectra are still important for studies of the Martian surface composition because this spectral range includes distinctive absorption features of candidate surface materials including several sulfates and CO_2 frost. This spectral region also includes absorption, emission, and scattering by CO_2 (4.3 and 4.8 μm), CO (4.6 μm), water vapor (> 4.8 μm), and airborne dust. These atmospheric contributions provide information about the atmospheric thermal structure and dust loading, but they are also a source of contamination that must be accurately accounted for in the analysis of surface features. Because of the complexity of these radiative processes, relatively sophisticated radiative transfer models are needed for the analysis of spectra at these wavelengths.

Spectra of several regions of Mars were taken by Blaney and McCord [1] in August of 1988 (L_s = 255) (Fig. 1) with the Cooled Grating Array Spectrometer (CGAS) [2] at the NASA IRTF. The spectral resolution ($\lambda/\Delta\lambda$) was about 300. No absolute radiometric calibration was performed, but telluric absorption was removed and an adequate relative wavelength-dependent calibration was achieved dividing each Mars spectra by that of a star of spectral type G8III (BS437). The resulting spectra show several distinct absorption features at wavelengths between 4.4 and 5.1 μm. Many of these features can be attributed to gases in the Martian atmosphere, but others are more difficult to identify.

To analyze these spectra more completely, we used a line-by-line multiple scattering model that was developed for studies of Venus night-side emission [3,4]. This model includes all atmospheric and surface radiative processes that are known to be important on Mars, including absorption, emission, and multiple scattering by CO_2, H_2O, CO, and airborne dust, and a spectrally-dependent surface albedo. The model atmosphere had 30 vertical levels between the surface (3.3 mbar for Tharsis and Solis Planum) and 60 km. The water vapor and CO mixing ratios were assumed to be constant, and were set to 24 ppmv (10 precipitable μm) and 700 ppmv, respectively. Surface and atmospheric temperatures and atmospheric dust loadings were estimated from Mariner 9 IRIS retrievals [5] and Viking IRTM observations [6,7]. A Mie-scattering algorithm [8] was used to derive dust optical properties from the optical constants of palagonite (Roush, personal communication) and basalt [9]. A log-normal size distribution with a modal radius of 0.5 μm and a variance of 0.15 μm was used for both constituents. The vertically-integrated dust optical depth was varied from 0.25 to 2.5. Surface albedos between 0.1 to 0.3 were used.

Results from our preliminary efforts to simulate the spectra taken near Tharsis and Solis Planum are shown in Fig. 1. The simulated Tharsis spectrum is shown at much higher resolution in Fig. 2 to illustrate the positions of the gas absorption features. A best fit to the Tharsis spectrum was achieved with an integrated dust optical depth of 0.25, a surface temperature of 270 K, and a surface albedo near 0.3. A much larger dust optical depth (2.25) was needed to fit the long-wavelength side of the Solis spectrum. These derived atmospheric and surface properties are not unique, but they provide an adequate fit to the overall shapes of the spectra as well as the depths of the CO_2 features at 4.3 and 4.8 μm, and the CO band near 4.6 μm. Further analysis of these spectra, and other spectra taken between 3.2 and 4.2 μm [1] are needed to evaluate other possible solutions and to place more stringent constraints on these surface and atmospheric properties.

The weak absorption features near 4.5 and 4.95 μm are not produced by atmospheric gases or other constituents that were included in this model. Both CO_2 frost and sulfate minerals have absorption bands at these wavelengths, but there are arguments against both of these candidate materials. For example, it is difficult to justify the presence of CO_2 frost even at high altitudes in spectra taken near the sub-solar point because the temperatures are usually much higher than the CO_2 frost point. Sulfate minerals in the airborne dust or on the surface would have absorption bands near 4.5 ($2\ \nu_3$) and 4.9 μm ($2\nu_1$), but most terrestrial sulfates have band structures that are much more complex than that seen here [10]. These and other materials are currently being studied further to explain these weak spectral features.

References:
1. D. L. Blaney and T. B. McCord, (1990) LPSC XXI, Lunar and Planetary Institute, Houston, Texas, 99-100. 2. A. Tokunaga et al. (1987) Infrared Astronomy with Arrays, Wynn-Willian and Becklin eds., 367-378. 3. J. F. Bell III et al. (1991) *Science* **252**, 1293-1296. 4. D. Crisp et al. (1991) *Science* (in press, 1991). 5. M. L. Santee and D. Crisp (1990) *Bull. Am. Astron. Soc.* **22**, 1078. 6. T. Z. Martin et al. (1979) *J. Geophys. Res.*, **84**, 2830-2842. 7. T. Z. Martin (1986) *Icarus*, **66**, 2-21. 8. W. Wiscombe (1977) *Appl. Opt.* **19**, 1505-1509. 9. J. B. Pollack et al. (1973) *Icarus*, **19**, 372-389. 10. V. Farmer (ed.) (1974) Mineralogical Society of London, Monograph 4, London England, 427-430.

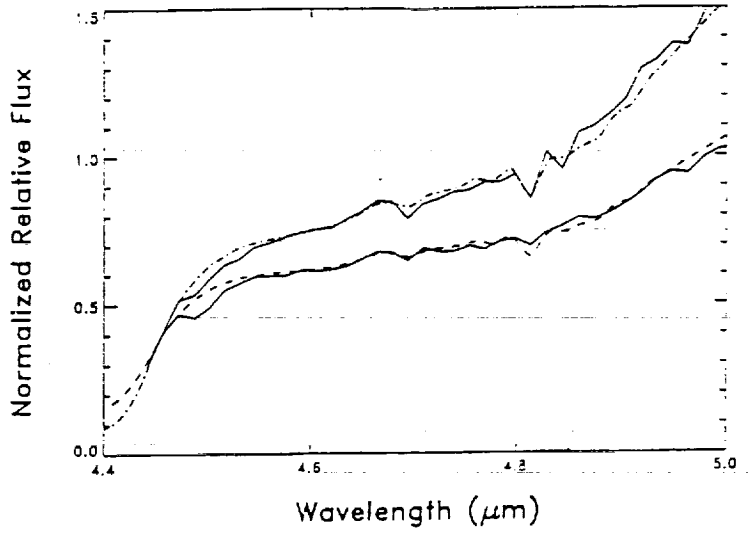

Figure 1. Simulations of Tharsis (top) and Solis Planum (bottom) spectra. Telescopic observations are shown as solid lines while model output is given by dashed lines. Description of model parameters is given in the text.

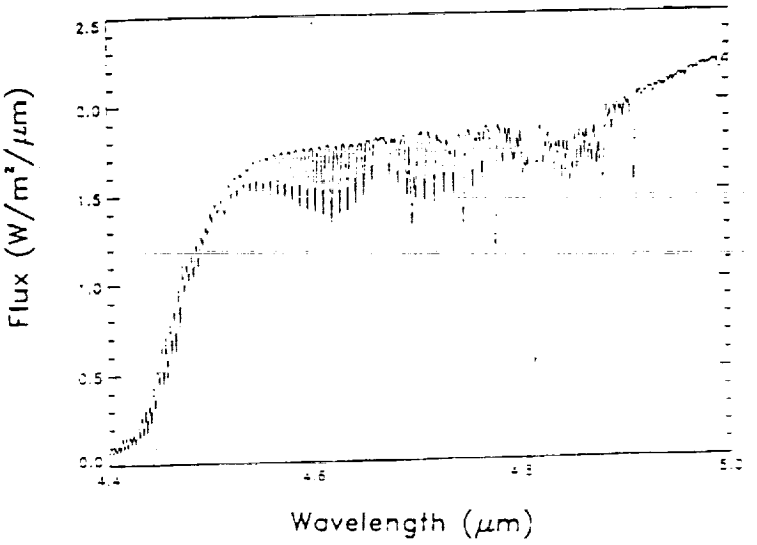

Figure 2. Reflected and emitted fluxes for the Tharsis simulation are shown at high resolution (1 cm^{-1}) to illustrate the positions of gas absorption bands.

MICRO WEATHER STATIONS FOR IN SITU MEASUREMENTS IN THE MARTIAN PLANETARY BOUNDARY LAYER: D. Crisp (MS 169-237, Jet Propulsion Laboratory, California Institute of Technology, 4800 Oak Grove Drive, Pasadena, CA, 91109), W. J. Kaiser (JPL), T. W. Kenny (JPL), T. R. VanZandt (JPL), and J. E. Tillman (Univ. of Washington, Seattle)

Viking Lander meteorological measurements show that the Martian planetary boundary layer (PBL) has large diurnal and seasonal variations in pressure (7 - 10 mbar), temperature (180 - 280 K), wind velocity (0 - > 30 m/s), relative humidity (1 - 100%), and airborne dust loading (0.3 - > 6 optical depths). An even larger range of conditions has been inferred from remote sensing observations acquired by the Mariner 9 and Viking orbiters. Numerical models indicate the these changes may be accompanied by dramatic vertical and horizontal wind shears (100 m/s/km) and rapid changes in the static stability [1]. In-situ measurements from a relatively small number surface stations could yield global constraints on the martian climate and atmospheric general circulation by providing "ground-truth" for remote sensing instruments on orbiters. A more complete understanding of the meteorology of the PBL is an essential precursor to manned missions to Mars because this will be their working environment. In-situ measurements are needed for these studies because the spatial and temporal scales that characterize the important meteorological processes near the surface cannot be resolved from orbit.

The Mars Environmental Survey (MESUR) Program will provide the first opportunity to deploy a network of surface weather stations for a comprehensive investigation of the martian PBL. The meteorological properties that should be measured by these stations include pressure, temperature, wind velocity, humidity, and airborne dust and ice optical depths. These properties should be sampled almost simultaneously, with sampling rates much greater than 1 Hz to resolve the turbulent processes that contribute to the fluxes of heat, mass, and momentum through this atmospheric layer. To maximize the scientific return from this mission, a relatively large number (> 20) of surface stations should be deployed in a global network. Recent advances in sensor design and integrated circuit technology should be utilized to develop compact, low-mass, low-power sensors that have greater longevity, reliability, and accuracy over a wider dynamic range than those deployed on the Viking landers.

We are assessing the feasibility and utility of a network of micro weather stations for making in-situ meteorological measurements in the martian PBL. The state-of-the-art silicon micro machining and semiconductor large-scale-integration technologies available in the JPL Micro Devices Laboratory (MDL) are being combined with other recent developments in sensor technology to substantially reduce the size, mass, and power consumption for meteorological sensors and their associated electronics. Prototype micro sensors for measuring pressure, temperature, winds, humidity, and dust/ice optical depth in the martian PBL are being designed and tested. If such sensors can be developed successfully, they could be incorporated into complete weather stations that are compact (1 - 5 cm^3), light weight (1 - 5 grams), and consume less than 0.1 Watt of power. Each micro weather station would consist of several, carefully-integrated subsystems including 1) the sensors, 2) sensor interface electronics, 3) a central processing unit, 4) communications, and 5) system power.

a. pressure: Pressure measurements are needed to monitor seasonal variations in the total atmospheric mass associated with the condensation and sublimation of CO_2 on the polar caps. On shorter time scales, they indicate variations associated with atmospheric thermal tides [2, 3], and the passage of weather fronts [4]. Diurnal pressure changes also provide an indirect measure of the atmospheric dust loading because the presence of dust significantly enhances the amplitude of the tides [5]. Pressure sensors for martian PBL should have a dynamic range of at least 0.5 to 12 mbars to accommodate pressure differences resulting from surface topography (-4 km to + 27 km) and the seasonal CO_2 cycle. Within this range, they should resolve pressure variations at the 1% level to adequately sample the phenomena listed above. A silicon micro-machined capacitive aneroid barometer is being tested for PBL pressure measurements.

b. Temperature: Temperatures near the Martian surface vary by almost a factor of two (145 - 280 K) between the polar regions and the sub-solar point. Large diurnal variations in temperature (> 80 K near the sub-solar point) and static stability have dramatic consequences for the dynamics of the boundary layer as well as the free atmosphere above it. The freezing and sublimation of the CO_2 during the very cold polar night modulates the atmospheric mass, and produces condensation flows [6]. Very low nocturnal temperatures also constrain the amount of water vapor that the atmosphere can hold. Accurate temperature measurements in the PBL could provide "ground truth" for remote sensing instruments in orbit. Temperature measurements from different altitudes within the PBL could yield direct estimates of the static stability near the surface. High resolution temperature

MICRO WEATHER STATIONS FOR MARS: D. Crisp, W. J. Kaiser, T. W. Kenny, T. R. VanZandt, and J. E. Tillman.

time series would give estimates of the vertical heat flux, the Obukhov stability parameter, and friction velocity [7]. To address these needs, temperature sensors for the martian PBL should provide absolute accuracies near 1K at temperatures between 145 and 300 K. In addition, much greater relative accuracies (0.01 - 0.1 K) over small temperature ranges, and rapid sampling rates (> 10 Hz) will be needed to resolve heat fluxes. Miniaturized thermal conductance, thermocouple, and sonic devices are being tested for PBL temperature measurements.

c. Winds: Wind velocity measurements in the PBL are needed for studies of saltation, and for estimates of the heat, mass, and momentum fluxes. They would also provide information about the passage of weather fronts, traveling synoptic waves, atmospheric tides, the strength of the Hadley circulation, and the dynamical consequences of local and regional topography [8, 9, 10]. Winds at the Viking Lander sites usually varied between 0 and $\pm$ 10 m/s, but much larger gusts (25 m/s) were occasionally seen. Much larger winds may be needed to raise appreciable amounts of dust in the thin martian atmosphere [11]. The Viking Landers made no direct measurements of vertical velocities. Wind sensors for the martian PBL should measure all three components of the winds (zonal, meridional, and vertical). They should be sensitive to winds as small as 0.1 m/sec, have accuracies better than 10% at velocities between 1 and 100 m/sec. Micromachined pitot-static and sonic anemometers are being considered for these measurements.

d. Humidity: The background atmosphere contains about 10 precipitable microns of water, but values ten times this large were seen in high northern latitudes in northern summer [12]. Humidity measurements in the martian PBL would constrain the surface-atmosphere exchange of water on diurnal and seasonal time scales. Humidity measurements taken by a network of surface stations could be combined with orbiter observations to determine the vertical and horizontal distribution of water and the total atmospheric water budget during the seasonal cycle. Humidity sensors for the PBL should measure water vapor mixing ratios between 0.1 and 100 ppmv, with relative accuracies of at least 10%. These requirements can best be achieved by measuring the dew point temperature. Miniaturized frost-point hygrometers that use micro Peltier coolers are being tested for this application.

e. Dust/ice optical depth: Estimates of the dust optical depths are essential for studies of atmospheric energetics, because small amounts of dust can dramatically alter the radiative heating rates and the thermal structure of the atmosphere and surface [6, 13]. Airborne dust also decreases the contrast of features in surface images taken from orbit, and can corrupt measurements of surface thermal inertia [14]. Passive measurements of the direct solar flux (or light from other bright astronomical objects, such as Phobos or Deimos) as a function of zenith angle may provide the simplest means of monitoring the total atmospheric dust or ice loading [13]. Optical depth accuracies around 10% would be adequate for most of the applications described above. A simple solid-state all-sky camera is being considered for optical depth measurements.

These devices, the testing program, and the proposed sampling and deployment strategies will be presented.

References Cited:

1. Zurek, R.W.,to appear in *Mars*, University of Arizona Press, 1991. 2. Zurek, R.W., *J. Atmos. Sci.* **33**, 321, 1976. 3. C. Leovy and R.W. Zurek, *J. Geophys. Res.* **84**, 2956. 4. Tillman, J.E., et al., *J. Geophys. Res.* **84**, 2947, 1979. 5. Zurek, R.W., *Icarus* **45**, 202, 1981. 6. Pollack, J.B., et al., *J. Geophys. Res.* **95**, 1447, 1990. 7. Tillman, J.E., *J. Appl. Meteor.* **11**, 783, 1972. 8. Ryan, J.A., and R.M. Henry, *J. Geophys. Res.* **84**, 2821, 1979. 9. Ryan, J.A., et al., *Geophys. Res. Lett.* **8**, 899, 1981. 10. Murphy, J.R., et al., *J. Geophys. Res.*, **95** 14555, 1990. 11. Arvidson, et al., *Science* **222**, 463, 1983. 12. Jakosky, B.J. and C.B. Farmer, *J. Geophys. Res.* **87**, 2999, 1982. 13. Pollack, J.B., et al., *J. Geophys. Res.* **84**, 2929, 1979.

SOIL TEXTURE AND GRANULOMETRY AT THE SURFACE OF MARS

A. Dollfus and M. Deschamps, Observatoire de Paris, 92195 Meudon (FRANCE).
J. Zimbelman, CEPS/NASM, Washington SDC 20560 (USA).

METHOD : The microtexture of the near-surface martian soil was sensed with three diagnostic parameters (Dollfus et al., 1991 - Dollfus, 1991) :
- The albedo A at normal incidence and phase angle 5°, which relates to the composition of the top surface exposed layer
- The polarization parameter b characterizes the texture of the top surface layer in terms of grain size (Geake and Dollfus, 1986)
- The thermal inertia parameter I which refers to the soil compaction through the first few decimeters below the top surface sensed by polarimetry, in terms of size for the pieces making a granular regolith (Kieffer et al., 1977 - Vodvine et al., 1980).

Parameter b was derived from instrument VPM on board the soviet spacecraft MARS-5 (Ksanfomaliti et al., 1975 - Dollfus et al., 1983 - Dollfus and Deschamps, 1986), inertia I is from IRTM on the american VIKING (Palluconi and Kieffer, 1981) and albedo A from both.

SOIL TEXTURE : The polarimetric scans racked strips covering two contrasted regions, the dark hued Mare Erythraeum and the adjacent bright orange Thaumasia.

Erythraeum is characterized everywhere by a same type of terrain, despite the large geomorphological diversity of the surface. There is an ubiquitous coating or mantling with small dark grains, of albedo 12.7% and particle size 10 to 20µm, above a sub-surface dislocated in pieces around 300 to 600µm in size. A simple model is with sand-size particles completely coated with 15µm dark grains, as schematized in the figure 1 at left.

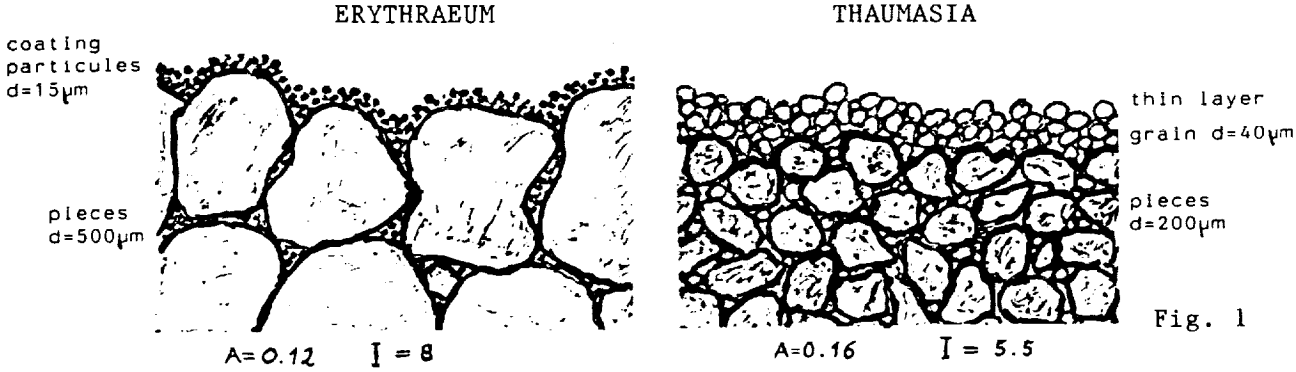

Fig. 1

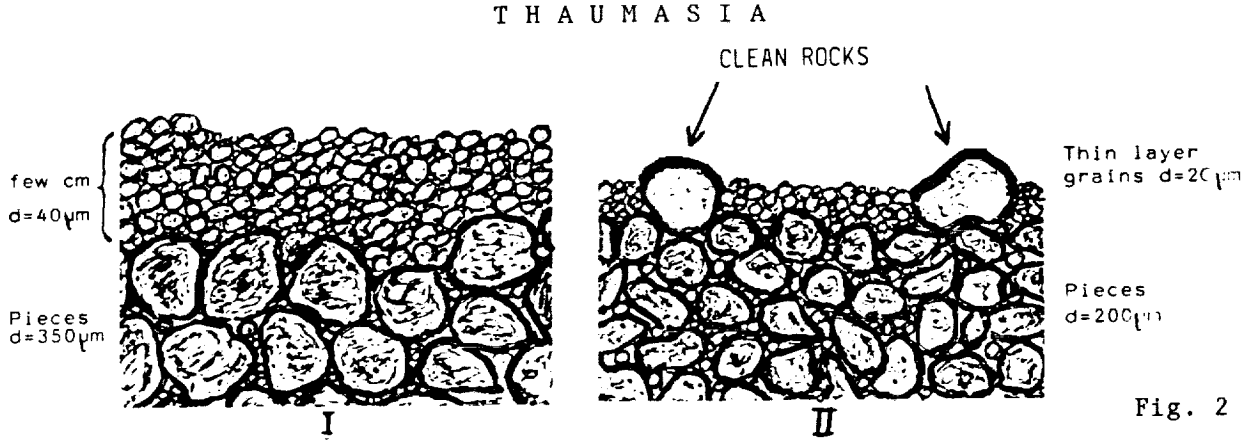

Fig. 2

Thaumasia, of average albedo 16%, discloses a surface covered with bright orange grains, probably very dispersed in size, the largest being several tenths of microns, overlaying and probably mixed with a subsurface dislocated into pieces 180 to 300µm or smaller if there is some cementation (figure 1 at right). If the surface layer is several centimeters thick, the thermal conduction requires larger pieces for the sub-surface (figure 2-I). If there is exposed rocks clean of dust, the excess polarization should be compensated by smaller surface grains (figure 2-II). Large variations in sizes occur from place to place, in contrast with the great textural uniformity over Erythraeum.

INTERPRETATIONS : On the basis of the terrestrial analogs of martian terrains identified by Morris et al. (1990), it is surmised that, on the dark areas, sand-size grains could be tachylite and the black particles a cohesive coating by titanomagnetite grains. In Thaumasia, the bright orange grains could be palagonite from weathered basalt glass particles of sideromelane.

DUST STORM PRODUCTION : Thaumasia is known, and was observed during our measurements, to be a source-area for dust storm production. The soil texture which is observed supplies both the large grains needed for saltation to occur and the intermixed small dust grains to be lifted by this process and carried in the atmosphere. A dark splotch observed in Thaumasia characterizes apparently an area completely deflated of its small orange grains storage, exhibiting darker soil of different texture.

DARK FEATURES PERENITY : The dark hued regions are permanent and must be protected against surface pollution by the accumulation of bright dust particles deposited after global dust storms. The soil texture which is observed is indeed made of grains with relevant size to be displaced at the surface by local wind. Impact of saltating sand grains ejects the non-cohesive dust grains into the air, which are eliminated by wind transportation, whilst the small local dark titanomagnetite grains remain stuck at the surface of the larger grains.

DUST STORM PARTICLES : The wind blown dust transportation models which were proposed (Zimbelman and Kieffer, 1979 - Christensen, 1982, 1986) usually assume that, among the components making the soil, only the bright small grains are able to be lifted in the air, not the dark particles. The implication is that only the palagonite type bright material have the mechanical properties required to be comminuted in non-cohesive small grains in the martian environment.

REFERENCES

Christensen P.R. (1982) : Jl. Geoph. Res. 87, 9985-9998.
Christensen P.R. (1986) : Jl. Geoph. Res. 91, 3533-3545.
Dollfus A., Ksanfomaliti L.V., Moroz V.I. (1977) : Cospar Space Res.XVII, 667-671 (Pergamon Press).
Dollfus A., Deschamps M. (1986) : Icarus 67, 37-50.
Dollfus A., Deschamps M., Zimbelman J. (1991) : 22th Lunar Planetary Science, Houston (Abstracts).
Dollfus A. (1991) pp. 101-104 in "The Environmental Model of Mars" (K. Szego Editor, Pergamon Press.
Geake J.E., Dollfus A. (1986) : MNRAS 218, 75-91.
Kieffer H.H. et al. (1977) : Jl. Geoph. Res. 82, 4249-4291.
Ksanfomaliti L.V., Moroz V.I., Dollfus A. (1975) : Kosm. Issled. 13, p. 92 (English UDC 543-47:523-43).
Morris R.V. et al. (1990) : Jl. Geoph. Res. 95, 14427-14434.
Palluconi F.D., Kieffer H.H. (1981) : Icarus 45, 415-426.
Vdovine V.V. et al (1980) : Kosm. Issled. 18, p. 809 (English UDC 523.43:629:196.64).
Zimbelman J.R., Kieffer H.H. (1979). Jl. Geoph. Res. 84, 8239-8251.

THE COMPOSITION OF MARTIAN AEOLIAN SANDS: THERMAL EMISSIVITY FROM *VIKING* IRTM OBSERVATIONS. *Kenneth S. Edgett and Philip R. Christensen*
Department of Geology, Arizona State University, Tempe, AZ 85287-1404.

Aeolian sands provide excellent surfaces for the remote determination of the mineralogic composition of martian materials, because such deposits consist of relatively well-sorted, uniform particle sizes and might consist of chemically unaltered, primary mineral grains derived from bedrock. Dark features on the floors of martian craters are controlled by aeolian processes [1-4] and many consist largely of unconsolidated, windblown sand [3, 5-7].

Measurement of the thermal emissivity of geologic materials provides a way to identify mid-infrared absorption bands, the strength and positions of which vary with mineral structure and composition [*e.g.*, 8, 9]. The *Viking* Infrared Thermal Mapper (IRTM) had four surface-sensing mid-IR bands, three of which, the 7, 9, and 11 μm channels, correspond to absorption features characteristic of carbonates, sialic, and mafic minerals, respectively [10]. In this study, the highest quality IRTM data were constrained so as to avoid the effects of atmospheric dust, clouds, surface frosts, and particle size variations (the latter using data obtained between 7 and 9 H); and selected for dark intracrater features such that only data taken directly from the dark feature were used, so as to avoid thermal contributions from adjacent but unrelated materials [6, 7, 11]. For any given dark feature, only 3 coincedent channels were available, because of the placement of the 7 and 9 μm IRTM detectors. Relative emissivities were computed for each IRTM spot by assuming that the highest of the three brightness temperatures (T_B) is the closest to the surface kinetic temperature (T_K). The radiance of each band at T_K is calculated using Planck's function. The relative emissivity is the ratio of the radiance at $T_B(\lambda)$ to the radiance at $T_K(\lambda)$ [12, 13]. Three-point emissivity spectra of martian dark intracrater features were compared with laboratory emission spectra of minerals and terrestrial aeolian sands convolved using the IRTM response function to the four IRTM spectral channels.

Results: Three-point spectra for 10 dark intracrater features for which the IRTM data met our strict constraint criteria are shown in Fig. 1. The vertical bars indicate the wavelength-dependent uncertainty due to detector sensitivity ("noise"). The numbers in Fig. 1 indicate the latitude and longitude locations of the relevant craters. Figure 2 shows four-point IRTM-convolved laboratory spectra of hand specimen-sized minerals and granular aeolian sands; the dotted lines indicate the shape of 3-point spectra where the 9 μm band is not present, for comparison with the results in Fig. 1. If the solid minerals of Fig. 2 were ground into sand-sized particles, their spectral shapes would remain about the same, but the relative depth of absorption features would be diminished [14]. The sand samples (with approximate major mineral abundances) include: (1) 100% quartz from Coral Pink Dunes, S.W. Utah, (2) 80% basalt, 20% quartz from the Moses Lake Dunes, Washington [15], (3) 100% basalt pyroclasts from aeolian drifts near Sunset Crater, Arizona, (4) 50% feldspar, 50% pumice from dunes in Christmas Lake Valley, Oregon [16], and (5) 100% pumice sand from an aeolian tuff in the Jemez Mts., New Mexico [see 17]. Also in Fig. 2 are three relative IRTM-derived 4-point spectra of portions of the martian regions Arabia, Syrtis, and Isidis [from 11] for comparison.

Discussion: The laboratory-derived spectra of calcite, quartz, and olivine show the shift in deep absorption features from 7 to 9 to 11 μm. Six of the martian spectra in Fig. 1 have a 7 μm observation, in all cases it is higher than the 11 and 20 μm emissivities, indicating a general lack of carbonate sand. Also in Fig. 1 there are 4 spectra with a 9 μm observation, which in all cases is also higher than the 11 and 20 μm emissivities, indicating that quartz cannot be a dominant mineral in these deposits. Feldspars, as well as quartz, have a 9 μm absorption feature which can be seen in the mineral and aeolian sand spectra in Fig. 2, but it is less-pronounced than the quartz feature. If only the spectra with 7 μm observations are considered, they appear to match very well with the 3-point spectra of basaltic and feldspar-rich dune sands in Fig. 2. In the cases where a 9 μm observation is present, the 9 μm emissivity is not only the highest, but the 11 and 20 μm emissivities are nearly equal; thus the best fit to these is the olivine spectrum, suggesting a dominance of ultramafic materials. Basalt (mafic) sands

have shallow absorptions in 9 μm, but only ultramafic sands would have deeper absortions near 11 μm. We note, however, that where a 9 μm observation is not available, we cannot be completely certain that more silicic materials are not present. We also note that many of the martian spectra in Fig. 1 resemble 3-point spectra for terrestrial sand samples where silicic materials (*e.g.*, quartz, pumice) are present in amounts up to 50%.

Conclusions: Mafic and ultramafic minerals and rock fragments may be the dominant materials comprising some of the windblown sands on Mars, but the presence of minor amounts of silicic minerals such as quartz cannot be ruled out when only the IRTM-derived thermal emission results are considered. The *Mars Observer* Thermal Emission Spectrometer (TES) will provide higher spatial and spectral resolution data with which to determine both the composition and mineralogic abundance of martian aeolian deposits.

References: [1] Sagan, C. *et al.* (1973) *J. Geophys. Res. 78*, 4163-4196; [2] Arvidson, R.E. (1974) *Icarus 21*, 12-27; [3] Christensen, P.R. (1983) *Icarus 56*, 496-518; [4] Thomas, P. (1984) *Icarus 57*, 205-227; [5] Cutts, J.A. and R.S.U. Smith (1973) *J. Geophys. Res. 78*, 4139-4154; [6] Edgett, K.S. (1990) M.S. thesis, Ariz. State Univ., Tempe, 196p.; [7] Edgett, K.S. and P.R. Christensen (1991) *Lunar Planet. Sci. XXII*, 335-336; [8] Lyon, R.J.P. (1965) *Econ. Geol. 60*, 715-736; [9] Farmer, V.C. (edt.) (1974) *The Infrared Spectra of Minerals*, The Mineralogical Society, London, 539p.; [10] Kieffer, H.H. *et al.* (1972) *Icarus 16*, 47-56; [11] Christensen, P.R. (1982) *J. Geophys. Res. 87*, 9985-9998; [12] Christensen, P.R. (1984) *Lunar Planet. Sci. XV*, 150-151; [13] Warner, T.A. and D.W. Levandowski (1990) *Proc. 2nd TIMS Workshop*, NASA JPL Publ. 90-55, p. 26-30; [14] Hunt, G.R. and R.K. Vincent (1968) *J. Geophys. Res. 73*, 6039-6046; [15] Petrone, A. (1970) M.S. thesis,Wash. State Univ., Pullman, 89p.; [16] Dole, H.M. (1942) M.S. thesis, Oregon State Coll., Corvallis, 98p.; [17] Smith, G.A. and D. Katzman (1991) *Geology 19*, 465-468.

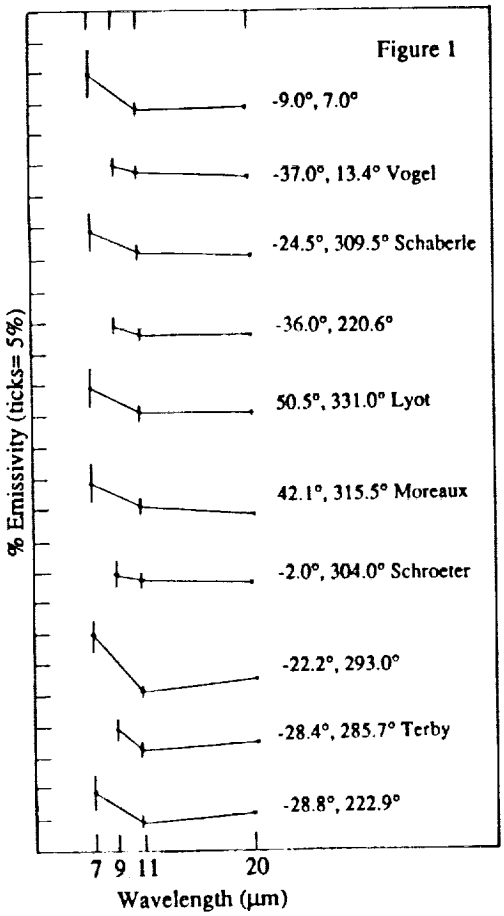

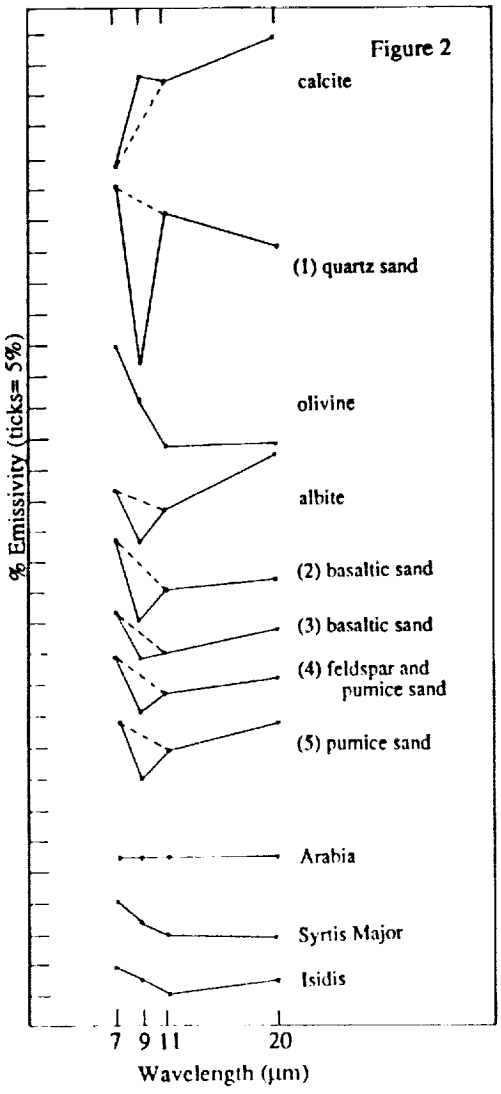

INFRARED PHOTOMETRIC BEHAVIOR AND OPPOSITION EFFECT OF MARS;

S. Erard[1], J-P. Bibring[1] and P. Drossart[2]. [1]Institut d'Astrophysique Spatial, bat.120, 91406 Orsay Campus, France; [2]DEpartement de recherches SPAtiales, Observatoire de Paris-Meudon, France.

Introduction: Although the instrument wasn't designed for this purpose, data from the imaging spectrometer ISM may be used for studying photometric variations of Mars reflectance, that are related to surface materials and aerosols physical properties. ISM flew aboard the Phobos-2 spacecraft which orbited Mars from January to March, 1989. About 40,000 spectra were acquired in 128 spectral channels ranging from 0.76 to 3.16 μm, with a spatial resolution of 25 km and a signal-to-noise ratio ranging up to 1000 (1) (2) (3).

Photometric function: A side task in reducing the spectral data was to correct them from viewing geometry changes, so as to compare the spectra in terms of normal albedo. This was achieved by using a simple Minnaert function, with an exponent fitted from the data (Fig. 1). Most of the values are ranging from k=0.55 to 0.80, with both bright and dark regions following such a law. However, small scale variations of surface material make evaluations of k difficult in the dark regions. The overall tendency is to get bigger values with increasing phase angle, albedo, and wavelength, in a range similar to that deduced by previous workers (4), though variation with phase angle is less steep. A similar method was used to infer aerosols properties (5).

Opposition effect: In other respects, we studied variations related to phase angles near the zero-phase. Reflectance measurements were used to fit five among six of Hapke's parameters, as the phase range was too small to allow roughness estimates. Single scattering albedo (0.66 to 0.80), and asymmetry factor (0.17 to 0,36) are consistent with previous observations at 0.9 μm of bright regions; there's a trend for narrowing and increasing amplitude of the opposition effect on brighter domains (Fig. 2), although maximum amplitudes are found upon Ophir Planum and S-E Syrtis Major, the latter being a very dark region.

Interpretation: Analysis of the results leads to the following conclusions: width variations of the opposition surge can be related to differences in porosity or grain size distributions on the various domains (6), with little or no effect from suspended dust. As the biggest effects are observed on dark and bright materials, intermediate behaviors on average-bright regions cannot result from a mixing process, but are more likely to come from either cementation processes or modifications of the grain size distribution under the influence of wind, which under martian conditions preferentially

removes the biggest particles (7). Thus, a surface dust consisting in big bright and small darker grains could explain the observations.

References : (1)Bibring *et al., Nature 341, 6242*, 591, 1989 (2)Bibring *et al., Proceedings of Lunar Planet. XX*, 461, 1990 (3)Erard *et al., Proceedings of Lunar Planet. XXI*, 437, 1991 (4)Pleskot and Kieffer, *Icarus, 30*, 341-359, 1977 (5)Drossart *et al.,Annales Geophysicae*, in press (6)Helfenstein and Veverka *Icarus 72*, 342, 1987 (7)Greeley *et al., Geophys. Res. Lett., 3*, 417,1976.

Figure 1: Example of Minnaert fit of ISM data at 0.9 µm, South of Olympus Mons. Phase angle is 14.5°, Minnaert exponent is 0.74.

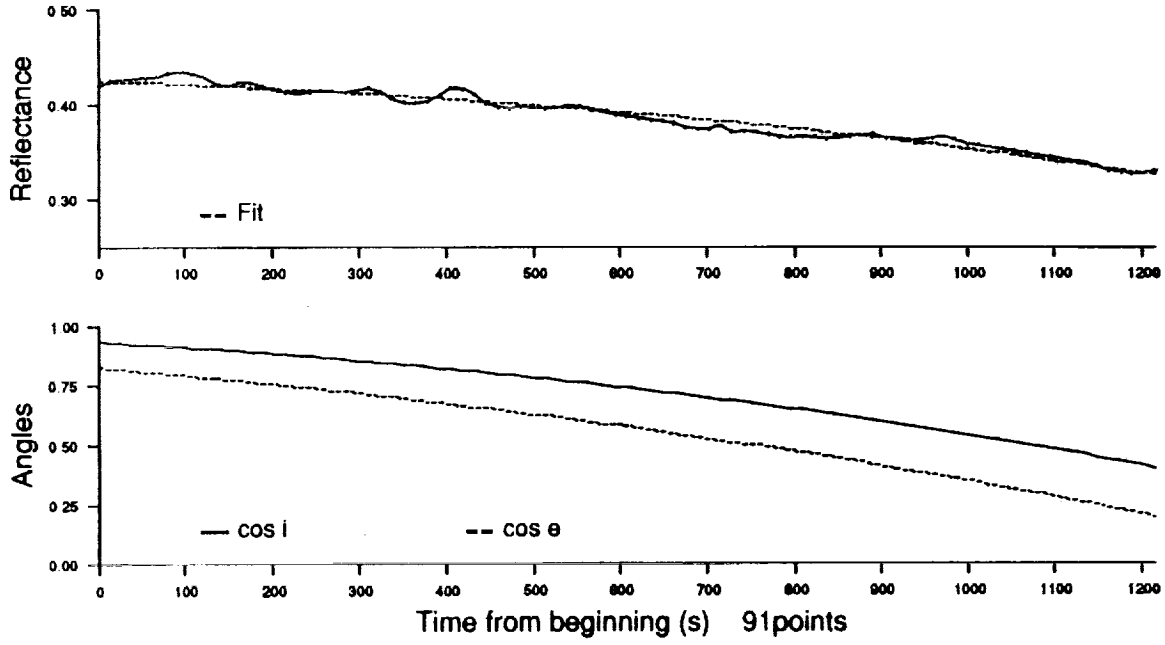

Figure 2: Relationships between single scattering albedo w, width h and amplitude B_0 of the opposition effect.

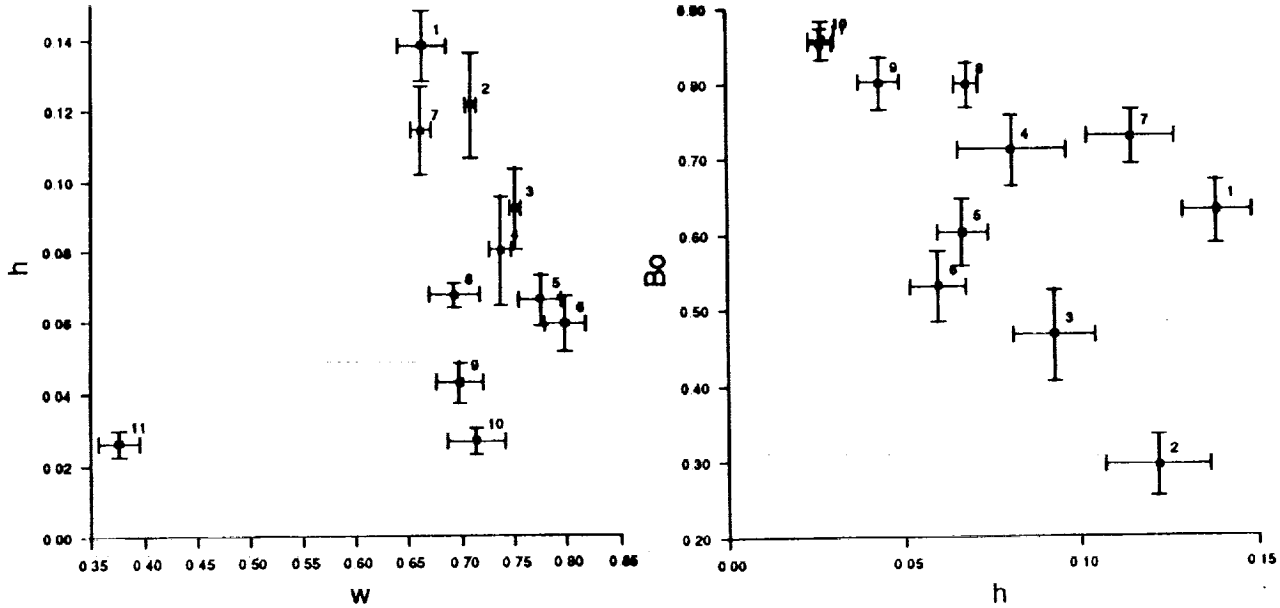

ATMOSPHERE–SURFACE INTERACTIONS AND ATMOSPHERIC EVOLUTION ON MARS;
Bruce Fegley, Jr., Department of Earth & Planetary Sciences and MacDonnell Center for Space Sciences, Washington University, St. Louis, MO 63130

Volatile Retention by Mars. A knowledge of the original volatile endowment of Mars is essential for any discussion of atmospheric loss on this planet. Cosmochemical models which postulate that planetary bulk compositions and volatile contents were controlled by the radial temperature profile in the solar nebula [1], and estimated bulk compositions based on the assumption that Mars is the parent body for the SNC meteorites [2] predict that Mars is volatile-rich. However, contrary views can also be found in the literature [3]. For illustrative purposes it will be assumed that Mars was initially as volatile-rich as the Earth. Taking terrestrial volatiles as the sum of atmospheric, crustal and oceanic volatiles [4] and assuming that Mars accreted with the same volatile content on a g/g basis, the volatile endowments for an Earth-like Mars correspond to $\sim$ 14 bars CO_2, $\sim$ 800 mbars N_2, and $\sim$ 1.2 km H_2O.

Composition of Outgassed Volatiles. Consideration of loss processes, such as atmosphere–surface interactions, also requires a knowledge of the composition of outgassed volatiles. Outgassing can occur during the accretionary phase and later during the post-accretionary phase. An important question is what fraction of the volatiles outgassed during accretion were retained by Mars and in what form (e.g., in the earliest atmosphere or trapped in the planetary interior). During both phases, the composition of the outgassed volatiles is dependent upon the prevailing oxygen fugacity. Quenching of gas phase and gas–grain reactions during outgassing – either from devolatilized planetesimals or from volcanic gases – is also likely to be important. Reducing conditions will lead to reduced C, N, and S gases such as CH_4, CO, NH_3, H_2S, and COS while oxidizing conditions will lead to oxidized gases such as CO_2, N_2, SO_2. Water vapor, HCl, and HF are expected in both scenarios. For reference, the average composition of present-day Hawaiian volcanic gases is 57.8% H_2O, 23.5% CO_2, 12.6% total S gases, 6.0% N_2 + Ar, 0.1% Cl gases, and 0.04% H_2 by volume [5]. Some (or all) of the reported N_2 + Ar may be atmospheric contamination and the reported molecular composition may be influenced by re-equilibration during collection. The relevance to outgassed volatiles on early Mars is unquantified, but an Earth-like volatile inventory and oxidation state will lead to similar outgassed volatiles.

Rates of Present-Day Atmosphere–Surface Reactions. As discussed in [6], many thermodynamically favorable gas–solid reactions are probably kinetically inhibited because of the low mean surface temperature (215 K) and pressure (7 mbars). An example shown in Fig. 1 is carbonate formation, which if facile, would drain all CO_2 from the Martian atmosphere leading to a N_2, Ar-rich atmosphere. However, recent studies of weathering products formed on Antarctic meteorites [7], which generally have been on Earth for less than 10^6 years [8], suggest that by analogy some gas–solid reactions may take place on Mars today. In one case, radiocarbon dating showed that formation of nesquehonite (and possibly other hydrous Mg-carbonates as well) on LEW 85320 apparently occurred at the rate of $\approx$ 1 gram per 30–40 years [9]. If pure nesquehonite is the only product formed, the implied rate is equivalent to $\approx$ 1 mole per 5000 yrs. The rate per unit area is much less certain because no details were given in [9]. However, a meteorite of this size probably has a surface area of $\leq$ 1 m^2 and assuming uniform coverage by the weathering product gives a very rough rate estimate of 10^8–10^9 molecules cm^{-2} sec^{-1}. This is probably an upper limit to the rate of gas–solid weathering on Mars because the lower temperature will exponentially decrease reaction rates.

Constraints on CO_2 Loss via Carbonate Formation. The following constraints are utilized in the absence of any kinetic data for the relevant carbonate formation reactions under Martian surface conditions. For illustration, a 10 bar CO_2 atmosphere, corresponding to an early Mars at least as volatile-rich as the Earth, will be assumed. Loss of this atmosphere over a 10^9 yr. period requires an average reaction rate of $\sim$ 10^{10} CO_2 molecules cm^{-2} sec^{-1}. This corresponds to the deposition of $\sim$ 0.2 μm calcite yr^{-1}. At 273 K and 10 bars pressure, about 2×10^{24} CO_2 molecules cm^{-2} sec^{-1} collide with a mineral on the Martian surface. Only a fraction of these collisions, which possess the necessary activation energy, will actually lead to carbonate formation. In order to have the average rate of 10^{10} molecules cm^{-2} sec^{-1}, the activation energy must be 75 kJ $mole^{-1}$ or less. As the reaction proceeds, the carbonate layer will build up and diffusion constraints will eventually slow down the carbonate formation process. Figure 2 illustrates the formation of such a product layer for another gas–solid reaction [10], but the principle is the same. The average reaction rate will be slightly lower if loss is assumed to occur over a longer period of 2–3 Gyr., but is about a factor of 10–100 larger than the (very approximate) rate estimated for hydrous carbonate formation on the Antarctic meteorite LEW 85320. It should also be noted that the reaction of 10 bars CO_2 will lead to the formation of large amounts of carbonate (e.g., equivalent to a global layer of calcite $\sim$ 200 meters thick).

Constraints on H_2O Loss. Water can be hidden in vast sub-surface ice deposits and/or permafrost layers. It can also be lost via atmospheric escape as discussed in [11]. For reference, loss of 100 meters H_2O in 10^9 yrs. also corresponds to a rate of $\sim$ 10^{10} molecules cm^{-2} sec^{-1}. Mass balance shows that production of a 1–2 km deep regolith containing 18% (mass) Fe_2O_3 consumes 50–100 meters H_2O if Fe is initially present as "FeO". Likewise, loss of 100 meters water by the formation of hydrated silicates leads to the production of $\sim$ 300 meters serpentine. It is important to assess the rates of these reactions relative to the rate of water loss via atmospheric escape.

Loss of Other Volatiles. As noted above, other species such as SO_2, HCl, and HF are plausible constituents of outgassed Martian volatiles. Also, NO_2 is a plausible product of atmospheric photochemistry and shock chemistry (e.g., lightning, impacts). The loss of these volatiles may occur by reactions exemplified by: $SO_2 + 0.5O_2 + MgSiO_3 \rightarrow MgSO_4 + SiO_2$, $SO_2 + 0.5O_2 + MgCO_3 \rightarrow MgSO_4 + CO_2$, $2HCl + MgSiO_3 \rightarrow MgCl_2 + SiO_2 + H_2$, $2HF + MgSiO_3 \rightarrow MgF_2 + SiO_2 + H_2$, $NO_2 + O_2 + CaCO_3 \rightarrow Ca(NO_3)_2 + CO$. However, no rate data are available for these reactions under Martian surface conditions. Furthermore, extrapolation of higher temperature rate data to Martian temperatures may be misleading because other mechanisms (e.g., grain-boundary vs. volume diffusion) may be rate-controlling at these temperatures. The predicted mineral assemblages and the predicted isotopic shifts (e.g., the ^{15}N enrichment in the nitrate relative to atmospheric N_2) are potential tests of how important such reactions were on Mars. Analyses of returned samples are required for these measurements.

Summary. Several questions need to be answered to provide better constraints on volatile loss via atmosphere–surface interactions. First, what is the nature of the outgassed volatiles on early Mars and what is their abundance? Second, what are the rates of important gas–solid reactions that act as volatile sinks? Third, how effectively do surface processes compete with atmospheric escape processes for water loss? Fourth, how efficient are the different surface sinks as conditions evolve toward the present-day?

Acknowledgments. This work was supported by the NASA Planetary Atmospheres Program and by the LPI, which is operated by the USRA under NASA Contract No. 4574.

References.[1] J.S. Lewis 1972 *EPSL* **15**, 286–290; [2] G. Dreibus & H. Wänke 1985 *Meteoritics* **20**, 367–381; [3] J.W. Morgan & E. Anders 1980 *Proc. Natl. Acad. Sci. USA* **77**, 6973–6977; [4] R.G. Prinn & B. Fegley, Jr. 1987 *Ann. Rev. Earth Planet. Sci.* **15**, 171–212; [5] W.W.Rubey 1951 *Geol. Soc. Amer. Bull.* **62**, 1111–1147; [6] B. Fegley, Jr. & A.H. Treiman 1991, "Chemistry of Atmosphere–Surface Interactions on Venus and Mars," in press in *Venus and Mars: Atmospheres, Ionospheres, and Solar Wind Interactions*, AGU; [7] M.A. Velbel, D.T. Long, & J.L. Gooding 1991 *GCA* **55**, 67–76; [8] K. Nishiizumi, D. Elmore, & P.W. Kubik 1989 *EPSL* **93**, 299–313; [9] J.L. Gooding , A.J.T. Jull, S. Cheng, & M.A. Velbel 1988 *LPS* **XIX**, 397–398; [10] B. Fegley, Jr. & R.G. Prinn 1989 *Nature* **337**, 55–58; [11] J. Luhmann 1991 in these abstracts.

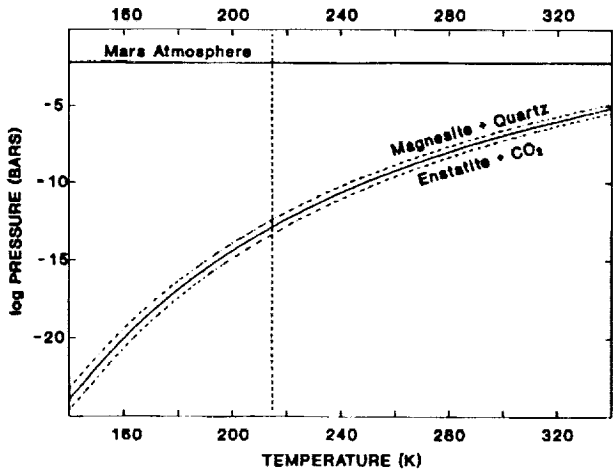

Fig. 1. The calculated CO_2 pressure required for magnesite formation from enstatite is significantly lower than the observed CO_2 pressure in the Martian atmosphere. If this reaction were facile, then no CO_2 should be left in the Martian atmosphere. The vertical dotted line indicates the global mean Martian surface temperature and the dashed lines indicate the uncertainties in the thermodynamic calculations. From Fegley and Treiman [6].

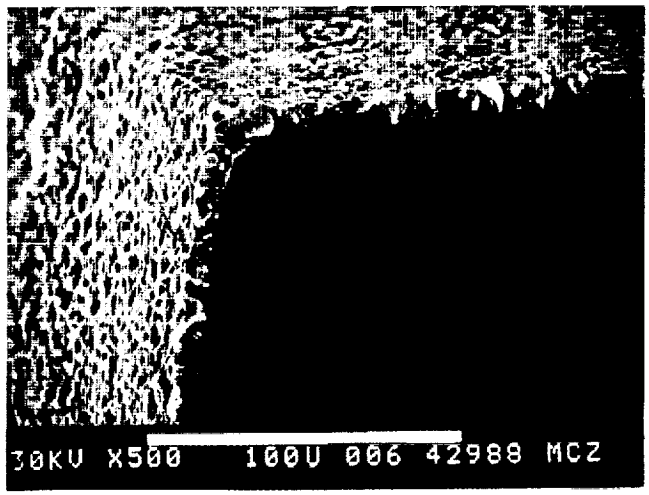

Fig. 2. A scanning electron micrograph of a calcite crystal covered by a layer of anhydrite formed by a gas–solid reaction. An analogous carbonate layer is expected on silicate minerals undergoing carbonation and if thick enough will slow down the carbonation reaction. The scale bar in this figure is 100 microns.

THE METEORITIC CONTRIBUTION TO DUST AND AEROSOLS IN THE ATMOSPHERE OF MARS; G. J. Flynn, Department of Physics, SUNY-Plattsburgh, Plattsburgh, NY 12901

The continuous, planet-wide accretion of meteoritic material onto the Earth and the Moon has been established by stratospheric sampling on Earth and chemical abundance analyses of the Lunar soils. The mass-frequency distribution of primary meteoritic material at the Earth is strongly bimodal, with mass peaks for particles of about 10^{-5} grams and 10^{17} grams (1). The lower mass peak, for particles near 250 μm in diameter, constitutes a continuous, planet-wide flux of meteoritic material, while the higher mass peak corresponds to rare impacts of large objects.

Although small particles make up only a tiny fraction of the mass of the Earth's atmosphere, these particles are important influences on the radiational energy transfer and optical properties of the atmosphere. In addition, these small particles serve as sinks for atmospheric gases, and as condensation nuclei influencing cloud formation and precipitation. Meteoritic material can make a significant contribution to the dust and aerosols.

At high altitudes a significant fraction of the particulate load of the Earth's atmosphere is derived from meteoritic material. Micrometeorites are the most abundant type of particle in the Earth's stratosphere in the 8 to 50 μm diameter range (2), except in the time period just after major volcanic eruptions. Micrometeorites would be the dominant particulate in the Earth's stratosphere down to an even smaller size limit were it not for the major contribution by aluminum-oxide rocket exhaust below 8 μm (3). Model calculations by Hunten et al. (4) indicate that recondensed meteoric material dominates the particle distribution in the sulfate layer of the Earth's atmosphere for particles below 0.5 μm in diameter, and direct collection of submicron particles at 35 km by Testa et al. (5) showed even higher particle concentrations than predicted by the Hunten et al. (4) model.

Meteoritic material must contribute in a similar manner to the atmospheres of all the planets and moons of the inner solar system. The micrometeorite contribution to the atmosphere of Mars was estimated for particles in the 10^{-14} to 10^{-9} gram mass range by Flynn (6) and for larger particles up to 10^{-1} grams by Flynn and McKay (7). However, only the contribution from primary micrometeorites, which survive atmospheric entry unmelted, was included in those calculations. Secondary contributions from:

1) recondensed vapor in meteor trails, and,
2) fragmentation debris from low density meteoroids,

are expected to be significant in the submicron particle size range. Hunten et al. (4) calculate that the secondary contribution exceeds the primary contribution for particles smaller than 0.2 μm at 30 km in the Earth's atmosphere.

The model developed by Hunten et al. (4) to estimate the contribution of material recondensed from meteor vapor trails to the aerosols in the Earth's atmosphere can also be applied to the Mars case, though recondensation may proceed differently in the CO_2 dominated atmosphere of Mars than on Earth. The amount of meteoritic material vaporized, and thus available for recondensation, can be estimated from the flux and entry heating temperatures calculated by Flynn and McKay (7). Taking 1900K as the temperature for onset of vaporization, the vaporized mass flux in each mass decade is given in Table 1. The total vaporized mass flux is estimated at 2×10^6 kg/year, about one-sixth of the estimate of total meteoritic flux at Mars. However this recondensed meteoric vapor is likely to be submicron in size, perhaps similar to the 0.25 nm size estimated for recondensation in the Earth's atmosphere (4). If so, the recondensed vapor would dramatically dominate the primary meteoric contribution in the submicron size range (see Table 2), since the mass flux of primary meteoritic material peaks at 250 μm.

Although meteor densities below 0.3 gm/cm^3 are frequently inferred from deceleration measurements (8), measurements on micrometeorites recovered from the Earth's stratosphere have, thus far, found no particles with densities below 0.3 g,/cm^3 (9). The micrometeorites recovered from the Earth's stratosphere frequently consist of very porous aggregates of submicron crystals weakly held together by amorphous material (2). It is likely that

Table 1: Surviving and Vaporized Meteoric Material on Mars

Mass Range (grams)	Size Range* (μm)	Mass Flux+ (kg/year)	Vaporized Fraction#	Vaporized Mass Flux (kg/year)	Unmelted Fraction@	Unmelted Mass Flux (kg/year)
$10^{1} - 10^{0}$	12400-26800	0.02×10^{6}	1	0.2×10^{5}	0	0
$10^{0} - 10^{-1}$	5760-12400	0.1×10^{6}	0.99	1×10^{5}	0.01	0.01×10^{5}
$10^{-1} - 10^{-2}$	2680-5760	0.3×10^{6}	0.9	3×10^{5}	0.05	0.2×10^{5}
$10^{-2} - 10^{-3}$	1240-2680	1×10^{6}	0.6	6×10^{5}	0.2	2×10^{5}
$10^{-3} - 10^{-4}$	580-1240	2×10^{6}	0.3	6×10^{5}	0.5	10×10^{5}
$10^{-4} - 10^{-5}$	270-580	3×10^{6}	0.1	3×10^{5}	0.7	20×10^{5}
$10^{-5} - 10^{-6}$	120-270	3×10^{6}	0.05	2×10^{5}	0.9	30×10^{5}
$10^{-6} - 10^{-7}$	60-120	1.5×10^{6}	0.01	0.1×10^{5}	0.98	15×10^{5}
$10^{-7} - 10^{-8}$	27-60	0.6×10^{6}	0	0	1	6×10^{5}
$10^{-8} - 10^{-9}$	12-27	0.2×10^{6}	0	0	1	2×10^{5}
$10^{-9} - 10^{-10}$	6-12	0.07×10^{6}	0	0	1	0.7×10^{5}
$10^{-10} - 10^{-11}$	3-6	0.006×10^{6}	0	0	1	0.06×10^{5}
$10^{-11} - 10^{-12}$	1-3	0.002×10^{6}	0	0	1	0.02×10^{5}
$10^{-12} - 10^{-13}$	0.6-1	0.0009×10^{6}	0	0	1	0.009×10^{5}
$10^{-13} - 10^{-14}$	0.3-0.6	0.0003×10^{6}	0	0	1	0.003×10^{5}
$10^{-14} - 10^{-15}$	0.1-0.3	0.00006×10^{6}	0	0	1	0.0006×10^{5}
TOTALS		12×10^{6}		2.1×10^{6}		8.6×10^{6}

* Assuming a spherical particle of density 1 gm/cm^3
+ As calculated by Flynn and McKay (1990) using the current terrestrial meteor flux in each mass decade (Hughes, 1978) and the Mars/Earth flux ratio for larger, crater producing objects (Shoemaker, 1977).
# Fraction of incident particles heated above 1900K from Flynn and McKay (1990).
@ Fraction of incident particles not heated above 1600K from Flynn and McKay (1990).

extremely low density particles of this type will fragment into their submicron crystalline constituents under the dynamic pressure experienced on atmospheric deceleration. Approximately 10% of the radar meteors detected at Earth have densities <0.1 gm/cm^3 (1). If 10% of meteoritic mass incident on Mars were to fragment on atmospheric entry this would contribute 1.2×10^{6} kg/year of fragmentation debris to the atmosphere of Mars.

Micrometeorites, recondensed meteoric vapor, and meteor fragmentation debris provide a continuous, planet-wide source of atmospheric particulates on Mars. In the size range >1 μm in diameter micrometeorites which survive atmospheric entry unmelted are the major contributor, accounting for about 8.6×10^{6} kg/year of material. For particles <1 μm in diameter the majority of the mass is likely to come from recondensed meteoric vapor, which could account for ~2×10^{6} kg/year.

Table 2: Meteoric Contribution to Particles <1 μm on Mars

Source	Mass Flux(kg/yr)
Unmelted Micrometeorites	4×10^{3}
Recondensed Meteoric Vapor	2×10^{6}
Fragmentation Debris	1×10^{6}

REFERENCES: 1. Hughes D. W. (1978) Meteors, in Cosmic Dust (ed. J. A. M. McDonald) John Wiley, New York, 123-185. 2. Fraundorf P., Brownlee D. E., and Walker R. M. (1982) Laboratory Studies of Interplanetary Dust, in Comets (ed. L. Wilkening), U. of Arizona Press, Tucson, 383-409. 3. Maurette M (1991) Nature, 351, 44-47. 3. Brownlee D. E., Ferry G. V., and Tomandl D. (1976) Science, 191, 1270-1271. 4. Hunten D. M., Turco R. P., and Toon O. B. (1980) J. Atmos. Sci., 32, 1342-1357. 5. Testa, J. P. Jr., et al. (1990) Earth and Planet. Sci. Lett., 98, 287-302. 6. Flynn G. J. (1991) in The Environmental Model of Mars (ed. K. Szego), Pergamon Press, New York, 121-124. 7. Flynn G. J. and McKay, D. S. (1990) J. Geophys. Res., 95, No. B9, 14,497-14,509. 8. Verniani F. (1969) Space Sci. Rev., 10, 230-261. 9. Flynn G. J. and Sutton S. R. (1991) Proc. Lunar and Planet. Sci. Conf., Volume 21, Lunar and Planetary Institute, Houston, TX, 541-547.

NITROGEN ESCAPE FROM MARS, J. L. Fox, Institute for Terrestrial and Planetary Atmospheres, State University of New York at Stony Brook

The mass spectrometer on the Viking spacecraft measured an anomalous ^{15}N:^{14}N ratio of about 1.62 times the terrestrial value (1). This enhancement presumably results from differential escape of ^{15}N. The escape of N is non-thermal and potential escape mechanisms include photodissociation, photoionization, and electron impact dissociative ionization of N_2, and ion-molecule reactions and dissociative recombination of N_2^+. The latter source was found to be the present most important by McElroy et al. (2) and by Fox and Dalgarno (3,4). Dissociative recombination of N_2^+ can proceed by a number of different channels, but sufficient energy is available for escape only from the channel which produces $N(^4S)$ + $N(^2D)$, for which the exothermicity is 3.45 eV, about twice the escape energy for ^{14}N at the Martian exobase, 1.74 eV. The escape energy of ^{15}N, 1.86 eV, is more than half the available energy and differential escape occurs if the N_2^+ is in the ground vibrational state. A detailed calculation by Wallis (5) showed that the escape probability for an ^{14}N released in dissociative recombination of N_2^+ in the ground vibrational level is 41.6%, and that for an ^{15}N is 23.7%. If the N_2^+ is vibrationally excited, 0.27 eV is added to the exothermicity and the isotope discrimination is reduced considerably. If we call $\phi(t)$ the $^{14}N_2$ flux at time t, $\mathcal{N}_{14}$ the column density of $^{14}N_2$, then the initial column density can be found by integrating

$$\frac{d\mathcal{N}_{14}}{dt} = -\phi(t) \tag{1}$$

over the age of the solar system. Similarly, the time rate of change of the isotope enhancement f is given by

$$\frac{df}{dt} = \frac{\phi f(1-R)}{\mathcal{N}_{14}}, \tag{2}$$

where R is the net relative escape rate of ^{15}N and ^{14}N (1). This equation can also be integrated backward in time, taking care to account properly for changes in the composition of the atmosphere and in the altitude of the exobase [cf. (4)]. The predicted isotope ratio is highly dependent on the fraction of dissociative recombinations assumed to proceed via the $N(^4S)$ + $N(^2D)$ channel. Fox and Dalgarno (4) assumed that the channels were produced in a statistical distribution, which would imply that 24% produced $N(^4S)$ + $N(^2D)$. The predicted isotope enhancement over the terrestrial value was more than 2.5, implying that the escape rate had been reduced in the past, possibly by the presence of a dense, early atmosphere. Later experiments on the dissociative recombination of N_2^+ by Queffelec et al. (6) suggested, however, that the major product channel is $N(^2D)$ + $N(^2D)$, for which the exothermicity is only 1.06 eV, much less than necessary for escape of N. A reanalysis based on this assumption shows that the predicted isotope enhancement is 1.71–2.0, not much larger than the observed value [cf. (7)]. The presence of an initially dense atmosphere is

not strongly required, but is not excluded, as long as it was lost relatively early in the history of the planet. Observations of branching valley networks on the surface of Mars have been interpreted as showing that liquid water was present early in the history of the planet, and and therefore the early atmosphere must have been warm and dense. Analyses suggest that such an atmosphere would, however, have been unstable, since CO_2 would have been rapidly deposited as carbonates in the presence of liquid water [e.g. Pollack et al. (8); Carr (9)].

Recently, Guberman (10) has carried out ab initio calculations that show that the major channel for dissociative recombination of N_2^+ in the ground vibrational state is the $N(^4S) + N(^2D)$ channel, with a yield of 0.88, significantly larger even than that assumed by Fox and Dalgarno (4), and much larger than indicated by the experiments of Queffelec et al. (6). Guberman noted that the yield of $N(^2D) + N(^2D)$ may be larger for DR from vibrationally excited N_2^+. Using the yield suggested by Guberman for dissociative recombination from ground state N_2^+ and that of Queffelec et al. for the vibrationally excited states, we find that ^{15}N-^{14}N isotope fractionation is significantly more effective than previous models have indicated. The predicted isotope enhancement after 4.5 billion years is about 4.5, much larger than the observed value, which is achieved after only 6.4×10^8 years. If the yields of Guberman are correct, some other mechanism must be found to inhibit the escape of N.

1. Nier, A. O., McElroy, M. B., and Yung, Y. L. (1976) *Science 194*, 68.
2. McElroy, M. B., Kong, T. Y., and Yung, Y. L. (1977) *J. Geophys. Res., 82*, 4379.
3. Fox, J. L. and Dalgarno, A. (1980) *Planet. Space Sci., 28*, 41.
4. Fox, J. L. and Dalgarno, A. (1983) *J. Geophys. Res., 88*, 9027.
5. Wallis, M. K., (1978) *Planet. Space Sci., 26*, 949.
6. Queffelec, J. L., Rowe, B. R., Morlais, M., Gomet, J. C., and Valee, F. (1985) *Planet. Space Sci., 33*, 263.
7. Fox, J. L., (1989) in *Dissociative Recombination: Experiment, Theory and Applications*, World Scientific, Singapore, p. 264.
8. Pollack, J. B., Kasting, J., Richardson, S. M., and Poliakoff, K. (1987) *Icarus, 71*, 201.
9. Carr, M. H. (1989) *Icarus, 79*, 311.
10. Guberman, S. L. (1991) *Geophys. Res. Lett., 18*, 1051.

IMPLICATIONS OF EARLY HESPERIAN AGES FOR PRESUMED NOACHIAN AGE VOLCANIC FLOWS ON MARS H. V. Frey, Geodynamics Branch, Goddard Space Flight Center, Greenbelt MD 20771

Introduction

Volcanic resurfacing has been important in martian history [1-7]. Major common-age resurfacing events are recorded in the cumulative frequency curves for the highland/lowland transition zone in eastern Mars [8] and elsewhere [9-12]. Most obvious in all these regions is a major resurfacing at the Early Hesperian (EH) time of ridged plains (unit *Hr*) eruption in Lunae Planum and elsewhere. This event seems to have occurred with greater or lesser efficiency in nearly all terrains studied: ridged plains, knobby terrain, smooth plains (if old enough) and adjacent cratered terrain. Volcanic processes have apparently dominated all other sources of resurfacing (aeolian, periglacial, impact, fluvial) throughout all martian history [7].

Ridged Plains of Noachian Age?

The identification of volcanic terrains is sometimes problematical, but there is near unanimous agreement that relatively smooth, lightly cratered plains with positive relief ridges (similar in appearance to lunar mare ridges) are such surfaces. The prominent ridged plains (*Hr*) of Lunae Planum, Coprates, Hesperia Planum and elsewhere are generally considered to have erupted in the EH [5,6]; their widespread nature and their occurance at the base of the Hesperian represents a major volcanic episode in martian history [2-4]. *Hr* plains are sometimes gradational with another ridged plains unit, mapped as *Nplr*, which are widely distributed in both hemispheres of Mars but cover much less area (4.5×10^6 km^2) than *Hr* units (13.3×10^6 km^2). The stratigraphic position (based on superposition relationships and total crater counts) of these apparently older ridged plains is **Middle Noachian**; the high density of impact craters on *Nplr* would certainly suggest a Noachian age.

But total crater counts can be misleading: Inefficient resurfacing events allow older surfaces to show through and give old TOTAL crater retention ages, which may not accurately reflect the age of the *resurfacing* unit. We have previously shown [13] that for at least two areas in Memnonia and Argyre, the *Nplr* ridged plains are the same age as - but significantly thinner (< 150 m?) than - *Hr* in Lunae Planum (>300-600 m?) or elsewhere [9,11,14]. If this conclusion holds in general for other *Nplr* outcrops, the eruption of ridged plains volcanism may have been more restricted in time but more widely distributed in space than previously thought.

Figure 1 shows the estimated percentage of Mars resurfaced by volcanism at different epochs [7]. Based on total crater counts (Figure 1a), volcanic resurfacing was greatest but similar in the Middle Noachian (MN) and Early Hesperian (EH), with a 50% decrease in the Late Noachian (LN) and Late Hesperian (LH) [7]. Figure 1b shows the case where all *Nplr* units are assumed to be EH in age [13]. The contribution of *Nplr* and *Hr* units alone to the EH volcanic resurfacing equals the total in the MN, and the LN volcanic resurfacing decreases to less than 1/3 that in the EH. If the volcanic fraction [7] of the LN *Npl2* unit also erupted in the EH, as resurfacing ages in such terrains suggest [10,11], then the EH peak dominates the MN peak by 25% and the LN volcanic resurfacing would decrease to almost nothing (Figure 1c).

Discussion

If Figure 1c actually represents the volcanic resurfacing on Mars, the ***major*** volcanic period in martian history occurred in the EH, following a period of quiescence in the LN after an earlier intense MN pulse (perhaps related to accretion, core formation and impact heating). Although absolute ages are poorly known for Mars, the quiescent interval (LN) may have been 400 my long [7,15,16]. The separate and likely shorter duration [15] MN and EH peaks and later steady decrease of volcanism may constrain thermal history models of Mars to those which warmed the interior of Mars over time after accretion [17,18].

The distribution of EH volcanism would have much greater continuity southwest, south and southeast of Daedalia Planum, and north and northeast of the Argyre Basin. Hesperian age resurfacing would nearly completely ring the Tharsis-Valles Marineris-Chryse outflow channel

region, except to the west and northwest where Amazonian age materials obscure older basement. Equally interesting are the Argyre deposits, which, with *Nplr*, *Npl2* and *Hr* units elsewhere in western and eastern Mars and in the south polar region, help to define near-continuous, sometimes extremely wide rings of possible Hesperian age volcanism surrounding the Hellas Basin at 1-2 basin diameters.

There are climatic implications to this possible younger age for *Nplr* ridged plains and volcanic *Npl2* units, since volcanism involves degassing of volatiles, including important greenhouse gases. Greeley [19,20] calculated the likely release of juvenile water over martian history estimated from the *volume* of volcanic materials at different times, which peak in the EH. Any increase in the amount of ridged plains volcanism in the EH would result in yet greater amounts of juvenile water being released at that time. This enhanced release (and likely wider distribution) was just prior to the long, episodic development of the martian outflow channels in the Late Hesperian (LH) [4]. Fluvial and periglacial resurfacing on Mars peaks in the LN and LH [7], following the major (and perhaps enhanced) peaks of volcanic resurfacing (Figure 1d). The *ratio* of these peaks (LN/LH = 0.65) is the same as the ratio of the MN/EH peaks in volcanism (0.68) for Figure 1c, which would be expected if volcanism were the source of the fluvial and periglacial resurfacing. The EH/LH was time of important change in the geologic style of Mars, with more restricted volcanism replacing former global distribution of materials (e.g., ridged plains) and fluvial discharge through outflow channels dominating over former more widespread valley networks [4]. The possibility that volcanism was even more prominant in the EH than previously thought only emphasizes the importance of this epoch in martian history.

References: [1] Arvidson, R.E. et al., Rev. Geophys. Space Phys. 18, 565-603, 1980. [2] Greeley, R. and P.D. Spudis, Rev. Geophys. Space Phys. 19, 13-41, 1981. [3] Neukum, G. and K. Hiller, JGR 86, 3097-3121, 1981. [4] Tanaka, K.L., Proceed. LPSC 17th, JGR 91, E139-E158, 1986. [5] Scott, D. H. and K.L. Tanaka, Geol. Map Western Equatorial Region of Mars, USGS Map I-1802-A, 1986. [6] Greeley, R. and J.E. Guest, Geol. Map Eastern Equatorial Region of Mars, USGS Map I-1802-B, 1987. [7] Tanaka, K.L. et al., Proceed. LPSC 18th, 665-678, 1988. [8] Frey, H. et al., Proceed. LPSC 18th, 679-699, 1988. [9] Frey, H. and T.D. Grant, JGR 95, 14,249-14,263, 1990. [10] Grant, T.D. and H.V. Frey, EOS Trans. Am. Geophs. Un. 68, 1342, 1987. [11] Frey, H.V. and T.D. Grant, LPSC XX, 313-314, 1989. [12] Frey, H. et al., LPSC XVIII, 304-305, 1987. [13] Frey, H. et al., Proceed. LPSC 21st, 635-644, 1991. [14] DeHon, R.A., NASA Tech Memo. 87563, 237-238, 1985. [15] Neukum, G. and D.U. Wise, Science 194, 1381-1387, 1976. [16] Hartmann, W.K. et al., Basaltic Volcanism, Chap. 8, 1049-1127, 1981. [17] Toksoz, M.N. and A.T. Hsui, Icarus 34, 537-547, 1978. [18] Stevenson, D.J. and S.S. Bittker, LPSC XXI, 1200-1201, 1990. [19] Greeley, R., Science 236, 1653-1654, 1987. [20] Greeley, R., LPSC XXII, 489-490, 1991.

FIGURE 1. RESURFACING OF MARS

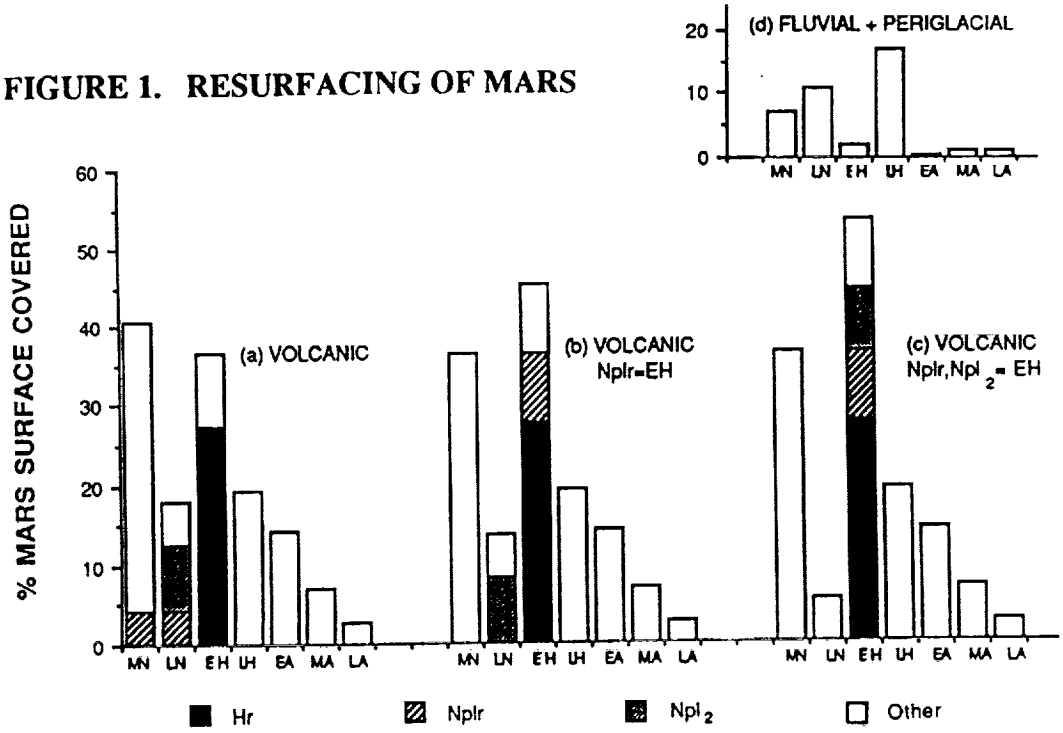

MARTIAN SURFACE SIMULATIONS; R.W. Gaskell, JPL/Caltech, 4800 Oak Grove Dr., Pasadena, CA 91109

Current scenarios for a Mars landing involve the extensive analysis of the surface near the landing site. Pinpoint landing, for example, requires a detailed mapping of the area from orbit for landmark identification and landing site selection, and the use by the lander of its own imaging data to recognize these landmarks and to guide itself safely to the surface. Hazard avoidance requires sufficient orbital imaging to ensure that safe landing sites exist, with the lander using its sensory data to find one of them. Once on the surface, a rover must be able to avoid or surmount obstacles, travel across surfaces with varying compositions and slopes, and navigate to a desired destination. Computer simulated martian surfaces are being constructed to aid in the development of these exploration technologies.

These surface simulations attempt to mimic the specific geologic episodes that built the surface, such as cratering, lava flows, and aeolian activity. Each episode takes a preexisting surface as a starting point, alters it in some way, and stores the new surface for further processing. This modular construction makes it possible for new processes to be included without altering existing software.

The image shown in figure 1 began as a fractally generated basement. A lava flooding then occurred, again with a fractally generated surface. The surface was then bombarded in a cratering episode. Crater sizes and surface locations were randomly generated according to a given distribution function. This was followed by a layer of dust, mimicked by using a fractal surface with variations controlled both by scale and by the underlying slopes. Rocks were then added according to another distribution function controlling their size and location. Other features such as crevasses can now be included in the simulations. Physical properties of the surface and sub-surface materials can be extracted for radar, thermal inertia and rover simulations.

All process models have random aspects. In fractal processes, heights are computed for a successively finer grid. A scale dependent random variation added at each stage determines the characteristic roughness of the surface. Statistical processes such as cratering are governed by predetermined distribution functions. Deterministic processes, such as wind and water erosion, are influenced by the physical properties of the surface. Models for such processes use these surface properties to constrain stochastic alterations.

The surface in figure 1 represents a region 25 km square viewed at a resolution of 50 meters, comparable to Viking orbiter resolution. The current software can zoom in on the lowest resolution images by a factor of up to 2^{22} (about four million), allowing any part of the surface to be explored in more detail. Figure 2 shows a 1600 meter square portion of the surface, outlined by the white square in figure 1, while figure 3 zooms in further to a region 50 meters on a side. This last picture, which reveals a lander amidst a boulder field, represents one pixel of the original image.

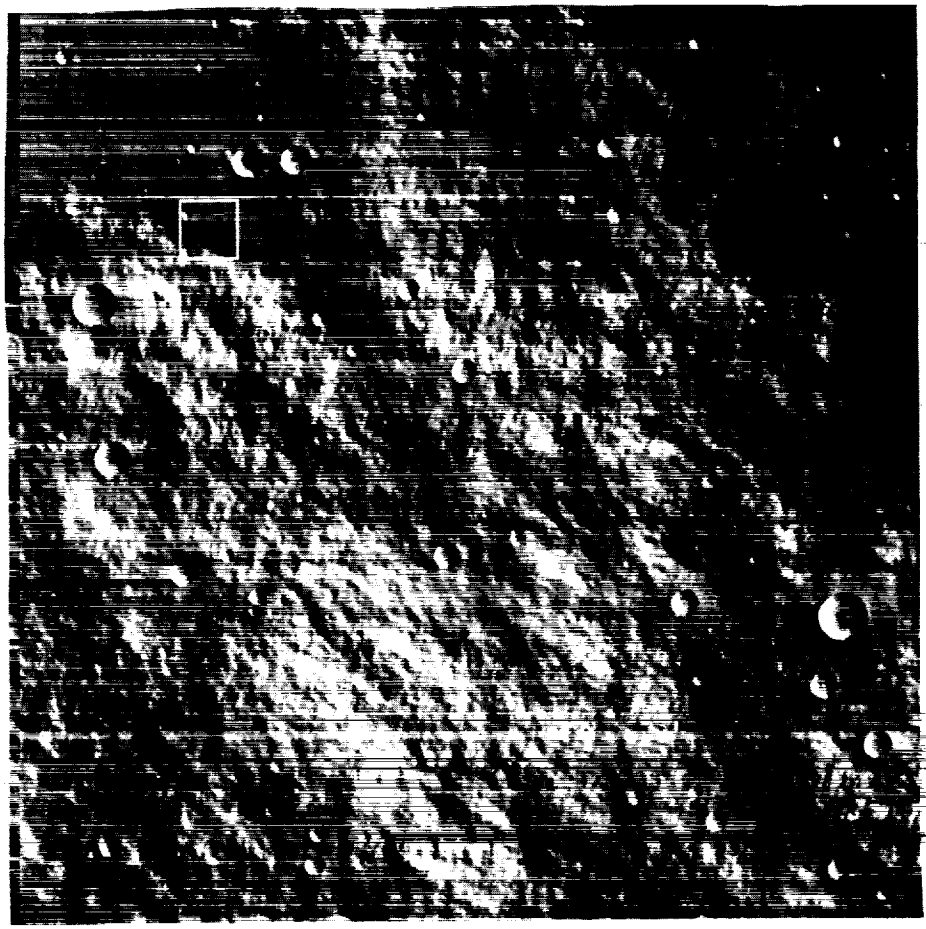

Figure 1

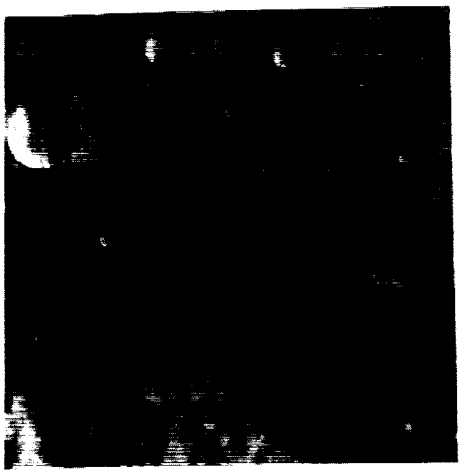

Figure 2

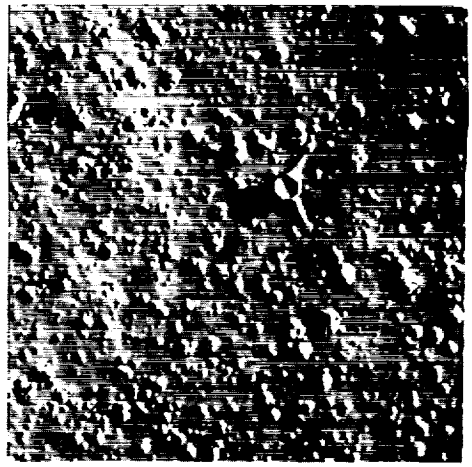

Figure 3

MARS SURFACE WEATHERING PRODUCTS AND SPECTRAL ANALOGS: PALAGONITES AND SYNTHETIC IRON MINERALS

D. C. Golden[1], D. W. Ming[1], R. V. Morris[1] and H. V. Lauer Jr[2].
[1]NASA, Johnson Space Center, Houston, TX 77058 and [2]Lockheed ESC, Houston, TX 77058

INTRODUCTION

There are several hypotheses regarding the formation of Martian surface fines. These surface fines are thought to be products of weathering processes occurring on Mars. Four major weathering environments of igneous rocks on Mars have been proposed by Berkeley and Drake [1]: (i) impact induced hydrothermal alteration; (ii) subpermafrost igneous intrusion; (iii) solid-gas surface reactions; and (iv) subaerial igneous intrusion over permafrost. Although one or more of these processes may be important on the Martian surface, one factor in common for all these processes is the reaction of solid or molten basalt with water (solid, liquid, or gas). These proposed processes, with the exception of solid-gas surface reactions, are transient processes. The most likely products of transient hydrothermal processes are layer silicates, zeolites, hydrous iron oxides and palagonites [2,3,4]. The long-term instability of hydrous clay minerals under present martian conditions has been predicted by Gooding [5]; however, the persistence of such minerals due to slow kinetics of dehydration, or entrapment in permafrost, where the activity of water is high, can not be excluded. Anhydrous oxides of iron (e.g., hematite and maghemite) are thought to be stable under present Martian surface conditions. Oxidative weathering of sulfide minerals associated with martian basalts has been proposed by Burns [6]. Weathering of sulfide minerals leads to a potentially acidic permafrost and the formation of Fe(III) oxides and sulfates. Weathering of basalts under acidic conditions may lead to the formation of kaolinite through metastab'e halloysite and metahalloysite [7]. Kaolinite, if present, is thought to be a thermodynamically stable phase at the martian surface [4].

Several terrestrial materials have been suggested as analogs for martian fines including palagonites and iron (III) oxides. Palagonites from Hawaii are considered to be some of the best analogs for the martian fines, based upon similar spectral properties [2]. Palagonitization of Hawaiian materials from Mauna Kea summit probably occurred during volcanic eruptions under a permanent ice cap during the Pleistocene period, causing quick alteration of basaltic glass followed by further alteration due to melt water. Volcanic eruptions through permafrost is a likely scenario on Mars. Iron oxides could result from alteration of primary mineral magnetite or direct precipitation during palagonitization or as an advanced weathering product of iron sulfide weathering. Whatever the mode of formation, iron oxides play a key role in Martian surface chemistry. In a weathering environment, very often the Fe(III) in iron oxides is substituted with other cations (e.g., Al) affecting their chemical and physical properties [8].

Fine materials on Mars are important in that they influence the surface spectral properties; these fines are globally distributed on Mars by the dust storms and this fraction will have the highest surface area which should act as a sink for most of the adsorbed volatiles near the surface of Mars. Therefore, the objectives of this study were to (i) examine the fine fraction mineralogy of several palagonitic materials from Hawaii and (ii) compare spectral properties of palagonites and submicron-sized synthetic iron oxides with the spectral properties of the Martian surface.

MATERIALS AND METHODS

The clay fractions ($<2\,\mu m$) of three palagonite samples-MK11 (red), MK12 (black), and MK13 (yellow) collected at an elevation of 4145 meters near the summit of Mauna

Kea volcano in Hawaii [9] were separated using centrifugation and sedimentation techniques [10]. In separate experiments, synyhetic magnetites were prepared by mixing appropriate amounts of $FeCl_2$ and $FeCl_3$, and the mixtures were precipitated in a strong ammonia solution. Aluminum up to 0.4 mole fraction of the starting Fe content was incorporated as $AlCl_3$. Precipitates of magnetite were washed in deionized water, freeze-dried, and heated in air to 400 ^{o}C for 4 hrs to form maghemite, and then heated again in air at 500 ^{o}C for 6 hrs to form hematite. Reflectance spectra of palagonite fine fractions and synthetic iron oxides were recorded from 0.35 μm to 2.2 μm wavelength range. Synthetic iron oxide minerals were characterized by infrared spectroscopy (IR), x-ray diffraction analysis (XRD), and transmission electron microscopy (TEM).

RESULTS AND DISCUSSION

The fine fraction of the red sample (MK11, <20 μm) had a reflectance spectrum band at 860 nm ($^{6}A_1$ to $^{4}T_{1g}$ electronic transition) which is normally found associated with bulk hematite particles. A feature at 450 nm in the MK12 and MK13 samples was due to Fe(III) in nanophase hematite (or possibly due to structural Fe in smectites) [11]. IR absorption studies indicated structural Fe(III) in clay fractions (<2 μm) of the MK12 and MK13 samples. The clay fraction of the MK11 sample contained well-dispersed submicron sized (0.1-0.4 μm) hematite particles on the surface of smectite particles. There was very little substitution of Fe in the structure of smectites in the MK11 sample as suggested by IR and microprobe analyses.

The synthetic Fe-oxides (i.e., maghemite and hematite) had similar reflectance spectra to those reported for synthetic Fe(III) oxides by Morris et al. [12]. The presence of maghemite in the martian regolith can significantly affect the magnetic properties of the bulk material and enhance the Fe(III) absorption bands in the reflectance spectra.

The palagonitic fine samples exhibited spectral features which are very similar to those observed in the martian bright regions. The fine fractions of the black (MK12) and yellow (MK13) samples were similar to those of martian bright regions in terms of their overall shape. It is possible to produce a pattern very similar to that of martian bright region spectra by mixing the fine fractions of the black or yellow palagonitic samples with small amounts of bulk hematite or a small amount of red MK11. As observed for the clays from palagonitic samples, a close association of the fine clay fraction with iron oxides is possible due to coulombic forces, and this association (phyllosilicates and iron oxides) is often observed in terrestrial soils. It is possible that such associations occur in Martian fines enabling these two phases to be distributed together uniformly over the Martian surface.

REFERENCES

(1) Berkley, J. L. and M. J. Drake (1981) *Icarus* 45:231-249. (2) Allen, C. C., J. L. Gooding, M. Jercinovic and K. Keil (1981) *Icarus* 45:347-369. (3) Banin, A., L. Margulies, and T. Ben-Shlomo (1988) *Lunar and planetary Science* XIX:27-28 (4) Ming, D. W. and J. L. Gooding (1988) *Workshop on Mars Sample Return science* (M. J. Drake et al., eds.), LPI Tech. Rpt. 88-07. Lunar and Planetary Institute, Houston.pp 124-125. (5). Gooding, J. L. (1978) *Icarus* 33:483-513. (6). Burns, R. G. (1987) *Lunar and planetary Science* XVII:141-142. (7) Ming, D. W., R. V. Morris, R. P. Bernhard, and J. B. Adams (1988) *Lunar and Planetary Science* XIX:780-781. (7) Ming, D. W., R. V. Morris, R. P. Bernhard, and J. B. Adams (1988) *Lunar and Planetary Science* XIX:780-781. (8) Norrish, K. and R. M. taylor (1961) *J. Soil Sci.* 12:294-306. (9). Golden, D. C., R. V. Morris, D. W. Ming, and H. V. Lauer Jr. (1991) *Clays and Clay Minerals* (in preparation). (10). Jackson, M. L. (1974) *Soil Chemical Analysis - Advanced Course*. published by the author. (11) Morris, R. V., and H. V. Lauer, Jr. (1990) *J. G. R.* 95:5101-5109. (12). Morris, R. V., H. V. Lauer Jr., C. A. Lawson, E. K. Gibson, Jr., G. Nace, and C. Stewart (1985) *J. G. R.* 90(B4):3126-3144.

Styles of Crater Gradation in Southern Ismenius Lacus, Mars: Clues from Meteor Crater, Arizona; J.A. Grant and P.H. Schultz, Brown University, Providence, RI 02912.

Introduction: Impact craters on the Earth and Mars provide a unique opportunity to quantify the gradational evolution of instantaneously created landforms in a variety of geologic settings. Unlike most landforms, the initial morphology associated with impact craters on both planets is uncomplicated by competition between construction and degradation during formation. Furthermore, pristine morphologies are both well-constrained and similar to a first order. The present study compares styles of gradation at Meteor Crater with those around selected craters (>1–2 km in diameter) in southern Ismenius Lacus (SIL; 30°–35°N, 325°–360°). Emphasis is placed on features visible in images near Landsat TM resolution (30–50 m/pixel) which is available for both areas. In contrast to Mars, vegetation on the Earth can modify gradation, but appears to influence overall rates and styles by 2X–3X rather than orders of magnitude. Future studies of additional craters in differing settings will refine the effects of this and other factors (e.g. substrate). Finally, by analogy with results from other terrestrial gradational surfaces (e.g.1) this study should help provide constraints on climate over crater histories.

Meteor Crater: Fluvial erosion currently accounts for approximately 1/2–2/3 primary ejecta erosion around Meteor Crater with eolian activity representing 1/3 primary denudation (2,3). Fluvial activity results in slope wash of fragments both into the crater along incised relict debris chutes and away from the rim through small radial gullies. Although specific source regions for individual alluvial fans and areas of more distal, diffuse drainage surrounding the crater are difficult to constrain, most gullies supplying lower flank deposits head in mid/upper flank locations. Therefore, the efficiency of fluvial erosion increases towards the rim-crest. Mapped drainage densities inside and outside the crater are 13.7 km/km^2 and 8.6 km/km^2, respectively; however, the small scale of gullies on the crater exterior precludes detection in Landsat imagery. By contrast, the location of many interior wall drainages within debris chutes results in exaggerated cross-sections and a drainage density of 4.3 km/km^2 at TM resolution. The smaller size and resultant lower apparent density of the exterior drainages likely reflects the lesser gradients and high infiltration capacity of the ejecta. Diffuse drainages are discerned around the crater in TM coverage; however, deposits are not visibly associated with gullies. Detection may reflect the multi-spectral image properties and/or vegetation changes.

Areas of fluvial incisement versus deposition at Meteor Crater remain controlled by ejecta topography and local gradients created during the impact. Hence, first-order styles of fluvial activity in and around the crater are gradient dependent: comparable morphology might be expected to evolve around other, larger and/or complex craters in areas of similar gradient and discharge.

Eolian activity at Meteor Crater causes considerable deflation off exposed ejecta surfaces and contributes to formation of deposits covering the crater floor and a patchy, but prominent windstreak northeast of the crater. Secondary eolian transport of a significant fraction of alluvial and colluvial deposits around the crater results in an overall dominance by eolian activity in gradation: only ~50–60% of the original alluvial/colluvial deposits remain in primary sinks.

A paucity of characteristic groundwater sapping morphology at Meteor Crater, coupled with the relatively large volume of alluvial deposits versus incised channel volume, indicates drainages are dominated by runoff from within their basins. In addition, the moderate hydrologic properties of the ejecta (hydraulic conductivity 7–9 m/day, fairly homogeneous grain-size properties) and the probable fractured nature of the country rocks due to the impact decreases the likelihood of subsurface aquitards. Hence, wetter than present conditions are likely to increase infiltration depths, but not increase the minimal role of sapping in erosion.

Mass-wasting played an important role in early modification of crater walls as evidenced by relict talus/debris chutes and continues to facilitate transport from high gradient, near-rim localities (4).

Southern Ismenius Lacus: Craters within SIL display a range of gradational morphologies largely evolved during discrete epochs of enhanced geomorphic activity in Noachian and Hesperian times (5). Many characteristics around the martian craters differ from those observed at Meteor Crater.

For example, ~25% of the craters lack raised-rims (raised-rim around <50% of crater) yet in many cases retain identifiable, but subtle ejecta deposits. The drainage density of valley networks within and around craters in the region is much lower than at Meteor Crater. Values range from 0.12 km/km² to 0.85 km/km² and between 0.13 km/km² to 0.36 km/km², for the 110 km diameter crater Cerulli (32°N; 338°W) and a ~30 km diameter crater at 34°N; 357°W, respectively. The partially buried or inverted relief appearance of some valley systems (e.g. in and around Cerulli) suggests original densities were slightly higher. Clear examples of alluvial deposits are rare and usually quite small. Deposits comparable to alluvial fans and diffuse drainages at Meteor Crater are not observed.

Eolian signatures also vary from those at Meteor Crater: prominent crater-associated windstreaks are rare, whereas many examples of partially filled craters occur (especially in eastern sections) whose primary features are subdued by remnants of air-fall deposits (5). Although air-fall deposits were emplaced during a late epoch of Hesperian gradation (5), mantling alone cannot account for the evolution of craters without raised rims (6,7). However, accelerated partial erosion of air-fall deposits on crater walls and rim-crests could smooth topography and produce rimless morphologies.

Some craters in SIL are obviously modified by mass-wasting with rare examples of both catastrophic wall failure and possible talus deposits/debris chutes observable (e.g. 33°N, 360°W). Because mass-wasting deposits in the form of landslides and/or debris flows are not easily associated with all craters, they must be either reworked, removed, or masked if the process is important in overall gradation. Relatively low drainage densities on crater walls indicates that fluvial redistribution of material is unrealistic. Several surface characteristics, such as low regional thermal inertia and proximity to fine-grained deposits in Arabia (8) suggest the substrate in SIL contains abundant fine-grained sediment (2); hence, eolian redistribution of fine-grained landslide/debris flow material might mask their identity. Maintenance of wall slopes at the angle of repose (27°-30°) throughout degradation supports inferences that sustained mass-wasting contributes to raised-rim removal.

Discussion: Based on the scale of preserved morphology at Meteor Crater, actual contributions to the overall gradational signature by fluvial processes might be missed at TM resolution during the early stages of erosion. Even when alluvial deposits such as the diffuse drainages at Meteor Crater are detected, their fluvial origin may not be obvious. Hence, a minimal fluvial signature at 30-50 m/pixel resolution around craters with preserved raised rims may not preclude a significant fluvial component in erosion, but may simply reflect a relatively well preserved crater (in the absence of features diagnostic of gradation by alternative processes). At Meteor Crater, the actual role of fluvial processes is best reflected in the density of interior wall gullies due to their exaggerated cross-sections. Because such fluvial enlargement of mass-wasting deposits might not characterize early gradation in all environments, an absence of these features may not rule out significant fluvial activity, but rather reflect development of drainages whose scale is unresolvable.

However, low drainage densities in and around rimless craters in SIL together with a paucity of recognizeable fluvial depositional features analogous to those at Meteor Crater demonstrates that fluvial processes were secondary to eolian deposition/deflation and/or mass-wasting in evolution of the current morphologies. Although possibly important prior to Hesperian times, fluvial activity since that period is limited by an absence of high magnitude precipitation events or groundwater release. By analogy with ejecta properies at Meteor Crater, martian ejecta/regolith deposits may possess moderate hydraulic conductivity and high infiltration capacity that further inhibit more recent fluviation.

References: (1) McFadden, L.D., Ritter, J.B. and Wells, S.G., 1989: *Quaternary Research*, v. 32, p. 276-290. (2) Grant, J.A., 1990: Ph.D. Dissertation: Geology, Brown University, Providence, Rhode Island, 401p. (3) Grant, J.A. and Schultz, P.H., 1991: submitted to *G.S.A. Bulletin*. (4) Shoemaker, E.M. and Kieffer, S.E. 1974: Arizona State University Center for Meteorite Studies Pulication 17, Tempe, AZ., 66p. (5) Grant, J.A. and Schultz, P.H., 1991: p. 485-486, in Lunar and Planet. Sci. XXII (abstracts), Lunar and Planetary Institute, Houston, Texas. (6) Zimbelman, J. and Greeley, R., 1981: p. 1233-1235, in Lunar and Planet. Sci. XII (abstracts), Lunar and Planetary Institute, Houston, Texas. (7) Craddock, R.A. and Maxwell, T.A., 1990: *Jour Geophys. Research*, v. **95**, p. 14,265-14,278. (8) Schultz, P.H. and Lutz, A.B., 1988: *Icarus*, v. 73, p. 91-141.

MAGMATIC INTRUSIONS AND HYDROTHERMAL SYSTEMS ON MARS. V.C. Gulick, Departments of Geosciences and Planetary Sciences, University of Arizona, Tucson, AZ 85721.

We are continuing our investigation of martian hydrothermal systems and the formation of fluvial valleys on Mars. Fluvial valleys formed on geologic features (*e.g.*, volcanoes, impact craters) and in regions (*e.g.*, intercrater plains) which would have developed vigorous hydrothermal systems in the presence of a permeable, water-rich subsurface [1]. Because the degree and nature of valley development in these regions appear to correlate with the magnitude and duration of the associated hydrothermal system [2] and because numerous fluvial landforms on Mars (*e.g.*, outflow channels) imply a subsurface water source [3], martian valleys might have formed from an endogenically derived hydrologic cycle [4]. Here we present our initial numerical modeling results of hydrothermal systems associated with magmatic intrusions on Mars.

To model such hydrothermal systems, we consider single, cylindrical intrusions of height 4 km emplaced 2 km beneath the martian surface. The modeled region extends to a distance, R, 20 times the radius of the intrusion, r_i. The intrusion is surrounded by a homogeneous, water-saturated medium having a porosity of 0.25. The intrusion is emplaced at time t = 0. Temperature and heat flow boundary conditions at the perimeter of the intrusion are derived from conductive cooling calculations [5]. We assume the magma has an initial temperature of 1100°C which is a typical temperature for basaltic magmas. The background geothermal gradient is neglected and an initial ground-water temperature of 0°C is assumed. Ground water is held at hydrostatic pressure along a permeable boundary at r = R.

The hydrothermal system was modeled using a cylindrical grid with a central cavity for the intrusion. We assumed that the intrusion itself remains impermeable and that conductive cooling is not appreciably affected by the surrounding hydrothermal systems until late in the lifetime of the system. These assumptions are validated by studies of terrestrial hydrothermal systems [6]. The finite-element, density-dependent ground-water flow simulation model SUTRA (Saturated-Unsaturated Transport) [7] is then employed to model the resulting ground-water flow and energy transport. We have replaced SUTRA's simplified treatment of the water properties with an accurate equation of state for H2O [8]. Stability of the numerical solution is preserved by restricting the size of the time step to less than the size of the cell divided by the maximum velocity, $\Delta t \leq \Delta z / |v_{max}|$.

Heat enters the system across the inner boundary with a time variation determined by a conductive cooling model. Water is allowed to flow into the system along the outside (right) boundary and allowed to flow into or out of the top boundary. The bottom boundary is impermeable to fluid flow as is the left or inner boundary. The inner boundary is conductive.

Our numerical modeling results reveal that significant quantities of water can be discharged to the surface over the lifetime of the hydrothermal system. In general, the larger the intrusion and the more permeable the subsurface, the larger the volume of the discharged water. The following graphs illustrate the preliminary results of our modeling of hydrothermal systems associated with martian volcanoes. Figures 1 a,b,c are temperature contours of a rising hydrothermal plume produced by a 50 km^3 intrusion of magma. The grid is assumed to lie in an infinite ground-water reservoir. Peak discharges are reached at about 27,000 years after the intrusion, yet discharge continues for approximately 100,000 years. Figure 1d illustrates the rising plume of hydrothermal water and the fluid flow field induced by the thermal anomaly, assuming there is no confining layer at the surface. The longest vectors represent a velocity of 10 m/year.

Figure 2a illustrates the flow field when an impermeable cap is added to the top right-hand side of the model. Total discharge is unaffected but replenishment of the aquifer by surface water is inhibited. Note that if this impermeable layer were an ice-rich permafrost, then any layer which was not melted by the initial emplacement of the magmatic intrusion would eventually be melted by the upward moving hydrothermal waters. Figure 2b illustrates the situation where multiple impermeable layers are present. The upper layer extends only a short distance, while the lower layer extends to the end of the modeled region. In this case, hydrothermal fluids can become 'perched' on the lower less permeable layer, flow around the upper layer and produce surface discharge farther down the flank of the volcano than in the homogeneous models (c). In this model, up to a third of the total discharge finds egress to the surface farther down the flank. Such geometry may be applicable to Alba Patera where the fluvial valleys begin a significant distance down the volcano's flank.

Figure 2d illustrates the total surficial discharge of a hydrothermal system associated with a 500 km^3 intrusion. The curves illustrate the dependence of discharge on the permeability of the system. Permeabilities of terrestrial basalts lie in this range. Megaregolith is thought to have a permeability of approximately 3000 darcies

[9]. The dashed, horizontal lines illustrate the rainfall rates over the same discharge region on the Hawaiian volcanoes. Ha and Hl refer to the average and leeward (dry side) rainfall rates, respectively, on Hawaii. The lengths of these lines show the approximate age of the Hawaiian valleys (*i.e.,* Mauna Kea volcano).

Our preliminary results of modeling hydrothermal systems associated with magmatic intrusions in the martian environment suggest that such systems, if associated with intrusions of several 10^2 km^3 or larger, in the presence of a permeable, water-rich subsurface should be able to provide adequate discharges of water over the time periods needed to form fluvial valleys. However, it is important to note that the amount of water ultimately available for erosion also depends on surface and subsurface lithology, water temperature, mineral concentration of the water, and atmospheric pressure.

References: [1] Gulick, V.C. et al.,1988, *LPSC* **XIX**, 441-442. [2] Gulick, V.C. and Baker, V.R., 1989, *LPSC* **XX**, 364-370. [3] Baker, V.R., 1982, *Channels of Mars* (Austin: Univ. of Texas Press). [4] Baker V.R. et al., in press, Mars Conference 1989 book chapter (Univ. of Arizona Press). [5] Jaeger, J.S., 1968, in *Basalts* (eds. H.H. Hess and A. Poldervaart), 503-536. [6] Norton, D. 1984 *Ann. Rev. Earth and Planet. Sci.* **12**, 155-178. [7] Voss, C.I., 1984, *U.S. Geol. Surv. Report* 84-4369. [8] Johnson, J.W. 1987, PhD. thesis (Univ. of Arizona). [9] Carr, M.H. 1979, *JGR* **84**, 2995-3007.

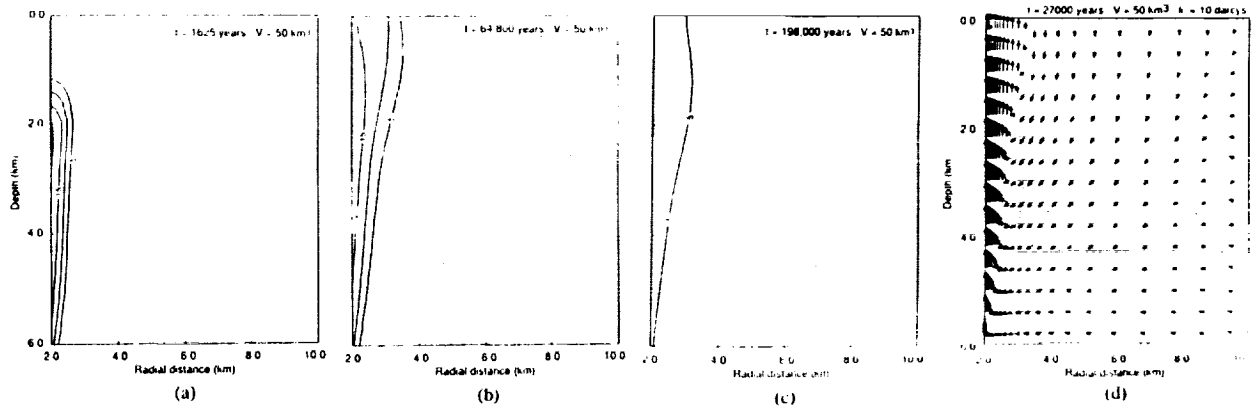

Figure 1

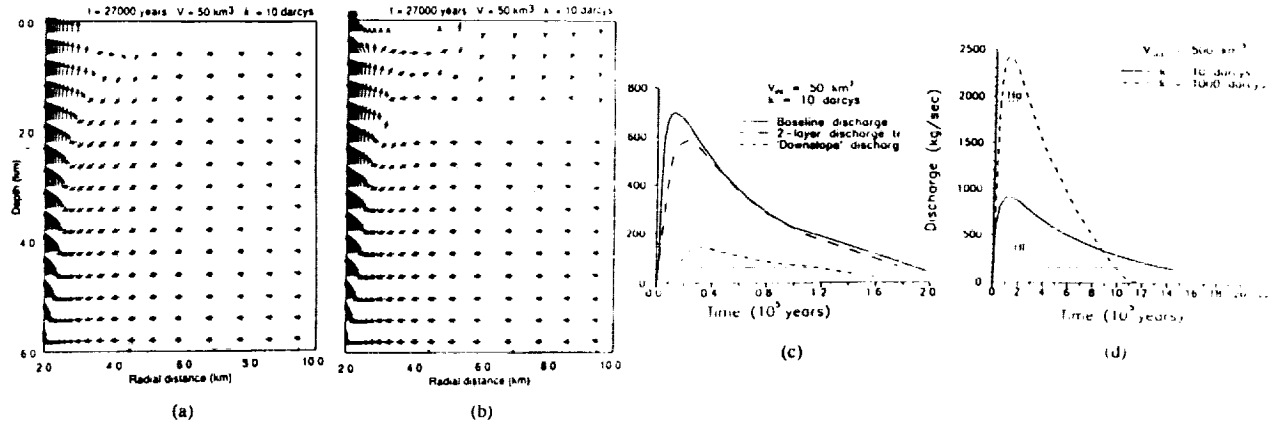

Figure 2

MARS: WAVELENGTH-DEPENDENT DUAL POLARIZATION GLOBAL SCATTERING; J. K Harmon, *NAIC, Arecibo, PR*, M. A. Slade*, *JPL/Caltech, Pasadena, CA*, and R. S. Hudson, *Washington State University, Pullman, WA*

During the 1988 and 1990 Mars oppositions, the first continuous-wave (CW) multi-wavelength radar observations were performed that include the entire echo in both polarizations. These observations, coordinated in subradar coverage when possible, were made with the Arecibo S-band (12.6 cm λ) and Goldstone X-band (3.5 cm λ) facilities. The CW spectra obtained during these oppositions have been studied using a variety of techniques to explore the spatial and wavelength dependence of both the Same-sense Circular (SC) and Opposite-sense Circular (OC) polarization returns. In addition to the Doppler tracking technique of Harmon *et al.* (1982) and Harmon and Ostro (1985), "Doppler imaging" techniques (Hudson and Ostro, 1990) have been used to construct SC ("depolarized") maps at the two wavelengths under various assumptions about the scattering law for depolarized echoes.

Earlier multi-wavelength comparisons (e.g., Simpson *et al.*[1977]; Downs *et al.* [1978]) dealt primarily with the quasispecular component of the echoes. Our work in contrast has much new information (at high signal-to-noise) for the SC "depolarized" component. The unique value of these radar observations lies in their potential for probing the subsurface scattering behavior in "appropriate" terrain. The clearest case for wavelength dependence in the SC component is the scattering behavior over Tharsis, where the X-band features are significantly weaker than the S-band features. This result supports the hypothesis by Christensen (1986) that the (apparently) rough scattering surfaces on Tharsis are mantled by a dust layer. This hypothesis was advanced to account for the low thermal inertia of Tharsis, but also can explain the S/X differences if the layer is about 40 cm. thick (assuming a conductivity of typical dry terrestrial soils). The presence of dust or ash in the "Stealth" region identified in the VLA Mars radar images to the west of Tharsis has been suggested also by Muhleman *et al.* (1991). Comparisons of the S-band CW maps of Stealth with the X-band VLA results and X-band CW maps will be presented which appear to fit into this same general scenario of deposits of layers of fines connected with the Tharsis volcano complex.

In contrast to the Tharsis results, the depolarized echo from the heavily cratered terrain is actually stronger at X-band. The obvious interpretation is that more scatterers exist at the scale of the shorter wavelength, either at the surface or as distributed subsurface scatterers.

The strongest depolarized feature of the X-band spectra is associated with the south residual polar cap. The radar cross section of this feature corresponds to an equivalent full-disk albedo of unity (assuming that it is a Lambert scatterer).

Other features of interest that will be discussed in the poster are results from CW maps and Doppler tracking covering the Amazonis and Elysium regions.

REFERENCES: Christensen, P.R. (1986). Regional dust deposits on Mars: Physical properties, age, and history. *J. Geophys. Res.*, *91*, 3533-3545. Downs, G. S., R. R. Green, and P. E. Reichley (1978). Radar studies of the Martian surface at centimeter wavelengths: The 1975 opposition. *Icarus*, *33*, 441-453. Harmon, J. K., D. B. Campbell, and S. J. Ostro (1982). Dual-polarization radar observations of Mars: Tharsis and environs. *Icarus*, *52*, 171-187. Harmon, J. K., and S. J. Ostro (1985). Mars: Dual-polarization radar observation with extended coverage. *Icarus*, *62*, 110-128. Hudson, R. S., and S.J. Ostro (1990). Doppler-radar imaging of spherical planetary surfaces. *J. Geophys. Res.*, *95*, 10947-10963. Muhleman, D.O., A. W. Grossman, B. Butler, and M. A. Slade. accepted by *Science*, August, 1991. Radar Images of Mars. Simpson, R. A., G. L. Tyler, and B. J. Lipa (1977). Mars surface properties observed by earth-based radar at 70-, 12.5- and 3.8-cm wavelengths. *Icarus*, *32*, 147-167.

The National Astronomy and Ionospheric Center (Arecibo Observatory) is operated by Cornell University under a cooperative agreement with the National Science Foundation and with support from the National Aeronautics and Space Administration. The work at the Jet Propulsion Laboratory was carried out under a contract with the National Aeronautics and Space Administration.

*presenter

The stable isotopic compositions of indigenous carbon-bearing components in EETA 79001. Hartmetz C.P., Wright I.P., Pillinger C.T. Planetary Sciences Unit, The Open University, Milton Keynes MK7-6AA, England.

It is now widely accepted that the most likely source of SNC meteorites is Mars. An oblique impact on Mars, or vaporization of permafrost, by an impactor seem to be the most likely ejection mechanisms capable of accelerating material to the 5 km/s velocity needed to overcome the gravitational field of Mars (1). These ejection mechanisms involve a large shock event and in the SNC class, the shergottites EETA 79001 and ALHA 77055 are the most heavily shocked samples, in which whole-rock pressures of 35-45 GPa have been estimated (2,3). In addition, discontinuities, possibly vugs, caused localized pressures above 80 GPa and this ultimately formed pockets of glass. This glass contains shock-implanted gases with noble gas, nitrogen, and carbon isotopic compositions (4,5,6) similar to the martian atmosphere as measured by the Viking spacecraft. Precisely determining the isotopic abundances of trapped atmospheric components in EETA 79001 has proved useful in modelling Mars' atmospheric evolution (7).

Also of great interest is constraining the carbon isotopic composition of the martian mantle. Because EETA 79001 is basaltic it is possible that by determining the isotopic abundance of magmatic carbon we can extrapolate this value to the carbon composition of the martian mantle.

Martian weathering products have also been identified in EETA 79001. Two types of Ca-carbonate have been recognized in the Antarctic shergottite EETA 79001 (8). The first, dubbed "white druse", was discovered in the sample's interior at the lithology A/C boundary. Druse has been described alternatively as a magnesium-rich granular calcite that contains dissolved phosphorus, or calcite with intergrown magnesium-bearing phosphate. Analyses of druse has shown that it decrepitates from 400°-800° C; carbon and oxygen isotopic abundances were also determined ($\delta^{13}C = +8.9‰$, $\delta^{18}O = +21‰$) that are inconsistent with the isotopic composition of terrestrial carbonates (9,10). A second type of carbonate in EETA 79001 consists of small anhederal highly fractured grains (10-20μm), trapped within mafic glass and rapidly quenched pyroxene, that are associated with laths and needles of sulfate grains, probably gypsum (8). This textural relationship is compelling evidence for the existence of these salt minerals prior to the event that formed the glass and pyroxene.

Herein, we started a series of analyses of EETA 79001 using a high-sensitivity static mass spectrometer, capable of measuring sub-nanogram quantities of carbon to precisions in $\delta^{13}C$ of ±0.4‰. A typical blank per step of 0.5±0.3ng is observed during stepped heating experiments performed on the extraction line used in conjunction with this instrument. Using high-resolution stepped combustion (25°-100° C steps depending on the amount of carbon released) we have analyzed lithologies A, B, and C along with band saw fines (powdered material left behind after the sample was sawed). These analyses will be used to further constrain martian weathering products (carbonate), trapped atmospheric CO_2, magmatic carbon, and any other indigenous carbonaceous components in EETA 79001. These studies will further enhance our understanding of the geological, weathering, and atmospheric evolution of Mars.

A previous analysis of EETA 79001 (11) reported four carbonaceous components that were thought to be indigenous (present prior to ejection of the samples from Mars). The first is a component released above 350° C, with a measured $\delta^{13}C = -27 \pm 1.5‰$ (calculated at $\delta^{13}C = -33‰$) that could possibly be an organic component (12). The second is a relatively ^{13}C-rich component that is released between 400°-700° C with a maximum measured $\delta^{13}C = +8.9 \pm 1.8‰$, assumed to approach $\delta^{13}C = +15.0‰$, the maximum measured thus far in SNC meteorites. This component has been positively identified as carbonate (a martian weathering product). The third was a relatively light component released at 1000° and 1100° C, with $\delta^{13}C$ between -22 and -27‰, that was

interpreted as magmatic carbon. The fourth is a heavy component released from lithology C at 1200° C, with measured $\delta^{13}C = +15‰$ (calculated at $\delta^{13}C = +36 \pm 10‰$) that is thought to be a shock-implanted sample of the martian atmosphere.

One of the objectives of this new study of EETA 79001 was to try and access the distribution of dispersed carbonate in the meteorite. Previous experiments (11) had already suggested that carbonates could be detected in lithology A samples where they were observed to decrepitate in the 600°-700° C step with an isotopic abundance of $\delta^{13}C = -11‰$. The combustion of isotopically light carbon-bearing components over the same temperature interval causes the observed isotopic value to be somewhat compromised. A re-examination of two splits of lithology A using the refined technique described above gives a different interval of decrepitation but was still unable to allow complete separation of the isotopically light component so $\delta^{13}C$ values of carbonates measured by this technique again remain compromised to some degree. However, the region where the inability to resolve the carbonate release exists is now more clear since further work has shown that the isotopically light component combusts between 350°-750° C (i.e., a similar temperature range as carbonate). Furthermore the $\delta^{13}C$ of this component has now been better constrained at -38‰. An intriguing experiment involves analysis of band saw fines obtained from several saw cuts through all lithologies of EETA 79001. In this case carbonate appears to be released in two components over the temperature range of 450°-700° C: the first decrepitated from 450°-575° C ($\delta^{13}C = -16.1 \pm 1‰$), the other from 600°-700° C ($\delta^{13}C = -12.9 \pm 1‰$). Although the carbon isotopic compositions of these components are compromised by the co-release of light carbon (measured in this sample with $\delta^{13}C = -40.2 \pm 0.8‰$ at 425° C) it is possible that two types of carbonate may have been resolved on the basis of thermal stability.

Contamination of samples with carbon that burns at high-temperature (introduced from a stainless steel mortar and pestle used to crush samples) and the removal of this problem from our later analyses has revealed that the previously reported magmatic carbon component with $\delta^{13}C$ between -22 and -27‰ was affected to some extent by contamination. Recent experiments devoid of this contamination reveal carbon that combusts between 700° and 1000° C which has a $\delta^{13}C$ from -7.4 to -16‰, with all the samples exhibiting a well-defined plateau in $\delta^{13}C$ over the this temperature range. Possible identifications of this component include: 1) graphite or poorly-graphitized carbon, but this has not been identified in SNCs and is expected to combust over a narrower range; 2) magmatic carbon, although this should also be released over a narrower temperature range as their host minerals melt; 3) a heterogeneous mixture of trapped martian atmospheric CO_2 and magmatic carbon, in this case the carbon released gives different isotopic compositions depending on the relative amounts of each component in the various samples. It is currently thought that latter possiblity provides the best explanation, but why the carbon is released over such a broad temperature range remains unknown.

Recent measurements of lithology C confirm that shock-implanted atmospheric CO_2 is released during the 1100°-1200° C step, the most recent measurement of its $\delta^{13}C$ is +27.0‰, which is 12‰ higher than measured previously. Note that this component is accompanied by a large release of SO_2 (~36 ppm) from the decrepitation of sulfate (an indigenous weathering product) which is also trapped within the glass.

References: 1) Nyquist L.E. (1982) Proc. LPSC 13th, Part 1, *J. Geophys. Res.* **88**, suppl., A779-A784. 2) McSween H.Y. and Stöffler D. (1980) *LPS*. XI, 717-719. 3) McSween H.Y. and Jarosewich E. (1983) *GCA* **47**, 1501-1513. 4) Bogard D.D. and Johnson P. (1983) *Science* **221**, 651-654. 5) Becker R.H. and Pepin R.O. (1984) *EPSL* **69**, 225-242. 6) Carr R.H. *et al.*, (1985) *LPS* XVI, suppl. A, 5-6. 7) Nier A.O. *et al.* (1976) *Science* **194**, 68-70. 8) Gooding J.L. *et al.* (1988) *GCA* **52**, 909-915. 9) Wright I.P. *et al.* (1988) *GCA* **52**, 917-924. 10) Clayton R.N. and Mayeda T.K. (1988) *GCA* **52**, 925-927. 11) Wright I.P. *et al.* (1986) *GCA* **50**, 983-991. 12) Wright I.P. *et al.* (1989) *Nature* **340**, 220-222.

GREENHOUSE WARMING BY MINOR GASES ON EARLY MARS; M.N. Heinrich, W.R. Thompson, and C. Sagan, LPS, Cornell Univ.

The early atmospheres of Earth and Mars were non-oxidizing mixtures likely derived from volcanic outgassing of a silicate mantle, with some fraction of the volatiles also contributed by impacting comets and meteorites. Volcanic gases, probably similar to those emitted by deep mantle volcanoes today, were rich in N_2, CO_2, CO, and H_2O, with a few percent of H_2 also present. H_2O and moderate to large amounts of CO_2 dominate "greenhouse" warming on the present-day Earth, while trace species such as CH_4 contribute substantially to the effect by blocking infrared radiance in "windows" where the absorption by H_2O and CO_2 is very low. As on present-day Earth, H_2O and CO_2 were important sources of atmospheric thermal opacity, but with an early solar luminosity less than 70% of today's value additional opacity is required to explain equilibrium temperatures compatible with the uninterrupted presence of Earth oceans and the possible presence of substantial amounts of liquid H_2O on Mars as well.

The composition of the early atmospheres of the terrestrial planets was a function of the rate of volcanic outgassing, the composition of volcanic gases (in turn, a function of the mantle redox state), atmospheric loss (for H_2), photo-, radiation, and other atmospheric chemistry, and (for CO_2 and other species) surface-atmosphere interactions [1]. To investigate the formation of minor species by energetic processes in such atmospheres, we have recently conducted plasma experiments on $N_2/CO/H_2/CO_2$ atmospheres [2]. In these experiments, N_2O, HCN, NCCN, simple aldehydes and other molecules are produced. These species would have resulted from radiation and shock processes acting on the primordial atmospheres of Mars and Earth, and, depending on the (poorly known) magnitude of available energy sources and removal mechanisms, could have existed in steady-state abundances sufficient to affect the spectral properties of the atmosphere. [Although photochemistry alone may not have been the dominant mechanism for the production of trace species, photochemical models [3] do predict that for moderately high CH_4 mole fractions $\sim 5 \times 10^{-4}$ the minor atmospheric species HCN and C_2H_6 could be present at mole fractions as high as $\sim 10^{-6}$ in the early Earth atmosphere, and that a nonnegligible steady state NH_3 abundance would have been maintained by HCN hydrolysis in the oceans.]

Here we investigate the potential of minor atmospheric constituents produced by ultraviolet and auroral chemistry to contribute to the thermal opacity of early Earth and Mars atmospheres. Using a very simple two-stream thermal opacity model, we show for example that HCN at 10 ppm and N_2O at 100 ppm can each block radiation in thermal infrared "windows" sufficiently to increase the surface temperature by 7 K separately, or 14 K together. Small quantities of other species (e.g., small, oxidized organic molecules like alcohols and acids) are also produced in such experiments. Some of these have especially complex infrared spectra and should be further investigated for their potential to help close "windows" in the CO_2+H_2O infrared transmission.

Enhancements of greenhouse warming by minor atmospheric species different from those present in today's atmospheres may have played important roles in the climates of early Mars and Earth. We emphasize that because the suite of energetic processes available to early atmospheres is poorly constrained, and the controls on bulk atmospheric composition are also complex and model-dependent, that the potential of minor species to affect climate should not be overlooked. But in addition to such physical effects, the removal of minor species to oceanic or regolith surface reservoirs allowed both the possibility of complex aqueous organic chemistry, and may have produced organic geochemical residues that have persisted below the oxidation zone of the Martian regolith to the present day.

REFERENCES: [1] Chang S., DesMarais D., Mack R., Miller S.L., and Strathearn G.E. (1983) in *Earth's Earliest Biosphere*,, ed. J.W. Schopf, Princeton Univ. Press, pp. 53–95. [2] Sagan C., Thompson W.R., Brower K., Singh S., and Khare B.N. (1988) *Bull. Amer. Astron. Soc. 20*, 860. [3] Zahnle K. (1986) *J. Geophys. Res. 91*, 2819.

N92-29023

THE MARTIAN POLAR CAPS: STABILITY AND WATER TRANSPORT AT LOW OBLIQUITIES; B.G. Henderson (1,2) and B.M. Jakosky (1,3): (1) Laboratory for Atmospheric and Space Physics, (2) Department of Astrophysical, Planetary and Atmospheric Sciences, and (3) Department of Geological Sciences, University of Colorado, Boulder, CO 80309.

Introduction: The seasonal cycle of water on Mars is regulated by the two polar caps. In the winter hemisphere, the seasonal CO_2 deposit at a temperature near 150 K acts as a cold trap to remove water vapor from the atmosphere. When summer returns, water is pumped back into the atmosphere by a number of mechanisms, including release from the receding CO_2 frost, diffusion from the polar regolith, and sublimation from a water-ice residual cap [1]. These processes drive an exchange of water vapor between the polar caps that helps shape the martian climate. Thus, understanding the behavior of the polar caps is important for interpreting the martian climate both now and at other epochs.

During the year that Viking visited Mars, the two poles had different residual cap compositions, the north being water ice and the south retaining CO_2 frost [2,3]. Significant amounts of water vapor were measured in the atmosphere over the northern summer cap, whereas the southern hemisphere contained amounts closer to the global average during its summer [4,5]. The implication is that the residual caps play a major role in determining the amount of water vapor in the martian atmosphere, at least at the current epoch [6,7].

Mars' obliquity undergoes large variations over 10^5- and 10^6-year time scales [8,9]. As the obliquity decreases, the poles receive less solar energy so that more CO_2 condenses from the atmosphere onto the poles. It has been suggested that permanent CO_2 caps might form at both poles in response to a feedback mechanism existing between the polar cap albedo, the CO_2 pressure, and the dust storm frequency [10]. The year-round presence of the CO_2 deposits would effectively dry out the atmosphere, while diffusion of water from the regolith would be the only source of water vapor to the atmosphere [11,12].

We have reviewed the CO_2 balance at low obliquity taking into account the asymmetries which make the north and south hemispheres different. Our analysis linked with a numerical model of the polar caps leads us to believe that one summertime cap will always lose its CO_2 cover during a martian year, although we cannot predict which cap this will be. We conclude that significant amounts of water vapor will sublime from the exposed cap during summer, and the martian atmosphere will support an active water cycle even at low obliquity.

Martian Hemispheric Asymmetries and the CO_2 Balance at Low Obliquity: A key issue is whether or not both caps can be covered year-round with CO_2 frost at low obliquity. At the current epoch, the south cap stays covered with CO_2 frost all year while the north cap loses its cover to expose a water-ice residual cap beneath. This compositional mismatch is the result of an unequal partitioning of CO_2 between the northern and southern hemispheres. This points to an energy imbalance between the poles, despite the fact that the two receive equal amounts of sunlight over the course of a year. Apparently, the current combination of factors that determines the energy budget at the two poles is asymmetric. Understanding these asymmetries is important for predicting the water cycle both now and at lower obliquities as well.

Mars' orbit is eccentric and varies between 0 and 0.14 over time scales of 10^5 and 10^6 years [8]. The southern hemisphere currently experiences shorter, hotter summers and longer, colder winters. This seasonal asymmetry does not affect the total annual insolation at the poles, but it does it seems to have an effect on the location and the timing of the dust storms [13]. The dust storms have the potential to alter the polar energy balance by affecting both the frost albedo and the solar insolation reaching the surface of the polar caps. The south cap is around 3 or 4 kilometers higher than the north cap [14]. As a result, the CO_2 frost condensation temperature is lower at the south pole than at the north pole. Aver-

aged over a year, CO_2 should preferentially sublime from the south cap and condense onto the north cap. Before Viking, this argument was used to argue against the presence of a permanent CO_2 polar cap at the south pole [15]. Viking showed us a permanent CO_2 cap in the south, which suggests that our understanding of the asymmetries in the system which cause the current CO_2 imbalance is incomplete.

The amount of CO_2 at either pole is determined by a balance between sublimation in the summer and condensation in the winter. As long as the two poles are in energy balance, the CO_2 inventory will be divided up more or less equally between the two polar caps. However, the equilibrium can be upset by the hemispheric asymmetries. If the polar regions are out of energy balance, then CO_2 will be transferred to one pole to make up for the deficit. There is no reason to believe that the two polar regions will be in energy balance over the course of a year, either now or at any other epoch. As long as both caps are trying to equilibrate with the same atmosphere, the asymmetry factors should effect a net CO_2 transfer to one pole, allowing the other cap to be exposed during its summer. Furthermore, this transfer will take place over short enough time periods so that seasonal exposure of a water-ice cap is possible at all epochs, regardless of the obliquity.

Model Description and Results: After the CO_2 migration has taken place, one pole should have a permanent CO_2 cap while the other will have a water-ice cap with a seasonal CO_2 covering during the winter. Once this configuration is achieved, is it stable, or is it just a temporary state? To answer this question, we modeled the energy balance at the poles to determine the stability of the caps at low obliquity. Our model assumes a polar cap in equilibrium with a CO_2 atmosphere and balances incoming solar radiation, outgoing surface thermal emission, subsurface conduction, and latent heat from CO_2 condensation or sublimation at the surface. We ran the model for combinations of obliquity (from 15° to 25°) and thermal inertia (0.01 to 0.05 cal-cm^{-2}-s$^{-1/2}$-K^{-1}) with other physical parameters appropriate for the north and south poles. Our results show that either pole can be stable in a state covered all year with CO_2 frost or in a state that loses its CO_2 cover during the summer to reveal an underlying surface, presumably water ice; this result holds at all obliquities between 15° and 25°. The implication is that once all the CO_2 has migrated to one pole, both the CO_2-covered cap and the water-ice cap are stable in that particular configuration.

Water should sublime to the atmosphere once the water-ice cap is exposed to summer insolation. We calculate the number of exposed days and the total annual water sublimation for the north and south poles individually.

Conclusions: The asymmetries in the martian polar cap system should allow CO_2 transfer to one pole over short enough time periods so that exposure of a water-ice cap is likely at low obliquity. Once this configuration is achieved, both the permanent CO_2 cap at one pole and the seasonally-exposed water-ice cap at the other pole can exist in a stable state. Thus, sublimation and atmospheric transport of water vapor are possible at low obliquities. At an obliquity of 15°, our calculations show that as much as 0.037 mm of water ice will sublime from the surface ice annually. Over a period of 10^5 years, 3 meters of ice could cycle between the caps at this annual rate. Clearly, the martian atmosphere at low obliquity should support an active water cycle and will contain a significant amount of water vapor.

References: [1] Jakosky, B.M. (1985) *Space Sci. Rev.* **41**, 131-200; [2] Kieffer, H.H., S.C. Chase, Jr., T.Z. Martin, E.D. Miner, F.D. Palluconi (1976) *Science* **194**, 1341-1344; [3] Kieffer, H.H. (1979) *J. Geophys. Res.* **84**, 8263-8288; [4] Farmer, C.B., D.W. Davies, D.D. LaPorte (1976) *Science* **194**, 1339-1341; [5] Farmer, C.B. and P.E. Doms (1979) *J. Geophys. Res.* **84**, 2881-2888; [6] Davies, D.W., C.B. Farmer, and D.D. LaPorte (1977) *J. Geophys. Res.* **82**, 3815-3822; [7] Haberle, R.M. and B.M. Jakosky (1990) *J. Geophys. Res.* **95**, 1423-1437; [8] Ward, W.R. (1979) *J. Geophys. Res.* **84**, 237-241; [9] Bills, B.G. (1990) *J. Geophys. Res.* **95**, 14137-14153; [10] Toon, O.B., J.B. Pollack, W. Ward, J.A. Burns, K. Bilski (1980) *Icarus* **44**, 552-607; [11] Ingersoll, A.P. (1974) *J. Geophys. Res.* **79**, 3403-3410; [12] Lindner, B.L. and B.M. Jakosky (1985) *J. Geophys. Res.* **90**, 3435-3440; [13] Zurek, R.W. (1982) *Icarus* **50**, 288-310; [14] U.S. Geological Survey (1989) Topographic map of the polar regions of Mars: U.S. Geological Survey Miscellaneous Investigations Series Map I-2030; [15] Murray, B.C. and M.C. Malin (1973) *Science* **182**, 437-443.

536-91
85105
72
p. 2

IJ5744 50

N92-29024

DARK MATERIAL IN THE POLAR LAYERED DEPOSITS ON MARS; Ken Herkenhoff, Geology and Planetology Section, Jet Propulsion Laboratory 183-501, California Institute of Technology, Pasadena, CA 91109

The Martian polar layered deposits probably record periodic variations in the deposition of dust and ice caused by climate changes over the last 10 to 100 million years or so [1,2]. It is widely believed that water ice is an important constituent of the layered deposits, and that the deposits were formed by eolian processes. The polar layered deposits appear to be the source of dark, saltating material that has been distributed over the surface of Mars, but the mechanisms by which this material is incorporated and eroded from the layered deposits is unknown. These mechanisms must be understood before the processes that formed and modified the layered deposits can be inferred and related to Martian climate changes.

Calculations of the stability of water ice in the polar regions of Mars [3,4] indicate that ice should not currently be present at the surface of the layered deposits. The present water ice sublimation rate is high enough to erode the entire thickness of the deposits in about a million years. This result suggests that sublimation of water ice from the layered deposits results in concentration of non-volatile material at the surface of the deposits. Such a surface layer would insulate underlying water ice from further sublimation, stabilizing the layered deposits against rapid erosion. The existence of a surface layer is consistent with thermal mapping in the south polar region [5], which indicates that the thermal inertia of the surface of the south polar layered deposits is very low.

The color and albedo of the layered deposits suggest that bright, red dust is the major non-volatile component of the deposits. However, the differences in albedo and color between mantling dust and exposures of layered deposits and the association of dark saltating material indicates that there is at least a minor component of dark material in the deposits [6,7]. If the dark material is composed of solid sand-size grains (hereafter called "sand" without compositional implications), poleward circulation is required to transport the sand (by saltation) into the layered deposits [8]. Saltating sand would eject dust into suspension, hindering codeposition of sand and dust. However, sand may have saltated over ice-cemented dust toward the poles at some previous time when winds blew onto the polar caps. In this case, the dark sand must have formed layers or lenses less than a few meters in size, or they would be visible in high-resolution Viking Orbiter images. Alternatively, dark dust (rather than sand) may be intimately mixed with bright dust in the layered deposits.

How can dark dust in the layered deposits form the dunes observed in the polar regions? Sublimation of dust/ice mixtures has been shown to result in the formation of filamentary sublimation residue (FSR) particles of various sizes [9]. Such particles can saltate along the Martian surface, and may therefore create dunes [10,11]. In order to form saltating material that is at least 3 times darker (in red light) than the bright dust that mantles much of Mars, dark dust grains must preferentially form FSR particles. Magnetic dust grains would be expected to form FSR more easily than non-magnetic dust, and are probably much darker. Experimental formation of FSR with magnetic material has not been attempted, and should be the subject of future research.

There is direct evidence for 1-7% magnetic material (magnetite or maghemite) in the surface fines at the Viking lander sites [12]. In addition, analysis of Viking lander sky brightness data indicates that suspended dust over the landing sites contains about 1% opaque phase, perhaps of the same composition as the magnetic material on the surface [12,13]. Within the uncertainties in these measurements, the percentages of magnetic material given above are identical to the volume of dark dune deposits in the polar regions expressed as a percentage of the estimated volume of eroded layered deposits [8,14]. This comparison indicates that the presence of magnetic dust in the layered deposits is likely, and that formation of dunes from dark FSR particles is plausible. Eventual destruction of the particles could allow recycling of the dark dust into the layered deposits via atmospheric suspension. Under the assumption that FSR can be formed by sublimation of mixtures of water ice and magnetic dust, the properties of this material have been estimated and compared with observational data, as detailed below.

Recent studies using Viking IRTM observations of the north polar dunes indicate thermal inertias between 2 and 8 x 10^{-3} cal cm^{-2} $sec^{-1/2}$ K^{-1} [15,16], the observed range perhaps caused by the effects of local dune slopes (D. A. Paige, personal communication, 1991). These results do not include the effects of atmospheric thermal emission, so that the actual thermal inertia of the surface (assuming a typical optical depth of 0.4) is probably about 4 x 10^{-3} [17]. Similarly, the apparent thermal inertias of dune fields elsewhere on Mars (8.0-8.3 x 10^{-3} [18]) correspond to actual thermal inertias near 6 x 10^{-3}. These data will be used below to constrain the properties of dark saltating material on Mars.

Previous interpretations of Martian thermal inertia data in terms of particle sizes have utilized the relationship between these quantities presented by Kieffer *et al.* [19], which is based primarily upon measurements

of the thermal properties of quartz sands [20]. The low albedos of Martian dunes are inconsistent with a siliceous composition, so basalt and magnetite are considered here (the thermal properties of maghemite have not been reported in the literature). The thermal conductivity of basaltic sands is about 3 x 10^{-5} cal cm^{-1} sec^{-1} K^{-1} (~40%) less than that of pure quartz sands of the same size (~100 microns). The thermal conductivity of solid magnetite [21] is identical (within measuremental uncertainties) to that of pure quartzite [22], so the thermal conductivity of magnetite sand is assumed to be the same as that of quartz sand. The thermal conductivities of the materials considered here are only weakly dependent on temperature between 200 and 300 K, so values measured near 300 K have been used in all cases. The density of magnetite is 5.2 g cm^{-3}, almost twice that of quartz (2.65 g cm^{-3}) or basalt (2.68-2.83 g cm^{-3}). The specific heat of magnetite is 0.13 cal g^{-1} K^{-1} at 220 K [21], only slightly less than the specific heat of various silicates [23]. Hence, the observed thermal inertias of mid-latitude dune fields on Mars are consistent with ~100-micron magnetite grains with 30% porosity, or ~150-micron magnetite grains with 47% porosity. Because the size of particles that are most easily moved by Martian winds is only weakly dependent on the ratio of the density of the particle to that of the atmosphere [24], 100-micron magnetite grains should be the first to saltate under Martian conditions.

If the polar dunes are composed purely of basaltic grains, their effective particle size is no greater than about 150 microns (45% porosity). More likely, ground ice is present below the diurnal skin depth with even lower-inertia material at the surface [15]. In any case, low-inertia materials that are capable of saltation must be examined as possible dune-forming materials on Mars. The thermal properties of FSR particles are therefore estimated below.

The porosity of clay FSR formed in laboratory experiments is 99% [9]. Magnetite FSR would therefore have a bulk density of only 0.052 g cm^{-3}. The thermal inertia of porous clay at 313 K, 740 torr ranges from 1.1 to 4.9 x 10^{-3}, depending on water content. The lowest value is identical to that of clay FSR [9]. When this dry clay is placed in a high vacuum, its thermal conductivity decreases only 7%. Therefore, the conductivity of clay FSR at 6 mbar is probably about 10^{-3}. The thermal conductivity of clay *minerals* is probably similar to that of most silicates, about 2.8 times less than the conductivity of magnetite. Hence, magnetite FSR should have a thermal conductivity near 2.8 x 10^{-3}, implying a thermal inertia of 4.3 x 10^{-3}. The thermal inertia of ensembles of FSR particles may be lower still, but generally compatible with the north polar erg thermal inertias derived from Viking data.

In summary, weathering of the Martian layered deposits by sublimation of water ice can account for the geologic relationships observed in the Martian polar regions. The non-volatile component of the layered deposits appears to consist mainly of bright red dust, with small amounts of dark dust or sand. Dark dust, perhaps similar to the magnetic material found at the Viking Lander sites, may preferentially form filamentary residue particles upon weathering of the deposits. Alternatively, dark sand-size basaltic particles may occasionally be transported onto the layered deposits, forming thin layers or lenses. Once eroded, particles of either type may saltate to form the dark dunes found in both polar regions. Both scenarios for the origin and evolution of the dark material within the polar layered deposits are consistent with the available data. Further experimental measurements of the thermophysical properties of magnetite and maghemite under Martian conditions are needed to better test these hypotheses.

REFERENCES

[1] Carr, M. H. (1982). *Icarus* **50**, 129-139. [2] Plaut, J. J., *et al.* (1988). *Icarus* **75**, 357-377. [3] Toon, O. B., *et al.* (1980). *Icarus* **44**, 552-607. [4] Hofstadter, M. D., and B. C. Murray (1990). *Icarus* **84**, 352-361. [5] Paige, D. A., and K. D. Keegan (1991). *Lunar and Planet. Sci.* **XXII**, 1013-1014. [6] Thomas, P. C., and C. Weitz (1989). *Icarus* **81**, 185-215. [7] Herkenhoff, K. E., and B. C. Murray (1990). *J. Geophys. Res.* **95**, 1343-1358. [8] Thomas, P. (1982). *J. Geophys. Res.* **87**, 9999-10008. [9] Storrs, A. D., *et al.* (1988). *Icarus* **76**, 493-512. [10] Saunders, R. S., *et al.* (1985). *NASA Tech. Mem.* **87563**, 300-302. [11] Saunders, R. S., and D. T. Blewett (1987). *Astron. Vestnik* **21**, 181-188. [12] Hargraves, R. B., *et al.* (1979). *J. Geophys. Res.* **84**, 8379-8384. [13] Pollack, J. B., *et al.* (1979). *J. Geophys. Res.* **84**, 4479-4496. [14] Lancaster, N., and R. Greeley (1991). *J. Geophys. Res.* **95**, 10921-10927. [15] Paige, D. A., and H. H. Kieffer (1987). *Tech. Rep.* **87-01**, Lunar and Planet. Inst., Houston, TX, 93-95. [16] Keegan, K. D., *et al.* (1991). *Lunar and Planet. Sci.* **XXII**, 701-702. [17] Haberle, R. M., and B. M. Jakosky (1991). *Icarus* **90**, 187-204. [18] Edgett, K. S., and P. R. Christensen (1991). *Lunar and Planet. Sci.* **XXII**, 335-336. [19] Kieffer, H. H., *et al.* (1973). *J. Geophys. Res.* **78**, 4291-4312. [20] Wechsler, A. E., and P. E. Glaser (1965). *Icarus* **4**, 335-352. [21] Touloukian, Y. S., *et al.* (1970). In "Thermophysical Properties of Matter," vols. 2 and 5, IFI/Plenum, New York. [22] Carte, A. E. (1955). *Am. J. Sci.* **253**, 482-490. [23] Winter, D. F., and J. M. Saari (1969). *Astrophys. J.* **156**, 1135-1151. [24] Iversen, J. D., and B. R. White (1982). *Sedimentology* **29**, 111-119.

MARS ENVIRONMENTAL SURVEY (MESUR): SCIENCE OBJECTIVES AND MISSION DESCRIPTION

G. Scott Hubbard, Paul F. Wercinski, George L. Sarver, Robert P. Hanel, and Ruben Ramos

NASA Ames Research Center
Moffett Field, CA 94035

ABSTRACT

In-situ observations and measurements of Mars are objectives of a feasibility study beginning at the Ames Research Center for a mission called the Mars Environmental SURvey (MESUR). The purpose of the MESUR (pronounced "measure") mission is to emplace a pole-to-pole global distribution of landers on the martian surface to make both short- and long-term observations of the atmosphere and surface. The basic concept is to deploy probes which would directly enter the Mars atmosphere, provide measurements of the upper atmospheric structure, image the local terrain before landing, and survive landing to perform meteorology, seismology, surface imaging, and soil chemistry measurements.

MESUR is intended to be a relatively low-cost mission to advance both Mars science and human presence objectives. Mission philosophy is to (a) "grow" a network over a period of years using a series of launch opportunities, thereby minimizing the peak annual costs; (b) develop a level-of-effort which is flexible and responsive to a broad set of objectives; (c) focus on science while providing a solid basis for human exploration; and (d) minimize project cost and complexity wherever possible.

Building up of the MESUR global network takes place over three launch opportunites using a total of five Delta II launch vehicles. The current MESUR baseline mission profile is a single launch of 4 probes in the 1998/99 opportunity, a dual launch of 4 probes and a communications orbiter in the 2001 opportunity, and a dual launch of 8 probes (4 on each ELV) in 2003. The lander network thus grows from 4 to 8 to 16 stations. Operations for the completed network is designed for at least one Mars year with planned nominal operations ending in 2005.

In order to meet the diverse scientific objectives, the each MESUR lander will carry the following strawman instrument payload consisting of; a) Atmospheric structure experiment, b) Descent and surface imagers, c) Meteorology package, d) Elemental composition instrument, e) 3-axis seismometer, f) Thermal analyzer/evolved gas analyzer.

Engineering features would include long life to support scientific data flow from the completed network, simple entry aeroshells with decelerator parachutes and landing air bags, low average rate data storage and high rate transmission when interrogated, and a small RTG consisting of a re-packaged single General Purpose Heat Source brick.

This feasibility study is primarily to show a practical way to design an early capability for characterizing Mars' surface and atmospheric environment on a global scale. The goals are to answer some of the most urgent questions to advance significantly our scientific knowledge about Mars, and for planning eventual exploration of the planet by robots and humans.

MESUR Mission

NASA Ames Research Center

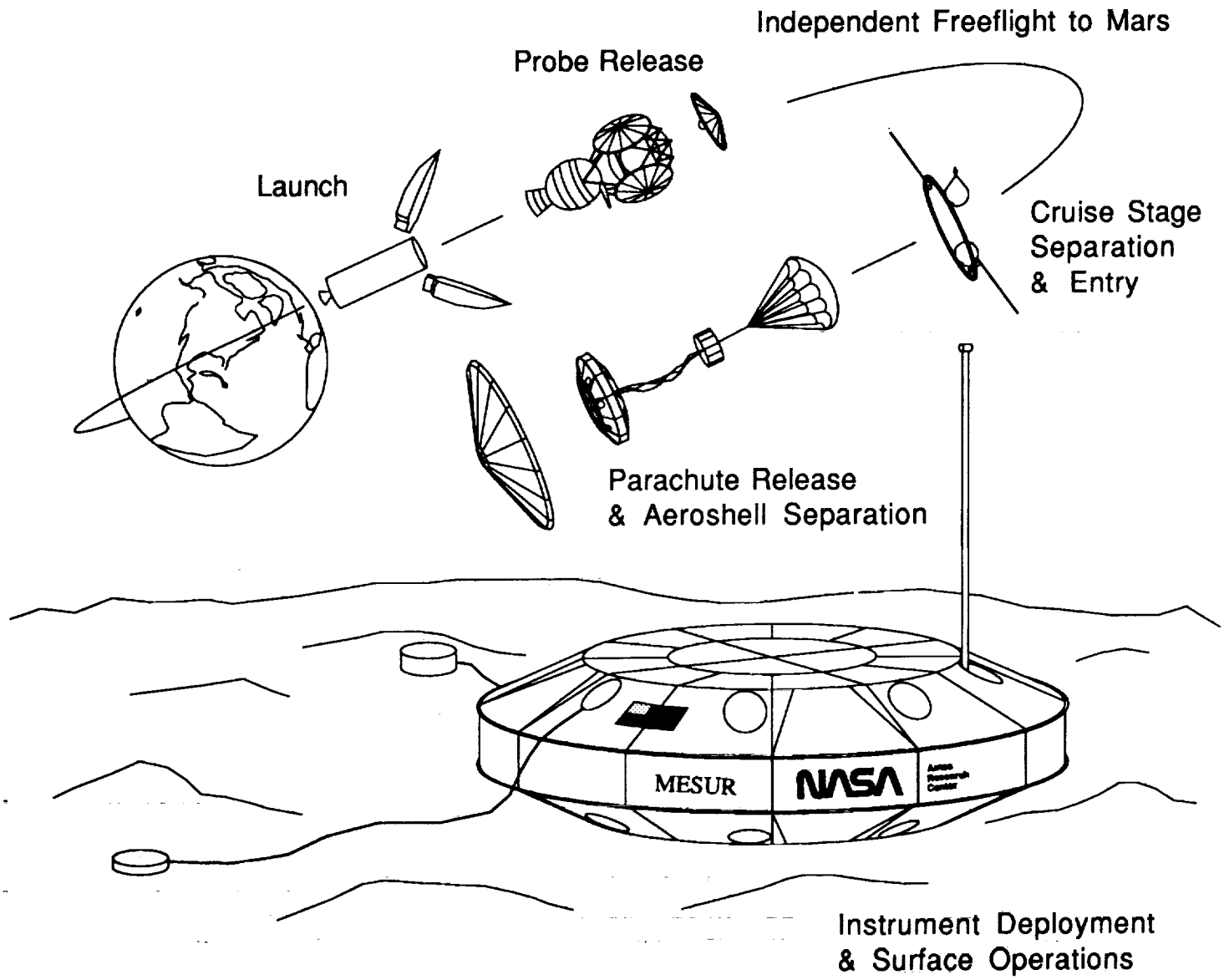

Observations of Mars Using Hubble Space Telescope

Philip B. James, Univ. Toledo, R. Todd Clancy and Steven W. Lee, Univ. Colorado, Ralph Kahn and Richard Zurek, Jet Propulsion Laboratory, Leonard Martin, Lowell Observatory, and Robert Singer, Univ. Arizona.

The lack of a continuous record of martian meteorology or of volatile cycles on Mars for extended periods of several martian years seriously hinders efforts to understand the physics of the martian atmosphere - surface system. The spacecraft observations are limited to only a few isolated time periods, and the earth based record is limited by the relatively short periods surrounding oppositions when telescopic observations can yield useful data. Our incomplete knowledge of the temporal distribution of major dust storm events on Mars is the best known consequence of the lack of such a record, but the situation is much the same for interannual variability in the behavior of surface condensates in the polar regions and for the behaviors of clouds in different years.

To test one possible technique for remedying this situation, we have embarked on a three year program of Mars observations using the Hubble Space Telescope. Although the solar pointing constraint eliminates 45% of the 780 day synodic cycle from possible observation, this is still a great improvement over the two to five months of each cycle (depending on the orbital geometry of the two planets at opposition) that can be profitably be used for earth based observations. During the initial phase of the project we have imaged Mars on five dates in a variety of spectral bands:

Date	Ls	Size	Scale	LCM	Filters
12-13-90	349	16.5"	17.7 km/px	190	890N,673N,588N,502N
				300	439W,336W,230W
				70	
01-02-91	359	13.5"	21.7 km/px	300	673N,413M,FOS
02-07-91	16	9.4"	31.1 km/px	300	673,413,336,230,FOS
03-20-91	35	6.6"	44.3 km/px	300	673N,413M
05-15-91	60	4.8"	60.9 km/px	190	673N,413M
				300	502N,336W,230W
				70	

The Richardson-Lucy algorithm was used to deconvolve the observed images with calculated point spread functions; the actual resolution obtained using this technique is estimated to be about

Preliminary analysis of the images obtained by HST during the five observation sequences has rewarded our optimism. Even at 4.8", details of the albedo boundaries on the surface are clearly resolvable. The images taken in May, when L_s equaled 60^0, clearly reveal the multicomponent "W" clouds in the Tharsis - Valles Marineris region as well as clouds associated with Elysium Mons. They also show the north polar surface cap, which is tilted earthward at this season. The potential scientific

value of these images augurs well for the investigation of the 1992 "classic dust storm" season which will use the similar scale images planned when Mars again emerges from the 50^0 solar interdict.

Several scientific investigations are being conducted using the images, including: a study of the albedo variations on the surface of the planet in the region of Syrtis major; unit mapping of spectral reflectances in the wavelength bands mentioned above; determination of optical depths due to aerosols and condensates; a study of the properties of condensate clouds and hoods; comparison of surface and atmospheric features observed by HST to the historical data base of terrestrial observations at the same season; observation of the size and shape of surface polar caps; and investigation of surface and atmospheric phenomena revealed by WFPC imaging in the ultraviolet portion of the spectrum and by spectral maps derived from FOS scans of the planet.

The ultraviolet imaging capabilities of HST provide a unique opportunity to study the surface and atmosphere of Mars in this relatively unexploited wavelength region. In particular, the strong ozone absorption near 230 nm makes it possible to map ozone concentration through differencing the 230 and 336 nm images. Preliminary use of this method reveals strong ozone absorption in the north polar region during late winter, as expected from the low water vapor content in the atmosphere at that time, and reveals other interesting correlations with various topographic and surface features. The differencing technique will be verified and calibrated using spectral scans of the planet in the ultra violet portion of the spectrum using the Faint Object Spectrograph (FOS); the latter data have been inspected to verify that signal to noise is as expected, but detailed analysis of those data has not yet been undertaken.

The preliminary data have firmly established that the deconvolved images of Mars will be sufficient to attain the scientific objectives of the program: even the smallest, May images are comparable in detail to Planetary Patrol photography during average oppositions. HST's Cycle 2 will encompass a major portion of the next dust storm season, and frequent monitoring of the planet has been proposed for that period. That Cycle will also afford the opportunity of revisiting the same seasons imaged during the last few months in order to search for existence and causes of interannual variability. Cycle 2 will provide monitoring of Mars leading into the Mars Observer Mission. We hope that, using the new instrumentation to be installed on HST in 1993, it will be possible to make observations which will complement the experiments to be conducted on that mission.

DISTRIBUTION OF WATER ON MARS: IMPLICATIONS FROM SNC METEORITES.

J.H. Jones, SN2, NASA/JSC, Houston, TX 77058.

There has been much speculation about the abundance of water and other volatiles on Mars. The geomorphologic evidence from Viking for widespread fluvial activity on Mars is compelling (e.g., Carr, 1987). Carr (1987) felt that the *minimum* amount of water on Mars (presented in units of depth of a hypothetical martian ocean) was ~500 m. Attempts to calculate abundances of water on Mars, using SNC meteorites as guides [e.g., Bogard (1987); Dreibus and Wänke (1987)], indicate that Mars should contain ~10-100 m of water.

Cooperative studies (Carr and Wänke, 1991) have suggested that water was effectively added as a late veneer. Water and metal tend to react to produce FeO. In the Carr and Wänke (1991) model, Mars remained dry until core formation was completed and that later-accreted water remained unreacted. Similar models have been proposed for the Earth (Jones, 1987; Ahrens, 1990). Finally, Greeley (1987) has used rates of basaltic volcanism on Mars, coupled with water contents of terrestrial basalts, to estimate total crustal water and its secular change. This type of analysis yields estimates of >~10 m of water.

Early Depletion of the Martian Mantle. There is abundant isotopic evidence from SNC meteorites to indicate that the martian mantle has been depleted since very early times. For example, Jones (1989) showed that a single well-mixed mantle that was depleted at ~4.5 Æ could be tapped at 1.25 Æ to produce the nakhlites and Chassigny and tapped again at 180 m.y. to produce the more mafic shergottites. In the Jones (1989) model, the more fractionated shergottites, Shergotty and Zagami, were produced by interaction of more primitive, mafic magmas with the martian crust.

Corroborating evidence for this simple model was found in the SNC Xe data (Jones, 1989). One SNC, EETA79001 contains Xe that is isotopically identical to the martian atmosphere, whereas the Xe isotopes of Chassigny are in solar proportions, which are quite different. Also, Chassigny does not have an ^{129}Xe anomaly, whereas martian air does. This is important because ^{129}Xe is produced from the decay of ^{129}I, which has a half-life of ~16 m.y. Apparently, the martian mantle was degassed of I [which is more incompatible than Xe (Musselwhite et al., 1990)] on the same timescale as the half-life of ^{129}I.

The recent data of Nyquist et al. (1991) have shown this model to be correct in some aspects and too simple in others. The nakhlite source region apparently was depleted very early because nakhlites have a ^{142}Nd anomaly from now-extinct ^{146}Sm ($t_{1/2}$ = ~100 m.y.). A complication to the model is that the most mafic shergottites do not have this anomaly and, therefore, their source region(s) must have differentiated later (Nyquist et al., 1991). However, it was already known on the basis of Pb isotopes that the model was somewhat oversimplified (Jones, 1989). A more realistic model would be for Mars to have outgassed incompatible atmophile elements and perhaps extremely incompatible elements very early, with subsequent removal of more-compatible elements from the mantle during the first 500 m.y. of martian history.

WATER ON MARS

J.H. Jones

Water on Mars. What does this model imply for the history of water on Mars? Water acts incompatibly during silicate partial melting. If U, Th, Rb and the LREE are depleted in the source regions of martian magmas, water should be depleted as well. Taken at face value, this observation indicates that, regardless of whether water-metal reactions were important during early martian history (they probably are), water budgets calculated from SNC meteorites are likely to be in error, because SNC's come from depleted source regions. Unlike the Earth, Mars apparently does not have subduction and plate tectonics to transport water to the mantle. Therefore, the surface of Mars could have been "wet," whereas the mantle remained "dry."

If this conclusion is correct there are some interesting consequences:

(i) The model put forth for the abundance of water on Mars by Dreibus and Wänke (1987) cannot easily be correct. Incompatible elements such as Br and Cl [that are used in the Dreibus and Wänke (1987) calculation] may follow water during martian magmatic processes in only a general way. For example, both halogens and water may be concentrated into the first melt from a mantle source. However, there is no guarantee that these elemental ratios will not be fractionated in the residuum. Unless, Br and Cl follow water exactly the Dreibus and Wänke (1987) model is likely to be in error.

(ii) The model of Greeley (1987) is also unlikely to be correct, because most of the water was outgassed early and degassing rates are probably not proportional to rates of volcanism.

Caveat. There is evidence against the model presented above. Johnson et al. (1991) infer that the Chassigny parent magma contained > 1.5 wt.% water and that the martian mantle contained >1000 ppm water. This is a lot of water for a depleted source region. Unlike the other estimates of martian water, the Johnson et al. (1991) value comes from experiments designed to constrain the stability field of the kaersutite (an amphibole) found in Chassigny. Perhaps some of the water in Chassigny was assimilated at shallow depths, either in a crustal magma chamber or by interaction with surficial permafrost. Either is possible and provides an alternative to the dilemma of water-rich, depleted source regions. Stable isotopic evidence may further constrain the origin of SNC water (Watson et al., 1991; Karlsson et al., 1991).

References. Ahrens T.J. (1990) In *Origin of the Earth* (Newsom and Jones, Eds.). pp. 211-227. Bogard D.D. (1987) In *Workshop on Mars Sample Return Science* (M.J. Drake et al., eds.) LPI Tech. Rpt. 88-07. pp. 41-42. Carr M. and Wänke H. (1991) *Lunar and Planetary Science XXII.* pp. 181-182. Dreibus G. and Wänke H. (1987) *Lunar and Planet. Sci. XVIII.* pp. 248-249. Greeley R. (1987) In *Symposium on Mars: Evolution of its Climate and Atmosphere* (V. Baker er al., eds.). pp. 40-42. LPI Tech Rpt. 86-01. Johnson M.C., Rutherford M.J. and Hess P.C. (1991) *Geochim. Cosmochim. Acta* **55**, 349-366. Jones J.H. (1989) *Proc. Lunar Planet. Sci. Conf. 19th.* pp. 465-474. Karlsson H., Clayton R.N., Gibson E.K., Mayeda T.K., and Socki R.A. (1991) *Meteoritics.* Submitted. Musselwhite D.S., Drake M.J. and Swindle T.D. (1990) *Lunar and Planet. Sci. XXI.* pp 833-834. Nyquist L.E., Harper C.L., Wiesmann H., Bansal B., and Shih C.-Y. (1991) *Meteoritics.* Submitted. Watson L.L., Ihinger P.D., Epstein S. and Stolper E.M. (1991) *Lunar and Planet. Sci. XXII.* pp 1473-1474.

A LIQUIDUS PHASE DIAGRAM FOR THE GROUNDMASS OF EETA79001A (Eg), A PRIMITIVE SHERGOTTITE COMPOSITION. J.H. Jones, SN2, NASA-JSC, Houston, TX 77058; A.J.G. Jurewicz and L. Le, Lockheed ESC, C23, 2400 NASA Rd. 1, Houston, TX 77058.

Introduction. Shergottites are members of the SNC meteorite suite, which may be samples of Mars. If so, the shergottite in our collection that most likely represents primitive liquid from the Martian mantle is EETA79001. EETA79001 has the Nd isotopic signature of a long-term depleted mantle [1], a relatively high Mg# [2], and a slightly olivine-normative composition [2]. In addition, unlike the other SNC's, EETA79001 is not a cumulate [3].

EETA79001A groundmass. Actually, these primitive characteristics do not universally apply to the EETA79001 whole-rock, an assemblage of lithologies, but specifically to the groundmass of a particular lithology, EETA79001A. EETA79001A is composed of a fine-grained groundmass and hartzburgitic xenoliths. The groundmass composition has been estimated by both [3] and [2].

To explore the phase relations for Eg, and also to see if there is any relationship between "primitive" shergottites such as Eg and "evolved" shergottites such as Shergotty and Zagami, we have performed experiments on an Eg composition. The two estimates for the Eg composition, McSween and Jarosewich [3] and Longhi and Pan [2], primarily differ in that the McSween and Jarosewich composition is richer in olivine. Our experiments use [2]. However, because olivine is the liquidus phase and our melts remain olivine saturated, these experiments should also apply for the McSween and Jarosewich composition [3] below 1300°C, the liquidus of Eg [2].

Experimental. Synthetic Eg glass was prepared by fusing an oxide-carbonate mix. Excess iron (2.4 wt% Fe_2O_3) was added to correct for iron loss to Pt. Charges were homogenized at 1350°C under flowing CO/CO_2 (QFM) at near one bar pressure for about 12 hours and then equilibrated isothermally. Run temperatures ranged from 1300 to 1100°C (QFM), at ~25°C intervals. Run durations ranged from about 12 hours to four days: the short times minimized volatile loss. Iron loss was not observed: FeO mass balances were 0.3 wt% (1.5% relative) at 1250°C, and 0.6 wt% (3% relative) at 1175°C. All compositions were determined using electronprobe microanalysis.

Attainment of Equilibrium. Several lines of evidence were used to assess the approach to equilibrium. For all experiments, $K_D(Fe/Mg)$ was 0.29-0.33 for olivine/liquid. The Mg#s of phases were systematic with temperature. In addition, the pyroxene lnD(Ca) vs 1/T plot yielded a slope of 41±6 kcal/mole (vs 33 kcal/mole for diopside formation; [4]) and the olivine D(CaO) was near that estimated from [5].

Phase appearance temperatures were generally comparable to the predictions of [6], except that augite was never observed. Comparison with natural Shergotty and Zagami pigeonites and with experimental pigeonites [7] indicates that our pyroxenes may be metastable below 1150°C (especially at 1100°C). Another problem was that only small melt pockets formed during low temperature runs. Accordingly, minor quench growth may have measurably modified the melts. Even so, because of both our internal consistency and our agreement with the literature, we report the preliminary results below.

Results. The Eg liquidus is approximately 1300°C, with Fo_{78} olivine (ol) as the liquidus phase. Sub-calcic pyroxene (pig: ~En_{78}, Wo_3) joins olivine near 1275°C. Changes in liquid composition (Figure 1) reflect the fact that, in the interval 1200-1150°C, pigeonite starts to become more calcic. Between 1150°C and 1100°C, plagioclase has appeared (plag: ~An_{63}). We think that the composition of the 1100°C liquid has probably been modified during quenching and should plot closer to the ol-pig-plag±cpx pseudo-invariant point (Figure 2). All charges except those at 1100°C consistently contain olivine. The charge run for four days at 1100°C contains olivine

which has the expected K_D(Fe/Mg) and D(CaO wt%) for the liquid, suggesting that olivine may be stable, even at these temperatures.

Comparison to calculated phase equilibria. We compare our results with the calculated phase relations predicted by Longhi [6] in Figure 2. The calculated liquidus is 1304°C, with the first olivine being Fo_{79}. Low-Ca pyroxene (En_{73}, Wo_4) is predicted to appear at 1245°C. Augite (En_{49}, Wo_{36}) and plagioclase (An_{73}) should appear at 1174°C and 1098°C, respectively.

Nature of the olivine-pyroxene boundary. Broadly, our experimental results compare quite favorably with prediction, although there is a systematic difference with normative silica. This difference probably reflects the fact that the calculation treats the Ol-Pig boundary as a cotectic, whereas our experiments suggest that, at least between about 1250-1150°C, the boundary is actually a peritectic. This probable change in the nature of the phase boundary is illustrated by the movement of the melts in Figure 2. Melts produced at temperatures greater than 1250°C move away from olivine, even though pigeonite first appears at 1275°C. Then, from 1250°C to 1150°C, the melts move back towards the olivine corner, and then move along the (1250°C pyroxene) - PL reference line. To support the above discussion, we note here that (1) we have a mass balance for FeO at 1250°C, and that (2) we have charges from duplicate 1250°C experiments.

Relationship to Shergotty and Zagami, and interstitial liquids. Figure 1 includes our results, the calculated phase relations predicted by Longhi [6], and also the Shergotty and Zagami melting experiments of [8]. It does not appear possible to derive bulk Shergotty or Zagami by either equilibrium or fractional crystallization of Eg. However, if Shergotty and Zagami are cumulates, it may be possible to derive the inferred interstitial liquid [8] from a composition like Eg. One complication is that our 1150°C and 1125°C experiments are olivine saturated, while comparable runs of Stolper and McSween [8] are not. If so, it may not be possible to derive the interstitial liquid of [8] by equilibrium crystallization of Eg. However, as discussed previously, our lowest temperature results are still preliminary. Moreover, two other possibilities, a slightly less olivine normative Eg or fractionation during crystallization of Eg, are yet to be evaluated.

References. [1] Jones JH (1989) *Proc LPSC, 19th* 465-474 [2] Longhi J and Pan V (1989) *Proc LPSC, 19th* 451-464 [3] McSween HY, Jr and Jarosewich E (1983) [4] Lange RA, De Yoreo JJ, and Navrotsky A (1991) *Am Min* 76 904-912 [5] Jurewicz AJG and Watson EB (1988) *Cont Min Pet* 99 176-185 [6] Longhi J (1991) pers. comm. [7] Ross M and Heubner JS (1979) *Am Min* 64 1133-1155 [8] Stolper EM and McSween HY, Jr (1979) *GCA* 43 1475-1498

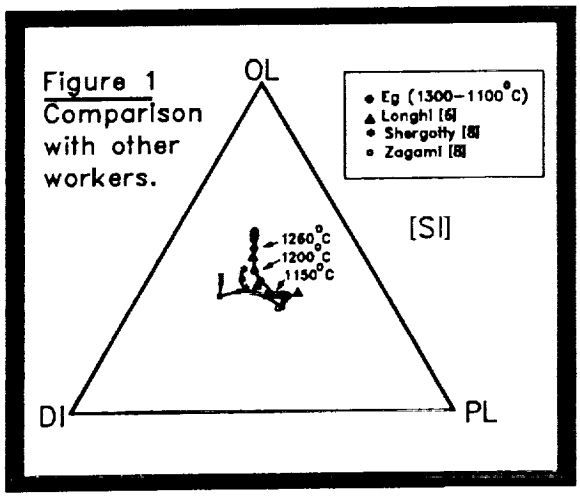

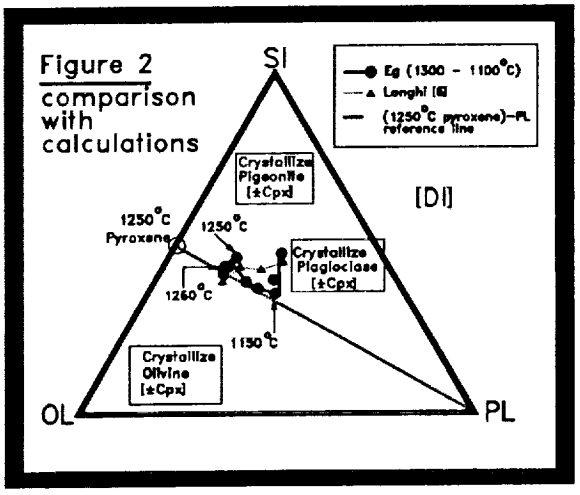

N92-29029

GLACIAL GEOMORPHIC EVIDENCE FOR A LATE CLIMATIC CHANGE ON MARS. J.S. Kargel and R.G. Strom, Lunar and Planetary Laboratory, University of Arizona, Tucson

In a series of preliminary reports (1,2,3) we documented evidence of former glacial epochs on Mars. Apparent glacial landforms seemed to be concentrated primarily at middle to high southern latitudes. More comprehensive articles (Baker, et al. (4), and Kargel and Strom (5)) summarized the concept of martian glaciation, including the probable occurrence in Middle Amazonian times, *i.e.*, late in martian history, of a vast Austral Ice Sheet. Also mentioned was the possible occurrence of comparable glaciation in the Northern Plains. We now have additional evidence supporting the view that glaciation was very widespread across middle and high latitudes of both hemispheres.

Recent studies of the Northern Plains indicate glaciation was widespread in this region. Although alternative explanations for individuals landforms are possible, we emphasis the difficulty of these diverse explanations to comprehensively explain associated, well ordered landforms that are readily explained by the single process of glaciation. The closely associated occurrence of landforms that resemble terrestrial glacial tunnel valleys, eskers, kame complexes, and moraines indicates glacial processes were present in the Northern Plains late in martian history.

Glacial landforms in the Northern Plains. The "thumbprint terrains" are interpreted by many workers as possible moraines. Scott and Underwood (6) recently put forward this interpretation and explained associated channel systems as the erosional products of glacial melt water. Ridges on some channel floors were interpreted as channel bedforms. However, they may also be eskers which often occur on the floors tunnel valleys. The close association of channels, ridges and thumbprint landforms is compelling evidence for subglacial meltwater erosion of tunnel valleys, deposition of eskers, and ice-contact deposition of moraines. This is a common terrestrial glacial association , and repeats itself across several areas of the Northern Plains (Fig. 1 is one example). The thumbprint ridges are strikingly similar to moraines deposited by glaciers calving directly into deep lakes or seas. This is consistent with the view that the Northern Plains were the site of an ancient ocean or multiple seas at the time of Middle Amazonian glaciation. The scale of these features is similar to the scale of analogous terrestrial moraines formed by deposition in deep water.

Summary and Conclusions. Martian glaciation appears to have been more extensive than previously recognized. Well integrated systems of landforms constituting probable glacial landscapes occur across much of

Glaciation on Mars: Kargel, J.S. and Strom, R.G.

the northern hemisphere. Some landforms can be interpreted as glacial till deposited by extensive marine ice sheets, consistent with the the presence of deep lakes or of Oceanus Borealis in the Northern Plains (4). The collective assemblage of glacial landforms in the Northern Plains, as with glacial landforms in the southern hemisphere, indicates rapid melting and collapse of vast ice sheets. The growth and collapse of ice sheets on Mars seems closely analogous to the growth and decline of Earth's great Pleistocene ice sheets. This implies that climate change was probably somewhat comparable on the two planets, although in the case of Mars the entire planet seems to have changed rapidly to a cold, dry present-day environment after the collapse of the ice sheets.

References: 1. Kagel, J.S. 1991. Terrestrial Glacial Eskers: Analogs for Martian Sinuous Ridges, Abstracts LPSC XXII, 683-684. 2. Kargel, J.S., *et al.*, 1991. Glacial Geology of the Hellas Region of Mars, Abstracts LPSC XXII, 687-688. 3. Strom, R.G., *et. al.*, 1991. Glacial and Marine Chronology of Mars, Abstracts LPSC XXII, 1351-1352. 4. Baker, V.R., *et al.*, 1991. Ancient Oceans, Ice Sheets and the Hydrological Cycle on Mars, Nature, in press. 5. Kargel, J.S. and Strom, R.G. 1991. Ancient Glaciation on Mars, Science, submitted. 6. Scott, D.H. and Underwood, J.R. 1991. Mottled Terrain: A Continuing Martian Enigma, Proc. Lunar and Planetary Sci., **21**, 627-634.

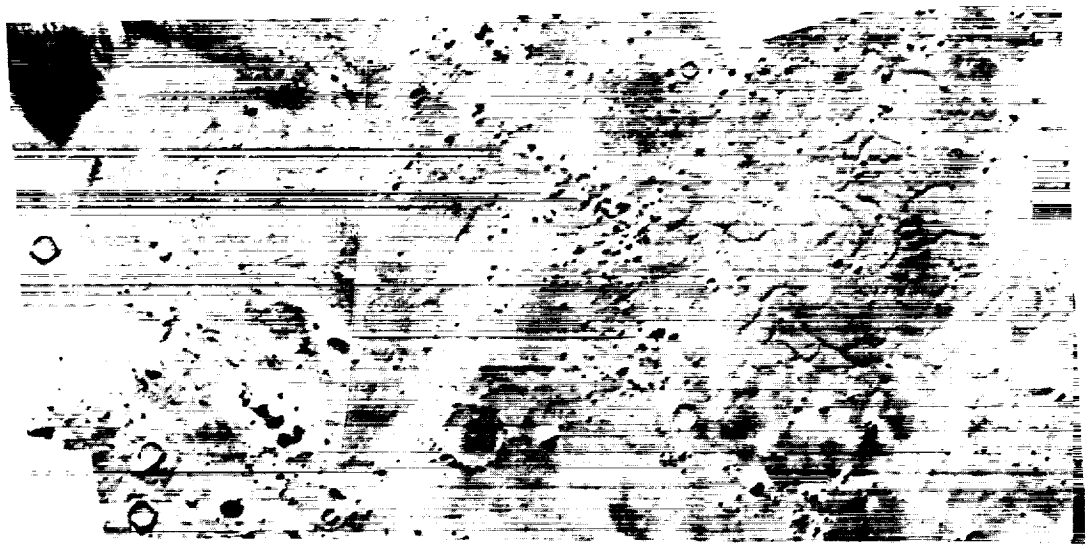

Figure 1. Photomosaic (Viking frames 776A32, 776A34, 810A31) of channels (tunnel valleys) and "thumbprint" terrain (glacial moraines) in the Northern Plains of Mars. Largest crater is 40 km diameter.

WAS EARLY MARS WARMED BY AMMONIA?; J.F. Kasting, L.L. Brown, and J.M. Acord, Department of Geosciences, Penn State University, University Park, PA 16802; J.B. Pollack, Space Science Division, NASA Ames Research Center, Moffett Field, CA 94035.

Runoff channels and valley networks present on ancient, heavily cratered Martian terrain suggests that the climate of Mars was originally warm and wet. One explanation for the formation of these channels is that the surface was warmed by the greenhouse effect of a dense, CO_2 atmosphere (1). However, recent work by Kasting (2) indicates that this mechanism does not work early in solar system history when the sun was less bright because the atmosphere condenses to form CO_2 clouds, thereby lowering the convective lapse rate and reducing the magnitude of the greenhouse effect. The CO_2 clouds may also reflect some of the incident sunlight, further lowering the surface temperature. The problem is illustrated by Figure 1, which shows the effective solar luminosity (i.e. the flux relative to the present solar flux at Mars' orbit) required to sustain various globally-averaged surface temperatures at different values of the surface pressure.

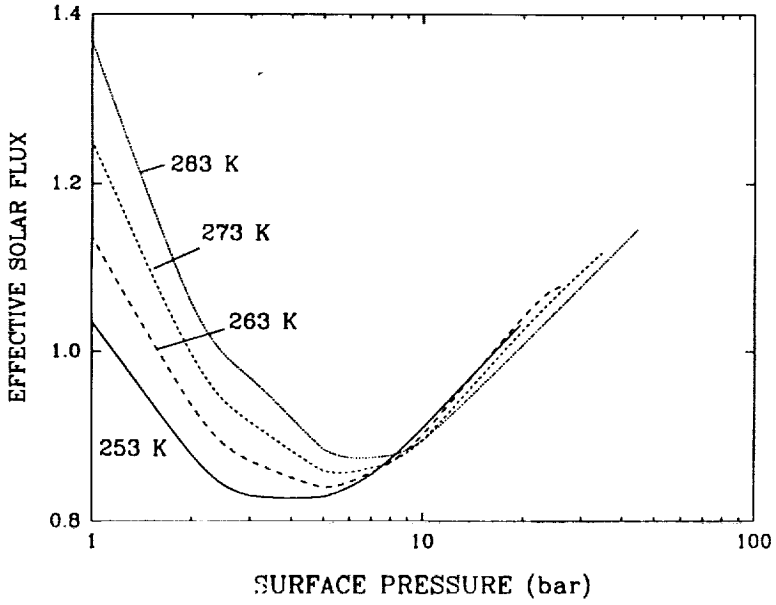

Fig. 1

Maintaining an average surface temperature of 273 K would require a solar flux of at least 86% of the present value according to this model. Using Gough's estimate (3) for the increase in solar luminosity with time, the solar flux would have been less than this value until roughly 2 billion years (b.y.) ago. If the valley networks are much older than this, as is commonly believed (1), some other mechanism must be found to keep early Mars warm.

One way to increase the surface temperatures predicted by the climate model is to assume that other greenhouse gases were present in Mars' atmosphere in addition to CO_2 and H_2O. A possible greenhouse gas that was suggested nearly twenty years ago (4) is ammonia, NH_3. An ammonia mixing ratio of ~5 x 10^{-4} by volume, combined with a CO_2 partial pressure of 4-5 bars, would be sufficient to generate a global average surface temperature of 273 K near 3.8 b.y. ago, when the solar flux was approximately 75% of the present value (Fig. 2).

WARMING EARLY MARS
J.F. Kasting et al.

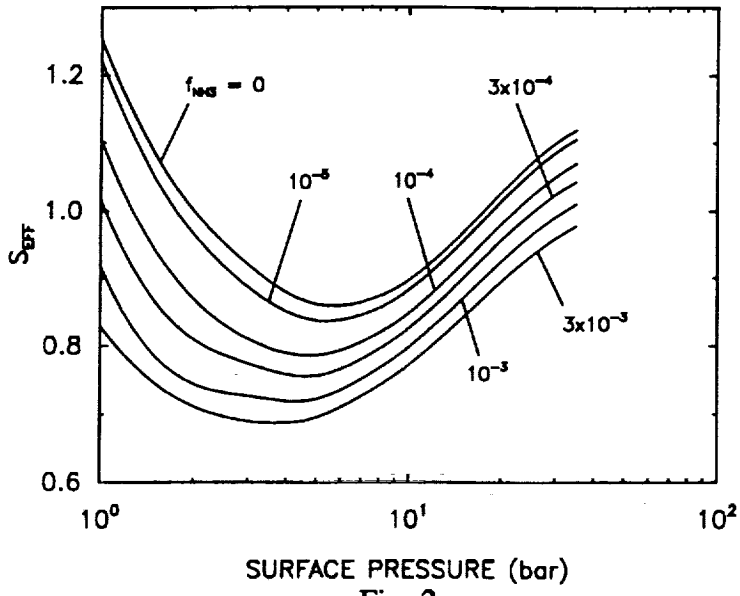

Fig. 2

Ammonia could have been present at this concentration only if it had a relatively large source and if it was shielded from photolysis by some effective UV absorber. Potential sources of ammonia include volcanic outgassing and photoreduction of N_2 on surface materials (5). Possible UV absorbers include hydrocarbons formed from methane photolysis (C. Sagan, private communication, 1991); this, of course, would require some source for atmospheric methane. Volcanic outgassing might suffice, particularly if the Martian mantle was more reduced than that of modern Earth. Methane is itself a greenhouse gas and would have added to the greenhouse effect; this effect has not yet been factored into the climate model.

Other possible mechanisms for warming early Mars include a brighter young sun (6,7), absorption of solar radiation by impact-produced dust, or the greenhouse effect of CO_2 ice clouds. These mechanisms merit further study, although none appears any more likely than the one suggested above. Alternatively, the runoff channels might have formed on a much colder early Mars (8); the problem then is to explain how groundwater reservoirs were recharged in the absence of precipitation.

References

1. Pollack, J.B. et al., Icarus 71, 203-224, 1987.
2. Kasting, J.F., Icarus, in press.
3. Gough, D.O., Solar Phys. 74, 21-34, 1981.
4. Sagan, C. and G. Mullen, Science 177, 52-56, 1972.
5. Henderson-Sellers, A. and A.W. Schwartz, Nature 287, 526-528, 1980.
6. Willson, L.A. et al., Comments Astrophys. 12, 17-34, 1987.
7. Boothroyd, A.I. et al., Ap. J., in press.
8. Peale, S.J. et al., Science 187, 273-274, 1975.

Erosional Landforms on the Layered Terrains in Valles Marineris.

G. Komatsu[1], R.G. Strom[1], V.C.Gulick[1] and T.J. Parker[2]
1.Lunar and Planetary Laboratory, University of Arizona, Tucson, AZ 85721
2.University of Southern California, Los Angels, CA 90089-0741

Many investigators have proposed potential ancient lakes in Valles Marineris based on the relationship with outflow channels [1], and a proposed lacustrine origin of layered deposits [2][3][4]. However, there has been no direct evidence for the existence of these lakes except the chaotic terrains [1]. We have investigated the erosional style of the layered terrains and evaluated their potential origin as sedimentation in and erosional modification by these lakes. The erosional features that will be discussed are distributed in the central canyon area and classified into terraces and layered depressions.

1. Morphology. There are two types of terrace morphology. Type I is benches about 500-800m wide in western Ophir Chasma (figure 1). A southern group is located in front of steep cliffs while a northern group does not have cliffs behind them. Type II (figure 2,3) in Candor and Melas Chasmata is similar in morphology and spacing, but less pronounced than Type I. At many locations these terraces seem to coincide with layers, but elsewhere image resolution is not sufficient to see this relationship. Layered depressions occurs in three areas in western Candor Chasma (figure 4,5).

2. Possible terrace erosional mechanisms. The terraces could be caused by one or more of three processes: eolian, mass wasting, or aqueous. Layered bedrock consisting of alternating weak and resistant layers may produce terrace morphology by wind deflation (figure 6) with the bench surfaces being resistant layers underlain by a less resistant layer. The southern group of Type I occurs in front of high cliffs and could be slump blocks enhanced by wind erosion. The layered terrains may be sediments deposited in a lacustrine environment [2][3][4], and the terraces could be wave-cut benches due to a late-forming lakes. Although water seepage and runoff [1] from the canyon walls, and potentially from its floors, could have eroded the layered terrains over a protracted period, it is unlikely to have caused the differential erosion of layers at the relatively high levels observed. Instead these terraces could be wave-cut benches similar to those in the Baltic coastal region due to post-glacial isostatic rebound (figure 7), or to those in Lake Bonneville due to lake retreat. Wave cutting produces a bench on a headland (figure 8). If uplift or subsidence occurs with respect to water level, benches form at different levels and do not necessarily coincide with layers. Thus, the terraces could represent wave-cut benches due to water level changes. If this is the case, then lakes were present in Valles Marineris relatively late in its history.

3. Erosional mechanism of the layered depressions. This erosional type can be explained by eolian process. However aqueous process also can dissect deep in the terrain. Eolian erosion may enhance the relief once the first order topography is established by the aqueous process. This first-order erosion could have been caused by catastrophic drainage of preexisting lakes that may have formed the deep valleys separating layered terrains from each other and from the canyon walls [1][4][6].

4. Conclusion. Many terraces in the layered terrains can be explained by coastal erosion in lakes as well as by eolian erosion. The lack of terraces on the canyon walls is probably due to more recent sapping and mass wasting of material with a different mechanical response to erosion than the layered terrains. Catastrophic water discharges in Valles Marineris as hypothesized by the ocean model [7] may have been the source of the lakes and eventual catastrophic release of the water from the canyons. Mars Observer may provide information to confirm the origin of these erosional features.

REFERENCES [1] Lucchitta, B.K and Ferguson, H.M., (1983), Jour. Geophy. Res., 88, A553-A568. [2] McCauley, J.F., (1973) U.S. Geol. Surv. Misc. Inv. Map I-897 [3] Lucchitta, B.K. (1982), Reports of Planetary Geology Program, p.233-234, NASA-TM 85127 [4] Nedell, S.S., Squyres, S.W., and Anderson, D.W., (1987), Icarus, 70, p.409-441. [5] Sharp, R.P., (1973), Jour. Geophy. Res., 78, p.4063-4072. [6] Komatsu, G. and Strom, R.G., (1991), LPSC 22, p.737-738. [7] Baker, V.R., Strom, R.G., Gulick, V.C, Kargel, J.S., Komatsu, G., and Kale, V.S., (1991), Nature, in press.

Figure 1. Type I terrace in western Ophir Chasma.

Figure 2. Type II terrace in Candor Chasma.

Figure 3. Type II terrace in Melas Chasma.

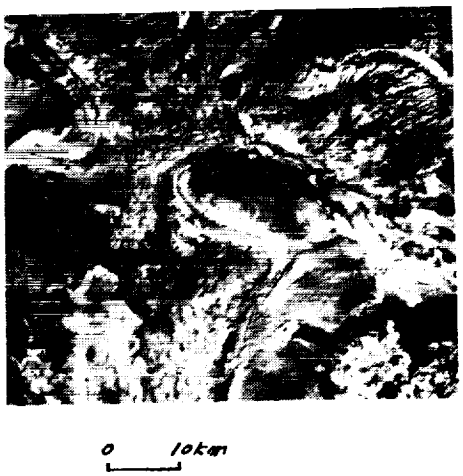

Figure 4. Layered depression in western Candor Chasma.

Figure 5. Layered depression in western Candor Chasma.

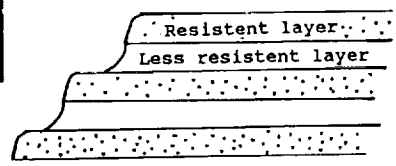

Figure 6. Enhancement of layers by wind deflation.

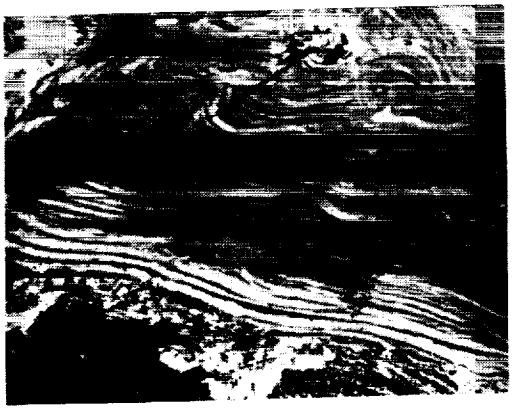

Figure 7. Elevated beach terraces on Ostergransholm, Eastern Gotland, Sweden. (Copyright holder, Arne Philip, Visby, Sweden, from Geodynamics by D.L. Turcotte and G. Schubert)

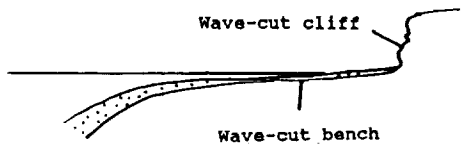

Figure 8. Beach bench formed by wave-cutting.

88

MARS: CORRECTING SURFACE ALBEDO OBSERVATIONS FOR EFFECTS OF ATMOSPHERIC DUST LOADING;

S.W. Lee and R.T. Clancy, Laboratory for Atmospheric and Space Physics, Univ. Colorado, Boulder, CO 80309

The Mariner 9 and Viking missions provided abundant evidence that aeolian processes are active over much of the surface of Mars [1; 2]. Past studies have demonstrated that variations in regional albedo and wind streak patterns are indicative of sediment transport through a region [3; 4], while thermal inertia data [derived from the Viking Infrared Thermal Mapper (IRTM) data set] are indicative of the degree of surface mantling by dust deposits [5; 6; 7; 8; 9]. The visual and thermal data are therefore diagnostic of whether net erosion or deposition of dust-storm fallout is taking place currently and whether such processes have been active in a region over the long term. These previous investigations, however, have not attempted to correct for the effects of atmospheric dust loading on observations of the martian surface, so quantitative studies of current sediment transport rates have included large errors due to uncertainty in the magnitude of the "atmospheric contamination".

We have developed a radiative transfer model which allows the effects of atmospheric dust loading on surface albedo to be investigated. This model incorporates atmospheric dust opacity, the single scattering albedo and particle phase function of atmospheric dust, the bidirectional reflectance of the surface, and variable lighting and viewing geometry. The most recent dust particle properties [10] are utilized.

The spatial and temporal variability of atmospheric opacity (τ) strongly influences the radiative transfer modelling results. We are currently using the approach described in [11] to determine τ for IRTM mapping sequences of selected regions. This approach allows τ to be determined at the highest spatial and temporal resolution supported by the IRTM data.

Applying the radiative transfer modelling and determination of τ described, IRTM visual brightness observations can be corrected for the effects of atmospheric dust loading at a variety of locations and times. This approach allows maps of "dust-corrected surface albedo" to be constructed for selected regions. Information on the variability of surface albedo and the amount of dust deposition/erosion related to such variability result.

To date, this study indicates that atmospheric dust loading has a significant effect on observations of surface albedo, amounting to albedo corrections of as much as several tens of percent. This correction is not constant or linear, but depends upon surface albedo, viewing and lighting geometry, the dust and surface phase functions, and the atmospheric opacity. It is clear that the quantitative study of surface albedo, especially where small variations in observed albedo are important (such as photometric analyses), needs to account for the effects of atmospheric dust loading. Maps of "dust-corrected surface albedo" will be presented for a number of regions.

REFERENCES: [1] Veverka, J., P. Thomas, and R. Greeley (1977). A study of variable features on Mars during the Viking primary mission. *J. Geophys. Res. 82*, 4167-4187. [2] Thomas, P., J. Veverka, S. Lee, and A. Bloom (1981). Classification of wind streaks on Mars. *Icarus 45*, 124-153. [3] Lee, S.W., P.C. Thomas, and J. Veverka (1982). Wind streaks in Tharsis and Elysium: Implications for sediment transport by slope winds. *J.Geophys. Res. 87*, 10025-10042. [4] Lee, S.W. (1986). Regional sources and sinks of dust on Mars: Viking observations of Cerberus, Solis Planum, and Syrtis Major (abstract), In *Symposium on Mars: Evolution of its Climate and Atmosphere* (V. Baker et al., eds.), pp. 71-72, LPI Tech. Rpt. 87-01, Lunar and Planetary Institute, Houston. [5] Kieffer, H.H., T.Z. Martin, A.R. Peterfreund, B.M. Jakosky, E.D. Miner and F.D. Palluconi (1977). Thermal and albedo mapping of Mars during the Viking primary mission. *J. Geophys. Res. 82*, 4249-4295. [6] Christensen, P.R. (1982). Martian dust mantling and surface composition: Interpretation of thermophysical properties. *J. Geophys. Res. 87*, 9985-9998. [7] Christensen, P.R. (1986). Regional dust deposits on Mars: Physical properties, age, and history. *J. Geophys. Res. 91*, 3533-3545. [8] Christensen, P.R. (1986). The distribution of rocks on Mars. *Icarus 68*, 217-238. [9] Jakosky, B.M. (1986). On the thermal properties of martian fines. *Icarus 66*, 117-124. [10] Clancy, R.T., and S.W. Lee (1991). A new look at dust and clouds in the Mars atmosphere: Analysis of emission-phase-function sequences from global Viking IRTM observations, *Icarus*, in press. [11] Martin, T.Z. (1986). Thermal infrared opacity of the Mars atmosphere. *Icarus 66*, 2-21.

SIMULATIONS OF THE SEASONAL POLAR CAPS ON MARS Bernhard Lee Lindner, Atmospheric and Environmental Research, Inc., 840 Memorial Drive, Cambridge, Mass. 02139-3794, USA

Introduction. One of the most puzzling mysteries about the planet Mars is the hemispherical asymmetry in the polar caps. Every spring the seasonal polar cap of CO_2 recedes until the end of summer, when only a small part, the residual polar cap, remains. During the year that Viking observed Mars, the residual polar cap was composed of water ice in the northern hemisphere [Kieffer et al., Science, 194, 1341, 1976] but was primarily carbon dioxide ice in the southern hemisphere [Kieffer, J. Geophys. Res., 84, 8263, 1979]. Scientists have sought to explain this asymmetry by modeling observations of the latitudinal recession of the polar cap and seasonal variations in atmospheric pressure (since the seasonal polar caps are primarily frozen atmosphere, they are directly related to changes in atmospheric mass). These models reproduce most aspects of the observed annual variation in atmospheric pressure fairly accurately. Furthermore, the predicted latitudinal recession of the northern polar cap in the spring agrees well with observations, including the fact that the CO_2 ice is predicted to completely sublime away. However, these models all predict that the carbon dioxide ice will also sublime away during the summer in the southern hemisphere, unlike what is observed. This paper will show how the radiative effects of ozone, clouds, and airborne dust, light penetration into and through the polar cap, and the dependence of albedo on solar zenith angle affect CO_2 ice formation and sublimation, and how they help explain the hemispherical asymmetry in the residual polar caps. These effects have not been studied with prior polar cap models.

Ozone, Clouds, and Airborne Dust. Since O_3 is more prevalent in the northern hemisphere than in the southern hemisphere, O_3 was suggested as a cause for the hemispherical asymmetry in the residual polar caps by Kuhn et al. (J. Geophys. Res., 84, 8341, 1979). However, Lindner (submitted to Icarus, 1991) has shown that O_3 has a minor effect on the atmospheric temperature, and hence on the infrared radiation which strikes the polar cap, and Lindner (J. Geophys. Res., 95, 1367, 1990) has shown that O_3 absorbs less than 1% of the total solar radiation absorbed by the polar cap. Thus, O_3 is not an important consideration in the polar cap energy budget.

Lindner (1990) has computed the solar and thermal flux striking the polar cap of Mars for various ozone, dust, and cloud abundances and for three solar zenith angles. These calculations have been inserted in the polar-cap model of Lindner (Eos Trans. AGU, 67, 1078, 1986). Vertical optical depths of dust and cloud ranging from zero to 1 cause little change in the total flux absorbed by the polar cap near its edge but increase the absorbed flux significantly as one travels poleward. Observations hint that hemispherical asymmetries in dust abundance and cloud cover exist, and these would combine to cause a significant hemispherical asymmetry in the total flux absorbed by the residual polar caps, which helps to explain the dichotomy in the residual polar caps.

Light Penetration. Penetration of solar radiation into the cap itself is included in the polar cap model of Jakosky and Haberle (J. Geophys. Res., 95, 1359, 1990), based on the theoretical work of Clow (Icarus, 72, 95, 1987). Lindner and Jakosky (B.A.A.S., 22, 1060, 1990) find that the inclusion of light penetration slightly decreases the albedo needed in the model to keep CO_2-ice year-round at the south pole by on the order of 1%. The required albedo is decreased because some solar radiation is used to heat the subsurface, and not all of this heat is transported back to the surface. Overall, we conclude that penetration of light into the polar cap has only a small effect on

the polarcap energy budget.

Albedo and the Solar Zenith Angle. Warren et al. (J. Geophys. Res., 95, 14717, 1990) have computed the dependence of the albedo of the martian polar caps on solar zenith angle, and these calculations have been included in my polar cap model. Since the albedo of ice increases and becomes more forward scattering at higher solar zenith angles, and since the solar zenith angle becomes higher as one approaches the pole, the albedo is greatest at the pole. This decreases absorption of sunlight, hence increasing survivability of CO_2 ice. In fact, this increases the survivability of ice enough to offset the decrease in survivability of ice due to radiative effects of clouds and dust.

Discussion. The combination of the effects of solar zenith angle on albedo and the radiative effects of clouds and dust act to extend the lifetime of CO_2 ice on the south pole relatively more than on the north pole, possibly explaining the hemispherical asymmetry in the residual polar caps without the need of a hemispherical asymmetry in polar cap albedo. This does not imply that a hemispherical asymmetry in polar cap albedo does not exist, but that one is not necessary.

Observations of the regression of the polar caps and the annual cycle in atmospheric pressure are reproduced fairly well by the model, as shown in the figures, although further improvement is needed. When CO_2 ice is retained at the south pole, the model predictions of the annual cycle in atmospheric pressure have a phase shift relative to the data, no matter what model input parameters are used. We are investigating other processes not included in prior polar cap models.

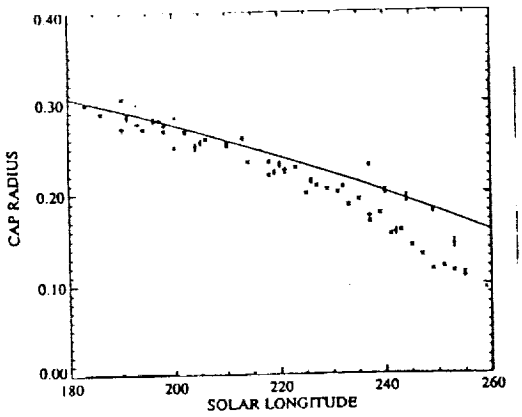

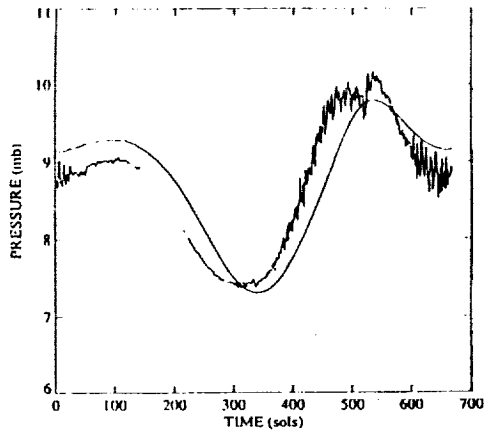

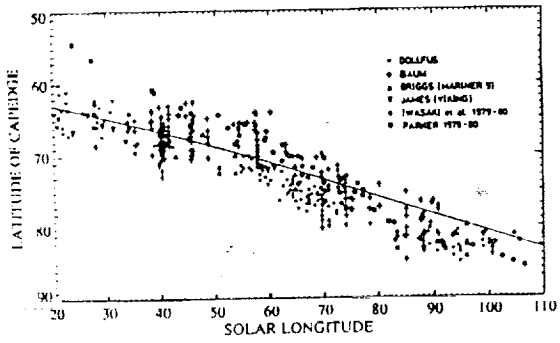

Comparison of the model to atmospheric pressure (upper right), south polar cap regression (upper left), and north polar cap regression (bottom)

MARS ATMOSPHERE EVOLUTION: ESCAPE TO SPACE: J. G. Luhmann, Institute of Geophysics and Planetary Physics, Los Angeles, CA 90024-1567

Both the loss mechanisms and the rates of escape of Martian atmosphere constituents to space must have changed throughout the history of the solar system. For the first billion years, Mars atmosphere escape was probably dominated by impact erosion related to the presence of debris left over from the accretionary phase (1). This loss may have been further augmented by hydrodynamic outflows related to the presence of an early denser atmosphere and a Sun that was brighter in the EUV wavelengths (2). Following this initial "catastrophic" phase, during which a large fraction of the original atmosphere may have been lost but then replaced by volcanism and cometary impact, the "modern" loss mechanisms which still operate today would have taken over. Those that now contribute to escape to space consist of classical thermal or Jeans escape, nonthermal escape due to chemical reactions in the atmosphere, and solar wind-related losses.

The state of the Martian atmosphere following the initial effects of impact erosion and hydrodynamic escape is difficult to assess. While information regarding the bombardment history in the inner solar system has been derived from the moon, the use of the lunar record may lead to incorrect estimates for Mars. One must also consider that "new" atmospheric gases can be released by both the foreign body and the planet on impact, so that impacts represent a source as well as a loss mechanism. The evolutionary role of comets is even more poorly constrained. Volcanism may have also been extant. Hydrodynamic outflow is thought to have left some indication of its importance in current isotope ratios as well as current composition, but the uncertainty of sources during the early history of the planetary atmosphere makes even that evidence difficult to interpret. (For example, a large comet impact can reset the D/H ratio (3).) Moreover the evidence for surface water following the early intense bombardment (4) means that substantial cycling with the surface was occurring (5), further complicating the evaluation of the effects of escape.

Both Jeans and nonthermal escape can be thought of simply as the loss of upward moving neutral particles that have thermal velocities in excess of the ~5 km/s escape velocity for Mars. However, particles contributing to Jeans escape derive their energy from the normal solar heating of the atmosphere, while the nonthermally escaping component derives its energy from chemical reactions such as dissociative recombination that impart excess energy to their products. The oxygen and nitrogen budgets of Mars are believed to have been particularly affected by nonthermal escape, while thermal escape is considered to have controlled hydrogen loss. The evolutionary importance of thermal and nonthermal losses is closely tied to the history of the Sun: the thermal mechanism because it derives its energy from solar heating, and the nonthermal mechanism because processes like dissociative recombination depend on both the underlying atmosphere scale height and the ionosphere properties. While the solar luminosity is believed to have been as much as 30% less in the past, the ultraviolet and EUV intensities are considered to have been higher (6), with the potential for enhancing these escape rates. Given the available knowledge from stellar evolution studies, the changes in these rates through time are in principle calculable.

The evaluation of the cumulative solar wind-related losses over time has perhaps received the least attention. This neglect appears to stem from uncertainties in the physical processes involved, and in the history of the solar wind. Significant progress has been made fairly recently on the former, as observations from the Pioneer Venus Orbiter, PHOBOS-2, and the cometary missions

MARS ATMOSPHERE EVOLUTION: ESCAPE TO SPACE
Luhmann, J.G.

have taught as a great deal about ion scavenging mechanisms in solar wind-ionosphere interactions. With historical models of the Mars atmosphere, the Sun, and the solar wind, we can begin to extrapolate the loss rates due to at least some of these mechanisms back in time. It has also recently been realized that not only ions, but also neutrals are removed by the solar wind interaction due to sputtering by energetic heavy scavenged ions that reimpact the atmosphere. The unknown history of the Martian intrinsic magnetic field also enters into the evaluation of this particular mode of atmosphere escape.

Much remains to be done concerning both the evaluation and prioritization of the various escape mechanisms through Mars' history. In particular, where possible, we need to evaluate the most reasonable range of all of the various types of loss rates, and to better define their interrelations. We need to evaluate the likelihood of various evolutionary scenarios and determine what additional observations can lead to further constraints on the number of possibilities. We need to fold in the effects of losses to the surface and surface interactions which may alter the rates of escape to space relative to what they would be for an inert surface, and to determine the relative importance of loss to the surface versus loss to space for different epochs and for different constituents. We also need to take into account historical evidence of post-accretionary period sources such as volcanism and comet or other gas-producing impacts. In the end, it may prove fruitless to attempt to quantify the earliest atmospheric states. However, we may be able to successfully work backward to the end of the initial "catastrophic" phase of atmosphere evolution by careful consideration of how present escape processes should have changed over time. We may at least be able to conclude whether in the most recent period of evolution (to ~3 Gyr ago) the atmosphere of Mars has been drastically altered via current-day processes.

References: (1) H. J. and Vickery, A. M. (1989) Nature, 338, p. 487.
(2) Hunten, D. M., Pepin, R. O., Owen, T. C. (1988) in Meteorites and the Early Solar System, edited by J. Kerridge and M. S. Matthews, University of Arizona Press, p. 565.
(3) Grinspoon, D. H. (1987) Science, 238, p. 1702.
(4) Carr, M. H. (1987) Nature, 326, p. 30.
(5) Kahn, R. (1985) Icarus, 62, 175.
(6) Zahnle, K. and Walker, J.C.G. (1982) Rev. Geophys. Space Phys., 20, 280.

CD 146017
MX 270710
CU 508845
ST 197060

54-91

N92-29035

P. 1 93

DISCOVERY CONCEPTS FOR MARS: Luhmann, J. G. and Russell, C. T., Institute of Geophysics and Planetary Physics, Los Angeles, CA; Brace, L. H. and Nagy, A. F., Space Physics Research Laboratory, University of Michigan, Ann Arbor, MI; Jakosky, B. M. and Barth, C. A., LASP, University of Colorado, Boulder, CO; Waite, J. H., Southwest Research Institute, San Antonio, TX.

Two focused Mars missions that would fit within the guidelines for the proposed Discovery line could deal specifically with 1) the issue of the escape of the atmosphere to space, an understanding of which is crucial to deciphering the evolution of the atmosphere, climate change, and volatile inventories, and 2) the investigation of remanent magnetization of the crust, and of the ionosphere and atmosphere which modifies these magnetic fields and is in turn modified by them.

Escape of the atmosphere to space is currently presumed to occur by means of a combination of Jeans escape, "Nonthermal" escape, and solar wind scavenging. The evaluation of these mechanisms and of the underlying physical processes requires an orbiting payload that makes direct measurements of both escaping ions and neutrals, together with essential additional information on ionization processes and rates, the altitude distribution of the atmospheric sources, and the dependence of the escape rates on solar wind conditions.

The history and present nature of the magnetic field of Mars, which are also relevant is considerations of atmosphere escape, remain controversial. We know by virtue of analogies with Venus that magnetic fields induced in the ionosphere by solar wind interaction processes are likely to dominate above altitudes of ~150 km. The Mars Observer is to orbit above 350 km. Therefore, a very low-altitude survey with supporting interplanetary measurements is necessary. A simple spacecraft in a highly elliptical orbit carrying magnetic field and basic aeronomical experiments could resolve this longstanding issue.

There is a great degree of commonality between the combined payloads of these missions, that of the yet to be approved Mars Aeronomy Orbiter, and that of the TIMED (Thermosphere, Ionosphere and Mesosphere Electrodynamics) spacecraft which is currently under study by the Space Physics Division of NASA. Creative approaches to joint division support could be investigated to determine whether a duplicate of the TIMED spacecraft could also fit within the Discovery cost limit, while achieving the science goals of both of the other concepts.

NONLINEAR STRATIFIED FLOW OVER LOCALIZED TOPOGRAPHIC OBSTACLES ON MARS; J. A. Magalhães, and R. E. Young (NASA/ARC).

The current dynamical influence of the Martian atmosphere on the surface is clearly revealed by dark surface albedo features which are associated with localized topographic relief and have been described in detail and classified as Type I(d) wind streaks[1]. The contrast of the streaks diminishes or disappears during the global dust storms, and the streaks are observed to quickly reform after the termination of the storms; the streaks remain stable after $L_S=0^o$ until the next dust storm. These observations, together with the ragged edges of the streaks, have been used to infer that the dark streaks are formed by the removal of bright dust from a darker substrate[2].

The Type I(d) streaks are concentrated in a band of latitude extending from roughly 20° S to 40° S[3]. Their longitudinal distribution and azimuths show a high degree of zonal symmetry, and the azimuths imply an easterly wind. The surface stress distributions predicted by a Hadley circulation model at the season of formation of the streaks show a band of easterly surface stress between 20° S and 40°S, in remarkable agreement with the streak observations[4,5]. However, the magnitude of the computed friction velocities in this latitude band ($u_* = 0.1\text{-}0.2$ m s^{-1}) is far less than the threshold friction velocity estimated for the initiation of saltation on Mars ($u_{*_t} = 1\text{-}2$ m s^{-1})[6]. Moreover, the predicted stresses in this latitude band represent a latitudinal minimum for this season.

We have studied analytically the two-dimensional nonlinear stratified, steady flow of a hydrostatic fluid over idealized topographic obstacles under Martian conditions. A fully nonlinear lower boundary condition for the topography is used. Two upper boundary conditions were studied. The first boundary condition was suggested by the recently developed theory of terrestrial severe downslope windstorms in the lee of major mountain ranges on the Earth[7,8]. Such windstorms are believed to be associated with reversals in the mean wind within a few kilometers of the surface, which act as critical layers for the stationary waves excited by the obstacle. Using an upper boundary condition which implicitly includes the trapping effects of the wind reversal, our model is identical to the semi-analytical theory of terrestrial severe downslope windstorms[7]. The theory predicts that the occurrence of the severe windstorm state depends on $Fr_h = h\,N_0/U_0$ and $Fr_H = H\,N_0/U_0$, where h is the obstacle height, H is the height of the wind-reversal, N_0 is the upstream Brunt frequency of the atmosphere near the surface, and U_0 is the upstream surface wind. The maximum downstream surface wind which is predicted by the theory is $3U_0$. For the surface winds predicted by the Martian Hadley circulation models at the time and location of formation of the dark streaks ($U_0 = 1\text{-}2$ m s^{-1}) and N_0 characteristic of the Martian nighttime thermal boundary layer[9], the theory predicts surface wind amplifications of a factor of three for mean wind reversals within a few kilometers of the surface and obstacle heights comparable to those associated with the dark streaks[10]. Hadley circulation models in fact predict such wind-reversals over the latitude band of the dark streaks at the time of their formation[4,5]. Therefore, 2-D terrestrial severe downslope windstorm theory seems to account well for the formation of the dark streaks at the time and locations of their formation. Moreover, the requirement of a near-surface wind reversal for the production of winds in the lee of the obstacle which are much larger than the upstream surface wind suggests a reason for the absence of dark streak formation at other locations and times.

NONLINEAR STRATIFIED FLOW ; J. A. Magalhães, and R. E. Young.

We have also considered a radiation upper boundary condition, which approximates the conditions over most locations over much of the Martian year. The radiation condition stipulates that the energy flux associated with the disturbance is directed upward. The solution of the model is completely determined by F_h and the shape of the obstacle. For F_h <0.85, the solution consists of a vertically propagating wave. For $F_h \geq 0.85$, the streamlines of the flow overturn, which results in a turbulent breakdown of the flow and deposition of momentum at the overturning height. We find that the strong stratification at night in the diurnal thermal boundary layer on Mars leads to wavebreaking within the lowest half scale height of the atmosphere over obstacle heights comparable to those associated with impact craters[10]. The nighttime boundary layer on Mars is strongly stratified and vertical turbulent diffusion is strongly suppressed[9]. Therefore, vertically propagating waves may represent an important means of vertically transporting momentum across the nighttime thermal boundary layer and thus could be an important factor in the dynamical coupling of the atmosphere and surface during the Martian night.

1. Thomas, P., J. Veverka, S. Lee, and A. Bloom (1981). **Icarus** *45*, 124-153.
2. Veverka, J. , P. Giersach, and P. Thomas (1981). **Icarus** *45*, 154-166.
3. Thomas, P., J. Veverka, D. Gineris, and L. Wong (1984), **Icarus** *60*, 161-179.
4. Magalhães, J. (1987) **Icarus** *70*, 442-468.
5. Haberle, R. M. (personal communication).
6. Greeley, R., R. Leach, B. White, J. Iverson, and J. Pollack (1980). **Geophys. Res. Lett** *7*, 121-124.
7. Smith, R. B. (1985). **J. Atmos. Sci.** *42*, 2597-2603.
8. Bacmeister, J. T. and R. T. Pierrehumbert (1988). **J. Atmos. Sci.** *45*, 63-80.
9. Gierasch, P. and R. Goody (1968). **Planet Space Sci.** *16*, 615-646.
10. Lee, S. W. (1984). **Icarus** *58*, 339-357.

VOLATILE TRACERS OF MARTIAN ATMOSPHERIC EVOLUTION: PRESENT MEASUREMENT STATUS AND REQUIREMENTS FOR FUTURE INVESTIGATIONS; ***Paul Mahaffy***, NASA/Goddard Space Flight Center, Greenbelt, MD 20771, ***Konrad Mauersberger***, University of Minnesota, Minneapolis, MN 55455

One of the most significant contributions to the detailed characterization of the molecular, atomic and isotopic composition of the Martian atmosphere came from the Viking mass spectrometer experiments[1]. Measurement of the abundance of the noble gases Ne, Ar, Kr, and Xe, as well as major molecular species was achieved together with some of the important isotopic compositions such as $^{15}N/^{14}N$, $^{36}Ar/^{40}Ar$ and others. The isotopic characterization, a key element to an understanding of atmospheric evolution advanced further with recent measurements[2] of the D/H ratio from HDO as well as the detailed study[3] of gases contained in meteorites thought to be of Martian origin.

Future Mars missions must verify past measurements and then extend these measurements to surface atmosphere exchange to determine the presence of volatiles in near surface material. An experiment is under development which will perform both atmospheric gas analysis and through pyrolysis of collected solid phase material will determine subsurface gas composition. The Viking gas chromatograph/mass spectrometer experiment which heated a sample to 500 C to desorb volatiles was primarily orientated to the question of the presence of organic molecules and did not provide detailed temperature profiles for inorganic molecules. The thermal desorption/pyrolysis experiment described, identifies first the presence of physically adsorbed species and then gaseous products from more permanently bound compounds such as carbonates, sulfur containing species, and hydrated minerals as the sample temperature is raised. The measurement of variations in the isotopic composition of the evolved gas with temperature are expected to be of particular value in tracing the history of surface exchange.

1.) T. Owen et al., Journal of Geophysical Research **82**, 4635 (1977).

2.) T. Owen et al., Science **240**, 1767 (1988).

3.) D. Bogard, et al., Geochimica et Cosmochimica Acta **48**, 1723 (1984).

AN EJECTION MODEL FOR SNC METEORITES: AN INDICATION FOR RECENT VOLCANISM ON MARS; J. P. Manker, Georgia Southwestern College

When compared to other achondrites, SNC meteorites have viewed as anomalous objects. This conclusion is based mainly on their extremely young crystallization ages and their short cosmic ray exposure times. Further, SNC's noble gas and nitrogen components indicate a martian origin for these objects (1). If these meteorites are from Mars, then the most confounding question facing the planetary science community is how were they ejected from the planet's surface.

At present, ejection by impact is considered to be the most viable mechanism. However, to accelerate surface material to the escape velocity of Mars by impact, then a shock pressure of 100 GPa would be generated (2) and/or the ejecta would be converted to a totally glass phase (3). SNC's display neither of these characteristics, but lack of these features could be accounted for by a highly oblique impact or by ejection of material from points distant from the center of impact. A modified version of this mechanism involves the explosive release of gas derived from the sudden melting of subsurface ice during impact (4). In this scenario, ejecta would be entrained in the gases and may achieve the critical velocity of 5 km/sec.

If impacting is the ejection mechanism, then why are SNC ages limited to 1.3 b.y. or less? Since cratering and subsequent ejection would not exclusively occur only in the younger terrains of mars, then at least some of the SNCs should display ages greater than 1.3 b.y. Assuming that there are older rocks on Mars, it is proposed the SNCs are derived from the youngest terrains on the planet (i.e., the Tharsis area) by explosive volcanism.

Muzzle velocities of particles associated with plinian eruptions on Earth have been determined to be 500 m/sec to 600 m/sec (5). Using Wilson's equations (5) and considering the values for g and the atmospheric density on Mars, then ejection velocities should be 1000 m/sec to 1500 m/sec during an explosive eruption on that planet at present atmospheric conditions. The calculated velocities are a significant shortfall of the required 5000 m/sec. Assuming that ground ice occurs at depth in mid to low latitudes on Mars, then a modified version of this mechanism is proposed. As magma moves rapidly toward the surface, it would encounter a continuous layer of ground ice and very rapid melting/sublimination would ensue to produce tremendous subsurface stream pressures. With continual melting, the ground ice would become too thin to contain the steam thus leading to a violent explosion which would entrain particles and accelerate them to high velocities. This mechanism has been partially verified by simulation at present martian atmospheric temperatures and pressures. The vent produced during experimentation very closely resembles that found in Candor Chasma which is considered to be the product of a fairly recent explosive eruption (6). A final phase of the simulation project will be carried out to determine ejecta velocities during the steam explosion. If velocities turn out to be near that which is required to eject materials from the martian surface, then it may give us an additional mechanism to consider for the origin of SNCs, but more importantly it may also give indirect evidence that Mars remains volcanically active.

REFERENCES

(1) Wood C.A. and Ashwal L. D. (1981) PLPSC 12th, p. 1359-1375.

(2) Vickery A. M. and Melosh H. J. (1983) ICARUS 56, p. 229-318.

(3) O'Keefe J. D. and Ahrens T. J. (1985) ICARUS 56, p. 328-338.

(4) Wasson J. T. and Wetherill G. W. (1979) Asteroids (T. Gehrels, ed.), p. 926-974.

(5) Wilson L. (1976) Geophy. Jour. Royal Astron. Soc. 45,p. 543-556.

(6) Lucchitta B. K. (1990) ICARUS 86, p. 476-509.

OBSERVED CHANGES IN LIMB CLOUDS IMMEDIATELY PRIOR TO THE ONSET OF PLANET-ENCIRCLING DUST STORMS; L. J. Martin, Lowell Observatory, P. B. James, University of Toledo and Lowell Observatory, R. W. Zurek, Caltech and Jet Propulsion Laboratory

(CN)

Of the several size and nomenclature groupings of Martian dust storms, it is the planet-encircling or truly runaway dust storms that are of most concern to both the theoreticians and mission planners. Once believed to be regularly seasonal, it has since been shown that they are not annual occurrences and that the few we know about occurred within at least one-third of Mars' seasonal cycle. We cannot confirm that any were observed before 1956, and none has been observed since 1982 (the classification of that event as "encircling" is an interpretation of observations from a single point on the planet's surface). If these storms occur in cycles, we do not know the lengths or causes of the cycles. Regional and local dust storms occur more frequently and throughout the Martian year, but the underlying question is how do some become runaways, encircling the planet, while the others die out, usually within a few days.

Although both Earthbased and spacecraft data really give only sporadic glimpses of these phenomena, we are optimistic that careful review and analysis of the data now on hand can greatly increase our knowledge of these storms. We believe that we have already made some important findings which hopefully may lead us to a goal of foreseeing circumstances observable on Mars that allow planet-encircling storms to develop.

The figure following was derived from two independent studies (1,2) of limb hazes recorded by the Viking cameras. Based upon Earthbased data covering a number of years before and since the mission, we believe that the Martian atmosphere was fairly dusty at the time of arrival of the Viking Orbiters. The diagram shows an increasing rise in the heights of limb clouds from early in the mission until the beginning of the first planet-encircling storm. The scatter in points is primarily attributed to the wide range of areas (latitudes and longitudes) on Mars that these images included. The data taken before L_s 150° suggests that some of the altitudinal rise may be seasonal since it was roughly repeated during the two Martian years following the storms. Unfortunately, there are no second- and third-year data points available after L_s 150°, when the cloud/haze heights rise above 60 km and then quickly to 80 km and higher. We suggest that this sudden rise just before the first of the 1977 planet-encircling storms is more than just coincidental or seasonal, although we would prefer to base this assertion upon more than one case. The increase in heights above 60 km occurred about 50 days (Earth time) before the storm began—enough time for providing a useful warning of possible imminent storms during future missions.

Another aspect of this research is the compilation of detailed storm-cloud maps based upon the Viking mosaics. We are establishing a classification system for the various cloud types seen on these images. Mapping clouded areas by type

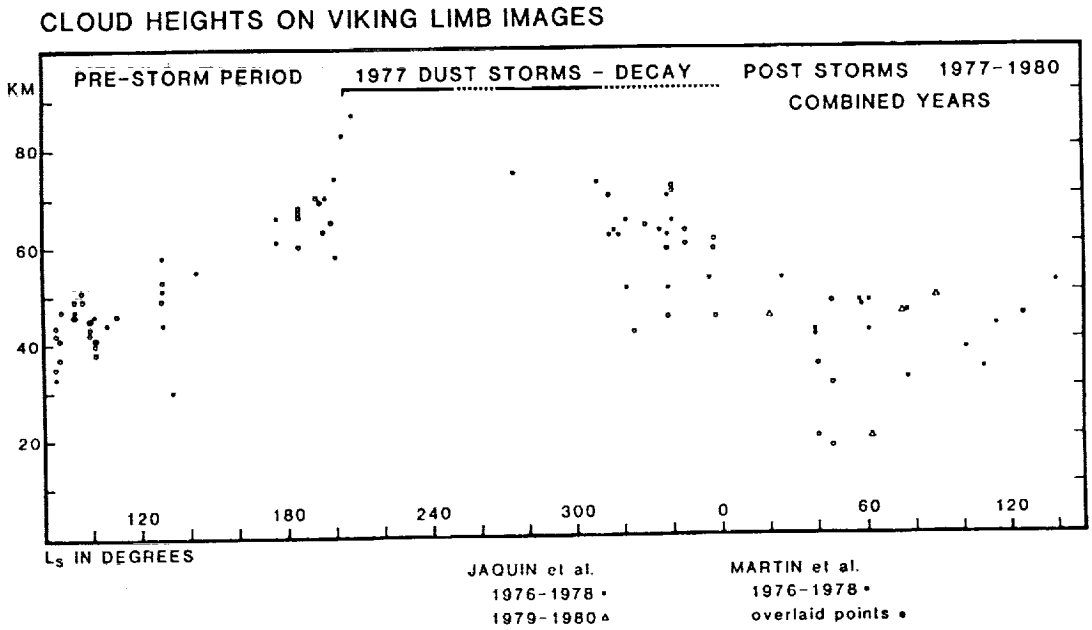

will provide a useful tool for evaluating how these storms evolved. Maps made from Earthbased data of earlier storms (3,4) are being used to fill gaps in the data where similarities between storms can be identified. This research has already convinced us that the recession of the seasonal South Polar Cap played a significant role in the development of the 1977 storms. Based upon earlier findings (5), correlations between the cap recession and dust activity need further investigations.

This research is supported by NASA grant NAGW-2257, as well as Lowell Observatory, the University of Toledo, Caltech, and the Mars Observer Project at the Jet Propulsion Laboratory

REFERENCES

1. Martin, L. J., Baum, W. A., Wasserman, L. H., and Kreidl, T. J. 1983. *Bull. Amer. Astron. Soc.* **15,** 847 (abstract).
2. Jaquin, F., Gierasch, P., and Kahn, R. 1986. *Icarus* **68,** 442–461.
3. Martin, L. J. 1974. *Icarus* **22,** 175–178.
4. Martin, L. J. 1976. *Icarus* **29,** 363–380.
5. James, P. B., Malolepszy, K. M., and Martin, L. J. 1987. *Icarus* **71,** 298–305.

NEW DUST OPACITY MAPS FROM VIKING IR THERMAL MAPPER DATA

T.Z. Martin, Jet Propulsion Laboratory, and M.I. Richardson, Imperial College London

Mapping of dust opacity of the Mars atmosphere, using the silicate-induced absorption of 9 μm radiation, has been performed with the Viking Infrared Thermal Mapper (IRTM) data by Hunt, Mitchell, and Peterfreund (1) for several local dust storms, and by Martin (2) in a global sense. Martin covered only the time period from L_s 168° in 1976 to 270° in 1977, ending before the second and larger dust storm of 1977.

We present here first results from an effort to extend the earlier mapping work to the period of the 1977b major storm, and to concentrate attention on the details of opacity behavior during the initial phases of the 1977a and b storms.

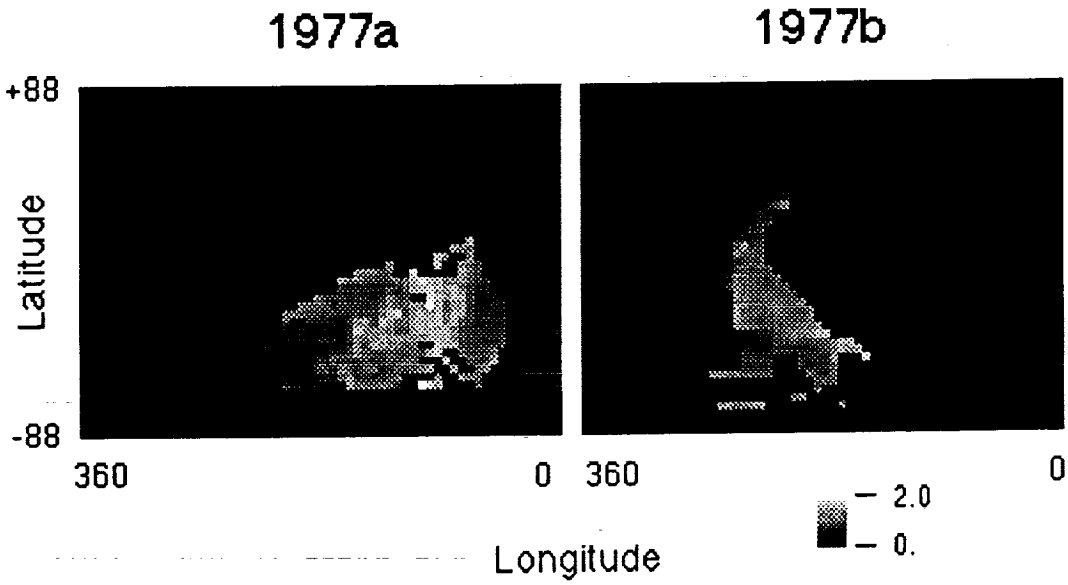

Images of 9 μm opacity obtained from IRTM sequences on 1977 day 49, UTC 4-8:30, VO2 rev 177 (left), and day 157, UTC 7:40-9:40, VO1 rev 353 and VO2 rev 286 (right). The white level corresponds to an opacity value of 2.0.

The figure shows the earliest evidence in the IRTM data for the inception of the two major 1977 storms. On day 49, opacities above

1.0 appear in the region from the equator south to about -44°, and from about longitude 84 to 156°. The L_s value at this time is 206.3°. The first evidence of this storm in visual images (3) occurs about 30 hours earlier, on VO2 rev 176, at L_s 205.6°.

The right figure shows opacities of 1.1 at latitude -36°, longitude 180°, surrounded by lower values grading to regional levels near 0.5. This coverage from nearly simultaneous VO1 and VO2 data was obtained at L_s 274.2°, preceding by about 15 hours the first imaging evidence for the storm at VO2 rev 287, L_s 274.5°. There is, however, no guarantee that the origin of the 1977b storm has been "captured" in these IRTM observations.

The 1977b storm is characterized by rapid changes in opacity and high spatial variability during its formative stages, and a much smoother distribution in later phases. Between L_s 275 and 280°, the storm was most intense in southern midlatitudes. Subsequently, opacities subside in the south, but equatorial regions remain dusty; the 9 μm opacity exceeds 1.0 near the equator until at least L_s 320°.

This work takes advantage of software developed by the Planetary Data System Radiometry Node by H.H. Kieffer and R. Gurule to treat radiometry data sets. That system, known as XG, allows access to the IRTM and other data sets under a TAE-driven interface operating on VAX VMS systems. Another PDS-developed item, the compact disk (CD-ROM) version of the IRTM data set, permitted ready access to the 650 Mbyte data set.

M. Richardson participated in this work as a 1991 Summer Undergraduate Research Fellow at the Calif. Inst. of Technology. The research described in this paper was carried out by the Jet Propulsion Laboratory, California Institute of Technology, under a contract with the National Aeronautics and Space Administration.

References:

1. Hunt, G.E., Mitchell, E.A., and Peterfreund, A.R. (1980) Icarus 41 p. 389-399.
2. Martin, T.Z. (1986) Icarus 66 p. 2-21.
3. Briggs, G., Baum, W.A., and Barnes, J. (1979) J. Geophys. Res. 84 p. 2795-2820.

TEMPORAL VARIABILITY OF THE SURFACE AND ATMOSPHERE OF MARS: VIKING ORBITER COLOR OBSERVATIONS

A. S. McEwen, USGS, Flagstaff, AZ 86001.

We are near the final stages in the processing of a large Viking Orbiter global color dataset. Mosaics from 57 spacecraft revolutions (or "revs" hereafter) have been produced, most in both red and violet or red, green, and violet filters. Phase angles range from 13° to 85°. A total of ~2000 frames have been processed through radiometric calibration, cosmetic cleanup, geometric control, reprojection, and mosaicking into single-rev mosaics at a scale of 1 km/pixel. All of the mosaics are geometrically tied to the 1/256°/pixel Mars Digital Image Mosaic (MDIM). Photometric normalization is in progress, to be followed by production of a "best coverage" global mosaic at a scale of 1/64°/pixel (0.923 km/pixel). Global coverage is near 100% in red-filter mosaics and 98% and 60% in corresponding violet- and green-filter mosaics, respectively. Soon after completion, all final datasets (including single-rev mosaics) will be distributed to the planetary community on compact disks.

Perhaps the most interesting portion of this dataset is the comparison of overlap regions, which show significant temporal variations in surface and atmospheric features. These are direct observations of atmospheric and surface processes and interactions. About half of Mars is covered at least twice by these mosaics, and many areas are covered up to five times. A few examples of these temporal comparisons are described below and will be presented in a poster at the MSATT workshop in Boulder. All of the color image comparisons were constructed from red-and violet-filter images only, even when green-filter images are also available, to insure comparability with color sets that lack green images. The images have been stretched to increase the contrast but with constant ratios between the stretch parameters for each color. This procedure preserves the relative color variations for comparison purposes.

Atmospheric Effects on Surface Observations

A very interesting result of the stretching procedure is that the very clear atmospheric observations are immediately obvious because the overall color of the scene is markedly redder than is the color of the same area viewed through a hazier atmosphere. This color relation applies only to seasons with a relatively dust-free atmosphere, when haze variations are primarily due to condensates. The bluer images also have more discrete atmospheric features and show correlations between color and local topography because the hazes settle into local topographic lows or because high mountains such as the Tharsis Montes rise through the low-lying regional haze. The relative atmospheric (versus surface) contribution to the scene brightness and color is increased by large angles of illumination, emission, or phase, as well as atmospheric opacity. These very clear atmospheric observations are crucial to accurate mapping of surface materials. Three examples are described below. All of the images described below were acquired during times of relatively low atmospheric opacity (1-4), and all of the Mars mosaics in this dataset were selected for processing because they appear relatively clear of atmospheric obscuration (except for the southern hemisphere dust storm initiation sequence, described below). Therefore, these relatively reddish scenes represent unusually clear atmospheric conditions.

The first example consists of three views of the Tharsis Montes. Controversy exists over the nature of dark materials on the volcano flanks. In two of the views (revs 735A and 334S) the Tharsis Montes appear markedly darker and redder than surrounding areas, and previous workers have concluded that these represent a distinct spectral (and compositional) unit (5, 6). This has been puzzling because the thermal inertia of the Tharsis Montes is consistent with atmospheric dust deposits (7-9), so we would expect the color and albedo to be similar to that of bright red areas over much of Mars. The very clear atmospheric conditions present during the third view (rev 583A) reveals that the color and albedo of the Tharsis Montes are indeed similar to surrounding regions. Although slope winds are clearly active on the Tharsis Montes (10), redistribution of only the very finest particles (1-20 μm) may be sufficient to explain the albedo variations (11, 12); the thermal inertia may be uniformly low for particles in this size range (13).

The second example consists of two views of the Mangala Valles/Memnonia Fossae region. Briggs et al. (14) suggested that this may be an exceptional area for atmosphere-surface exchange of water vapor and of potential interest for future lander missions. This is another example of a very clear atmosphere observation (rev 614A) compared to a hazy view (rev 690A). In the rev 690A mosaic we see haze concentrated in discrete topographic lows such as craters and channels, as has been described previously (10). In addition, comparison with the rev 614A mosaic reveals greater haze concentrations over lowland plains than highlands regions; the resultant color variations could be mistakenly related to the surface materials.

A third comparison shows the central region of Valles Marineris. In the clear atmosphere view (rev 583A) we see a spectral unit associated with some of the interior layered deposits that is brighter and less red than other bright red (probably dust-mantled) regions; in the rev 334S view this spectral unit is not distinguishable. This unit corresponds both to an exposure in a steep slope of evenly layered deposits in Ophir Chasm and the major surface exposure of irregular layered deposits in western Candor Chasm (15). The irregular layered deposits are of special interest because they consist of a thick sequence that is superimposed over major landslide deposits and must have been emplaced very late in Martian history (late Amazonian).

Temporal Variability of Surface Units

There are three major non-polar color/albedo units or endmembers: bright red (dust), dark red, and dark grey (bluish in enhanced images) (6, 16, 17). Many of the color comparisons illustrate variability in bright red and/or dark grey surface deposits. We have found no evidence in any of our temporal comparisons to contradict the suggestion that the dark red unit is relatively immobile, supporting the suggestions that this unit is either a duricrust or a lag deposit. There are many changes

in "small" (10s of kilometers) discrete features. Changes in the Claritas Fossae/Syria Planum region (revs 583A and 334S) may have occurred during the 1977 global dust storm, but changes in the Memnonia Fossae/Daedalia Planum region (revs 614A and 690A) occurred during northern summer, perhaps due to slope winds from the Tharsis region.

Drifts of bright red dust appear to have migrated in southern Acidalia Planitia during the period between revs 590A and 334S. This period included the dusty northern winter of 1979 in which no global storm occurred (18). Arvidson et al. (17) suggested that the bright red dust border south of Acidalia accumulated because the dust carrying capacity decreases at the border between smooth dark gray and rough intermediate-albedo red units. The color comparisons do seem to illustrate the southward migration of dust over Acidalia Planitia. This migrating dust may account for the thin (< 1 cm) dust layer hypothesized to cover the region of Mutch Memorial Station (VL1) (19).

A remarkable set of images cover a portion of Terra Cimmeria (latitude -42°, longitude 210°). The first observation (rev 459A) was acquired soon after the end of the 1977 global dust storms, and all of the southern hemisphere mosaics acquired during this period (revs 426A-469A) appear mantled with seasonal dust which has not yet been completely removed from dark areas. The second observation (rev 605A), acquired during northern spring (L_s 46°), shows a distinctive dark feature where only scattered dark areas were present during rev 459A. In the third observation (rev 323S), the eastern half of the dark feature is absent. The second observation reveals a plume-shaped structure covering the eastern dark area with several km of apparent vertical relief. It is unlikely that a surface unit more than a kilometer thick was both deposited and removed within a little more than a Martian year, so, unless the appearance of vertical relief is deceptive, this must be an atmospheric plume. Its morphology is similar to other Martian dust plumes (20), but its low albedo and relatively neutral color are anomalous.

Large-scale color and albedo changes in the region south of Capri Chasm are revealed by a four-image comparison. Geissler and Singer (21) interpreted the changes seen between revs 586A and 334S as due to the southward movement by saltation of dark material out of the canyons, but movement by more than 1000 km in a Martian year exceeds reasonable migration rates via saltation. Although dark materials may migrate southward from the canyons over longer time periods, analysis of mosaics from two additional revs reveals that the observed color/albedo changes were due to removal of a regional dust mantle deposited during the global storms of 1977. The rev 469A observations are part of the post dust storm sequence (L_s 342°) that shows a residual dust mantling throughout the southern hemisphere following the 1977 global storms, as discussed previously. The second observation, acquired in early northern spring (L_s 38°, rev 586A), shows that dark erosional streaks and coalesced streaks (22) have removed some of the bright cover. (The rev 469A mosaic also shows many dark erosional streaks, so much of the dust had already been removed before this rev.) The third observation (rev 663A) was acquired in late northern spring (L_s 72°), and shows the same pattern of bright and dark patches seen in the final view, acquired almost a full Martian year later (rev 334S, L_s 70°). A similar sequence of albedo change in this region is apparent in the IRTM albedo maps (23). Therefore, the large-scale albedo changes occurred during northern spring, not during southern summer when the north-to-south near-surface flow from the Hadley cell would be most likely to transport materials southward from the canyons. Removal of a thin layer of dust fallout probably accounts for the reemergence of classical large-scale albedo patterns throughout the equatorial region of Mars following global dust storms (24).

Southern Hemisphere Dust Storm Initiation Sequence

A series of nine color mosaics (revs 165B through 182B, L_s 198°-210°) show portions of the southern hemisphere just before and during the initial stages of the first 1977 global dust storm. In addition, color observations of almost the entire southern hemisphere from six revs (441A-469A) were acquired soon after clearing of the atmosphere in the southern hemisphere following the 1977 storms. These mosaics will be reprojected to a common format for detailed comparisons of the surface and atmosphere before, during the initial stages, and after the dust storm activity. Although Mars appears uniformly bland during mature stages of global storms, the dust clouds have considerable structure during the initial stages. Preliminary examinations have revealed many interesting relations between the dust clouds and surface topography, albedo, and the seasonal CO_2 frost margin, which have not been previously described (14, 20, 25).

(1) Martin, T. Z., **Icarus 66**, 2-21, 1986. (2) Thorpe, T. E., **JGR 84**, 6663-6683, 1979. (3) Thorpe, T. E., **JGR 86**, 11419-11429, 1981. (4) Colburn, D. S. et al., **Icarus 79**, 159-189, 1989. (5) Soderblom, L. A. et al., **Icarus 34**, 446-464, 1978. (6) McEwen, A. S., **LPSC XVIII**, 612-613, 1987. (7) Zimbelman, J. R., and H. H. Kieffer, **JGR 84**, 8239-8251, 1979. (8) Palluconi, F. D., and H. H. Kieffer, **Icarus 45**, 415-426. 1981. (9) Christensen, P. R., **JGR 91**, 3533-3546, 1986a. (10) Lee, S. W. et al., **JGR 87**, 10,025-10,042, 1982. (11) Wells, E. N. et al., **Icarus 58**, 331-338, 1984. (12) Thomas, P., and J. Veverka, **Icarus 66**, 39-55, 1986. (13) Jakosky, B. M., **Icarus 66**, 117-124, 1986. (14) Briggs, G. et al., **JGR 82**, 4121-4150, 1977. (15) Lucchitta, B. K. et al., in Mars, edited by H. H. Kieffer et al., in press. (16) Kieffer, H. H. et al., **PLPSC 12B**, 1395-1417, 1981. (17) Arvidson, R. E. et al., **JGR 94**, 1573-1587, 1989b. (18) Leovy, C. B. et al., in Recent Advances in Planetary Meteorology, edited by G. Hunt, Cambridge University Press, 69-84, 1985. (19) Jakosky, B. M., and P. R. Christensen, **Icarus 66**, 125-133, 1986. (20) Briggs, G. et al., **JGR 84**, 2795-2820, 1979. (21) Geissler, P. E., and R. B. Singer, **Bull. AAS 22**, 1061, 1990. (22) Thomas, P. et al., **Icarus 45**, 124-153, 1981. (23) Christensen, P. R., **JGR 93**, 7611-7624, 1988. (24) Martin, L. J., in Mars, edited by H. H. Kieffer et al., in press. (25) Kahn, R. A. et al., in Mars, edited by H. H. Kieffer et al., in press.

Regional Variations in the Stability and Diffusion of Water-Ice in the Martian Regolith: Michael T. Mellon [*,†] and Bruce M. Jakosky [*,‡], [*] Laboratory for Atmospheric and Space Physics, [†] Department of Astrophysical, Planetary, and Atmospheric Sciences, [‡] Department of Geological Sciences, University of Colorado, Boulder, CO 80309

Introduction:

Geologic evidence suggests subsurface water-ice has played an important role in the formations of Martians landforms. Forms of mass-wasting such as debris aprons and flow patterns on valley floors suggest creep deformation of ice-laden soil, [1,2] while thermokarst and chaotic terrain suggest once extensive deposits of ground ice that were later removed [1]. Squyres and Carr [2] mapped the global distribution of ice-related morphology. Their study showed regional variation, in both latitude and longitude, in the distribution of debris aprons, concentric fill craters, and "softened" crater profiles.

Previous studies of the stability of subsurface ice have assumed the thermophysical properties of the regolith are regionally invariant and that latitudinal variations in insolation alone account for changes in water ice stability [3-5]. Using the current mean annual atmospheric water vapor abundance, Farmer and Doms [3] calculated a frost-point temperature of about 200K and concluded that water-ice would remain stable poleward of about 40 degrees and would be seasonally stable down to 30 degrees latitude. Fanale *et al* [4] and Zent *et al* [5] additionally allowed for the exchange of water vapor with the atmosphere and reached a similar conclusion. These studies provide an explanation for the latitudinal variation in the geomorphic features mapped by Squyres and Carr, but do not provide an explaination for the longitudinal dependence.

A comparison of the map of Squyres and Carr with maps of thermal inertia and albedo from Palluconi and Kieffer [6] reveal a correlation between low thermal inertia/high albedo regions and regions of ice-related surface morphology. This correlation suggests that thermal inertia and albedo play an important role in determining water-ice stability in conjunction with latitude. By allowing for regional variability of the thermophysical properties of the regolith we show that the regions containing ice-related features have colder mean annual surface and subsurface temperatures and would therefore act as preferential sinks of atmospheric water vapor.

Models and Results:

To study the effects of the regional variations in water-ice stability we developed a thermal model of the Mars subsurface. In this model each latitude and longitude define the thermal inertia, albedo, and insolation. The mean annual subsurface temperatures are then computed. Colder regions are, to first order, more stable with respect to the condensation of water-ice. Specifically, if the current mean atmosphere is in equilibrium with existing subsurface ice, we expect all regions colder that about 200K to act as sinks of atmospheric water. Results indicate a strong regional dependence of water-ice stability at the current epoch as well as past epochs (*i.e.*, high and low obliquity). The equatorward-most extent of ice stability varies in the northern hemisphere by about 30 degrees of latitude from one longitude to another. These variations are less in the southern hemisphere. The evolution of Mars' orbit affects these results, showing regions of episodic stability. During high obliquity stable regions extend furthest equatorward. Regions of stability correspond well with the ice-related features, particularly in the northern hemisphere where the Squyres and Carr map is more complete. These regions include areas north and north-east of Tharsis and fretted terrain between 280 and 0 degrees longitude.

To further refine our understanding of water ice stability we plan to model the diffusion of water vapor within the regolith and in exchange with the atmosphere. We expect to find that regions of low mean annual temperature will preferentially act as sinks of atmospheric water. We hope to characterize the time-scale on which water will exchange with the atmosphere; seasonal or climatological. We also hope to clearly identify regions of permanent stability and episodic stability as a function of the Martian orbital cycles (*i.e.*, obliquity, eccentricity, and argument of perihelion).

References:

[1] M. H. Carr and G. G. Schaber, **JGR** 82, 4039-4054 (1977), [2] S. W. Squyres and M. H. Carr, **Science** 231, 249-252 (1986), [3] C. B. Farmer and P. E. Doms, **JGR** 84, 2881-2888 (1979), [4] F. P. Fanale, J. R. Salvail, A. P. Zent, and S. E. Postawko, **Icarus** 67, 1-18 (1986), [5] A. P. Zent, F. P. Fanale, J. R. Salvail, S. E. Postawko, **Icarus** 67, 19-36 (1986), [6] F. D. Palluconi and H. H. Kieffer, **Icarus** 45, 415-426 (1981)

EXPLORING COMPOSITIONAL VARIATIONS ON THE SURFACE OF MARS APPLYING MIXING MODELING TO A TELESCOPIC SPECTRAL IMAGE

E. Merényi, J. S. Miller and R. B. Singer
Planetary Image Research Laboratory
University of Arizona, LPL
Tucson, AZ 85721

The linear mixing model approach of Adams *et al.* (1989) has successfully been applied to data sets of various natures, where the measured radiance could be assumed a linear combination of radiance contributions [e.g. Adams *et al.* 1986, Pieters *et al.* 1985, Smith *et al.* 1990].

The present work is an attempt to analyze a spectral image of Mars with linear mixing modeling. This endeavor is pioneering in that we use, as described below, a quite unique data set; at the same time, we apply mixing modeling on a very large spatial scale, 200-500 km/pixel. Since earlier applications typically dealt with 0.1-40 m/pixel (e. g. for Earth remote sensing and Viking Lander images) to about 10 km/pixel (Viking Orbiter pictures, for example), we have to exercise special care in verifying the validity and interpretation of the mixture modeling results. Our results will be directly compared with our conventional analysis of these data.
Bell *et al.* (1990) collected a very similar data set at the same time ours was recorded, which can also provide a valuable comparison for our results.

This paper reports the first step of a continuing analysis - exploration of compositional variations of the Martian surface in terms of spectral endmembers that were selected from the image itself. The second step will be to relate the image endmembers to known earth-based reference spectra from laboratory and field measurements.

The visible and near-IR spectral region contains primarily information about Fe^{3+} and Fe^{2+} mineralogy of Mars surface materials, as discussed by Singer (1982, 1985) and others. Relatively subtle spectral shapes and differences are of importance in terms of the exact mineralogies of the ferric iron bearing phases present, and therefore reflect the parent materials and modes of formation. Most of the low-albedo regions also show Fe^{2+} absorptions near 0.95 microns, attributable to pyroxenes in the basaltic crustal material. Differences in pyroxene abundance and composition among low-albedo regions have been observed based in these and other data, using more conventional spectral analysis methods.

The data under investigation with mixture modeling [Singer *et al.* 1990] consist of a visible/NIR spectral image cube of Mars in approximate orthographic view, centered just south of Sinus Meridiani and including the NW and SE limbs. The spectral range is 0.442μm to 1.040μm in 300 channels, resampled from a set of eleven prism-dispersed 800-channel spectrograph images. The image cube scale is 6.7 pixels per arc second along the spectrograph slit (vertical), and 1 image per arc second in the scan direction (horizontal), expanded to 7 pixels for display. Seeing was better than 1 arc second, with best-case resolution near 280 x 150 km at the subearth point. Data values are Mars / HD 1835, where HD 1835 is 9 Ceti, a G2V solar analog star. The values have only a multiplicative offset from Radiance Factor; the zero level is accurate. The data have been corrected for effects from the instruments and the terrestrial atmosphere. The source images for the spectral image cube were taken 07:21 - 08:08 UT September 26, 1988 at the 61" telescope at the University of Arizona's Catalina Station near Tucson, Arizona. Martian L, was

279 degrees (southern summer), subearth latitude 21.5 degrees S, subsolar latitude 25 degrees S, illumination phase 4 degrees.

Following the methodology of Adams *et al.* (1989), we can satisfactorily model the given area of Mars with 4 or 5 image endmembers. (An independent PCA analysis supports that this many endmembers are justified.) These endmembers are representative spectra from Arabia, Sinus Meridiani, South Acidalium, the Chryse region, and from a smaller area located just south of Sinus Meridiani. Shade was also always used as an endmember, as advocated by Adams and co-workers. The shade fraction, however, became quite featureless as we were improving on the model fit by the inclusion of additional spectral endmembers. This corresponds to the fact that at this large spatial scale there is not much shadowing/shading except for limb darkening.
Two small areas, to the south and to the west of Sinus Meridiani - collectively referred to as 'Meridiani Border' from now on - look spectrally distinct from everything else. Earlier natural color and color ratio images from the Viking Orbiter [Kieffer *et al.* , 1981] possibly support this; the much weaker distinction there may be attributed to the low spectral resolution and smaller spectral range. Possible compositional causes for this distinction will be discussed.

We successfully separated condensates over the edge of the north polar region, by including a 'cloud' endmember, in addition to the ones mentioned above.

Studying the residuals from the linear mixing model fit, we see several spatially coherent features around .782μm, .802μm, .822μm and .942μm, which do not coincide with any known surface unit on Mars. Discussion on the possible origin of these residuals will be given.

References

Adams, J. B., M. O. Smith, P. E. Johnson, Spectral Mixture Modeling: A New Analysis of Rock and Soil Types at the Viking Lander 1 Site, *JGR* **91** B8, pp 8098- 8112, 1986

Adams, J. B., M. O. Smith and A. R. Gillespie, A Mixing Model Strategy for Analyzing and Interpreting Hyperspectral Images, *Remote Geochemical Analysis: Elemental and Mineralogical Composition*, Pieters and Englert ed., 1989

Bell III, J. F., T. B. McCord, and P. G. Lucey, Imaging Spectroscopy of Mars (0.4 - 1.1μm) During the 1988 Opposition, *Proceedings of the 20th LPSC*, pp. 479-486, 1990

Kieffer, H. H., P. A. Davis, and L. A. Soderblom, Mars global properties: Maps and applications, *Proc. Lunar Planet. Sci. Conf., 12th*, 1395-1417, 1981

Pieters, C. M., J. B. Adams, P. J. Mouginis-Mark, S. H. Zisk, M. O. Smith, J. W. Head, and T. B. McCord, The Nature of Crater Rays: The Copernicus Example, *JGR* **90** B14, pp 12,393-12,413, 1985

Singer, R. B., J. S. Miller, W. K. Wells, E. S. Bus, Visible and near-IR spectral imaging of Mars during the 1988 opposition, *Lunar and Planetary Science XXI*:1164-1165 (abstract), 1990

Singer, R.B., Spectral evidence for the mineralogy of high-albedo soils and dust on Mars. *J. Geophys. Res.*, **87** pp. 10159-10168, 1982.

Singer, R.B., Spectroscopic observation of Mars. *Adv. Space Res.*, **v.5**, #8 pp. 59-68, 1985.

Smith, M. O., S. L. Ustin, J. B. Adams, A. R. Gillespie, Vegetation in Deserts: I. A regional Measure of Abundance from Multispectral Images, *Remote Sensing of Environment* **31**:1-26, 1990. II. Environmental Influences on Regional Abundance, *Remote Sensing of Environment* **31**:27-52, 1990

Simulation of Martian Surface-Atmosphere Interaction in a Space-Simulator: Technical Considerations and Feasibility

D. Möhlmann and H. Kochan
Institut für Raumsimulation, DLR ,5000 Köln 90, Germany
P.O.Box 906058

The Space Simulator of German Aerospace Research Establishment at Cologne, formerly used for testing Satellites, is nowadays (since 1987) the central unit within the research sub-program "Comet-Simulation" (KOSI). This is part of the program "Small Bodies in the Solar System" funded by the Deutsche Forschungsgemeinschaft. Meanwhile the KOSI-team investigated physical processes relevant for real comets and their surfaces.As a byproduct we gained experience e.g. in sample-handling under simulated space conditions. In broadening the scope of the research activities of the DLR Institute of Space Simulation an extension to "Laboratory-Planetology" is planned.Following the KOSI-experiments a Mars-Surface-Simulation with realistic minerals and surface soil in a suited environment (temperature, pressure,CO_2-atmosphere) is foreseen as the next step.Here,our main interest is centered on thermophysical properties of the Martian surface and energy transport (and related gas transport) through the surface.Focusing these activities in the direction of the planned Mars missions it seems very meaningful to cooperate with the Mars Observer Participating Scientists e.g. on the field of "surface-atmosphere interaction" (thermal properties and temperature,thermal conductivity and mechanical properties,outgassing, recondensation, weathering, interrelation of minerals and volatiles, material science aspects of permafrost soil,....).
These laboratory simulation-activities can be related to space missions as typical pre-mission and during-the-mission support of the experiments design and operations (simulation in parallel).Post mission experiments for confirmation and interpretation of results seem to be very valuable.The physical dimensions of the Space Simulator (cylinder of about 2.5m diameter and 5m length) give also the possibility to test and qualify experiment hardware under realistic Martian conditions.

p.1

MARS DUST STORM SIMULATIONS: ANALYSIS OF SURFACE STRESS;

J.R. Murphy, NRC Research Associate / NASA Ames; C.B. Leovy, Univ. of Washington

The primary mechanism by which dust is inserted into the martian atmosphere is the interaction of low-level atmospheric motions with the planet's surface. Near-surface winds exert a shear stress upon dust particles resting on the martian surface, and at some lower threshold limit of stress magnitude, ~0.04 N m^{-2} (1), particles are set into motion. Wind tunnel studies indicate that the first particles to be moved under martian surface conditions have radii of ~100 μm (2). Such particles are too large to remain in suspension in the martian atmosphere, but their impact back upon the surface can set smaller suspendable particles into motion. This process is termed saltation.

Numerical simulations of martian dust storms have been carried out via the interactive coupling of the NASA Ames Mars general circulation Model (3) with an aerosol transport/microphysical model (4). These simulations, though not explicitly employing calculated surface stress values for determination of surface dust lifting (which is prescribed), do allow for the investigation of the relationship of various circulation components, topographic features, and regions of enhanced surface stress under dusty atmosphere conditions.

In the absence of suspended dust, maximum calculated surface stress magnitudes occur at northern middle latitudes during a northern hemisphere winter solstice simulation. The introduction of dust into the model atmosphere at southern subtropical latitudes leads to the development of localized time-mean stress maxima there and a reduction in northern hemisphere stress magnitudes. As suspended dust becomes widespread, southern hemisphere stress maxima become well correlated with topographic features. Semidiurnal variations of stress magnitude at northern middle latitudes during dust storm simulations suggest the role which the dynamic effects of thermal tides can play in the generation of enhanced surface stress. The lack of such temporal stress variations at more equatorial and southern hemisphere latitudes is consistent with the apparent inability of the model to properly account for near-surface semidiurnal wind variations there.

The results to be presented indicate that neither positive nor negative feedbacks between atmospheric dust loading and calculated surface stress are ubiquitous features of these simulations. The results suggest that specific circulation components are important in generating enhanced surface stress values at particular locations and times and that temporal variations of these components might lead to renewed dust raising after an initial large lifting event.

(1) R. Greeley and J. D. Iversen (1985), Wind as a geological process, Cambridge Press. (2) J.B. Pollack *et al.* (1976), Icarus, **29**, 395-417. (3) J.B. Pollack *et al.* (1990), JGR, **95**, 1447-1474. (4) O.B. Toon *et al.* (1988), JAS, **45**, 2123-2143.

IS GROUND ICE STABLE NEAR THE MARTIAN EQUATOR? D. A. Paige, Dept. of Earth and Space Sciences, UCLA, Los Angeles, CA 90024.

Determining the present distribution of subsurface water ice on Mars will undoubtedly be a prime objective for future spacecraft missions. Past theoretical studies (1,2,3) have predicted that Martian ground ice should be stable to evaporation only at latitudes poleward of approximately ±50° . Presented here are a new set of calculations which show that bright surficial dust deposits can protect subsurface ice deposits from evaporation at much lower latitudes than previously expected.

Figure 1 shows thermal model calculations of annual minimum, annual maximum, and annual average temperatures as a function of latitude for three sets of soil thermal and reflectance properties. The first has a thermal inertia of .0065 cal cm^{-2} $sec^{-1/2}$ and an albedo of 0.25, which are values that have been used in many previous studies as representative of average Martian soil. The second has a thermal inertia of 0.015 cal cm^{-2} $sec^{-1/2}$ and an albedo of 0.25, and is representative of the highest thermal inertia surfaces mapped by Palluconi and Kieffer (4). The third has a thermal inertia of 0.002 and an albedo of 0.3, and is representative of the widespread low thermal inertia material that is mapped in the Martian equatorial and temperate latitudes. Because of the non-linear surface boundary condition, the low thermal inertia surfaces have substantially lower annual averaged temperatures. If the effects of subsurface heat flow are neglected, then the calculated annual average surface temperatures will be equal to the expected annual mean temperatures at depth.

Ground ice will be stable to evaporation if its temperature never exceeds the local frost point. Since water vapor in Martian soil is transported by diffusion, the water vapor concentration at depth can be determined if the water vapor concentration at the surface is known. In the mid-latitude regions, night time surface water vapor concentrations are extremely low due to saturation at low surface temperatures, which results in the formation of nightly surface frost and ground fog (5,6). During the day, surface water vapor concentrations increase sharply in the morning, but are not saturated by mid-day due to vertical atmospheric mixing in the boundary layer. The Viking MAWD instrument measured daytime total column water vapor abundances of 10 to 18 precipitable microns in the northern equatorial and temperate latitudes (7). If daytime atmospheric water vapor is assumed to be mixed uniformly with pressure to the top of the boundary layer, then the daytime water vapor concentration at the surface can be estimated if the height of the boundary layer is known. Diurnally averaged surface water vapor concentrations, and corresponding frost point temperatures, can also be estimated by assuming that nighttime surface water vapor concentrations are essentially zero, and that the daily average is half the calculated daytime value. Figure 2 shows estimated frost point temperatures as a function of daytime column water abundance for boundary layer heights of 10, 5 and 2 km. The results show that the daily averaged water vapor abundances at the surface of Mars imply that the subsurface frost point is 201K, with ±6K uncertainties due to observed spatial and temporal variations in column water vapor abundances, and weak observational constraints on the variation of water vapor concentration with altitude. This range of expected subsurface frost point temperatures is shown in Figure 1.

Before using the results of this analysis to make specific conclusions regarding the latitudinal distribution of Martian ground ice, it is extremely important to point out that the calculated average temperatures in the low thermal inertia regions in Figure 1 have been overestimated. This is because Palluconi and Kieffer's fits to the IRTM diurnal surface temperature observations excluded data obtained between 2pm and 8pm Mars local time, because actual surface temperatures are systematically lower than the model predictions during this period (4). Ditteon has studied these anomalously low temperatures in detail (8). Figure 3 shows his compilation of the differences between actual observed surface temperatures and Palluconi and Kieffer best fit predicted temperatures for low thermal inertia regions between 0° and 30° latitude. These results imply that, on average, surface and subsurface temperatures in low thermal inertia regions are 2.6K colder than the Palluconi and Kieffer best fit predictions would indicate. With this additional qualification, the results shown in Figure 1 imply that ground ice could well be stable within low latitude, low thermal inertia regions.

A set of more detailed studies are presently underway to simulate the formation of high thermal inertia ground ice in low thermal inertia regions. Preliminary results indicate that dust covered ground ice deposits are thermally stable, and that the permafrost boundary may be just a few centimeters below the surface in these regions. It is interesting to note that Ditteon's own thermal model calculations explained the low afternoon temperatures in these regions by the presence of high thermal inertia rock

or duracrust material approximately one diurnal skin depth below the surface (8).

Determining whether or not stable ground ice deposits are present near the Martian equator will require a great deal of further study. For instance, Haberle and Jakosky have recently proposed that some of the afternoon cooling observed by IRTM may be due to atmospheric effects (9) and there is a wide range of other types of spacecraft and ground-based remote sensing data for these regions which need to be synthesized into a more complete picture. If near-surface water ice is indeed found to be present in these regions, it would have enormous implications for future Mars exploration, as access to water at low Martian latitudes could greatly facilitate a permanent human presence.

(1) Leighton R. B. and B. C. Murray, Science 153, 136-144, (1966). (2) Farmer, C. B. and P. E. Doms, JGR 84, 2882-2888, (1979). (3) Fanale, F. P. *et al.*, Icarus 67, 1, (1986). (4) Palluconi, F. D. and H. H. Kieffer, Icarus 45, 415-426, (1981). (5) Flasar, F. M. and R. M. Goody, Planet. and Space Sci. 24, 161-181, (1976). (6) Ryan, J. A. and R. d. Sharman, JGR 86, 503-511, (1981). (7) Jakosky, B. M. and C. B. Farmer, JGR 87,2999-3019, (1982). (8) Ditteon, R., JGR 87, 10197-10214, (1982). (9) Haberle, R. M. and B. M. Jakosky, Submitted to Icarus, (1991).

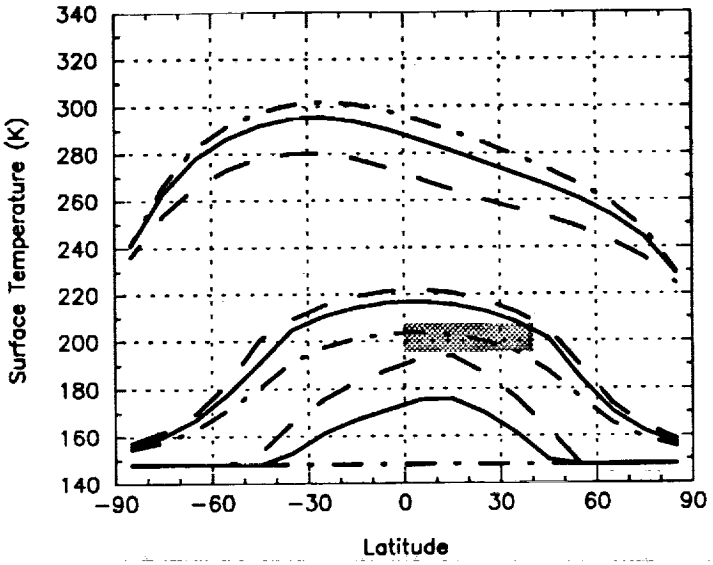

Figure 1. Model calculated annual maximum, minimum and average surface temperatures as a function of latitude for Mars high thermal inertia (dashed), low inertia (dot-dashed) and average inertia (solid) soils. The shaded region indicates the expected range of subsurface frost point temperatures in the northern equatorial region.

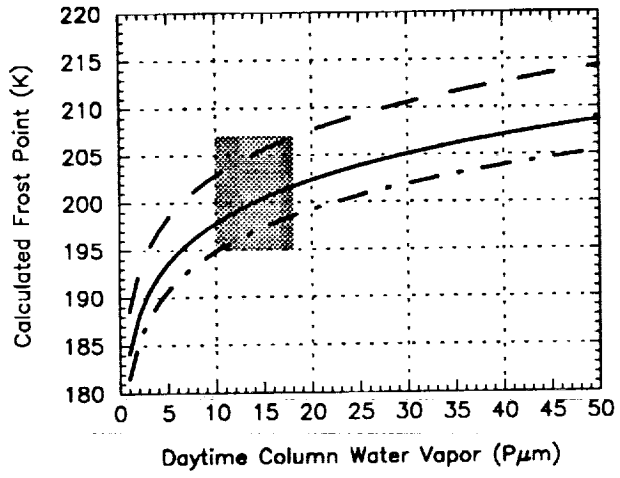

Figure 2. Calculated subsurface frost point temperatures as a function of daytime column water abundance assuming boundary layer heights of 2 km (dashed), 5 km (solid) and 10km (dot-dashed). The shaded region indicates the expected range the northen equatorial region based on the MAWD observations.

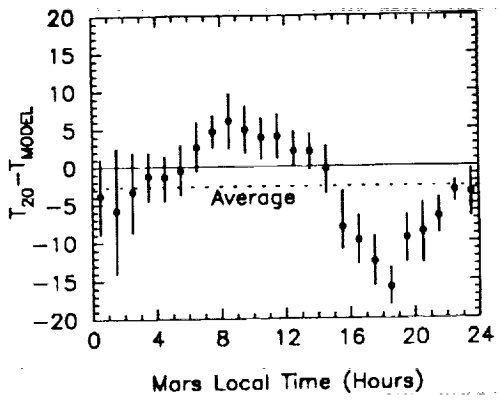

Figure 3. Ditteon's compilation of differences between IRTM observed and model calculated surface temperatures for low thermal inertia regions as a function of Mars local time for latitudes from 0 to 30N (8). The average difference is -2.6 K.

DISTRIBUTION OF COASTAL MORPHOLOGY IN THE MARTIAN NORTHERN LOWLANDS. T. J. Parker and D. S. Gorsline, University of Southern California, Dept. of Geological Sciences, Los Angeles, CA 90089-0740.

The northern plains of Mars exhibit boundary morphologies that have been interpreted as shorelines of a sea that formed as a result of flooding from the major outflow channels along the perifery of the lowlands (1). Parker et. al (1) focused on a morphologic description based on the very high resolution images available in the west Deuteronilus Mensae region where these boundaries and their relationships to pre-existing features could be most readily characterized. Here, we wish to describe the criteria used in their identification.

In the west Deuteronilus Mensae region, as many as seven distinct boundaries were identified (1). Because their recognition often depended on the availability of the rare, very high resolution Viking Orbiter images (in the neighborhood of 10m/pixel), however, many of these boundaries cannot be traced laterally for great distances. Two notable exceptions, labeled contacts #1 and #2 (in 1, figure 1), can be traced with nearly complete closure within the northern plains. These contacts were identified based on the following criteria:

Contact #1 is expressed in two ways:

(I) As a sharp albedo contact in which the plainward surface is usually darker than the upland surface. In this case, the cratered uplands dip gently northward into the lowland plains over several tens of kilometers and appear onlapped by plains materials along a "Gradational Boundary" (2). Locally, this contact is deflected southward into topographic lows such that the lowland plains material appears to embay the cratered uplands. Evidence for both onlapping of the cratered uplands by the plains material and erosion of the cratered uplands at the contact is described by Parker et al.(1). This type of contact is best expressed in southwest Chryse Planitia, along the northeast margin of Tempe Terra, in southeast Acidalia Planitia, and in southern Isidis Planitia.

(II) As a break in slope at fretted terrain and massif-outlier escarpments both with and without debris aprons. Escarpments with debris aprons often exhibit concentric striae on the apron surface. In high resolution images, these striae resolve into a system of low ridges and swales, parallel to the cliff base. These appear similar to multiple strandlines associated with regression of terrestrial lakeshores (e.g., lake Bonneville, Utah). Debris aprons with striae *radial* to the escarpment are also present in many fretted terrain regions and may post-date contact #1. These were not included when delineating this contact.

Morphological associations:

"No" small valley networks lie plainward of contact #1 (a few, non-typical small valleys associated with relatively young flow-ejecta craters characterize an exception). Many small valley networks and some of the older outflow channels (e.g., Mawrth Vallis, Ma'adim Vallis, Al Qahira Vallis) terminate at contact #1, and may have shared a common base level.

Contact #2 is typically expressed as a smooth, lobate or arcuate contact with most of its concave segments facing plainward. This contact is usually very distinct and readily traceable over great distances, however in regions with only low resolution coverage or with extensive evidence of eolian modification (e.g., Amazonis Planitia), establishing continuity can be difficult.

Morphological associations:

No small valley networks lie plainward of contact #2. Virtually no outflow channels lie plainward of contact #2 (a few possible relict channels can be identified by their softened outlines or as sinuous dark albedo features (e.g., N of Erebus Montes in Arcadia Planitia), suggesting they may have been drowned by plains flooding (lacustrine rather than volcanic).

Sharp-crested curvilinear ridges and arcuate terrain boundaries (3) occur along and just plainward of contact #2. "Stepped" massifs (3) are numerous plainward of contact #2 such

that much of the knobby terrain plainward of contact #2 consists of stepped massif. (Step "levels" appear relatively consistent in regions where these massifs are clustered). This type of massif may also be found in scattered examples between contacts #1 and #2 in places such as northern Acheron Fossae, southern Chryse, northwestern and southern Isidis, and along the lowland/upland boundary between Isidis and Tharsis. The step "levels" represented by these massifs are relatively hard to correlate from one massif to another (because they are typically far apart).

Giant polygonal terrain lies plainward of contact #2. Large impact craters (above ~10 km diameter) appear either very fresh with well-developed ejecta blankets, or are highly degraded and may exhibit stepped rims. Wrinkle ridges are rare plainward of contact #2. They often appear "rounded" or softened and may have small stepped massifs associated with them. Small wrinkle ridges typically terminate at contact #2. Sharply defined fretted terrain occurs exclusively outside contact #2. Rounded, softened fretted terrain can be identified in Deuteronilus Mensae, Protonilus Mensae, and perhaps northeast of Nilosyrtis Mensae. Thumbprint terrain occurs exclusively plainward of contact #2.

REFERENCES: (1) Parker et al. 1989, Icarus 81, p. 111-145. (2) Rossbacher, L. A., 1985, in Models in Geomorphology (Woldenberg, Ed.), p. 343-372. (3) Parker et al., 1987, NASA Tech. Memo. 89810, p.502-504.

JJ 574450

N92-29048

115

RECENT ELYSIUM VOLCANISM - EFFECTS ON THE MARTIAN ATMOSPHERE; J. B. Plescia and J. Crisp, Jet Propulsion Laboratory, California Institute of Technology, Pasadena, CA.

A vast area of smooth plains in southeastern Elysium near 5°N, 195° has been identified as young (Upper Amazonian) volcanic plains (1). These plains represent flood eruptions of very low viscosity lavas at a point in time much later than the volcanism that produced the major volcanoes of Elysium. Since volcanism is a principal mechanism by which gases are supplied to the atmosphere, and since these gases can have important climatic effects, it is important to consider the amount of H_2O, CO_2, and other gases that might have been erupted. We present estimates of input and release rates from this volcanic episode. The age is defined by the density of superposed craters; there are 89±15 craters $\geq$ 1 km per 10^6 km^2 corresponding to the Upper Amazonian (2) making this the youngest major volcanic episode. Lavas, covering 1.5 x 10^6 km^2 and presumably erupted through fissures, filled a topographic low and then flowed through knobby terrain into westernmost Amazonis. The western plains are characterized by scattered low shields having radial lava flows. Unit thickness is uncertain, individual flows are about 10 m thick; the entire deposit buries older knobby terrain having local relief of 200-400 m (estimated by Earth-based radar data (3)); hence the volcanics must be thick enough to bury that relief. On the basis of unit morphology, length of flows, and the extent of the deposit, it can be inferred that the lava was of low viscosity and mafic to ultramafic composition. The age and petrology of the shergottites suggest they may have come from this unit.

Volatile release can only be estimated, since compositions, volumes, and eruptive conditions are speculative. The H_2O content of terrestrial mafic to ultramafic lavas is relatively low (less than a few percent) but hydrous amphibole in melt inclusions from SNC meteorites (which presumably come from Mars) indicates potentially high water content in martian magma. Most terrestrial basalts have H_2O contents of >0.5% by weight (our lower estimate) and Johnson et al. (4) estimated the water content of the Chassigny parent magma at 1.5% (our upper estimate). Therefore, assuming these H_2O contents, the amounts released can be estimated for different volumes of erupted lava.

Total H_2O Release (g)				
Magma H_2O Content (wt %)			Rock	Unit
0.5	1.0	1.5	Mass (g)	Thickness (m)
9.5 x 10^{17}	1.9 X 10^{18}	2.9 X 10^{18}	1.9 X 10^{20}	50
2.0 X 10^{18}	3.9 X 10^{18}	5.9 X 10^{18}	3.9 X 10^{20}	100
4.7 X 10^{18}	9.4 X 10^{18}	1.4 X 10^{18}	9.4 X 10^{20}	250
9.5 X 10^{18}	1.9 X 10^{19}	2.9 X 10^{19}	1.9 X 10^{21}	500

The present mass of H_2O in the martian atmosphere has been estimated to be 10^{15} g (5). Therefore, this volcanic episode would have released total H_2O amounting to 10^2 to 10^4 times the present atmospheric mass. However, the critical point is not simply the H_2O amount, but the rate at which it was injected because a large release rate could substantially effect the local and or global climate.

Estimating release rate requires an estimate of the lava effusion rate. Eruption rates have been observed directly for only a few terrestrial volcanoes; rates have never been directly observed for massive flood eruptions such as Columbia River Basalts. Crisp (6) presented average long-term (300-10^8 yr) eruption rates for volcanoes and volcanic centers. Eruption rates are 1.6 X 10^{-1} km^3 yr^{-1} for the Karroo volcanics; 8 X 10^{-2} km^3 yr^{-1} for the Columbia Plateau; and 7 X 10^{-3} km^3 yr^{-1} for the Snake River Plains; Mauna Loa averages about 8.5 X 10^{-2} km^3 yr^{-1}. These long-term rates provide a lower bound on the actual effusion rates, as individual eruptions were probably separated by periods of quiescence. The effusion rate for the Roza member of the Columbia River Basalts is estimated at 10^6

m^3 sec^{-1} (7) which would correspond to a long-term average of 3.2 X 10^4 km^3 yr^{-1}; but the eruption probably lasted only a matter of days. Using these various rates, an estimate of the duration of volcanic activity for the Elysium flood lavas can be made.

	Time to Erupt Volcanics (Years)			
Volume Erupted	Long-Term Rates (km^3 yr^{-1})			
(km^3)	1.6 X 10^{-1}	8 X 10^{-2}	7 X 10^{-3}	3 X 10^4
1.4 X 10^4	9.4 X 10^4	1.9 X 10^5	2.1 X 10^6	<1
7.3 X 10^4	4.6 X 10^5	9.1 X 10^5	1.0 X 10^7	2
1.5 X 10^5	9.4 X 10^5	1.9 X 10^6	2.1 X 10^7	5
3.6 X 10^5	2.3 X 10^6	4.5 X 10^6	5.1 X 10^7	11
7.3 X 10^5	4.6 X 10^6	9.1 X 10^6	1.0 X 10^8	23

The gas loading rate depends on the actual magma effusion rate during eruption. The Elysium volcanic province is similar in volume to the Columbia Plateau and is presumably grossly similar in composition (i.e., mafic). Therefore, estimates of the eruptive history of the Columbia Plateau allow at least a point of comparison for Elysium. The Roza rate is probably a reasonable estimate of the actual effusion rate and such rates would imply a few short-lived periods of eruption separated by periods of quiescence. The entire Elysium volcanic episode probably spanned 10^6 - 10^7 years.

Assuming 1.0 weight % H_2O, a total eruption of 3.6 X 10^5 km^3, and 10 eruptive episodes of 100 days length each, the inferred effusion rate would be similar to the Roza event. H_2O loading rates would be 9.4 X 10^{15} g day^{-1}; about 10 times the present H_2O would be loaded into the atmosphere each day during the eruption. Greater eruption rates (i.e., shorter episodes) would inject correspondingly greater fluxes. The net activity would add about a factor 10^3 times the current water mass.

CO_2 typically varies from 0.01 to 1.5 % weight in mafic lavas. Assuming 1%, the volume of CO_2 and the release rate would be similar to H_2O. The current CO_2 mass of the martian atmosphere is about 2.5 X 10^{19} g. Under the above conditions, 9.4 X 10^{15} g day^{-1} would be released. This would correspond to an increase in mass to the atmosphere of only a factor of 3.8 X 10^{-4} per day, however the net influx of CO_2 would be similar to the present total atmospheric CO_2 mass. The amount of other volcanic gases are poorly constrained (and their concentration in the martian atmosphere is uncertain) but some rough estimates can be made based on their concentrations in terrestrial mafic lavas (8). The total release amounts would be: 8 X 10^{17} g for S; 6 X 10^{16} g for Cl, and 9 X 10^{16} g for Fl.

The actual amounts of released gas are small compared with the total masses released by all of martian volcanism (9), but they are important because of their very young age. Release of significant quantities of H_20 and $C0_2$ as well as other gases into the atmosphere in the recent past would have significantly affected the climate, at least on a local scale. The results of such volcanic gas release may be manifested as an influx of ground water, surface chemical alteration, or climate changes.

REFERENCES: (1) Plescia, J. B., 1990, Icarus, **88**, 465-490; (2) Tanaka, K., 1986, J. Geophys. Res., **91**, E139-E158. (3) Downs, G., et al., 1982, J. Geophys. Res., **87**, 9747-9754. (4) Johnson, M., Rutherford, M., and Hess, P., 1991, Geochim. Cosmochim. Acta, **55**, 349-366. (5) Jakosky, B., 1985, Space Sci. Rev., **41**, 131-200. (6) Crisp, J., 1984, J. Volc. Geotherm. Res., **20**, 177-211. (7) Shaw, H., and Swanson, D., 1970, Proc. 2nd Columbia river Basalts Symposium, 271-299; Swanson D., et al., 1975, A.J.S., **275**, 877-905; (8) Sigurdsson, H., 1990, Geol. Soc. Amer. Spec. Paper 247, 99-110. (9) Greeley, R., 1987, Science, **236**, 1653-1654.

DETERMINING THE pH OF MARS FROM THE VIKING LABELLED RELEASE REABSORPTION EFFECT

Robert C. Plumb
Worcester Polytechnic Institute and
Brown University, Dept. of Chem., Worcester MA 01609

The acid-base properties and redox potentials of solids are two of the more fundamental chemical parameters characterizing a material. Knowledge of these parameters for martian regolith fines would be of considerable value in determining what specific compounds are present and making judgements on what reactions are possible.

The observed magnitude (21-23%) of the reabsorption of $^{14}CO_2$ upon successive injections of nutrient in the Viking LR experiments provides a rather precise measure of the acid-base properties of martian regolith and the pH which one would measure in an appropriate experiment. The reabsorption process can be described quantitatively by a chemical model using well-established theory and thermodynamic parameters. The principal variables (unknowns) addressed in the calculations are 1) the amount of soluble acid species or base species present in the LR regolith sample and 2) the solubility product of the carbonate of limiting solubility, including the extreme case that no soluble carbonate is present. The model considers that acid-base and solubility equilibria are established and that the exchangeable $^{14}CO_2$ pool includes $CO_3^=$ from dissolved carbonates. Calculations show that there is a narrow zone of composition which will produce the observed reabsorption effect. The similar magnitudes of second and third injection reabsorption limits the zone of acceptable compositions. Observations of the amount of $CO_2(g)$ released upon wetting in the GEX experiments limit the zone still further.

The calculations indicate that a carbonate with the chemical properties of calcite or aragonite and at most 2 micromoles of soluble acid were present in the 0.5 mL LR samples and the pH of this material (as measured in a sealed volume with martian atmosphere at 298 K) would be $7.6 \pm .2$.

Both the model and the composition deduced from it have been verified by laboratory simulations with apparatus which accurately mimics the Viking LR experiments.[1] As added confirmation of the conclusions, it has been found that the kinetics of $^{14}CO_2$ evolution after the first injection are sensitive to the composition parameters and that it is necessary to have $CaCO_3$ present to reproduce the Viking kinetics.

(1) R. C. Plumb, R. Tantayanon, M. Libby and W. W. Xu, *Nature* **338**, 633-635 (1989).

562-91
85132
p.2

118

GU 597082

N92-29050

CHEMICAL REACTION PATH MODELING OF HYDROTHERMAL PROCESSES ON MARS: PRELIMINARY RESULTS;

Geoffrey S. Plumlee and W. Ian Ridley, *U. S. Geological Survey, MS 973, Denver Federal Center, Denver, CO, 80225*

Introduction: Hydrothermal processes have been postulated to play significant roles in the development of surficial mineralogies and morphological features on Mars. For example, a significant proportion of the martian soil could consist of the erosional products of hydrothermally altered impact melt sheets [1]: in this model, impact-driven, vapor-dominated hydrothermal systems hydrothermally altered the surrounding rocks and transported volatiles such as S and Cl to the surface. Further support for impact-driven hydrothermal alteration on Mars has been provided by studies of the Ries crater, Germany [2], where suevite deposits were extensively altered to montmorillonite clays by inferred low-temperature (100–130°C) hydrothermal fluids. It has also been proposed that surface outflow from both impact-driven and volcano-driven hydrothermal systems could generate the valley networks, thereby eliminating the need for an early warm wet climate [3,4].

We use computer-driven chemical reaction path calculations to model chemical processes which would likely have been associated with postulated martian hydrothermal systems. These calculations: 1) provide insight into the chemical feasibility of martian hydrothermal processes proposed by previous workers, and; 2) place constraints on possible hydrothermal alteration and precipitant minerals which might have formed at or near the martian surface in either a warm or cold climate.

Examples of processes which we model include:

1) Chemical aspects of the generation of hydrothermal fluids from groundwaters or ice by heat from magmas or meteorite impacts.
2) Chemical reactions between hydrothermal fluids and various rock types (such as basalts, komatiites, carbonates) inferred to be present on Mars.
3) Chemical processes which occur during the near-surface "quenching" of hydrothermal fluids via interactions with an ice cap or ground ice.
4) Boiling of hydrothermal fluids at depth in martian hydrothermal systems, the resulting transport of volatile species to the surface, and interactions of the condensed volatiles with near-surface rock/regolith material.
5) Interactions of magmatic gases with hydrothermal fluids and/or groundwaters in martian volcanoes.
6) Near-surface condensation of magmatic gases in volcanic edifices, and the resulting alteration of the volcanic host rocks.

Theory of chemical reaction path modeling: Computer-based chemical reaction path calculations determine heterogeneous chemical equilibrium conditions among minerals, gases, and/or aqueous solutions along an incremental series of specified temperature, pressure and/or bulk composition changes [5]. Based upon measured or estimated thermodynamic data, reaction path modeling thus predicts the changes in aqueous solution composition, the resulting amounts of minerals precipitated, and/or the amounts of gases formed during specific chemical processes. Because they are computer-based, large numbers of reaction path calculations can be carried out to address the full range of factors influencing a particular chemical process. The chemical speciation and reaction path programs SOLVEQ and CHILLER [5,6] were used in this study because they were specifically designed to model hydrothermal processes such as boiling, fluid mixing, water-rock interactions, and gas condensation.

Constraining input parameters for the modeling: In order to carry out the reaction path calculations, input parameters such as the initial chemical compositions of groundwaters, ground ice, rocks, regolith materials, and magmatic gases must be constrained. Because the Viking chemical analyses [7] are the only "hard" compositional data available, we are forced primarily to constrain these parameters by analogy to terrestrial data. For example, if liquid water was once stable at the martian surface, a wide range of water compositions must be evaluated in the calculations; these range from dilute ground and surface water compositions (such as those found in terrestrial basaltic terrains), to saline compositions (rich in Na, Mg, Ca, Cl, sulfate, and carbonate) such as are found in terrestrial seawater. Saline compositions could also approximate sub-zero °C groundwaters speculated to be currently present in the martian subsurface [8]. Rock compositions used in our calculations include those of the SNC meteorites and those of terrestrial basalts, komatiites, and carbonates. Magmatic gas compositions used include those measured at various active terrestrial volcanoes such as Kiluea, Hawaii [9], and modifications of these compositions.

Examples of results: Preliminary results of our modeling studies provide several interesting implications for the types of hydrothermal alteration and precipitant mineralogies that could have formed at or near the martian surface. For example, if SO_2- and CO_2-rich volcanic gases (similar to those from Kiluea) emanated from martian volcanoes in a cold climate, they would probably form a limited amount of acidic condensates in the volcano throat that would alter only small amounts of the basaltic rocks to silica, alunite, anhydrite, hematite, chlorites, and carbonates. If, however, groundwaters were present in the volcanoes (possibly in a warmer climate?) to absorb the volcanic gases, large volumes of very low pH (<1 – 1.5) fluids could form and generate volumetrically-extensive silica-alunite-anhydrite-chlorite-carbonate hydrothermal alteration; such alteration is observed within many active terrestrial volcanoes.

As another example, our modeling predicts that near-surface quenching of hydrothermal fluids outflowing from impact- or volcano-driven hydrothermal systems should produce significant amounts of silica- and/or carbonate-rich precipitants. These products are directly analogous to the silica sinter terraces and travertine terraces observed at the outflow of terrestrial geothermal systems.

Modeling of boiling processes in impact-driven hydrothermal systems indicates that such systems were likely too low-temperature to effectively transport signifcant chloride to the surface in the vapor phase, a proposed mechanism for the source of the high Cl values in the martian regolith [1].

References: [1] Newsom, H.E., 1980; *Icarus*, v. 44, p. 207-216. [2] Newsom, H. E., Graup, G., Sewards, T., and Keil, K., 1986; *J. Geophys. Res.*, v. 91, no. B13, p. E329-E251. [3] Brakenridge, G.R., Newsom, H.E., and Baker, V.R., 1985; *Geology*, v. 13, p. 859-862. [4] Gulick, V. C., Marley, M. S., and Baker, V. R., 1991; *LPSC XXII*, p. 509-510. [5] Reed, M. H., 1982; *Geochim. et Cosmochim. Acta*, v. 46, p. 513-528. [6] Spycher, N. F., and Reed, M. H., 1989; *Econ. Geology*, v. 84, p. 328-359. [7] Toulmin, P, III, Baird, A.K., Clark, B.C., Keil, K., Rose, H.J., Jr., Christian, R.P., Evans, P.H., and Kelliher, W.C., 1977; *J. Geophys. Res.*, v. 82, p. 4625-4634. [8] Zent, A.P., and Fanale, F.P., 1986; *J. Geophys. Res.*, v. 91, no. B4, p. D439-D445. [9] Gerlach, T. M., 1980; *J. Volc. Geotherm. Res.*, v. 7, p. 295-317.

Short- and Long-Term Climate Changes on Mars

James B. Pollack
Space Science Division
NASA/Ames Research Center
Moffett Field, CA 94035-1000

The present climate of Mars is dominated by the seasonal cycles of dust, water vapor, and carbon dioxide. Understanding these cycles represents a first step towards interpreting climate changes in the past. Past climates on Mars may have been different from the present one due to astronomical variations of orbital and axial properties, to major changes in atmospheric pressure and/or composition, and to long-term changes in solar luminosity.

In this talk, I focus on recent developments in modelling the seasonal cycle of carbon dioxide and in modelling the early climate of Mars. The Viking lander meteorology experiment provided an accurate record of the changes in atmospheric mass due to the waning and waxing of the seasonal carbon dioxide polar caps. Key factors that affect this seasonal cycle include the caps' albedo, heat advected by the atmosphere from low to high latitudes, clouds at high latitudes (polar hoods), and thermal inertia of the bare ground. I and my colleagues have attempted to simulate quantitatively the observed seasonal pressure curves using results from general circulation model (GCM) calculations of the impact of atmospheric heat transport on the deposition and sublimation rates of carbon dioxide ice in the polar regions. These GCM runs were performed on a dense grid of seasonal dates and dust optical depth. We also developed simple parameterizations for the effects of other variables, such as cap albedo.

The valley networks, which occur almost exclusively on the old cratered uplands, imply that liquid water flowed over much of the surface on early Mars. They may have resulted from a combination of a warmer climate, due to an enhanced greenhouse, and a steeper geothermal gradient. A dense, carbon dioxide atmosphere, having a pressure of at least several bars, could have raised the surface temperature to above the freezing point of water. However, if the Sun's luminosity, was 20-25% less than its current value at the times of interest, as suggested by most models of the Sun's evolution, carbon dioxide condensation may have made it very difficult to emplace the needed amount of carbon dioxide in the atmosphere. Possible solutions to this problem include: (1) a higher solar luminosity 4 billion years ago than that given by conventional models; (2) the presence of other greenhouse gases; or (3) valley network genesis almost exclusively by a steeper geothermal gradient than today's gradient.

INFLUENCE OF HEAT FLOW ON EARLY MARTIAN CLIMATE.

Susan Postawko & Fraser P. Fanale, Planetary Geosciences, Univ. of Hawaii Honolulu, HI 96822

It has been argued (1) that the formation of the valley networks on Mars may be explained by higher internal regolith temperatures associated with a much higher heat flow early in the planet's history. Squyres (1) has suggested that this higher heat flow would cause groundwater to be closer to the martian surface 3.8 billion years ago, and thus allow the formation of the valley networks by groundwater sapping, without having to invoke surface warming due to an atmospheric greenhouse effect.

It was previously shown (2) that, in fact, it may not be possible to completely separate the effects of higher heat flow and atmospheric greenhouse on early Mars. The mean residence time of CO_2 in the martian regolith (in the form of carbonates) is dependent on the rate at which these carbonates are broken down and the CO_2 recycled into the atmosphere. This recycling time can be quantitatively related to the heat flow. The depth to the water table is dependent not only on heat flow, but on surface temperature, which is a boundary condition. Surface temperature depends, at least in part, on the amount of CO_2 in the atmosphere. Thus, a set of equations was derived which simultaneously calculate surface temperature and depth to the water table for any value of heat flow. In addition to heat flow, other variables are the total CO_2 available, regolith conductivity, and atmospheric mean residence time of CO_2.

We have more fully explored the parametric space of our set of equations to better determine the sensitivity of the system to variations in any of the above factors. The limiting factor in the effectiveness of an atmospheric greenhouse to significantly increase surface temperature is the total CO_2 available in the system.

We find that a combination of higher heat flow and atmospheric greenhouse effect on early Mars may more easily explain valley network formation and distribution, even for a cool early sun, than either of these mechanisms separately.

References: (1) Squyres, 1989, Fourth International Conf. on Mars, Tucson, AZ. (2) Fanale & Postawko, 1990, Proc. 21st Lunar Planet. Sci. Conf., Houston, TX.

MID-INFRARED SPECTRA OF MARTIAN KOMATIITE

David P. Reyes, Department of Geology, Arizona State University, Tempe, AZ 85287-1404.

Synthetic mid-infrared emissive spectra of basalts of possible Martian komatiitic compositions were generated to show what might be seen in data returned from the Thermal Emission Spectrometer (TES). TES is flying on Mars Observer arriving at Mars in late 1993. The synthetic Martian komatiite spectra were generated using mineralogy based on SNC and Viking XRF data. These data sets provide strong evidence for the existence of ultramafic lavas on Mars, particularly lavas of komatiitic composition.

Terrestrial komatiite is an ultramafic extrusive characterized by compositional and textural layering within individual flow units, and by high MgO content. Komatiites were generated at depths of 150-200 km by massive partial melting of the mantle [1]. They were emplaced mostly during the Archean (>2.7 Ga), at very low viscosity (0.1 to 1 Pa·s), and very high temperature (1400-1700^{0} C) [2,3]. Komatiite may be sub-divided by MgO content into peridotitic (>20 wt.% MgO), pyroxenitic (12-20 %), and basaltic (9-12%) [4]. Peridotitic komatiite (PK) consists mainly of olivine, with lesser pyroxene, and no plagioclase. Pyroxenitic komatiite (PyK) is dominated by pyroxene, with less olivine, and increasing plag. Basaltic komatiite (BK) is dominated by pyroxene or plagioclase, with little or no olivine.

The existence of komatiite on Mars is strongly supported by SNC composition [5] and texture [6], and also by Viking XRF data [7]. Common features SNC's share with terrestrial komatiites are: low Al_2O_3 content, cumulate textures, high MgO content, and similar mineralogy. The major difference between SNC and terrestrial komatiite is that SNC's are relatively enriched in Fe relative to Mg. This is reasonable because it reflects the relative mantle chemistry of Mars and Earth [7,8]. Interestingly, SNC's have about the same mineralogy and MgO contents as the 3 types of komatiite [4,9]. Shergotty, Nahkla, and Chassigny correspond to BK, PyK, and PK, respectively. Additionally, Nakhala has a cumulate texture common to the basal portions of terrestrial komatiites.

Viking XRF data suggests evolution of current Martian surface fines from mafic to ultramafic basalts. Major oxide data of the silicate portion of the Martian fines adjusted to CIPW normative mineralogy predicts that a pyroxene rich mafic to ultramafic lava, analogous to terrestrial PyK or BK is the best fit [7]. Additional evidence from VXRF data is the relatively high sulfur content of the fines which may be due to the weathering of Fe-sulfide minerals from komatiitic basalts [8,10].

The mineral and komatiite spectra were gathered on Arizona State University -TES Lab's Fourier transform interferometer measuring emission at a spectral resolution of 4 cm^{-1}, from 7 to 25 μm. The spectral resolution of TES is comparable to the lab spectrometer but ranges from 6 to 50 μm. Using the gathered spectra, synthetic spectra are generated using a program called *imath*, developed by Don Anderson for ASU-TES Lab. To create the synthetic spectra, the measured spectra of constituent minerals are combined linearly in arbitrary percentages to produce a synthetic rock spectrum. Mixing in reflectance is linear in the MIR region [11], and presumably also in emission by Kirchoff's Law (E=1-R, E=emission, R=reflectance). This is important in that it allows the creation of synthetic whole rock spectra from known or given mineral abundances, and will also allow for spectral unmixing to determine minerals and abundances, even from remotely gathered data such as TES will provide.

The synthetic spectra shown in Figure 1 represent several potential Martian komatiite spectral signatures based on information in Table 1 from [7,9,12]. The synthetic spectrum of Shergotty was not included because one mineral endmember was unavailable. All synthetic Martian spectra are shown with their terrestrial komatiite counterpart, and one has an additional synthetic spectrum. The real spectra were taken from komatiitic rocks from Ontario, Canada. Due to their great age the original mineralogy has been slightly altered by mild metamorphism and replacement by serpentine. Additionally, the actual mineral content of these rocks is not listed pending thin-section analysis.

The synthetic spectrum based on V-XRF data compares well with the spectrum of BK in Fig. 1. They both show two prominent absorption features centered near 9.6 and 20 μm. Both of these locations are areas of prominent pyroxene absorption features and thus are significant in the spectra due to the large percentages of pyroxene these rocks contain. The synthetic spectrum of Nahkla is essentially the spectrum of pyroxene because it contains such a dominant percentage of pyroxene relative to other constituent minerals. In comparison, the synthetic spectrum of PyK shows some similar absorption features as synthetic Nahkla, having a large pair of absorption features near 9.1 & 11.1 μm, and another single large absorption feature at 20 μm caused by pyroxenes. However, the depth and precise location of the absorption bands for the synthetic Pyk are tempered by a large addition of olivine. The real spectrum of PyK has the same general shape as Nahkla and the synthetic PyK, having a large doublet near 10 μm and a large single absorption feature near 20 μm. Differences between the real and synthetic spectra are due to some alteration in the PyK specimen. The synthetic spectrum of Chassigny in Fig.3 is practically that of olivine. The real spectrum of PK also has strong olivine absorption features, but is not

exactly the same due to replacement of some portion of olivine by mild alteration, and possibly due to variations in species of olivine, with Chassigny having Fe-rich and PK Mg-rich olivine.

The spectra presented here give a rough idea of what Martian komatiite may look like if detected by TES. Each of the 3 types of komatiite and their Martian counterparts have individually distinctive spectral signatures. These spectral signatures are specific due to the simple and unique mineralogy of rocks having komatiitic compositions. Additionally, komatiitic basalts are easily distinguished from other ultramafic and mafic basalts by their sharp features and greater band depths [13]. If komatiite exists on Mars as suggested, then they will be easily identified where sufficiently exposed.

FIGURE 1 Comparison of synthetic spectra of Martian komatiite analogs and real spectra of terrestrial komatiite.

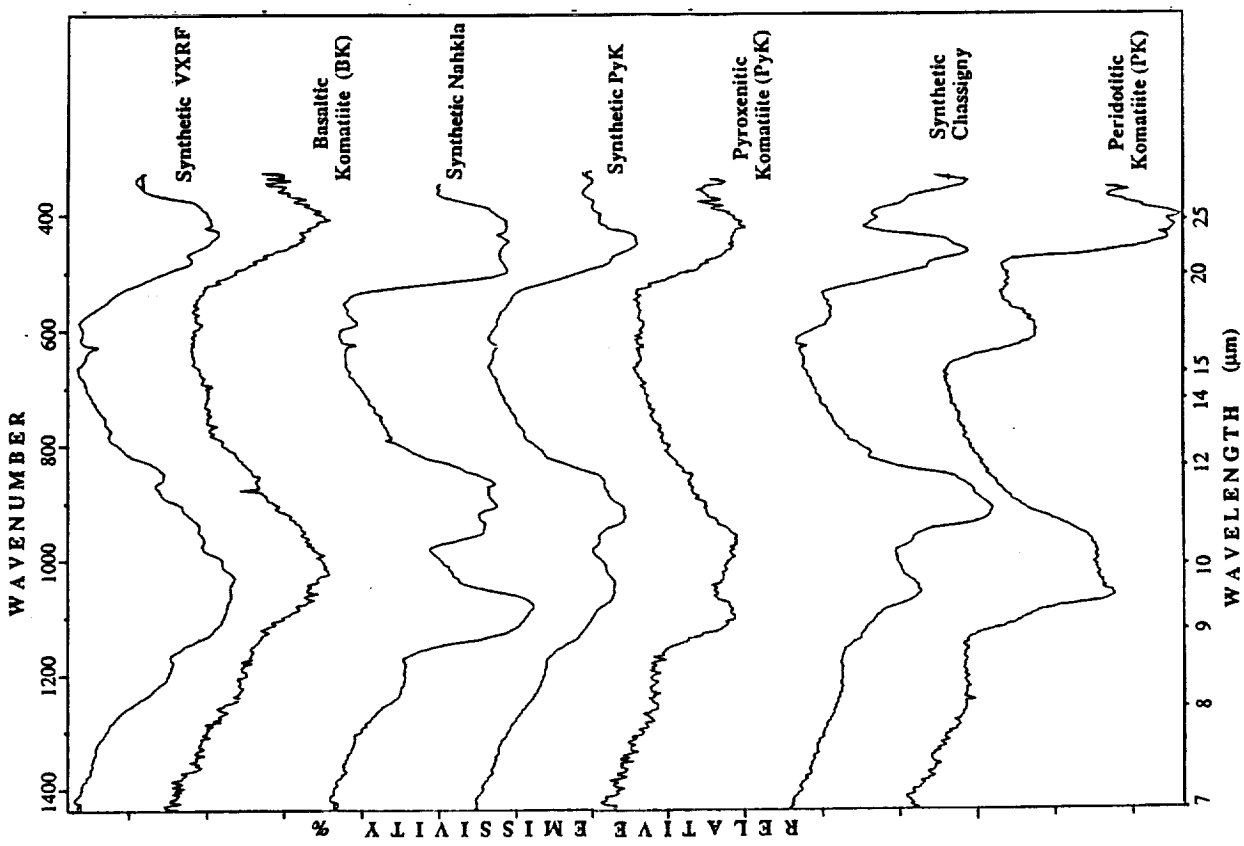

[1]Takahashi,&Scarfe(6/1985)Nature,v315,p566-568.[2]Arndt,et al(1979)CanadnMinrlgst, v17, p147-163. [3]Huppert, et al (3/1984) Nature, v309, p19-22. [4]Arndt,et al (1977)JPet, v18, pt2, p319-69.[5]Longhi&Pan(1988)LPI TechRpt 88-05, p76-8. [6]Treiman (1987)LPSCXVIII, p1022-3.[7]Baird&Clark(1981)ICARUS45,p113-23.[8]Burns& Fisher (1989)LPI TechRpt 89-04,p20-2. [9]McSween (1985)RevsGeophys, v23,n4,p391-416. [10]Burns&Fisher (1990)JGR, v95,nB9,p14169-73.[11]Thomas&Salisbury (1991)pre-print submt to RmtSensngEnvirn. [12]Naldrett&Mason(1968)Candn.J.Erth.Sci,n5,p 11145.[13]Reyes&Christensen(1990)LPSC XXI, p.1023.

TABLE 1 - Percent Constituents

	VXRF [7]	Nahkla [9]	Chassigny [9]	PyK [12]
olivine	-	15.5	88.5	37.2
Cpx	19	78.6	7.8	19.6
Opx	50	-	-	23.6
Plag	25	3.7	2.6	16.3
K-spar	-	1.1	-	0.5
compares to:	BK	PyK	PK	PyK

Chryse Planitia region, Mars: Channeling history, flood-volume estimates, and scenarios for bodies of water in the northern plains; Susan L. Rotto and Kenneth L. Tanaka, U.S. Geological Survey, Flagstaff, Ariz., 86001.

The Chryse Planitia region of Mars includes several outflow channels that debouched into a single basin. Here we evaluate possible volumes and areal extents of standing bodies of water that collected in the northern lowland plains, based on evidence provided by topography, fluvial relations, and channel chronology and geomorphology.

The large channels do not cross-cut one another; thus determination of channeling history must rely on crater counts [1,2]. Appropriate sites for new crater counts (Fig. 1) have been identified by our geologic/geomorphologic mapping in the region (work in progress). Our work further indicates that channel activity in the Chryse region was prolonged and highlighted by a major Late Hesperian/Early Amazonian channeling episode (spanning 1.2 to 2.4 b.y. [3]), in which large floods carved the Kasei, Maja, Shalbatana, and Ares-Tiu-Simud Valles channel systems.

Estimates for the volumes of water released through each channel (Table 1) are based on the volumes of eroded rock [4] and a sediment load of 40 percent [5]. These estimates may be low if the sediment load was less; on the other hand, they may be high if the missing material was removed chiefly by debris flows [6]. Topographic data [7,8] indicate three possible basins in which the water and sediment could have ponded (Table 2). At the mouths of the major outflow channels, where erosional features are not present and wrinkle ridges are subdued, the *proximal Chryse basin* (PCB) forms the smallest basin (centered at ~ lat 23^0 N., long 43^0). The *extended Chryse basin* (ECB) consists of Chryse Planitia and Acidalia Planitia, approximately delineated by the -2 km contour [7]. The *northern plains basin* (NPB) is the region below datum and north of the highland/lowland boundary scarp, covering an area ranging in size from that of the extended Chryse basin to nearly 30 percent of the planet; the NPB actually consists of more than ten large closed basins [8]. The sizes of the three basins (Table 2), however, must be viewed with suspicion given the 1- to 1.5- km precision of the topography [7].

We investigated the formation of lakes resulting from estimated discharges based on the following scenarios for Chryse channel activity (Table 3): (1) singular channel events (the largest being Kasei Valles) and (2) concurrent, multiple channel activity. Discharges of smaller floods, such as Maja Valles, would have been entirely contained within the PCB. Larger singular floods and multiple floods would have filled and overflowed the PCB. We infer that such spillover water carved the longitudinal grooves and streamlined features north of the PCB, which are traceable into Acidalia Planitia as far north as lat 40^0 N (possible evidence for flooding farther north is provided by polygonal terrain and other periglacial features). Even the largest flood volumes could have been contained in the ECB, which covers ~15 percent of the northern plains.

Implications for an "Oceanis Borealis". Although we cannot entirely rule out the possibility that an extensive "Oceanis Borealis" (which would fill the NPB) [9] was produced by Chryse flooding, we think that it is highly unlikely, for the following reasons: (1) the water sources are confined to the Chryse region, which at most covers only one-sixth of the planet [10]; therefore, the equivalent of the drainage of at least several hundred meters of water from the *entire* Chryse region would be required; (2) the "peak" episode of channel activity may have spanned more than 1 b.y.; therefore, it is likely that some channels were carved by multiple flood events [e.g., 11], each of which was relatively small; (3) part of the missing rock volumes represented by the channels may be due to post-flood modifications such as mass-wasting and erosion [12]; and (4) much of the discharged water would have filled the pore spaces of the deposited sediments and infiltrated underlying rocks. The only other major contemporary contributors to northern plains flooding were Mangala Valles, which may have added <0.01X10^6 km^3 of water [13], and the Elysium channels, whose deposits cover <2X10^6 km^2 [cf. 14], or <5 percent of the area of the northern plains. On the other hand, if smaller discharges were the norm, plenty of time would be available

for intermittent aquifer recharge. Thus we prefer to think that large, *lake-sized* bodies of water and muddy sediments were emplaced that endured for short periods.

Figure 1. Relative ages and cumulative densities of craters (no. >2 km diam. per 10^6 km^2) for Chryse channel systems

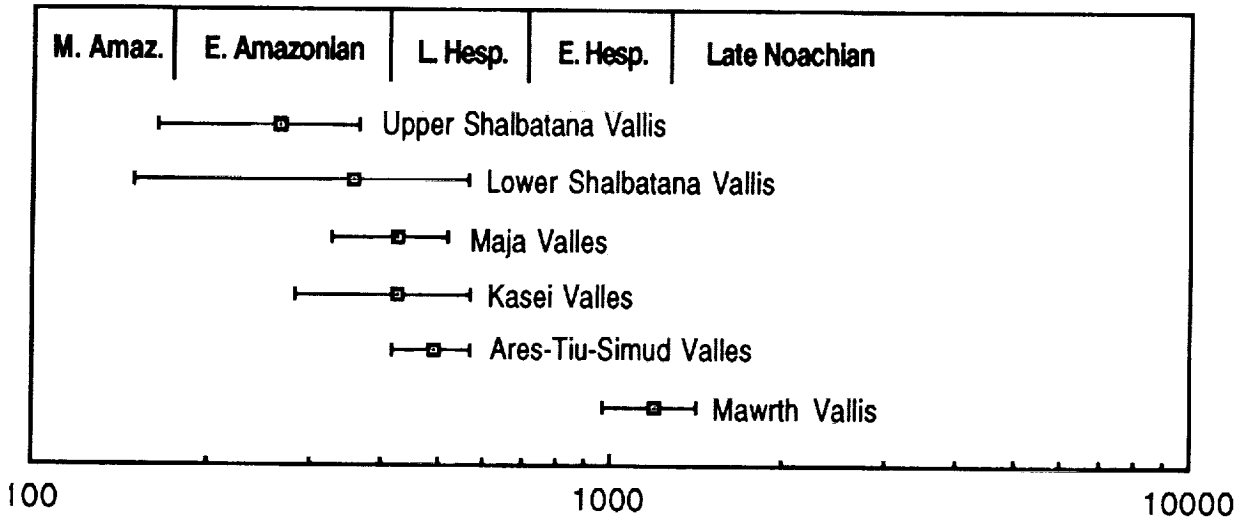

Table 1. Water discharges estimated for Chryse channel systems [based on 4,5]

Feature	Volume (10^6 km^3)
Kasei Valles *(includes Echus Chasma)*	1.36
Ares-Tiu-Simud Valles *(includes associated chaos and chasmata)*	3.36
Maja Valles *(includes Juventae Chasma)*	0.11
Shalbatana Vallis	0.07
Total	**4.90**

Table 2. Dimensions of possible basins for Chryse discharges

	Average depth (km)	Area (10^6 km^2)	Volume (10^6 km^3)
Proximal Chryse basin	1	0.27	0.27
Extended Chryse basin	1	5.32	5.32
Northern plains (data from [8])	<1.7	<38.00	<65.00

Table 3. Possible Chryse flood events and resulting lakes

Flood event	Probable extent and depth of lake
Maja Valles	Fills proximal Chryse basin ~400 m
Kasei Valles	Fills extended Chryse basin ~250 m
Ares-Tiu-Simud Valles	Fills extended Chryse basin ~630 m
All channels at once	Fills extended Chryse basin ~920 m

References: [1] H. Masursky et al. (1977) *JGR* 82, 4016-4038. [2] S.L. Rotto and K.L. Tanaka (1991) *LPSC XXII Abstracts*, 1135-1136. [3] K.L. Tanaka et al. (in press) chapter in *Mars*, Univ. Ariz. Press. [4] M.H. Carr et al. (1988) *LPSC XVIII Abstracts*, 155-156. [5] P.D. Komar (1980) *Icarus* 42, 317-329. [6] D.J. MacKinnon and K.L. Tanaka (1989) *JGR* 94, 17,359-37,370. [7] U.S. Geological Survey (1989) USGS Misc. Inv. Ser. Map I-2030. [8] D. H. Scott et al., (1991) *LPSC XXII Abstracts*, 1203-1204. [9] Baker V. R. et al. (in press) *Nature*. [10] K.L. Tanaka and D.J. MacKinnon (1987) *LPSC XVIII Abstracts*, 996-997. [11] M.G. Chapman and D.H. Scott (1989) *PLPSC* 19, 367-375. [12] R.C. Kochel and J.R. Miller (1990) *LPSC XXI Abstracts*, 643-644. [[13] K.L. Tanaka and M.G. Chapman (1990) *JGR* 95, 14,315-14,323. [14] K.L. Tanaka et al. (1988) *PLPSC* 18, 665-678.

DORSA ARGENTEA TYPE SINUOUS RIDGES, MARS : EVIDENCE FOR LINEAR DUNE HYPOTHESIS;

Steven W. Ruff, Department of Geology, Arizona State University

Unusual ridges with sinuous, dendritic, and braided morphologies near the south pole of Mars (Figure 1) as well as in the Argyre basin have recently begun to receive attention. Originally proposed by Howard (1) to be glacially formed eskers, recent work by Kargel and Strom (2) continues to argue for this hypothesis. Indeed, an entire glacial model has been built up around these ridges. A brief examination by the author (3) of possible ridge forming processes included an esker origin but also examined other mechanisms. Of the alternative hypotheses, an origin as linear dunes is the most reasonable. The current study focuses on evidence for this mode of origin.

On Earth, dunes of linear form are the most widespread of all dune types (4). Though all linear dunes share common attributes, there are many shapes, sizes, and patterns of occurrence. Simple, compound, and complex forms range from a few meters high and several meters wide to 200 m high and several hundred meters wide. Lengths vary from a < 1 km to a few hundred kilometers.

Linear dune patterns vary from widely spaced straight ridges to complex reticulate patterns of Y- junctions and intersecting ridges (5) (Figures 2 & 3). These more complex patterns of coalescing dune ridges have been compared to a stream network (6). This analogy allows for the comparison of dynamic equilibrium in a fluvial landscape and a dune system.

The origin of linear dunes is the subject of continuing debate. An origin by horizontal roll vortices is the most often cited explanation for their development but this remains a poorly supported hypothesis (see 7). Relationships between dune height, spacing, and junctions is fairly well established. Mabbutt and Wooding (6) noted a direct relationship between dune height and spacing while Lancaster observed that Y - junctions become more frequent with decreasing dune spacing (8). Thomas and Shaw (9) state that height and spacing of linear dunes is determined by the availability of sediment and the characteristics of the wind regime. Lancaster (8) concludes that different dune patterns are in part, a function of age, history of initiation, stabilization, and reactivation.

Extensive dune fields and sand seas (ergs) have been observed on Mars (10, 11). These appear to be composed exclusively of transverse and barchan type dunes. Linear dunes are notably absent from the areas observed by these authors. The lack of linear dune forms is to be expected according to Tsoar et al. (10) due to a lack of vegetation to constrain sand movement, although there is no evidence to support a causal relationship between vegetation and linear dune development (12,13).

Figure 1. *Viking photomosaic of sinous ridges in Dorsa Argentea*

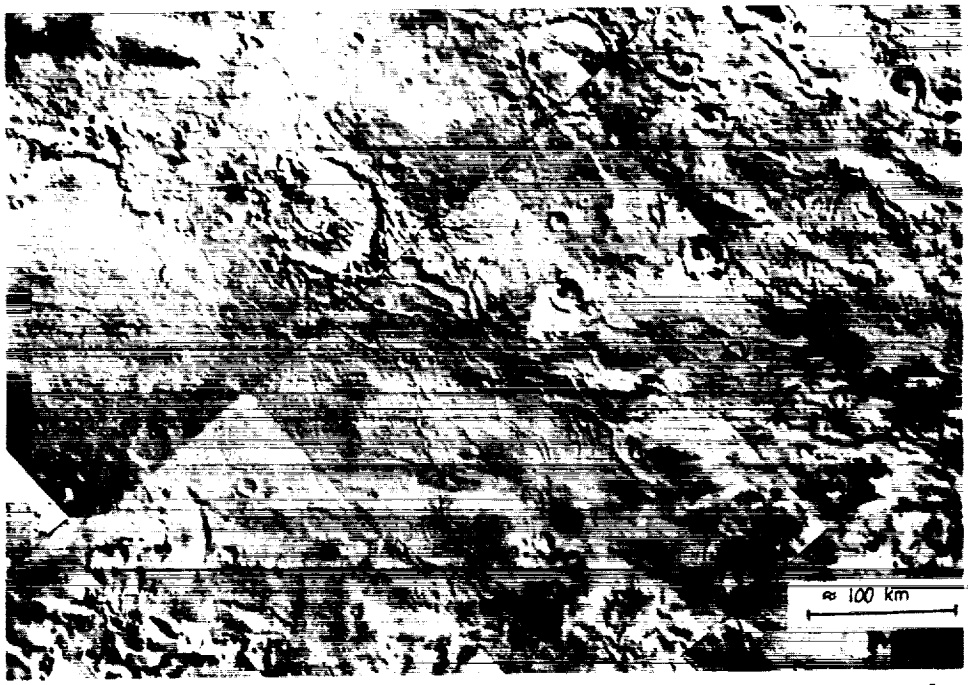

MARTIAN RIDGES: LINEAR DUNE HYPOTHESIS S.W. Ruff

Evidence for net erosion of sediments in the midlatitudes of Mars and net deposition at the poles (14,15) would seem to suggest that the south pole may also be a site for sand seas. The Dorsa Argentea region may be an erg in the process of burial or exhumation. The sinuous ridges here are, in some places, mantled or covered by material and in others, completely exposed (Figure 1). It is not clear whether they are being buried by or exhumed from the overlying material. What is clear is that they share many of the features of terrestrial linear dunes, especially the complex reticulate dune forms (Figures 2 & 3). The sinuous ridges of the Argyre basin farther north share many of the features of Dorsa Argentea ridges and should be examined together.

The martian ridges tend to be longer, wider, higher, and more widely spaced than terrestrial linear dunes but no more or less complicated in pattern. Because the morphometry of linear dunes varies widely depending on location, it does not seem unreasonable that they would have different size characteristics on another planet. The spacing relationship seen in terrestrial dunes does seem to hold up in the case of the ridges. If the martian sinuous ridges are linear dunes, clearly they are the result wind and sand parameters much different than those found on Earth.

REFERENCES

1) Howard, A.D. 1981. *Reports of Planetary Geology Program-1981,* NASA TM 84211, 286-289.
2) Kargel, J.S. and Strom, R.G. 1991. *Lun. Planet. Sci. XXII,* 683-684.
3) Ruff, S.W and Greeley, R. 1990. *Lun. Planet. Sci. XXI,* 1047-1048.
4) Lancaster, N. 1982. *Prog. Phys. Geogr.,* **6**, 475-504.
5) Thomas, D.S.G. 1986. *Zeit. Geomorph.,* **30**, 231-242.
6) Mabbutt, J.A. and Wooding, R.A. 1983. *Zeit Geomorph. Suppl.,* **45**, 51-69.
7) Pye, K. & Tsoar, H. 1990. *Aeolian Sand and Sand Dunes,* Unwin Hyman, London 396pp.
8) Lancaster, N. 1988. *J. Arid Envir.,* **14**, 233-244.
9) Thomas, D.S.G. and Shaw, P.A. 1990. *The Kalahari Environment,* Cambridge University Press, 284 pp.
10) Tsoar, H., Greeley, R., and Peterfreund, A.R.,1979. *J. Geophys. Res.,* **84**, 8167-82.
11) Breed, C.S., Grolier, M.J., & McCauley, J.F.1979. *J. Geophys. Res.,* **84**, 8183-204.
12) Ash, J.E. and Wasson, R.J. 1983. *Zeit. Geomorph. Suppl.,* **45**, 7-25.
13) Thomas, D.S.G. 1988. In *Geomorphological Studies in Southern Africa,* G.F Dardis and B.P.Moon (eds.), 145-156.
14) McCauley, J.F. 1973. *J. Geophys. Res.,* **78**, 4123-4137.
15) Soderblom, L.A., Malin, M.C., Cutts, J.A., and Murray, B.C. 1973. *J. Geophys. Res.,* **78**, 4197-4210.

Figure 2. *Linear dunes of Kalahari desert*

Figure 3. *Linear dunes of Simpson desert*

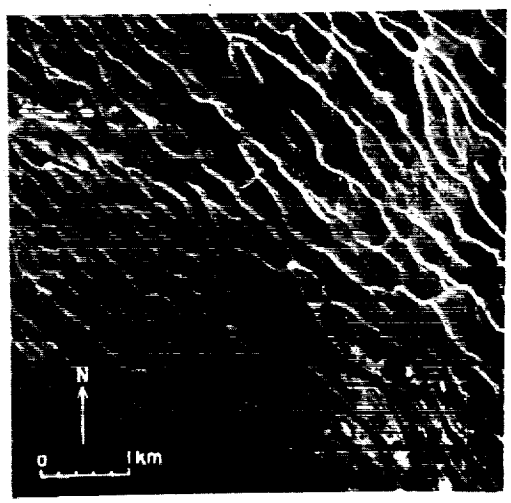

ATMOSPHERIC AND SURFACE TEMPERATURES AND AIRBORNE DUST AMOUNTS DURING LATE SOUTHERN SUMMER FROM MARINER 9 IRIS DATA;

M. Santee, 170-25 Caltech, Pasadena, CA 91125 and D. Crisp, JPL, Pasadena, CA 91109

The temperature structure and dust loading of the Martian atmosphere are investigated using thermal emission spectra recorded in 1972 by the Mariner 9 infrared interferometer spectrometer (IRIS). The analysis focuses on a subset of data consisting of $\sim$ 2400 spectra obtained near the end of the southern summer season ($L_S = 343° - L_S = 348°$), after the global dust storm had largely abated and airborne dust amounts were subsiding to background values. Simultaneous retrieval of the vertical distribution of both atmospheric temperature and dust optical depth is accomplished through an iterative procedure which is performed on each individual spectrum. The atmospheric transmittances are calculated using a Voigt quasi-random band model [1], which includes absorption by CO_2 and dust, but neglects the effects of multiple scattering. Vertical profiles of temperature and dust optical depth are obtained using modified versions of the retrieval algorithms proposed by Smith [2]. These profiles are used to construct global maps of temperature and dust optical depth as functions of latitude ($\pm 90°$), altitude ($\sim 0 - 50$ km), and local time of day.

Pole-to-pole descriptions of dayside and nightside atmospheric temperatures are shown in Fig. 1. The highest atmospheric temperatures (> 260 K) are found at low altitudes near the sub-solar latitude ($\sim 6°$S), while the coldest temperatures (< 150 K) are found at levels near 1.0 mbar at high northern latitudes, which are in polar night during this season. A comparison of temperature maps at 2 pm and 2 am reveals diurnal temperature variations as large as 80 K at low altitudes near the sub-solar latitude, whereas diurnal temperature changes at pressures less than 1.0 mbar rarely exceed 10 K. Both dayside and nightside atmospheric temperatures above the 0.1 mbar ($\sim$ 40 km) level are warmer over the winter (north) pole than over the summer (south) pole, suggesting the existence of a pole-to-pole circulation which transports heat (and mass) from the south to the north with maximum northward advection at an altitude above 40 km, and return flow at lower levels. This thermal structure and the accompanying meridional circulation have not been identified before at these altitudes.

Previous efforts to retrieve temperature profiles from the IRIS data set neglected the additional opacity due to the presence of airborne dust. Including dust in the retrieval algorithm produces changes in the derived temperatures of more than 10 K in some atmospheric layers. The largest 9 μm optical depths (~ 0.4) occur over the equatorial regions. These values correspond to visible optical depths approximately 2.5 times larger [3]. These moderately large dust amounts are consistent with the amplitude of the diurnal temperature variations near the surface. This distribution of dust agrees well with the findings of Anderson and Leovy [4] from Mariner 9 television data and Martin [3] from Viking IRTM data.

REFERENCES: [1] Crisp, D. (1990) *JGR* **95**, 14,577-14,588. [2] Smith, W. L. (1970) *Appl. Opt.* **9**, 1993-1999. [3] Martin, T. Z. (1986) *Icarus* **66**, 2-21. [4] Anderson, E. and Leovy, C. (1978) *JAS* **35**, 723-734.

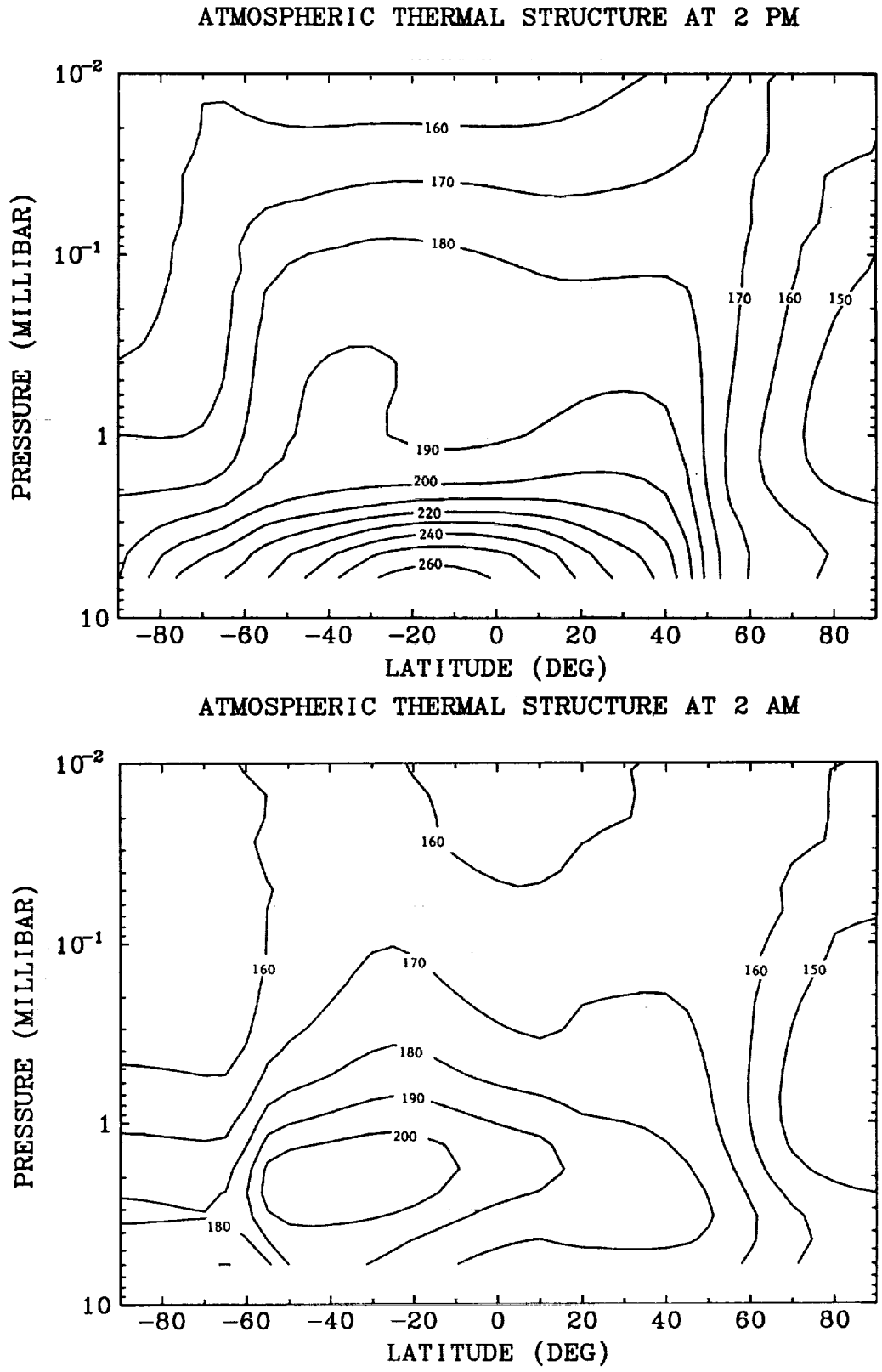

Fig. 1. Pole–to–pole dayside and nightside atmospheric temperature variations.

A CARBONATE - SILICATE AQUEOUS GEOCHEMICAL CYCLE MODEL FOR MARS; M. W. Schaefer, University of Maryland, College Park, MD, and H. Leidecker, NASA/Goddard Space Flight Center, Greenbelt, MD

A model for the carbonate-silicate geochemical cycle of an early, wet Mars is under development. The results of this study will be used to constrain models of the geochemical history of Mars and the likely mineralogy of its present surface.

Although Mars today is a cold, dry planet, it may once have been much warmer and wetter. Values of total outgassed CO_2 from several to about 10 bars are consistent with present knowledge (Pollack *et al.* 1987), and this amount of CO_2 implies an amount of water outgassed at least equal to an equivalent depth of 500 - 1000 meters (Carr 1986). Pollack *et al.* (1987), in addition, estimate that a thick CO_2 atmosphere may have existed for an extended period of time, perhaps as much as a billion years. The greenhouse effect of such an atmosphere would permit the presence of liquid water on the surface, most likely in the form of a shallow sea in the lowest regions of the planet, such as the northern plains (Schaefer 1990).

The treatment of geochemical cycles as complex kinetic chemical reactions has been undertaken for terrestrial systems in recent years with much success (Lasaga 1980, 1981; Berner *et al.* 1983; Lasaga *et al.* 1985). Although the Martian system is vastly less well understood, and hence less well-constrained, it is also a much simpler system, due to the lack of biogenic reactions that make the terrestrial system so complex. It should be possible, therefore, to use the same techniques to model the Martian system as have been used for terrestrial systems, and to produce useful results.

A diagram of the carbonate-silicate cycle for Mars (simplified from the terrestrial system) is shown on the next page.

Berner, R. A., Lasaga, A. C., Garrels, R. M., *Am. J. Sci. 283*, 641, 1983. Carr, M.H., *Icarus*, *68*, 187, 1986. Lasaga, A. C., *Geochim. et Cosmochim. Acta 44*, 815, 1980. Lasaga, A. C., in *Kinetics of Geochemical Processes*, ed. A. C. Lasaga and R. J. Kirkpatrick, MSA, 1981. Lasaga, A. C., Berner, R. A., Garrels, R. M., in *The Carbon Cycle and Atmospheric CO_2: Natural Variations Archaean to Present*, ed. E. T. Sundquist and W. S. Broecker, AGU, 1985. Pollack, J.B., J.F. Kasting, S.M. Richardson, K. Poliakoff, *Icarus 71*, 203, 1987. Schaefer, M. W., *J. Geophys. Res. 95*, 14291, 1990.

GEOCHEMICAL CYCLE MODEL FOR MARS, M.W. Schaefer and H. Leidecker

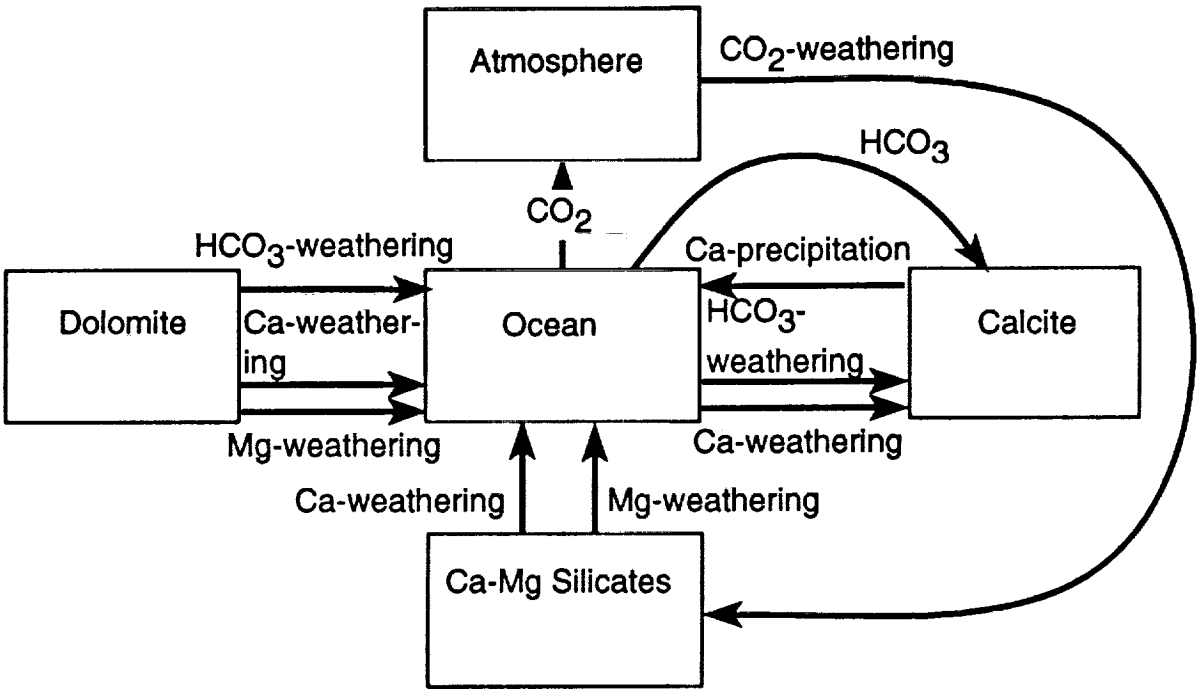

AMAZONIS AND UTOPIA PLANITIAE: MARTIAN LACUSTRINE BASINS.

David H. Scott, James W. Rice, Jr., James M. Dohm, and Mary G. Chapman

Amazonis and Utopia Planitiae (Fig. 1) are two large (>10^6 km^2) basins on Mars having morphological features commonly associated with former lakes. The investigation of these areas is an extension of our previous paleolake studies in the Elysium basin. Using Viking images, we are searching for familiar geologic forms commonly associated with standing bodies of water on Earth. Like Elysium, the two basins exhibit terraces and lineations resembling shorelines, etched and infilled floors with channel-like sinuous markings in places, inflow channels along their borders, and other geomorphic indicators believed to be related to the presence of water and ice. In some areas these features are better displayed than in others where they may be very tenuous; their value as indicators can be justified only by their association with related features. Even though these postulated paleolakes are very young in the Martian stratigraphic sequence, their shoreline features are poorly preserved and they are probably much older than large Pleistocene lakes on Earth.

Amazonis Planitia - Our work in the Amazonis basin is an extension of geologic mapping and paleolake studies in the Elysium basin [1].

Among the geomorphic indicators produced by water that we have observed within Amazonis Planitia are the following: (a) Etched and eroded materials similar to those observed on the floor of the Elysium basin and in large outflow channels leading to Chryse basin. (b) Sinuous, bifurcating channel markings extending from Amazonis Planitia northward across the divide (elevation about -1500 m) separating Amazonis from the Diacria basin; these and other channels in the area are associated with whorled ridge patterns that may represent ice related structures or the differential solution of carbonate deposits [2]. Elsewhere these whorled patterns are commonly found with meander relics [3] and other features that collectively may be good indicators of paleowater [4]. (c) A possible strandline extends partly along the sharp termination of the Olympus Mons aureole deposits against the plains (Fig. 1A). The abrupt termination of the aureole deposits resembles a wave cut terrace and bordering platform. A similar type of "shoreline" extends along the base of a topographic rise on the west side of the Amazonis basin at about the same elevation. Numerous breached and partly buried craters, as well as partly buried mesas, suggest the presence of sedimentary deposits as well as fluvial erosion. High-resolution images of areas within the planitia show channels eroded into plains materials. The postulated paleolake may have been relatively shallow, having been reduced at waning stages to mere meandering channels slowly transporting water to the northern plains.

Utopia Planitia - Most of the indicators thought to be associated with areas once occupied by ponded water (or by ice) are present in both the Utopia and adjacent Isidis basins (Fig. 1B). In addition, small (≥1 km diameter) cones, many with summit craters, occur within both basins where they form linear and curvilinear chains in places. Interpretations of their origin include pseudocraters [5,6] formed by the interaction of ground ice or water with volcanic flows; pingoes and ice-cored ridges [7] that develop in poorly drained lakes and channels as in the Mackenzie river delta of the Northwest Territories, Canada [8]; moraines [9]; and mounds formed by the disintegration of stagnant ice covers [10]. All of these origins require the presence of water or ice. Double-ringed features across the center of the Utopia basin resemble concentric-ring structures described on flood-eroded basalt surfaces in the channeled scablands of Washington State [11]. The scabland structures are outlined by dikes that appear to have been more resistant to flood erosion than surrounding basalt flows. The Martian rings, however, may exceed their terrestrial look-alikes in diameter by an order of magnitude or more.

Terraces bordering raised platforms are visible in places near and around the margins of Utopia and Isidis Planitiae; generally they occur near or slightly above the -1000 m contour. The extensive areas of knobby and etched material [12] that border the highland-lowland boundary along the southwestern margin of Utopia and Elysium Planitiae conceivably might represent shore cliffs and pinnacles of rock (stacks) detached from the main shore cliff by wave erosion. However, much more work needs to be done to separate "fact from fancy" and hard evidence from interesting supposition.

Martian Lacustrine Basins: David H. Scott, James W. Rice., Jr., James M. Dohm, and Mary Chapman

References: [1] Scott, D.H., and Chapman, M.G., 1991. Proc. Lunar and Planet. Sci. Conf. 21, p. 669-677. [2] Schaefer, M.W., 1990. Icarus, v. 83, p. 244-247. [3] Scott, D.H., 1983. In Conference on Planetary Volatiles (R.O. Pepin and R. O'Connell, eds.), p. 157-166. LPI Tech. Rpt. 83-01, Lunar and Planetary Institute, Houston. [4] Scott, D.H., and Underwood, J.R., Jr., 1991. Proc. Lunar and Planet. Sci. Conf. 21, p. 627-634. [5] Frey, H., and Jarosewich, M., 1982. J. Geophys. Res., v. 87, p. 9867-9879. [6] Carr, M.H., 1986. Icarus, v. 68, p. 187-216. [7] Rossbacher, L.A., and Judson, S., 1981. Icarus, v. 45, p. 39-59. [8] Lundquist, J., 1969. Periglacial Processes, Ross Publications. [9] Lucchitta, B.K., 1981. Icarus, v. 45, p. 264-303. [10] Grizzafi, Patricia, and Schultz, P.H., 1989. Icarus, v. 77, p. 358-381. [11] Baker, V.R., 1978. In Baker, V.R., and Nummedal (eds.), Field Conference held in the Columbia Basin, June 5-8, 1978. [12] Greeley, Ronald, Guest, J.E., 1987. U.S. Geol. Surv. Misc. Inv. Ser. Map I-1802-B, scale 1:15,000,000.

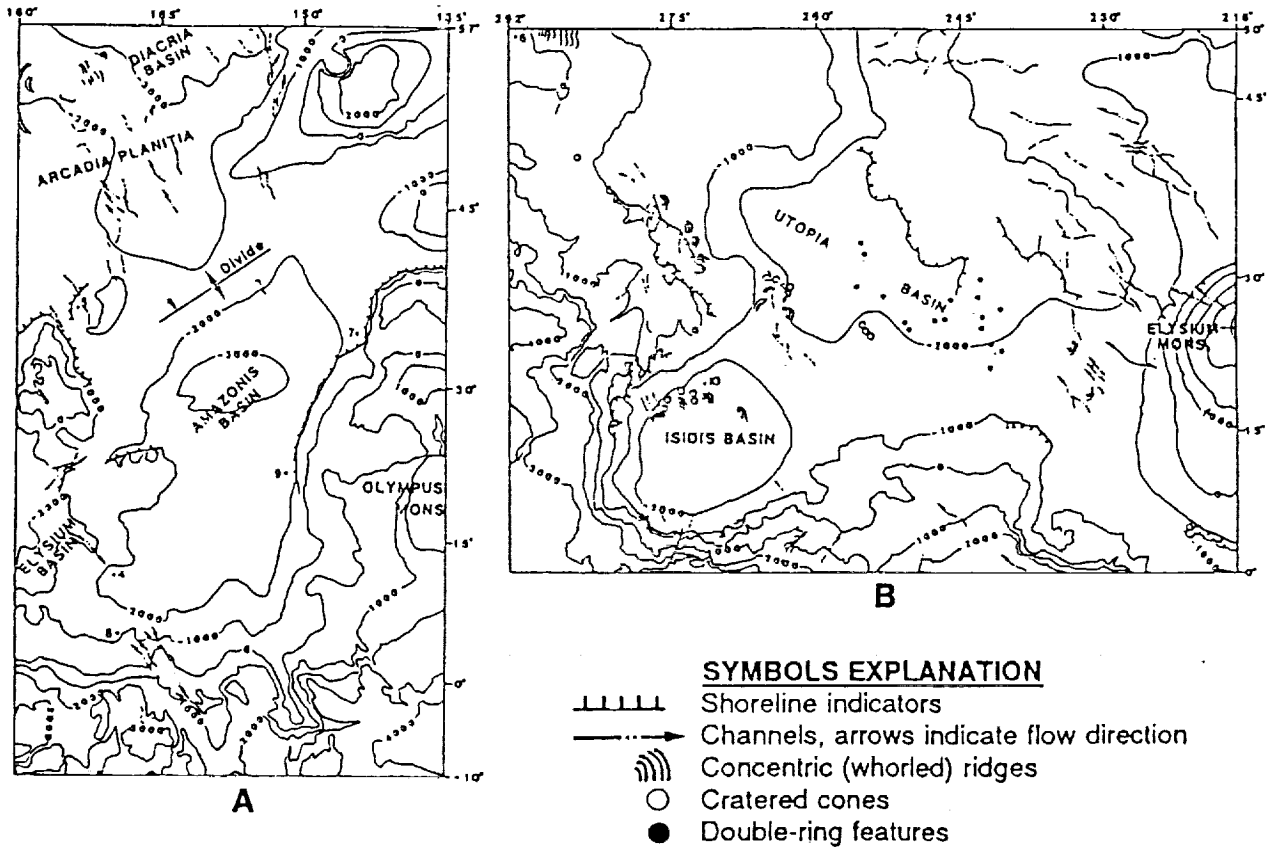

FIGURE 1

p. 2

EVIDENCE FOR CRYSTALLINE HEMATITE AS AN ACCESSORY PHASE IN MARTIAN SOILS

R.B. Singer and J.S. Miller, Planetary Image Research Laboratory, LPL, University of Arizona

Based on visible and near-IR spectral images of Mars obtained by us in 1988, we have confirmed the occurrence of bulk crystalline hematite as a minor or accessory phase on the surface. This hematite is not uniformly distributed being less abundant or absent in certain northern low-albedo regions. Even where most abundant, bulk hematite is not the primary coloring agent of heavily weathered materials on Mars. The primary coloring agent is apparently an amorphous or nanophase Fe^{3+} phase, analogous to the coloring agent in certain Hawaiian palagonites (e.g. Adams and Evans, 1980; Singer, 1982; Morris *et al.*,1989).

Background The characteristic coloration of Mars has long been known to be caused by Fe^{3+}, but the exact mineralogies have not been conclusively demonstrated. The relatively smooth and featureless spectral slope from the near-UV to the near-IR has made exact mineralogic interpretations difficult. Huguenin *et al.* (1977) were the first to make specific interpretations based on subtle spectral details. They noted a change in slope at 0.53μm, another at 0.62-0.64μm, and a weak absorption band sometimes present near 0.86μm. They interpreted these features as consistent with crystalline hematite, although in Mars spectra they are much weaker than for the pure mineral. Evans and Adams (1979) demonstrated that spectral reflectance of Mars was well matched by a specific palagonite (oxidized and hydrated basaltic glass) from Mauna Kea, Hawaii. Evans and Adams (1980) showed that an amorphous ferric iron/silica gel developed in the laboratory had similar spectral characteristics. Singer (1982) spectroscopically measured bulk crystalline ferric oxides physically diluted in a neutral powder. Even 1% bulk hematite or goethite in the laboratory mixtures imparted distinct crystal-field absorption features characteristic of that phase, much stronger than observed for Mars. He concluded that crystalline ferric oxides were not the primary coloring agent on Mars. The best palagonites, however, are not perfect matches to Mars. Morris *et al.* (1989) demonstrated that *nanophase* hematite produces a smooth but steep absorption edge similar to Hawaiian palagonites. Nanophase hematite is crystalline, but at such a small particle size (<7nm) that crystal-field bands do not develop. (The word *bulk* is used, in contrast to nanophase, to indicate crystalline ferric oxide with larger crystal sizes.) To better simulate spectra of high-albedo regions Morris *et al.* (1989) combined nanophase hematite with a small amount of bulk hematite. New observational data and interpretations by Bell *et al.* (1990) indicate that bulk crystalline ferric oxides may be more common on Mars than previously thought, and show some variation in regional distribution.

1988 Spectral Imaging Data Our results are interpreted from spectral imaging obtained during the 1988 apparition, using the Univ. of Az. 1.5m telescope on Mt. Bigelow and a CCD spectrograph. Wavelength coverage is 0.44 to 1.02 μm with resolution of 2 nm. Best-case spatial resolution is about 280 x 150 km. The data are calibrated relative to the solar-type star HD1835 (G2V). Further details are given by Singer et al (1990). The specific observations discussed here were obtained on September 26, 1988 (UT) at an Ls = 279° (early northern winter). The spectral behavior of the low-albedo regions Acidalia Planitia and Oxia Palus (hereafter Type 2) is different from more typical near-equatorial low-albedo regions such as Meridiani Sinus and Margaritifer Sinus (hereafter Type 1). Representative spectra from Meridiani and Acidalia are shown in Figure 1. The spectrum of Meridiani is more steeply sloped in the visible. Acidalia is more reflective in the blue, but less reflective in the near-IR. (An additional difference is that while Meridiani shows evidence for an Fe^{2+} pyroxene absorption near 0.95 μm, Acidalia does not.) Similar spectral characteristics for these regions were observed McCord and Westphal (1971) and Singer and Blake (1982), but not interpreted by them.

Spectral Evidence for Bulk Hematite The overall spectral difference between these two types of low-albedo regions indicates a greater amount of Fe^{3+} in Type 1. Evidence for the existence and regional variation of bulk hematite on Mars is clearly demonstrated by the spectral ratio between Meridiani Sinus and Acidalia Planitia shown in Figure 2. The rougher line is the spectral ratio. The smooth line is a laboratory spectrum of a heavily altered hematite-rich soil from the Cuprite, NV. Both spectra show spectral characteristics of bulk hematite: significant absorption in the blue, with a distinct change in slope at 0.53μm, a change in slope near 0.6μm leading to a flattened shoulder from 0.6 to somewhat beyond 0.7μm, and a broad crystal-field absorption centered near about 0.87μm. Most of the detailed deviation of the Mars ratio from the Cuprite spectrum in the near-IR is due to minor atmospheric water vapor problems. Somewhat beyond 0.9μm the

Mars ratio rises more steeply than the Cuprite spectrum: this is due primarily to the difference in pyroxene content between these two Mars regions. One potential complication for our interpretations is the presence of a north polar hood (a white condensate cloud) over northern Acidalia Planitia at the time of our observations. The hood is relatively optically thin, affecting data most strongly in the blue where the surface reflectance is lowest. It is not possible in our data to define a strict southern boundary for the hood. However, we have three different lines of evidence that condensates are not seriously affecting our results. First, these overall spectral differences have been observed three different martian seasons. Second, we have compared Meridiani/Acidalia ratios along spatial traverses from north to south. The characteristic hematite spectral shape is best developed for southern Acidalia where the condensates are absent or minimal. Lastly, Type 2 spectral characteristics are also observed for the low-albedo region Oxia Palus, which is close to the equator (0-10° N.) and unlikely to be seriously affected by condensates.

Discussion Based on these results we can say with considerable certainty that bulk crystalline hematite exists on Mars in small amounts, in addition to the more ubiquitous nanophase or poorly crystalline ferric oxide phase(s). We conclude that Type 2 low-albedo regions (typified by Acidalia Planitia) contain less of this hematite than Type 1 regions (typified by Meridiani Sinus). Oxia Palus shows indication of *slightly* more oxidation and bulk hematite than Acidalia. This may be a real compositional difference, indicating that Oxia is in some sense transitional between Type 2 and Type 1 regions, but we cannot rule out the possibility of some optical mixing with surrounding higher-albedo regions. We are currently investigating the relationship of ferric-oxides in high-albedo regions to both types of low-albedo regions. As expected, spectral ratios of data from western Arabia to dark regions show considerably greater Fe^{3+} in Arabia. There are not obvious spectral indications of a difference in ferric-oxide composition between Arabia and Type 1 low-albedo regions, implying that Arabia also contains minor bulk hematite.

References

Bell, J.F. III, *et al.*, J. Geophys. Res., 95, 14447-14461 (1990).
Evans, D.L. and J.B. Adams, Proc. LPSC 10th, 1829-1834 (1979).
Evans, D.L. and J.B. Adams, Proc. LPSC 11th, 757-763 (1980).
Huguenin, R.L., *et al.*, LPSC VIII abstract (1977).
McCord, T.B. and J.A. Westphal, Ap. J., 168, 141-153 (1971).
Morris, R.V. *et al.*, J. Geophys. Res., 94, 2760-2778 (1989).
Singer, R.B., J. Geophys. Res., 87, 10159-10168 (1982).
Singer, R.B. and P.L. Blake, Bull. A.A.S., 14, 755 (1982).
Singer R.B., *et al.*, LPSC XXI abstract, 413-314 (1990).

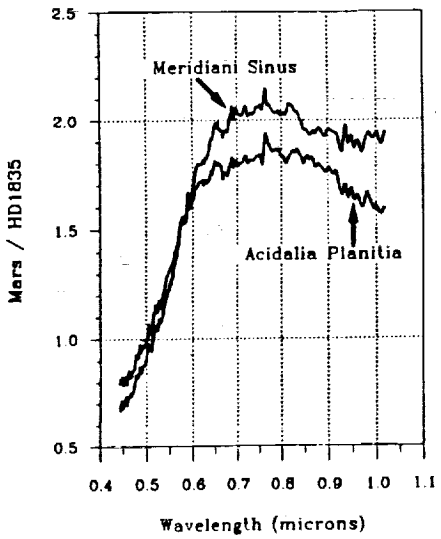

Figure 1.

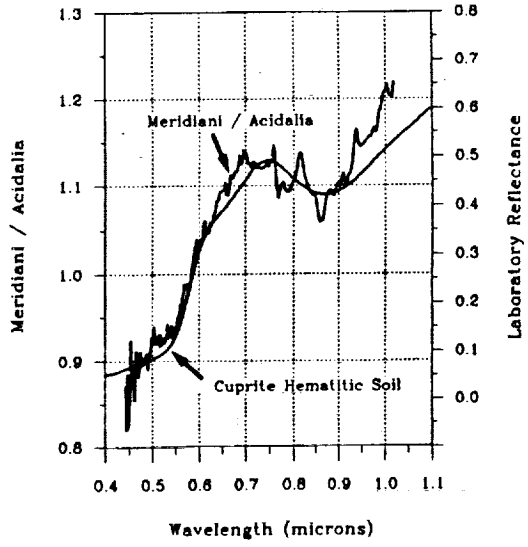

Figure 2.

CARBONATE FORMATION ON MARS: HISTORY OF THE CO_2 ATMOSPHERE FROM MODELS OF DIFFUSION-LIMITED GROWTH IN NON-AQUEOUS ENVIRONMENTS. Stuart K. Stephens and David J. Stevenson, Division of Geological and Planetary Sciences, California Institute of Technology, Pasadena, CA 91125.

History of CO_2 pressure on Mars: Getting from a (possible) greenhouse to (the present) 7 mb. If Mars had a $\gtrsim$1 bar CO_2 atmosphere prior to ~3.5 b.y. ago -- as many believe on the basis of geological evidence [e.g., 1,2] -- then the transition to the present pressure of 7 mb may require a loss mechanism other than carbonate formation in liquid water.

Previous work suggests that storage of CO_2 by adsorption in the Martian regolith [3] will not account for the early CO_2 inventory, while continued carbonate formation under ice-covered lakes [4,5] proceeds only until the pressure drops to ~0.5 bars. The removal of CO_2 by impact erosion [6] works only if the end of heavy bombardment postdates further recycling [7] or replenishment [2] of CO_2. Kahn's (1985) [8] mechanism for continued growth of carbonate in pockets of disequilibrium water may be tenable, but it awaits experimental verification.

Past experimental work. Booth [9,10] investigated the storage of CO_2 by non-aqueous carbonate formation, i.e., by gas-solid reaction or by reaction involving water vapor. His results -- that (a) the kinetics are sufficiently rapid to store the entire early inventory of CO_2, (b) an adsorbed monolayer of water-derived OH^- is involved, and (c) diurnal temperature-cycling below ~240 K (to get ~1 monolayer adsorbed OH^-) appears to be important -- require qualification, in addition to verification of the reaction mechanism. We have pointed out previously [11] that the results are difficult to extrapolate since (a) Booth's experiments did not proceed beyond a monolayer, and (b) the limiting effect of the formation of a non-porous rind was not examined.

Models of diffusion-limited carbonate formation. (a) Assumptions. We assume that the carbonate rind that builds up is non-porous, causing the process to be diffusion-limited [11]. This criterion is satisfied (using the reaction rate of Booth (1980) [10]) for $D \lesssim 10^{-10}$ cm^2s^{-1}, a limit consistent with extrapolations from available data [see 11]. The reaction mechanism we envision involves carbonate formation at the CO_2-silicate interface in the presence of carbonate or bicarbonate ions formed by the interaction of gaseous CO_2 with a thin film (monolayer?) of adsorbed OH^- [10]. The layer of water-derived ions would probably have to be at the reaction interface, within the solid, and we require an overabundance of water vapor relative to CO_2 -- a criterion most likely fulfilled by consideration of atmospheric water vapor abundances and relative diffusion rates. In addition to assuming a regolith depth of 1 km and a particle radius of 20 μm, we use a T-P relation similar to that used by Pollack et al. (1987) [7]. Recent (unpublished) models by Kasting have not been considered yet.

(b) Equations. We use $T = T(P)$, diffusivity $D = D_o\exp(-\Delta E/RT)$, and rind thickness $\ell \propto P_o - P$ to numerically iterate forward in time with $dP/dt \propto -D[T(P)]P/T(P)\ell(P)$. This relation arises from consideration of the tarnishing reaction [e.g., 12], for which the thickness of product formed on a solid by a gas reacting with it is given instantaneously (constant D) by $\ell(t) \propto (Dt)^{1/2}$. Our use of the tarnishing reaction further assumes ideality of gas solubility (i.e., Henry's Law).

(c) Results. With the constraint of today's pressure, and the simplification of uniform global temperature at each time-step, we can calculate the history of CO_2 pressure for a given diffusivity pre-exponential and activation

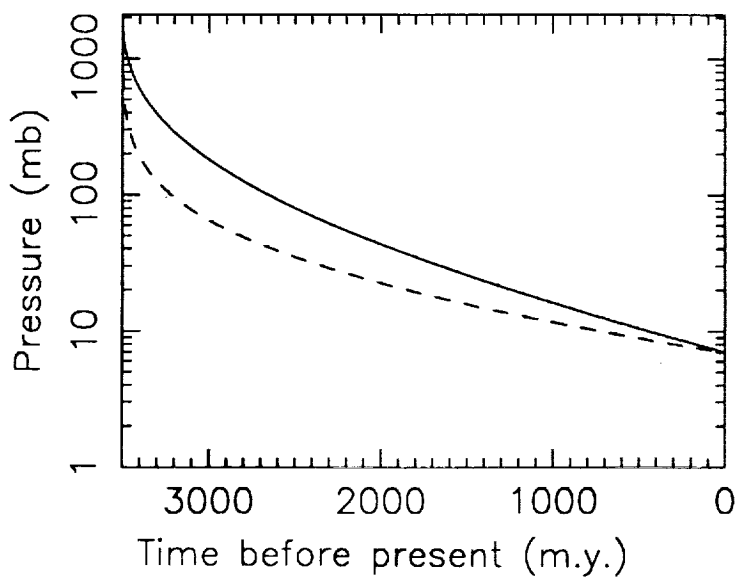

energy. The curves in the figure at left start with P_o = 2.1 bars (consistent with early greenhouse models) and are for two examples of the diffusivity -- $D_o = 10^{-18}$ cm^2s^{-1} and $\Delta E = 2.1x10^{11}$ ergs/mole (solid line), and $D_o = 10^{-10}$ cm^2s^{-1} and $\Delta E = 5.3x10^{11}$ ergs/mole (dashed line) -- both of which give a present-day D ~ 10^{-24} cm^2s^{-1}. Note that the pressure decays very rapidly in the first few 100 m.y., as a result of higher temperatures and therefore higher diffusivities. More recently than ~2 b.y. ago, the pressure declines gradually -- roughly exponentially with a 1-2 b.y. time constant. At present, the pressure is decreasing very slowly. Significantly, the exponential dependence of diffusivity on temperature in this non-aqueous CO_2-storage mechanism results in a decline in pressure more dramatic than that resulting from aqueous means [e.g., 5]. Geologic conditions on early Mars may have changed over time-scales of just a few tens of m.y.

We do not consider the effect of CO_2 rejuvenation, which would have been important prior to 3.5 b.y. ago due to volcanic recycling. By starting our calculations where we do, we begin with a situation in which sinks of CO_2 dominate over sources. However, we also ignore the important buffering effects of CO_2 storage in the regolith and polar ice caps [3]. These would result in small modifications to the CO_2 pressure beginning 2-3 b.y. ago.

Present experiments. We have conducted preliminary experiments designed to measure the amount of CO_2 reacted from a simulated Martian atmosphere to form carbonate on silicate grains. Warm experiments at constant T (300-350 K) and with no water (vapor or liquid) yielded no detectable reaction, suggesting the following result: If we are indeed operating in a thermodynamically-favorable regime (supported by Gooding (1978) [13] for the gas-solid reaction), then the lack of a reaction at warm temperatures suggests that a reaction in the 200-300 K regime will be less favored if reaction kinetics dominate. The completely dry scenario is thus not favored. An additional experiment, with abundant water vapor and at T ~ 300 K (constant), yielded a negative result as well. However, this is not inconsistent with Booth's findings, since lower temperatures may be required for the adsorption of a monolayer of water. We plan further (lower-T) experiments.

References. [1] J.B. Pollack (1979), Icarus, 37, 479-553. [2] M.H. Carr (1989), Icarus, 79, 311-327. [3] F.P. Fanale et al. (1982), Icarus, 50, 381-407. [4] C.P. McKay and S.S. Nedell (1988), Icarus, 73, 142-148. [5] C.P. McKay and W.L. Davis (1991), Icarus, 90, 214-221. [6] H.J. Melosh and A.M. Vickery (1989), Nature, 338, 487-489. [7] J.B. Pollack et al. (1987), Icarus, 71, 203-224. [8] R. Kahn (1985), Icarus, 62, 175-190. [9] M.C. Booth and H.H. Kieffer (1978), J. Geophys. Res., 83, 1809-1815. [10] M.C. Booth (1980), Ph.D. thesis, UCLA. [11] S.K. Stephens and D.J. Stevenson (1990), LPSC XXI Abs., 1198-1199. [12] F. Booth (1948), Trans. Faraday Soc., 44, 796-801. [13] J.L. Gooding (1978), Icarus, 33, 483-513.

ATOMIC OXYGEN IN THE MARTIAN THERMOSPHERE; A.I.F. Stewart, M.J. Alexander, LASP, U. of Colorado, R.R. Meier, NRL, L.J. Paxton, APL, Johns Hopkins U., S.W. Bougher, LPL, U. of Arizona, and C.G. Fesen, Dartmouth College

The Mariner 9 Ultraviolet Spectrometer (UVS) made extensive observations of airglow emissions from the thermosphere of Mars throughout the nominal mission (November 1971 - February 1972), during late summer in the southern hemisphere. Limb and disc measurements of the 130 nm triplet emission from thermospheric atomic oxygen were modelled by Strickland et al. [1]. They used a composition model in which oxygen was in diffusive equilibrium above 100 km (where the opacity of CO_2 at 130 nm reaches unity), and a complete frequency redistribution radiative transfer code which adopted a Doppler line profile whose width was independent of altitude. They concluded that the limb data were best explained by oxygen fractional abundances, f_O, of 0.5-1.0% at the 1.2 nbar pressure level. The disc data were generally consistent with about 1% atomic oxygen, but considerable local time and/or geographic variation was indicated. This earlier analysis did not attempt to extract a latitude dependence.

Recently, the thermospheric general circulation models (TGCMs) developed for the Earth and Venus have been applied to Mars [2]; we refer to it as the MTGCM. Radiative transfer modelling has also advanced considerably since the time of Mariner 9. Meier and Lee [3] describe a Monte Carlo partial frequency redistribution (MCPFR) code that allows for realistic altitude- and temperature-dependent line profiles. We have adapted this code to Martian conditions, and have compared the predictions of the MTGCM/MCPFR models with the Mariner 9 data.

Our analysis shows that the oxygen mixing ratio is the fundamental unknown controlling the 130 nm brightness. Our radiative transport calculation shows that the emergent intensity at 130 nm is not very sensitive to variations in thermospheric temperature. Then by fixing temperature and varying the oxygen abundance (via the parameter f_O) we use the μ and μ_0 (cosines of the emission and illumination angles) dependence of the data and the overall magnitude of the brightness to constrain the average value for f_O in the Martian thermosphere. The μ, μ_0 dependence is best reproduced by a model thermosphere with an oxygen fractional abundance at 1.2 nbars of 0.25% relative to CO_2, while the overall brightness of the observed 130 nm signal is best reproduced by a model with f_O=0.7%. These two tests suggest $f_O \simeq 0.5\%$ at the 1.2 nbar pressure reference level which corresponds to a vertical optical depth of several hundred in the 130 nm triplet.

The pattern of diurnal variation derived from our analysis is roughly the same as Strickland et al. [1] although with somewhat lower values for the O mixing ratio. The main reasons for this difference are the more important role played by the photoelectron source in our model, and the somewhat larger 130 nm solar flux, so we require less oxygen to match the observed brightnesses. Strickland et al. [1] also found that the OI 130 nm

emission on Mars is correlated with solar activity. We find that the correlation is virtually non-existent during the early orbits when the planet was covered with a thick global dust storm, but later orbits, during the clearing of the storm, show a persistent correlation.

Figures 1 and 2 compare distributions of f_O in latitude and local time derived from inversion of the Mariner 9 data (Fig. 1) and predicted by the MTGCM (Fig. 2). Focusing on the well-sampled region of the data map below the dashed line, the overall values of f_O are quite similar, about 0.8% deduced from the data and about 1.3% predicted by the MTGCM. However, the most striking result of the comparison is that both the local time trend and the latitude trend predicted by the models are the reverse of the trends in the data. The occurrence of a global dust storm just prior to the Mariner 9 arrival at Mars, and its gradual abatement during the period covered by the present data, suggest that the thermospheric structure, wind systems, and composition may have been profoundly affected during the acquisition of this data by the effects of waves and tides propagating upwards from the lower atmosphere.

ATOMIC OXYGEN AT 1.2 NBARS

Figure 1

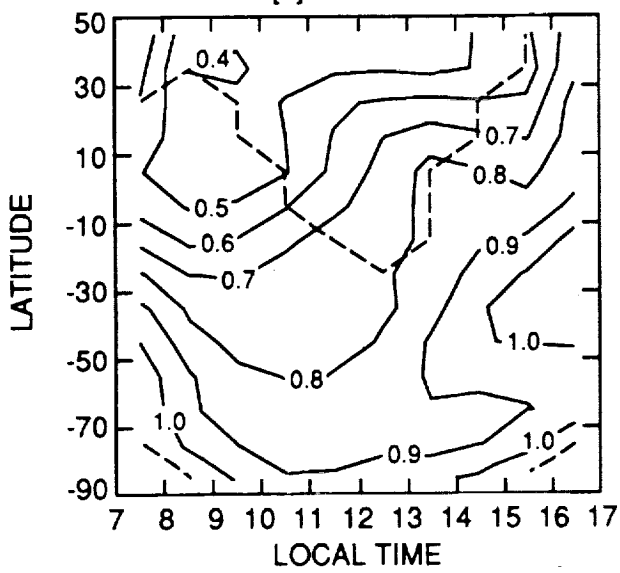

Figure 2

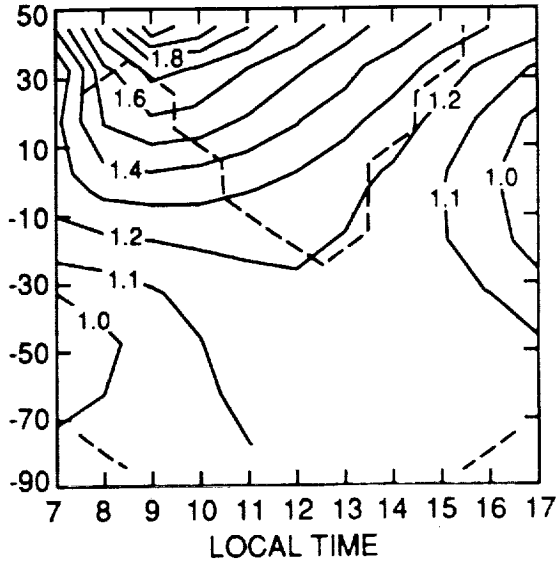

References: [1] Strickland, D.J., A.I. Stewart, C.A. Barth, C.W. Hord and A.L. Lane (1973) *J. Geophys. Res.* **78**, p. 4547. [2] Bougher, S.W., R.G. Roble, E.C. Ridley and R.E. Dickinson (1990) *J. Geophys. Res.* **95**, p.14,811. [3] Meier, R.R. and Jong-Sen Lee (1982) *J. Geophys. Res.* **82**, p.439.

p. 2

PHYSICAL INTERPRETATION OF THERMAL AND REFLECTED DATA ON MARTIAN SURFACE UNITS

Edwin L. Strickland III, 12717 Bullick Hollow Rd. Austin TX 78726

None of the available Viking Orbiter Infrared Thermal Mapper's thermal datasets can be uniquely interpreted in isolation from other data in terms of variations of a single, simple physical parameter of the martian surface. Other thermal datasets of a target area, thermal observations of adjacent materials, and visible and near-infrared observations of the same region can often sufficiently constrain interpretations to obtain one that is nearly unique. The major datasets, their derived information, and their ambiguities are as follows.

A.) Apparent Thermal Inertias: These can be determined from diurnal observations or estimated from single observations. The latter are partially dependent on surface albedo, which may be approximated from Pleskot and Miner's (1) map . The apparent inertia of a single target can be interpreted in terms of **(a)** the mean particle size of a loose sediment, **(b)** a mosaic of materials with different particle sizes and inertias, **(c)** the bonding of small, lower inertia particles to yield a higher inertia material, or **(d)** the presence of materials with different inertias within a few skin depths of the surface. The apparent inertia depends to a smaller degree on the surface's bulk density, the atmosphere pressure, and the atmosphere opacity at the time of measurement (2). Since elevations are approximately known on Mars, the dependence of inertias on elevation can be analyzed for a set of samples of one unit.

B.) Fine Component Thermal Inertias: These are estimated from observations of characteristic patterns of diurnal or (less precisely) predawn brightness temperature spectral differences (3). These are nearly as ambiguous as apparent inertias: only the ambiguity due to the presence of both high and low inertia materials at the surface has been approximately removed.

C.) Rock Abundance Estimates: These are derived from the same data as fine component inertias, and they are somewhat less ambiguous than the inertias. Though atmosphere dust emissions and surface emissivity variations can corrupt the analysis for rock abundance (3), the first effect is probably minor, while the second can approximately be compensated for (4). The main problem in interpreting rock abundance estimates is the uncertainty in the size of the "rocks". In regions with high "fines" inertias (implying particles about a millimeter in size), material with high enough inertias to be readily detected as a "rock" component must be at least centimeters across: presumably rock. However, in regions with low fine component inertias (characteristic of silt-sized or finer powders), higher inertia patches of either sand-sized particles or bonded fines could produce the spectral contrast interpreted as rocks. Christensen (3) presented rock abundance estimates and models that assumed I = 30 (about 13 cm) rocks. He provided limited indications on the corresponding abundances that would be estimated for other "rock" inertias, but these were given only for relatively low abundances of "rocks" and only for "rock" inertias greater than about 10 to 20.

D.) Surface Emissivity Estimates: These primarily sense spectral features related to the composition of the top few tens of micrometers of the surface, but they are also influenced by particle size effects, temperature gradients within the emitting layer (2), and by optically thin dust layering or unit mosaics (the last two are also detectable in visible and near-infrared reflected light observations). Little emissivity data is yet available, only the estimates of emissivity vs. albedo given for each IRTM channel by Christensen (4) and the preliminary 20 micrometer map of Christensen (5).

E.) Surface Phase Function and Emission Angle Observations: These, in principal, can provide direct information on surface roughness once effects of the atmosphere are removed, but they cannot discriminate between the effect of large, solid rocks and small, soft soil clumps. The only useful thermal data published so far is that of Kieffer *et al* (6) for the Viking 1 landing site. Related data is potentially available from visual and near-infrared data, but only limited studies of a few regional features have been done so far.

F.) Non-Ideal Diurnal Temperature Variations: These may have a variety of causes, summarized by Ditteon (7). **a.)** High atmosphere dust opacity produces a characteristic small departure from ideal diurnal behavior (late morning warming and afternoon cooling). This effect is undetectably small for "normal", tau << 1, dust opacities, and it is also assignable to dust because of the dust's characteristic spectral properties. **b.)** Smooth mosaics of materials with different thermal inertias will produce a similar behavior, but this will result in readily observed spectral effects due to surface anisothermality. Both **c.)** surface roughness and **d.)** non-Lambertian solar energy absorption cause a different type of non-ideal diurnal behavior (post-dawn and pre-sunset cooling) from those caused by atmosphere dust and mixed-inertia surfaces. However, roughness should produce the spectral signature of an anisothermal surface and cause non-ideal emission and phase-angle dependent brightness temperature variations, while non-Lambertian behavior should be detectable by analyzing imaging and IRTM broadband albedo photometric function data. An increase in thermal inertia with depth **(e.)** is probably the primary cause (2) of the morning warming and afternoon cooling mapped by Ditteon. Layered surfaces can be reliably inferred from this behavior when dust opacities are low and when "rock" abundance mapping has shown that

"rock" abundances (or equivalently the thermal contrasts of exposed materials) are low to moderate.

Without additional information, afternoon cooling cannot be interpreted unambiguously. The amount of cooling depends on both the thermal contrast between the surface layer and the substrate, and on how rapidly the inertia changes with depth. The strongest observed cooling values (-20° to -25°) require about 1/3 skin depth (l_t) of low inertia material on a high inertia substrate and require that the two materials have large inertia contrasts (2). I = 2 material on an I = 30 substrate, for example, can produce afternoon cooling as strong as -28°.

For compatibility with early versions of Christensen's (3) rock abundance estimates, Ditteon presented model results that almost exclusively assumed an I = 30 high inertia substrate. Cooling less extreme than -28° will be produced by materials with a smaller inertia contrast, but Ditteon's examples of predicted behavior do not clearly indicate what the maximum effect any given pair of inertias (besides I = 2 and 30) can produce. A few examples were given for other inertia combinations: I = 5 and I = 9 top layers on I = 30 "rock" can produce at least -15° and -9° cooling, respectively; while I = 1 "dust" on I = 10 "rock" can produce at least -25° cooling. Inertia differences of at least three times are apparently needed to produce afternoon cooling values of -10° or more.

Top layers that are either thinner or thicker than 1/3 l_t will produce smaller amounts of afternoon cooling than the maximum possible with a given pair of inertias. Typical observed afternoon cooling values (-10° to -20°) are compatible with a low inertia top layer that is either 1/10 to 1/5 or 1 to 2 l_t thick on a much higher inertia substrate. They are also compatible with a top layer about 1/3 l_t thick that has only moderate inertia contrast with the substrate.

Independent information on apparent thermal inertias can provide additional information to discriminate between these cases. For the thin-top-layer case, inertias will nearly equal that of the bottom layer. Increasing the top layer's thickness will decrease inertias and increase the amount of afternoon cooling. For the transitional-case (circa. 1/3 l_t top layer), the inertias will be intermediate between the inertias of the two layers, and inertias will be very sensitive to changes in the top layer's thickness while afternoon cooling will vary only moderately. For the thick-top-layer case, inertias will approach those of the top layer, and afternoon cooling will diminish as the inertia decreases. In addition, information from visual and thermal observations of a region surrounding a specific target can sometimes restrict plausible top and/or bottom layer candidate materials to units with known or constrained inertias.

G.) Supporting Information from Visible and Near-IR Data: Visible images and IRTM Lambert albedo data provide information on surface layers no more than a very few tens of micrometers thick. For these layers, color data can discriminate between materials of different mineral composition, particularly the degree of weathering of iron-bearing materials. Albedo data can discriminate between materials of similar color and thus possibly similar composition but of different grain sizes: finer-grained materials generally have higher albedo. However, very small amounts of a dark, spectrally neutral, opaque material, like magnetite or carbon-black, can drastically reduce the reflectance of moderate albedo powders while changing their colors little.

Images of units present in an area can directly indicate whether units mix on scales below image resolution limits, form partially resolved mosaics, or remain well separated even on kilometer scales. Multispectral albedo mixing data in the visible and near infrared can indicate whether unresolved mixtures of materials are mixing by deposition of a continuous layer of variable optical thickness on a substrate, or as a discrete "checkerboard" mosaic of optically thick unresolved patches. The morphologies of color/albedo features and their changes of shape or albedo and color with time may indicate if units are effectively immobile, can move slowly across the surface, or can be deposited and stripped from an area rapidly, constraining their grain sizes and degree of bonding. These empirical principals and analysis techniques were used to interpret the physical properties of previously identified martian surface units (8, 9), as discussed in the accompanying abstracts.

REFERENCES: (1) Pleskot and Miner [1981] Icarus, 45, 179-201, (2) Strickland [1988] Lunar and Planetary Science XIX, 1139-1140, (3) Christensen [1986] Icarus, 68, 217-238, (4) Christensen [1982] J. Geophys. Res., 87, 9987-9998, (5) Christensen [1984] Lunar and Planetary Science XV, 150-151, (6) Kieffer *et al.* [1977] J. Geophys. Res., 82, 4249-4292, (7) Ditteon [1982] J. Geophys. Res., 87, 10197-10214, (8) Strickland [1982] Lunar and Planetary Science XIII, 780-781, (9) Strickland [1986] Lunar and Planetary Science XVII, 839-840.

PHYSICAL PROPERTIES OF DEUCALIONIS, EOS, AND XANTHE-TYPE UNITS IN THE CENTRAL EQUATORIAL REGION OF MARS

Edwin L. Strickland III, 12727 Bullick Hollow Rd., Austin, TX 78726

Classification and mapping of surficial units in the central equatorial region of Mars (30°N. - 20°S., 57°E. - 75°W.) using enhanced color images and Mars Consortium data, identified three distinct, high albedo, relatively red surficial units in regions with intermediate to high thermal inertias. These units have distinctive properties and morphologies, occur in different, well-defined areas, and show different seasonal and secular patterns of albedo change. **Deucalionis** units occupy the classical albedo area of Deucalionis Regio, south of Meridiani Sinus and Sabaeus Sinus, and adjacent areas. **Eos** forms a bright band that separates the dark, relatively blue Meridiani-type units that dominate the southern part of the study area from intermediate albedo, relatively red Oxia units common in the north. **Xanthe** forms moderately bright, relatively red, *Type 1B* crater-streaks and uniform sheet-deposits in and adjacent to parts of Chryse Planitia, including the Viking 1 landing site. Xanthe is always associated with Oxia deposits, and has significantly lower albedos than the Eos materials, which it can be confused with.

DEUCALIONIS: All available data indicates Deucalionis deposits are thin bright "red" dust deposits on Meridiani (and occasionally Oxia) materials of normal macroscopic roughness. Visible and broadband data indicate that the dust is nearly optically thick in the visible but not the near infrared. Bright Deucalionis is probably no more than 10 micrometers or so thick for an assumed bulk density of 1.0. The Dark Deucalionis deposits are probably only 1-2 micrometers thick, and are extremely variable. They can be deposited by a single dust storm, and are episodically eroded in patches until the next storm. Bright Deucalionis may be many years accumulation of dust.

Emissivities of both units are near unity, indicating that thermal infrared opacities are like visible opacities and higher than near-infrared opacities. Deucalionis deposits may be an ideal location to study possible thermal gradient effects in thin bright dust deposits on darker substrates that may simulate the effects of atmospheric dust.

Thermal data indicates that Dark Deucalionis deposits' thermal properties are controlled entirely by their substrate. Bright Deucalionis materials have slightly lower inertias than most of their surroundings. About 0.1 mm of 0.1 gm^{-3} density, micrometers-sized dust might be able to reduce inertias by the observed amount, and this might be compatible with Bright Deucalionis being only partially optically thick in the near infrared. However, the imperfect correlation of locally low inertias with the Bright Deucalionis distribution and a total lack of afternoon cooling caused by a thermally detectable dust layer probably rule out that model out. Models assuming that discrete low inertia dust patches are present in Deucalionis Regio under an optically uniform dust mantle could be consistent with multi-wavelength thermal data and afternoon cooling observations, but barely. It seems more likely that the lower inertias in Deucalionis Regio and adjacent parts of Sabaeus Sinus is not caused by the Deucalionis dust, but by properties of their Meridiani substrates.

Afternoon cooling data show that unusually small amounts of afternoon cooling, and possibly actual afternoon warming, are present in the reduced inertia areas of Deucalionis Regio and southern Sabaeus Sinus. This data tends to exclude models for the reduced inertia that invoke low inertia dust patches on the Meridiani. Afternoon warming, if confirmed, probably indicates a decrease in the thermal inertia with depth in this area. One model consistent with the reduced inertias and possible afternoon cooling would have several cm of Meridiani on a lower inertia substrate of Dark Oxia in this area. Better data and numerical models are needed to confirm the possible warming and model the effects of inverted inertia layering.

EOS: All available information indicates Eos materials are thin dust deposits on Meridiani materials and probably thicker, but still thermally thin dust deposits on Oxia. Eos materials are all "red" and all have high albedos. However, two or more materials identified as "Eos", but with slightly different albedos, are probably present in the eastern Oxia crater-streaks region. Eos probably forms discrete, optically thick, relatively stable patches on Oxia, continuous, variable optical thickness, and less stable dust deposits on Meridiani. Eos surfaces probably have similar average macroscopic roughness to Oxia and Green-blue" Meridiani surfaces.

Only depositional morphologies of Eos on Oxia or Meridiani are observed, suggesting that the results of erosional events have not been observed or are not as readily recognizable as the typical *Type Id* erosional forms observed in Deucalionis Province. Mobility of their substrates probably controls the thickness and stability of Eos deposits. Eos is preferentially deposited at and near contacts between Oxia and Meridiani, but no obvious explanation for this has been identified.

Christensen's rock abundance data suggests that large patches of Eos on Oxia may be in slightly rockier areas than Eos-free Oxia. Increased surface roughness may promote Eos deposition in those areas, but smoother patches of Eos may counter the photometric effect of the roughness. Rock abundances in the Eos border area cannot be readily compared with Eos' distribution without Consortium-type analysis.

PROPERTIES OF DEUCALIONIS, EOS, AND XANTHE UNITS, MARS; Strickland, Edwin L., III

An Eos border between Arabia and Deltoton Sinus has larger T_7T_{20}brightness temperature differences than adjacent Arabia surfaces. This may be caused by wavelength-dependent emission at variable depths along a temperature gradient in the dust layer, and is probably not, as attributed by Christensen in 1982, caused by a localized concentration of atmospheric dust.

Thermal inertia data shows Eos on Oxia decreases thermal inertias slightly without obviously changing the afternoon cooling (which is probably caused by the presence of a low inertia disaggregated Oxia layer on a consolidated or cemented Oxia substrate). This requires the Eos to be less than about 1/3 thermal skin depth thick but probably more than 1/10th skin depth. If Eos is 20 micrometer dust with an density of 1.7 and an inertia of 2, it should be a few millimeters thick. If Eos is 2.5 micrometer dust in a very low density "fairy castle" structure with a density of 0.1 and an inertia of 0.16, it could be about 0.4 millimeter thick. In either case, it should be optically thick.

Eos was observed to expand north over Oxia between 1969 and 1972, and deposition of an estimated annual global atmosphere dust loading of 4.10^{-3}g cm $^{-2}$(by Pollack et al. in 1979) could produce the visually observed deposits and possibly the observed thermal properties, but only if ultra-low density deposits are formed, or if selective dust deposition in restricted locations produces deposits with masses and thicknesses well above the global average. Alternately, the new Eos deposits could be thermally invisible, and only many years of accumulation could produce the observed lower inertia patches.

South of the Eos-obscured Oxia/Meridiani contact within the Eos border, Meridiani is visible, inertias are lower, and afternoon cooling is diminished. In this border, Eos must be thin enough, patchy enough (not preferred), or must physically mix with the Meridiani (also not preferred) so that Meridiani is visible in the transition zone. One allowed class of models has a sharp Oxia/Meridiani contact. Patchy Eos on the Meridiani or Eos mixing with the Meridiani south of the contact could be responsible for the changing inertias and afternoon cooling. These models are implausible and are not preferred but cannot be ruled out. Models with variable thicknesses of Oxia (or Meridiani) between the Eos and the underlying Meridiani (or Oxia) were rejected.

The preferred model has a mosaic of thermally thick Oxia and Meridiani patches under the Eos. To the south, an increasing Meridiani proportion increases the inertia and decreases the afternoon cooling. Eos must obscure the Oxia in the transition zone, but progressively reveal the Meridiani. Unfortunately, in both of these models, either Oxia or Meridiani can be stratigraphically higher, so long as the unit on top is sufficiently thick to thermally obscure its substrate in most locations.

XANTHE: Xanthe's high albedo and "red" color are entirely consistent with highly oxidized dust. Significantly lower albedos than on nearby Eos surfaces suggest slightly different compositions or grain sizes. Colorimetric properties suggest that like Eos, Xanthe covers Oxia in discrete opaque patches, Meridiani as a variable-opacity deposit. Photometric properties suggest Xanthe surfaces' roughness resembles Oxia's and Eos'. Like Eos, Xanthe on Oxia appears relatively stable, Xanthe on Meridiani is more mobile. Their principal visual difference, besides Xanthe's lower albedo, is that Eos forms sharp-edged, solitary and coalesced Type Ib streaks , while Xanthe forms highly diffuse Type Ib sheet deposits. These materials were probably deposited under similar, but significantly different conditions.

Thermal properties of Xanthe are surprisingly complex. In the southern part of Chryse, inertias are about 1 unit lower than on adjacent Oxia surfaces. Rock abundances are low, and mapped afternoon cooling is the same as that of adjacent Oxia. Xanthe's predawn temperatures and inertias increase gradually and uniformly toward the north, across first a sharp increase in the inferred "rock" abundances and then a fairly sharp decrease in the strength of the observed afternoon cooling. A model that can probably explain the coordinated variations of predawn temperature and afternoon cooling in the Eos border region seems unable to easily explain the lack of correlation in Xanthe, and no better model was found.

Dark streaks in the vicinity of the Viking 1 lander suggest that Meridiani materials may be present under the Xanthe at the landing site, and dark, relatively "blue" soils were observed at the site by Strickland in 1979. "Dark red" soils present at the site may well correspond to Oxia materials. As the Lander is adjacent to or on the mapped afternoon cooling gradient crossing the Xanthe in Chryse, and a mosaic of Oxia and Meridiani under Xanthe dust was proposed to explain thermal properties of Eos border, Lander data are crudely compatible with that model. Lander data may be able to choose between alternate models for the low inertia of Xanthe: millimeters of approximately I = 2 silt or << 1 mm of a very-low-density layer of I < 1 micrometer- sized dust. However, the local complexity of the site was largely hidden from the Lander by the bright "red" Xanthe dust, and unexpected regional complexity of the ares is indicated by the poor correlations between inertias, rock abundances, and afternoon cooling datasets. This means that a more thorough study of the site using both Lander and Orbiter data will be needed to resolve the many ambiguities that currently hinder using the site as ground-truth for interpreting remote sensing data on Mars.

PHYSICAL PROPERTIES OF MERIDIANI SINUS-TYPE UNITS IN THE CENTRAL EQUATORIAL REGION OF MARS:

Edwin L. Strickland III, 12717 Bullick Hollow Rd., Austin, TX 78726

Classification and mapping of surficial units in the central equatorial region of Mars (30°N - 20°S, 57°E-75°W) using enhanced color images and Mars Consortium data (1, 2) identified four major color/albedo units in the dark, reddish-gray regions that form the classical dark albedo markings of Mars, including Meridiani Sinus. The darkest, least red (relatively "blue") materials form splotches (some with dune forms) in craters, inter-crater depressions, and parts of Valles Marineris. These form the "Dark Blue" Meridiani unit. Abundant materials that have higher albedos and are somewhat redder than the "Dark Blue" unit have uniquely high green/(violet+red) color ratios in Viking Orbiter images. These materials, named "Green-blue" Meridiani, surround and mix with "Dark Blue" Meridiani patches and are abundant on crater rims and local elevations. Discontinuous, patchy deposits with still higher albedos and much redder colors have morphologies characteristic of the *Type Ib* bright depositional dust streaks and sheets that were classified by Thomas *et al.* (3) These dust deposits, which appear to be optically thin and patchy and are darker and not as red as other *Type Ib* dust deposits on Mars, and their Meridiani substrates, were designated the "Red" Meridiani unit. Distinctive deposits that form highly eroded mesas and escarpments in northern Meridiani Sinus were named "Light Blue" Meridiani since they are not as red as other materials with moderately high albedos. Large areas dominated by these units form Meridiani Province (2) in the central equatorial region of Mars. This abstract presents a systematic interpretation of these units' properties based on currently available remote sensing data.

Meridiani Province is dominated by dark, relatively "blue" and unoxidized mafic materials, probably derived from basalt or other mafic rocks. Exposed surfaces are usually partially coated with a mixture of a spectrally distinct weathering product (4), probably derived from the Meridiani materials, plus some of the globally distributed "red" dust. Surface thermal emissivities are variable and are highly correlated with albedo: visible amounts of the "red" dust and the weathering coatings sharply increase emissivity over the circa. 0.9 values (5) of the "Dark Blue" unit's.

The darkest and least "red" surfaces of the "Dark Blue" Meridiani unit may be nearly free of the weathering coatings and dust because a highly mobile surface component, most likely fine sand, ejects dust and abrades any weathered grain coatings. The "Dark Blue" unit accumulates in topographic lows, and photometric data (6) indicates that it is smoother than most units in the study area, consistent with most deposits being dunes and sand sheets. The darkest splotches have unusually high thermal inertias (7), but do not have high rock abundances. The highest observed inertias require that those splotches contain particles from coarse sand to pebbles in size or are partially cemented, but the splotches' ability to eject dust indicates that a highly mobile finer component is present

The "Green-blue" and "Red" Meridiani units' colors are attributed to the presence of abundant but optically thin "green" weathering coatings (4) and "red" dust, respectively. Their thermal inertias are not distinctive in the available data. The "Green-blue" Meridiani present in the Oxia-region *Type II* splotch-related crater streaks is apparently mobile and was probably deflated from source splotches of "Dark Blue" Meridiani (8). It may be finer grained, possibly well sorted, and may contain considerable amounts of the "green" weathering product despite its mobility. "Green-blue" and especially the "Red" units within Meridiani Province may be relatively immobile, and may be fine-grained but weakly cemented material that does not readily eject dust or weathering coatings. Other deposits of these units could be coarse lag deposits, depleted of mobile fine-grained sand

and equally unable to eject dust. Both deposits' photometric properties (6) indicate that they are rougher than "Dark Blue" Meridiani, consistent with partially cemented and then eroded sand or coarse lag deposits.

Thermal inertias of Meridiani surfaces decrease with elevation considerably more than expected for unbonded sediments (9). This could be due to elevation-dependent particle size sorting, but data outside the study area suggests that high inertia materials are under-represented at relatively high elevations in the study area. Rock abundances (10) are highly variable, but high abundances are not characteristic of the province within the study area. Small amounts of afternoon cooling are consistent with small or locally restricted thermal inertia increases in the top centimeters of Meridiani surfaces (11), but not the widespread presence of bedrock under less than about 10 cm of sand.

"Light Blue" Meridiani, found only within northern Sinus Meridiani, is a high inertia, probably partially lithified, eolian deposit. It mixes with "Green-blue" Meridiani, and while relatively "red", has higher violet albedos than the "Red" Meridiani dust. The pure "Light Blue" unit may not have been sampled at kilometer resolution in available colorimetric data (12). Therefore, it is unclear whether it is a spectrally distinctive "blue" unit with a high albedo and unusually low green color-ratios (the reverse of the "Green-blue" unit), or a very high albedo "red" dust-related material exposed in at most a 50-50 (or so) mosaic with the "Green-blue" unit. The only color/albedo unit with major topographic relief in the study area, this highly distinctive material deserves concentrated study.

The bulk of the Meridiani Province materials show no systematic regional color/albedo variations suggestive of regional composition variations. This could mean that the bulk of these materials have been transported and mixed on at least sub-global scales and are not locally derived. However, discrimination of small color/albedo differences between Meridiani materials from different igneous sources may be impossible with Viking-like color cameras in the presence of the overwhelming contamination of weathering products and dust deposits. Until the mapping spectrometers of the Mars Observer and other future missions start returning data, earthbased spectral observations, and possibly Viking color observations of the darkest, least contaminated splotches, may be the only means, of searching for regional composition variations of Meridiani-type mafic sediments on Mars.

More rewarding work clearly possible with Viking data is research directed at understanding the relation between the thermal properties of Meridiani materials and their morphology, mobility, colors, and photometric properties. Within Meridiani Province, thermal inertias are uniquely poorly correlated with albedos, except for the high inertias of many intra-crater "Dark Blue" Meridiani splotches. It should be possible to discriminate between the proposed physical models of "Green-blue" and "Red" Meridiani with Viking data. It should also be possible to characterize and better understand the currently obscure causes of the regional and global variations in thermal inertias and rock abundances of the non-splotch Meridiani materials.

REFERENCES: (1) Strickland [1982] Lunar and Planetary Science XIII, 780-871 (2) Strickland [1987] Lunar and Planetary Science XVIII, 958-959, (3) Thomas *et al.* [1981] Icarus, 45, 124-153. (4) Strickland [1983] Third International Colloquium on Mars, LPI Contribution 441, 253-255, (5) Christensen [1984] Lunar and Planetary Science XV, 150-151 (6) Strickland, these abstracts, (7) Christensen [1983] Icarus, 56, 496-518, (8) Thomas and Veverka [1979] J. Geophys. Res., 84, 8131-8146, (9) Strickland [1988] Lunar and Planetary Science XIX, 1139-1140, (10) Christensen [1986] Icarus, 68, 217-238, (11) Strickland [1988] Lunar and Planetary Science XIX, 1137-1138, (12) Strickland [1986] Lunar and Planetary Science XVII, 839-840.

PHYSICAL PROPERTIES OF OXIA/LUNAE PLANUM AND ARABIA-TYPE UNITS IN THE CENTRAL EQUATORIAL REGION OF MARS

Edwin L. Strickland III, 12717 Bullick Hollow Rd., Austin TX 78726

Introduction: Classification and mapping of surficial units in the central equatorial region of Mars using enhanced color images and Mars Consortium data (1, 2) identified the relatively dark but "red" materials that cover Lunae Planum and surround the Meridiani materials of Oxia Palus as portions of a major surficial deposit that extends from Lunae Planum east to the low thermal inertia region of Arabia. Oxia Province (3) consists of the regions dominated by the characteristically dark "red" Oxia materials, but it includes darker streaks and splotches of relatively "blue" Meridiani materials and brighter "red" deposits of dust belonging to Eos Province (the bright "red" border between Oxia and regional Meridiani deposits to the south) and Xanthe Province (the moderately bright "red" dust deposits in western Chryse Planitia and its vicinity, including the VL-1 landing site). Two Oxia units were recognized: a darker unit present on Lunae Planum and east of Oxia Palus that has distinctive low thermal inertias, and a higher albedo unit in the Chryse trough that has intermediate to high inertias. Oxia Province surrounds the extremely low thermal inertia Arabia Province in the east part of the study area, and occurs as isolated patches within Arabia (often including splotches of Meridiani materials within the Oxia patches). Arabia Province's materials have been widely interpreted as unconsolidated dust deposits which are currently forming at this stage of Mars' precessional climate cycle (5, 6), though the persistence of stable, moderately strong albedo contrasts among Arabia materials has not been addressed in those models (7). This abstract presents a systematic interpretation of Oxia and Arabia Province materials based on currently available remote sensing data.

Oxia Province Materials: Oxia's homogeneous "red" color indicates that it consists of oxidized materials without any less "red", less oxidized Meridiani mixed in to account for its distinctive low albedo. Shadowing caused by unusual surface roughness (8) cannot readily explain Oxia's low albedo, as photometric data (9) indicates Oxia is not unusually rough, and Oxia's low albedos persist at low phase angles. One plausible explanation is the presence of small amounts of a dark, spectrally neutral material like magnetite in Oxia materials. Another possible explanation (10) is that Oxia materials are more hematitic than the Hawaiian palagonite-like higher albedo "red" dust materials of Eos and Xanthe. If Oxia, like the "dark red" soil at the Viking 1 site (11), can be shown to have lower green ratios than the brighter "red" units (resulting from hematite's characteristic spectral shape), their hypothesis would be strongly supported.

Except for superimposed deposits of higher albedo "red" units, Oxia's remarkably uniform optical properties suggests it was deposited as a regional dust mantle. Its continuity, stability, apparent resistance to erosion, and generally low rock abundance (12) suggest Oxia is relatively thick (many centimeters to a few meters) and cohesive. The drifts of "dark red" soil at the VL-1 site have these properties, supporting the hypothesis that these are Oxia deposits.

The moderate to high thermal inertias of Light Oxia imply that its materials have a coarse grain size or are partially cemented. Only the latter is consistent with other observations. The only major physical difference between the two Oxia units, which differ primarily in thermal inertia, may be that Dark Oxia is less cemented than Bright Oxia. Each Oxia units' thermal inertias vary by approximately the expected amount with elevation (13), but after effects caused by high rock abundances at low elevations and atmospheric dust are removed, Oxia inertias may decrease by less than the expected amount. This would be more consistent with thermal properties expected for cemented silt instead of unbonded sand.

Moderately strong afternoon cooling (14) is observed for all Oxia surfaces. Surface roughness, atmospheric dust opacity, or other suggested causes cannot account for Oxia's observed non-ideal diurnal thermal behavior. Only an increasing thermal inertia with depth appears capable of explaining Oxia's afternoon cooling (15). Models with rock-like high inertia material under a moderate inertia Oxia top-layer are implausible, and Meridiani does not have enough thermal inertia contrast with Oxia to be the substrate. The preferred model of Oxia's afternoon cooling has a substrate of partially cemented Oxia with slightly higher inertia than the observed value, covered by a thermally thin, low inertia top layer formed by mechanical disaggregation of the Oxia back into silt-sized or finer grains. Confirmation of this hypothesis using VL-1 site data will be difficult because of the site's obscuring deposit of Xanthe dust, the complex mix of units present at the site (11), and because VL-1 is near or on a sharp regional decrease in the strength of the afternoon cooling.

Arabia Province Materials: Arabia consists of two major units, Bright and Dark Arabia. Both are bright and "red", but the dark unit has significantly lower visible albedos at low phase angles than proven "red" dust units (16). However, Arabia units have higher IRTM broadband albedos (approximately near-IR reflectances) than the "red" dust, indicating that Arabia and the "red" dust materials may have significantly different compositions. Higher visible albedos than other units seen at high phase angles (9) suggest that Arabia surfaces have unusually low macroscopic surface roughness.

Arabia's albedo patterns were not obviously changed by two global dust storms (7), indicating that Arabia does not consist of a uniform recent dust deposit and that widespread dust deposition and erosion did not occur during and after the storms. Though a few bright,

depositional streaks are present, most albedo features in Arabia are not interpretable in terms of recognized depositional or erosional wind streaks and related features (17). Dust deposits on Meridiani surfaces are unacceptably poor analogs of Arabia's albedo features. Dust deposits on Oxia, though their morphologies do not resemble Arabia's units, have some similarities: widespread deposition is uncommon, *Type Ib* bright dust deposits are much more stable than in Meridiani Province, and dark *Type Id* erosional features are not visible. Either unfamiliar depositional or erosional mechanisms are responsible for these features, or Arabia's albedo markings are not formed by simple, thin, bright dust deposits on a darker substrate.

Arabia (and related materials in Tharsis and Elysium) have uniquely low apparent thermal inertias and predawn temperatures. Apparent inertias of about 3.0 may actually correspond to an inertia of 1.4 after removing the effects from higher inertia "rocks" and atmospheric dust (13), implying particle sizes near 10 micrometers. Dark Arabia areas have higher predawn temperatures than Bright Arabia, but not higher thermal inertias, possibly due to differences in their diurnal thermal behaviors. Arabia inertias appear essentially independent of elevation, contrary to the expected behavior of particles larger than 1-3 micrometers (15). This might be explained if Arabia materials were about 1 micrometer in size, but were sufficiently bonded to raise their inertias to observed values. "Rock" abundances (12) are small, and do not obviously correlate with albedo patterns. Predawn brightness-temperature differences, attributed to the presence of a rocks covering a few percent of the surface, can probably be better explained by a varying surface fraction of moderate inertia material with Dark Oxia-like inertias, but models needed to quantitatively evaluate this hypothesis are not available.

Arabia and Tharsis surfaces have large systematic departures from ideal diurnal behavior, most notably morning warming and strong afternoon cooling (14). This cannot be explained by the presence of rocks, atmospheric dust, high surface roughness, or non-Lambertian photometric behavior (13). The only reasonable explanation yet proposed is that thermal inertias of Arabia surfaces increase sharply within less than 2 cm of the surface. Models with low inertia material on a high inertia (Oxia, Meridiani, or bedrock) substrate are implausible, though not entirely excluded. Models with very low inertia material on a low inertia substrate, analogous to the preferred Oxia model, are preferable. A few millimeters of uncemented, micrometer-sized material on a low inertia substrate can probably explain observed non-ideal diurnal temperature variations, but quantitative models needed to test this hypothesis are again not available. The overall inertia will be dominated by the substrate, which was proposed on independent grounds to consist of weakly cemented micrometer-sized dust, so the top layer could simply be disaggregated substrate. Albedo and predawn temperature patterns could reflect varying exposures or amounts of disaggregation of the substrate.

Comparison of Oxia and Arabia materials: Arabia and Oxia-like deposits appear to be fundamentally related in many ways, despite their great thermal inertia differences. Both are "red" but have lower visible albedos than demonstrably recent bright "red" dust deposits. Both have higher broadband albedos than many of the dust deposits, suggesting that the dust units and the Arabia and Oxia units have significant spectral differences not yet detected in earthbased spectra. Both materials occur in close association within the north equatorial region (which they dominate) and both become rapidly less abundant to the north and south of this band. Oxia materials show a systematic inertia decrease as they approach Arabia/Tharsis Province edges, and they appear to surround all Arabia/Tharsis deposits except on the southern sides. Oxia occurs within Arabia, but neither have been shown to occur as outliers outside of these two provinces, particularly within Meridiani Province. Neither areas currently tend to accumulate dust deposits, except for isolated areas of Eos and Xanthe deposits in Oxia Province and isolated bright streaks in Arabia. Both have stable albedo patterns, and both lack recognized dark erosional features. Both areas have large afternoon cooling values, best interpreted as indicating a strong thermal inertia increase within 2 skin depths of the surface. Both are most easily interpreted as old eolian dust deposits, originally up to meters thick, cemented to varying degrees, and currently being disaggregated at the surface to form thin lower inertia top layers.

The similarities between Oxia and Arabia-like materials, despite the great range of their thermal inertias, indicate that these materials are fundamentally similar in nature and origin. They form a distinct class of surficial materials with physical properties clearly distinct from both the "blue" Meridiani sands and the various thin, mobile, "red" dust deposits.

REFERENCES: **(1)** Strickland [1982] Lunar and Planetary Science XIII, 780-781, **(2)** Strickland [1983] Third International Colloquium on Mars, LPI Contribution 441, 228, **(3)** Strickland [1987] Lunar and Planetary Science XVIII, 958-959, **(4)** Kieffer *et al.* [1981] Proc. Lunar. Planet. Sci. Conf., 12th., 1395-1417, **(5)** Christensen [1986] J. Geophys. Res., 91, 3533-3545. **(6)** Zimbelman and Kieffer [1979] J. Geophys. Res., 84, 8239-8251, **(7)** Strickland [1986] Lunar and Planetary Science XVII, 837-838, **(8)** Guinness and Arvidson [1988] Lunar and Planetary Science XIX, 439-440, **(9)** Strickland, in these abstracts, **(10)** Arvidson *et al.* [1987] draft of article to be submitted to J. Geophys. Res., **(11)** Strickland [1979] Proc. Lunar. Planet. Sci. Conf. 10th, 3055-3077, **(12)** Christensen [1986] Icarus, 68, 217-238, **(13)** Strickland [1988] Lunar and Planetary Science XIX, 1137-1138, **(14)** Ditteon [1982] J. Geophys. Res., 87, 10197-10214, **(15)** Strickland [1988] Lunar and Planetary Science XIX, 1139-1140, **(16)** Strickland [1986] Lunar and Planetary Science XVII, 839-840, **(17)** Thomas *et al.* [1981] Icarus, 45, 124-153.

SURFACE PHOTOMETRIC PROPERTIES AND ALBEDO CHANGES IN THE CENTRAL EQUATORIAL REGION OF MARS

Edwin L. Strickland III, 12717 Bullick Hollow Rd. Austin TX 78726

Comparison of the Viking Orbiter 2 Approach mosaic (1) with a Viking Orbiter 1 apoapsis mosaic taken 11 Mars months later (2) provides qualitative information on the photometric properties of the martian surface, the stability of the dust and sand deposits responsible for the classical martian albedo features, and the distribution of dust and ice aerosols in the martian atmosphere near the northern summer solstice. The approach mosaic was taken at L $_s$106° (early N. summer), phase angle 106°, and airmasses varying from 4.6 at 30°N to 3.3 near 10°S. The apoapsis mosaic was taken in four sequences between L $_s$72° and 76° (late N. spring), near phase angles of 47°, and at airmasses near 2.5. Systematic differences in the photometric decalibrations used to generate these mosaics may induce multiplicative errors of 5-10% of the observed albedos in comparisons of the mosaics, but they are probably nearer 3% of the albedos

In the study area (30°N - 20°S, 57°E - 75°W), scene-average approach Minnaert albedos were about 10% greater than apoapsis albedos and slightly less "red". Guinness' observations of surface photometric functions at the Viking landing sites (3) indicate that soil surface reflectances dropped 30% between 47° and 106° phase angle, but there was little shift in color between these two phase angles. The relatively high approach albedos and the color shift relative to the approach mosaic are probably due to the abundance of forward-scattering dust and ice hazes in the atmosphere observed through greater airmasses in the approach mosaic (4 & 5).

Since the surface albedo markings are clearly visible in both mosaics, the approach and apoapsis orange-band (red filtered) albedos (affected least by the non-uniform ice-haze distribution) of the surface units in this region (classified and mapped in (6)) were compared to search for differences attributable to secular albedo changes or surface photometric function variations. The raw plot of approach vs. apoapsis albedos of 48 targeted features showed a wide scatter. The only interpretable trend in the plot is that in the approach mosaic, targets for each unit were systematically brighter in the northern part of the study area and darker in the south. One unit had an orange albedo of 11.8-12.6% in the apoapsis mosaic, but varied from 9.5% near 20°S to 19.1% near 30°N in the approach mosaic. This latitudinal trend is probably due to the combined effects of increased atmospheric opacity in the northern part of the approach mosaic (7) and the greater line-of-sight airmasses over northern targets in that mosaic.

In a second attempt to compare approach and apoapsis albedos, the orange albedo differences (approach minus apoapsis) of the 48 targets were plotted as a function of latitude. For all units, the approach-apoapsis difference generally increased with latitude. The albedo differences at any given latitude were similar for most units, scattering about a "normal" latitudinal trend by only ±1%. However, the darkest, least "red" unit ("Dark Blue" Meridiani, DBM) and the high-albedo, "red," low thermal inertia materials of Arabia were both relatively bright in the approach mosaic. "Green-blue" Meridiani (GBM) materials (slightly brighter and redder than DBM) plotted slightly above the remaining units' trend. The Eos unit's targets (located in the high albedo border that separates the intermediate albedo, relatively "red" Oxia materials in the north from the dark, relatively "blue" Meridiani materials further south) all fall slightly below the "normal" trend of most units. Since both the "Dark Blue" Meridiani unit and the Arabia units plot approximately 3.5% above the trend, scattering about ±1% about their own trends, their behavior is clearly anomalous.

What is responsible for the unusual behavior of these two units? Can their relatively high apoapsis albedos be due to secular albedo changes during the 11 Mars months between observations? Visual comparison of the two mosaics shows that contacts between most units were stable at the resolution and noise level of the approach mosaic. These included the abundant, moderate-contrast albedo features within Arabia. Major exceptions were the contacts between the "blue" Meridiani materials (DBM & GBM) and most of the overlying dust deposits of the "Red" Meridiani and Deucalionis units. Discrete patches of "Red" Meridiani material appeared slightly more numerous and had higher contrast with their surroundings in the apoapsis mosaic. However, the total amount of "Red" Meridiani material on "blue" Meridiani deposits appeared generally similar in the mosaics, and the albedo difference vs. latitude plot showed no obvious change in "Red" Meridiani albedos when compared with the other "normal" units' albedos.

For most "normal" units, there is no indication that any systematic, regional albedo change occurred. Certain targets (which were intentionally located in areas that were known from earthbased and spacecraft studies to have highly variable albedos) scatter further from the "normal" latitudinal trend than most targets, but their behaviors can readily be explained by albedo changes that are easily visible upon comparison of the mosaics. Eos targets do appear to have brightened during the interval between observations, based on observations of the mosaics and other images, and this is reflected in their somewhat low approach - apoapsis albedo differences.

The "Dark Blue" Meridiani materials appear to have less contrast with their surroundings in the approach mosaic than they did later. If they were lightly coated with high-albedo dust at the time of the approach mosaic and were dust-free later, this could explain the unit's relatively high albedo in the approach mosaic. However, the similar "Green-blue" Meridiani unit shows at

most weak brightening in the approach mosaic, and red dust deposits on Meridiani materials appear slightly more widespread in the apoapsis mosaic than earlier. In addition, while regional albedo increases from widespread dust deposition were observed (Eg. Eos, some Deucalionis deposits), albedo decreases from erosion do not appear to be synchronized and uniform over regions as large as the study area. Finally, "Dark Blue" Meridiani appears to be the last dust-covered unit and/or the first dust-scoured, based on the appearance and behavior of dark, intracrater Meridiani splotches in Eos, Meridiani, and Deucalionis dominated areas. Thus, a systematic regional albedo decrease of only "Dark Blue" Meridiani -- leaving other Meridiani units unchanged -- is an implausible explanation for the unit's relative brightness in the approach mosaic.

The Arabia materials also appear anomalously bright in the approach mosaic when compared with their appearance in the apoapsis mosaic. This area is widely considered to be an area of active dust deposition and accumulation (8), though the persistence of stable albedo markings in this area is inconsistent with that hypothesis. A dust deposit present in the approach mosaic and absent later could causer a relatively high approach albedo. However, a comparison of features in the two mosaics shows that the albedo patterns formed by darker and brighter Arabia materials appear the same in the two mosaics. Deposition and removal of a regional dust deposit from Arabia should cause substantial changes in the region's albedo patterns, similar to changes seen in the Deucalionis and "Red" Meridiani units' patterns. Thus, regional albedo changes due to dust deposition or erosion appear unlikely to cause the relatively high approach albedos of the Arabia materials.

At high phase angles, particularly at and beyond the 106 ^{0}phase of the approach mosaic, addition of a forward scattering atmosphere dramatically increases albedos. Thus, an increase in atmospheric optical depth over specific areas can greatly increase their approach albedos. However, such highly localized (but fairly uniform) increases in atmospheric opacity over specific surface materials -- but not their surroundings -- are entirely hypothetical, yet they would be needed for this hypothesis to be plausible.

An third explanation for the distinctive behavior of the Meridiani and Arabia units is that these units' scattering properties are different from those of the other units. If these surfaces had a less strongly back-scattering photometric function than the "normal" units have, they would appear relatively bright in the high phase angle approach mosaic. To evaluate whether differences in surface photometric functions could explain these effects, photometric models of the martian surface were constructed by combining Hapke's photometric functions (9) with the atmospheric attenuating and scattering effects modeled by Lumme and Bowell (10). Surface packing-density variations can vary the width of the opposition-effect back-scattering peak, but they are not significant at intermediate to high phase angles. Strongly forward scattering particle phase functions could explain the effect, but *ad hoc* explanations are needed to explain the differences between these units and other "normal" units with similar apoapsis colors and albedos.

A simpler and more plausible explanation of high-phase brightening is that relatively smooth surfaces have higher albedos at high phase angles than rougher but otherwise identical surfaces. This is because shadows (less abundant on smoother surfaces) are preferentially observed at high phase angles. This effect is independent of the particle micro-properties of a surface, and depends only on the surface's roughness over distances larger than the mean optical path length in the surface. Thus, it can easily explain photometric differences between units made of similar materials (eg. DBM and GBM).

The preferred explanation for the observed approach - apoapsis albedo differences is that both Arabia and Meridiani materials are smoother on millimeter and larger scales than other units in the study area. This is in good agreement with preliminary conclusions of Thorpe (11) and (for dark intracrater Meridiani splotches) Regner *et al.* (12). This is also consistent with reasonable models of these surfaces. "Dark Blue" Meridiani surfaces are interpreted (13) as consisting of sand dunes and sand sheets, which would be expected to have macroscopically smooth, nonshadowing surfaces. Viking Lander images of the surfaces at both landing sites show that smooth drift area's brightnesses are close to those of adjacent rough soil areas at low phase angles, but drifts become much brighter than rough soils when looking up-sun at high phase angles. Smooth patches of duricrust at both landing sites, interpreted by Strickland (13) as eolian deposits (regardless of how they became salt enriched and cemented), also show this behavior. Arabia surfaces, widely thought to be uncemented eolian dust deposits, could well be smoother than more cemented dust deposits, even after erosion (13). Further study of the photometric properties of martian surface materials clearly has the potential to provide valuable information on physical properties of the materials' component grains and the macroscopic surface properties of the materials' deposits.

REFERENCES: **(1)** Soderblom *et al.* [1978] Icarus, 34, 446-464, **(2)** Kieffer *et al.* [1981] Proc. Lunar. Planet. Sci. Conf., 12th, 1395-1417, **(3)** Guinness [1981] J. Geophys. Res., 86, 7983-7992, **(4)** Thorp [1977] J. Geophys. Res., 82, 4161-4165, **(5)** Pollack *et al.* [1979] J. Geophys. Res., 84, 2929-2946, **(6)** Strickland [1982] Lunar and Planetary Science XIII, 780-781 and Strickland [1981] Third International Colloquium on Mars, LPI Contrib. 441, 258, **(7)** Strickland [1987] Lunar and Planetary Science XVIII, 960-961, **(8)** Christensen [1986] J. Geophys. Res., 91, 3533-3545, **(9)** Hapke [1984] Icarus, 67, 264-280, **(10)** Lumme *et al.* [1981] Icarus, 45, 379-397, **(11)** Thorpe [1982] Icarus, 49, 398-415, **(12)** Regner [1988] Lunar and Planetary Science XIX, 968-969, **(13)** Strickland, these abstracts, **(14)** Strickland [1979] Proc. Lunar. Planet Sci. Conf., 10th, 3055-3077.

GLACIAL AND MARINE CHRONOLOGY OF MARS

Robert G. Strom, Jeffrey S. Kargel, Natasha Johnson, and Christine Knight; Lunar and Planetary Laboratory, University of Arizona, Tucson AZ 85721

A hydrological model involoving episodic oceans and ice sheets on Mars has been presented by Baker, et al. (1). An important aspect of this model is the age and correlation of these events, particularly the glacial epochs. Also important are their absolute ages. Based on stratigraphic and cratering evidence, the most recent occurrence of these events was relatively late in Martian history.

The cratering record on Mars can be divided into three general periods: 1) the period of late heavy bombardment, 2) a transition period at the end of late heavy bombardment, and 3) the post heavy bombardment era (3). The crater size/frequency distribution represented by the period of late heavy bombardment is characterized by a complex curve with a differential -2 slope (cumulative -1) at diameters less than about 50 km diameter. The post heavy bombardment size distribution has a differential -3 slope (cumulative -2) over the same diameter range (Fig. 1). On the Martian time-stratigraphic scale, the period of late heavy bombardment occurred during Noachian and Early Hesperian time and came to an end during the Middle Hesperian. The post heavy bombardment era began in Late Hesperian time and extends through the Amazonian Epoch to the present day (2).

Although a Noachian ocean is suggested as a theoretical consequence of a warm, wet early Mars (3,4), as an element in the hydrological cycling responsible for the widespread Noachian valley networks, and a cause of an erosional episode near the end of late heavy bombardment (5), there is no direct evidence for such an ocean. Evidence for a more recent sporadic formation of great northern plains oceans has been presented by Parker, et al. (6). Since most of the northern plains are Late Hesperian (2,7) these oceans cannot be older. The outflow channels, thought to be the sources of the oceans, show multiple flow episodes and ages ranging from Late Hesperian to Late Amazonian (7). High density valleys on Alba Patera have been attributed to water runoff possibly associated with a nearby ocean (8). The age of the surface on which these valleys occur is Early Amazonian indicating the valleys and ocean are younger (Early to Middle Amazonian). Chapman, et al. (9) present evidence that the Elysium basin was occupied by an ephemeral sea which they date as Amazonian based of stratigraphic evidence. This "sea" may have been a part or a remnant of the late ocean mentioned above.

There is mounting evidence that widespread episodic glaciation occurred in the both hemispheres mostly above 40 degrees (10, 11, 12, 13). The most detailed studies are of the Argye and Hellas regions (11, 12, 13). Crater counts in the Hellas basin indicate that the Hellas glaciation occurred during the Middle Amazonian. We also counted craters on the floor of Argyre occupied by ridges (eskers). Although there is evidence for at least two glacial epochs, the esker plains appear to be the most recent. The craters were divided into three types: 1) craters with ejecta blankets, 2) craters with no visible ejecta blankets but relatively sharp rims, and 3) no ejecta blankets and highly degraded rims. The craters with ejecta blankets are probably post glaciation and equivalent to ejecta blanket craters in Hellas. Fig. 2 is an "R" plot of the size/frequency distribution of eject blanket craters on the Argyre esker plains and similar craters in Hellas. Also shown for reference are the Northern Plains (Late Hesperian) and the Tharsis Volcanic Plains (Amazonian). The Hellas and Argye curves are essentially identical within the errors, indicating similar ages of glaciation during Middle Amazonian time. The glacial features (eskers, outwash plains, etc.) recognized in Argyre, Hellas and elsewhere (10,11. 12, 13) require glacial melting and running water for relatively long periods of time. This in turn suggests a temperate climate with temperatures above the melting point of ice during Middle Amazonian time.

Fig. 3 summarizes the martian ages of various events including the latest glacial and marine epochs. The absolute ages of these events is very uncertain and depend on ones

assumptions about the origin of the impacting objects and the cratering rate. If the period of late heavy bombardment ended the same time on Mars and the Moon, then the Middle Hesperian is about 3.8 Gy old. However, if the objects responsible for late heavy bombardment were accretional remnants, their sweep-up time at Mars would be extended by about 1 Gy due to perturbations of the objects into the u_6 secular resonance (14). In this case the Middle Hesperian is about 2.8 Gy old. Thus, ocean and ice sheet formation on Mars is surely younger than 3.8 or 2.8 Gy. Depending on different models (15, 16), the Middle Amazonian could be anywhere between about 2.3 to 0.25 Gy, and therefore ice sheets and apparently a temperate climate were present sometime during this time span.

References. 1. Baker et al., 1991, Nature, in press. 2. Strom et al., 1991, Mars, Univ. Arizona Press, in press. 3. Pollack et al., 1987, Icarus, **71**, 203-224. 4. Schaefer, M.W., 1990, J. Geophys. Res., **95**, 14291-14300. 5. Chapman and Jones, 1977, Ann. Rev. Earth Planet. Sci., **5**, 515-540. 6. Parker et al., 1989, Icarus, **82**, 111-145. 7. Tanaka, K.L., 1986, Proc. Lun. Planet. Sci. Conf. 17th, J. Geophys. Res., **91**, E139-E158. 8. Gulick and Baker, 1990, J. Geophys. Res., **95**, 14325-14344. 9. Chapman, et al., 1990, Lun. Planet. Sci. Conf. XXI, 180-181. 10. Kargel and Strom, 1991, Science, submitted. 11. Kargel et al., 1991, Lun. Planet. Sci. Cong. XXII, 687-688. 12. Kargel and Strom, 1991, Lun. Planet. Sci. Conf. XXII, 683-684. 13. Johnson, et al., 1991, Lun. Planet. Sci. Conf. XXII, 651-652. 14. Wetherill, G.W., 1975, Proc. Lunar Planet. Sci. Conf. 6th, Pergamon Press, 1539-1561. 15. Neukum and Wise, 1976, Science, **194**, 1381-1387. 16. Hartman, et al., 1981, Basaltic Volcanism on the Terrestrial Planets, Pergamon Press, New York, 1049-1127.

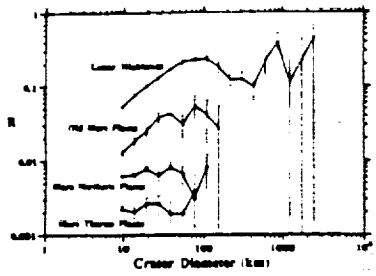

Fig. 1. "R" plot of the crater size/frequency distribution of the lunar highlands, martian old plains (Early Hesperian), Mars Northern Plains (Late Hesperian), and Mars Tharsis Plains (Amazonian).

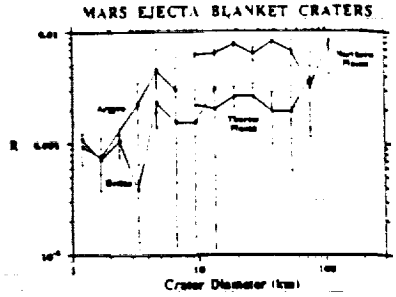

Fig. 2. "R" plot of the size/frequency distributions of post-glacial craters in Argyre and Hellas compared to the martian Northern and Tharsis Plains.

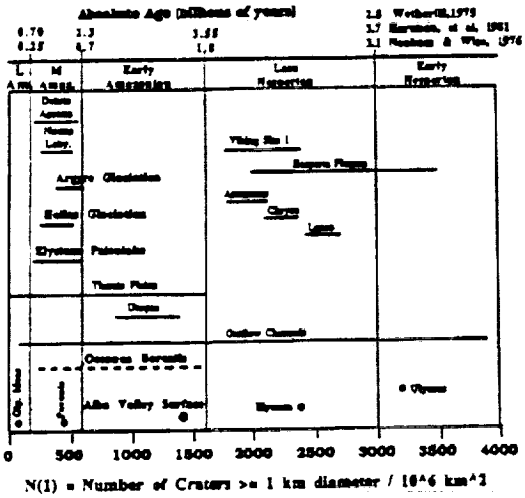

Fig. 3. Summary of the time-stratigraphic age of ice sheet and ocean formation together with several other major events in Martian history.

CHARACTERIZATION OF MARTIAN NEAR-SUBSURFACE MATERIALS BY DETERMINATION OF COHESION AND ANGLE OF INTERNAL FRICTION; R. J. Sullivan, Department of Geology, Arizona State University, 85287.

The strengths of geological materials, from the strongest, most pristine varieties of bedrock to the weakest soils and debris, can be described by the Coulomb criterion in which the two material-dependent parameters are ϕ, the angle of internal friction, and c, the cohesion. Values of ϕ range from 0 to ~60°, although values of 30-45° are most common. Values of c, however, range over several orders of magnitude, from 0 to 10^8 Pa.[1] Many classes of geological materials can be distinguished from one another on the basis of their strengths. In the present study, martian near-subsurface materials are characterized by performing stability back-analysis on small martian avalanche chutes in order to determine ϕ and c for these materials at time of failure. Additionally, the strengths of these materials and the depths to which they are indicated (i.e., depths of failure) have implications for the effectiveness of the weathering process(es) responsible for having weakened the material to the point of failure.

The gradation of steep slopes generally reveals much about the geological surface environment of a planet. Steep slope morphologies often reflect the gradational processes that have shaped them, and the past or present activity of these processes usually implies other important information about the planet's surface environment (e.g., on Earth the drainage basin is a common geomorphic unit on steep slopes, and this implies specific surface/atmospheric conditions needed for liquid water to precipitate and to be stable at the surface). Steep slopes are not widespread on Mars, but do occur along the margins of outflow channels, within the calderas of volcanos, and along the walls of Valles Marineris.

The steepest slopes within the Valles Marineris occur just below scarp brinks and are characterized by fine scale crenulations (previously described as U-shaped chutes, fluted scarps, rocky ribs, etc.).[2-6] On close inspection, these small features typically have narrow triangular or half hour-glass shapes, with acute (but usually open) ends pointing downslope, generally resembling some types of terrestrial landslide scars. The features under study here are similar in form to the much larger, more frequently studied Valles Marineris "spurs and gullies" although, besides being smaller, they are less arcuate, more acute, and occur on generally steeper slopes at higher elevations subjacent to scarp brinks. Sharp identified these features as avalanche chutes.[2,3] Following on Sharp's identification, the hypothesis investigated here is that these smallest spur-and-gully features result from repeated catastrophic mass-wasting governed by development of a debris mantle of reduced strength (compared with the original bedrock) on steep slopes. The mass-wasting cycle begins when a weak mantling layer develops and grows through some unidentified weathering process(es) at the expense of the underlying sloping rock, until the layer eventually fails catastrophically under its own weight and slides down the mantle/rock interface.

In civil engineering, stability analysis commonly involves determining the factor of safety, FS, for a standing slope. Input variables include the two-dimensional topography of the slope, and material parameters such as specific weight, ϕ, and c. If ϕ and c cannot be directly measured, then only minimum strength values required to maintain the integrity of the slope can be determined. This type of analysis, performed for a few areas in Noctis Labyrinthus and Valles Marineris, suggests that the strength of martian slope materials varies with location, and in some places may be relatively weak.[7]

MARTIAN NEAR-SUBSURFACE MATERIALS: Sullivan, R. J.

In this work, *back*-analysis (reconstruction) of the stability of thirty avalanche chutes was performed in the very limited areas where high resolution imaging overlapped with available 1:500K topographic map coverage. Back-analysis of slip failure is a tool used in terrestrial civil engineering for determining, after slip failure has occurred, the strength of geological material along the slip-surface at time of failure. Stability back-analysis involves approximating the geometry of the failure scar (often as a two-dimensional infinite slab), setting the factor of safety equal to unity, and deriving a function relating the angle of internal friction and the cohesion to each other. Some ambiguity exists in this derived relation; different values of cohesion and angle of internal friction may be combined to yield the same strength. Terrestrial workers usually have additional means available to remove this uncertainty. In cases of remotely sensed features, such as the small martian avalanche chutes, no such additional means are available.

However, a new technique has been developed to incorporate the third dimension (width) of an avalanche chute in stability back-analysis in order to yield unambiguous values of cohesion and angle of internal friction. The procedure is based upon extending the ordinary method of slices to three dimensions, in order to construct avalanche chute cross-sections whose widths and depths vary as a function of gradient, gravity, density of material, and ϕ and c. Applying the technique to the well-documented slide at Lodalen, Norway[8] as a test produces excellent correspondence with field reality. Generally, the technique reveals that the width:depth ratio of any avalanche chute decreases with increasing contrast between the average slope angle and the angle of internal friction.

Applying this technique to the martian avalanche chutes yields results consistent with indications from earlier work,[9] but with greater certainty: values of cohesion and angle of internal friction identify the materials at time of failure as moderately cohesive debris. If Sharp's identification of these features as avalanche chutes is correct, then results here imply that (1) weathering processes have had a significant effect to depths of tens of meters (where failure has occurred) below the martian surface; and thus (2) on relatively steep slopes within Valles Marineris, sizeable, unaltered, unmantled bedrock exposures for high-resolution spectral and spatial scanning by Mars Observer may be scarce.

References

(1) Hoek, E., and J. Bray, *Rock Slope Engineering*, 3rd ed., (London: Institution of Mining and Metallurgy), 358 pp., 1981. (2) Sharp, R. P., Mars: Troughed terrain, *J. Geophys. Res. 78*, pp. 4063-4072, 1973. (3) Sharp, R. P., Mars: Fretted and chaotic terrains, *J. Geophys. Res. 78*, pp. 4073-4083, 1973. (4) Lucchitta, B. K., Morphology of Chasma Walls, Mars, *Interagency Report: Astrogeology 83*, 51 pp., 1977. (5) Lucchitta, B.K., Morphology of chasma walls, Mars, *Jour. Res. U. S. Geol. Survey, 6*, No. 5, pp. 651-662, 1978. (6) Blassius, K. R., J. A. Cutts, J. E. Guest, and H. Masursky, Geology of the Valles Marineris: First analysis of imaging from the Viking 1 orbiter primary mission, *J. Geophys. Res. 82*, 4067-4091, 1977. (7) Clow, G. D., H. J. Moore, P. A. Davis, and L. R. Stichartz, Stability in Chasma walls in the Valles Marineris, Mars, (abstract) *Lun. Plan. Sci. Conf. XIX*, pp. 201-202, 1988. (8) Sevaldson, R. A., The slide in Lodalen, 6 October 1954, *Geotechnique, 6*, pp. 1-16, 1954. (9) Sullivan, R. J., and M. Malin, Cohesion and angle of internal friction of martian slope materials (abstract) *Bull. Am. Astron. Soc., 22*, No. 3, p. 1062, 1990.

TOPOGRAPHY OF APOLLINARIS PATERA AND MA'ADIM VALLIS

G. D. Thornhill, D. A. Rothery, J. B. Murray, Dept. of Earth Sciences, Open University, Walton Hall, Milton Keynes, MK7 6AA, T. Day, A. Cook, J-P. Muller, J. C. Iliffe, Dept. of Photogrammetry and Surveying, University College London, Gower Street, WC1

1. Introduction

The automated extraction of detailed topographic information from Viking Orbiter images will provide constraints on the geomorphology of Martian features, and improve our understanding of the processes that have shaped the Martian surface. Digital elevation models (DEMs) of a small area of Mars have been obtained using automated terrain extraction software developed at University College London.

Two stereo pairs covering part of the Aeolis quadrangle (MC23 -NE and SE) have been stereo-matched, providing topographic information of the northern part of Ma'adim Vallis and crater Gusev, and of the volcano Apollinaris Patera.

2. Method

The software uses an adaptive least squares correlation technique, to grow regions of matched points, based on a few user-supplied seed points (1,2,3). This can produce good coverage of the overlapping area on the Viking photographs, although in some areas where there is insufficient texture, or where albedo streaking is present, the matcher fails to converge. Work is under way at University College London to develop shape from shading techniques to complement the stereo matching. The matching process is constrained by range limits on a variety of parameters, including the eigenvalues of the covariance matrix, the distortion matrix between the two patches, and various radiometric measures. However, for Viking imagery, most of these constraints have to be rather loose to ensure sufficient coverage of the area, and as a result, the matcher makes errors (blunders). Methods of automatically identifying and removing blunders, where no independent topographic information exists, are being investigated. At present, some blunder removal is carried out manually.

After blunder removal, the image is geocoded, translating the disparities into heights using a network of control points developed by Wu (4), and then interpolated onto a grid using kriging (5). The results can then be viewed by overlaying the image on the DEM (terrain rendering) or by plotting contours and profiles.

3. Results

Digital elevation models of the northern part of Ma'adim Vallis (603a41 607m/pix, 639a91 721m/pix), and Apollinaris Patera (603a42 612m/pix, 639a92 717m/pix), covering the area between 180° to 190° long. and -2° to -20° lat. were obtained using the method outlined above.

The results for the Ma'adim Vallis area show broad agreement with the USGS topographic map of the area (6) with a channel depth of 1-2 km. This is also in agreement with Roth *et al.* (7), who obtained Earth-based radar profiles of the area, including an echo from Ma'adim Vallis, showing a depth of 2km. Detailed study of the variations in the channel depth along its course, and calculations of discharge rate from channel cross-section and slope are currently being undertaken. Unfortunately, comparison of the profile of crater Gusev with the results of Roth *et al.* (7) has not been possible, as the dark, featureless, aeolian streak prevented stereo-matching on the floor of the crater.

Results for Apollinaris Patera have also been obtained, (fig. 1), though the absolute heights relative to the Mars datum are not well constrained. However, the relative heights are sufficient for some analysis. Again, the topographic map is in reasonable agreement with the USGS map of the area (8), although there are significant differences. The data derived here suggest that the construct stands some 5-6km above the terrain on the western side, which is a difference of 2km from the USGS map. This discrepancy has already been noted by Robinson (9), who calculated the height of the construct from shadow measurements and photoclinometry. The slopes of the volcano are approximately 6° on the western side, and 3° on the eastern side, consistent with its

classification as a shield volcano. On the south-eastern flanks, there is a considerable bulge, which corresponds to the fan-shaped flows visible on the image. The implications of the volcano's morphology for the eruption style and magma composition are being considered.

The hypothesis suggested by Scott and Chapman (10) that a lake in the Elysium basin was fed in part by water from Ma'adim Vallis will be examined in the light of the topographic information, in particular the relationship between the flows of Apollinaris and channel routes to the proposed lake.

4. Conclusions

The results from the automated stereo matching of these two image pairs has demonstrated the practicability of the method for Viking photographs. The additional topographic infomation will prove invaluable for geologic interpretation of Mars.

References.

(1) Muller, J-P., (1989), Surveying and Mapping 89, Univ. of Warwick, 17th - 21st April, 1989. (2) Otto, G. P., Chau, T. K. W., (1989), Image and Vision Comput. 7 no. 2 p. 83-94. (3) Day, T., Muller, J-P., (1989), Image and Vision Comput. 7 no. 2 p. 95-101. (4) Wu, S. C., Schafer, F. J., (1984), Proc. ASP-ACSM 50th Annual Meeting, Washington DC, 11th-16th March, p. 456-463. (5) Agterberg, F. B., 'Geomathematics' chap. 10 Elsevier, (1974). (6) USGS Topographic Map of Aeolis SE Quadrangle of Mars, M-22/191 T (1988). (7) Roth, L. E., Saunders, R. S., Downs G. S., Schubert G., (1989), Icarus 79 p. 289-310. (8) USGS Topographic Map of Aeolis NE Quadrangle of Mars, M 2M-7/191 T (1988). (9) Robinson, M. S., (1990), LPSC Abstracts XXI p. 1027. (10) Scott, D. H., Chapman, M. G., (1991) Proceed. LPSC Vol. 21 p. 669-677.

Acknowledgment. We would like to thank Mark Robinson for providing the images of Apollinaris Patera and Ma'adim Vallis used in this work.

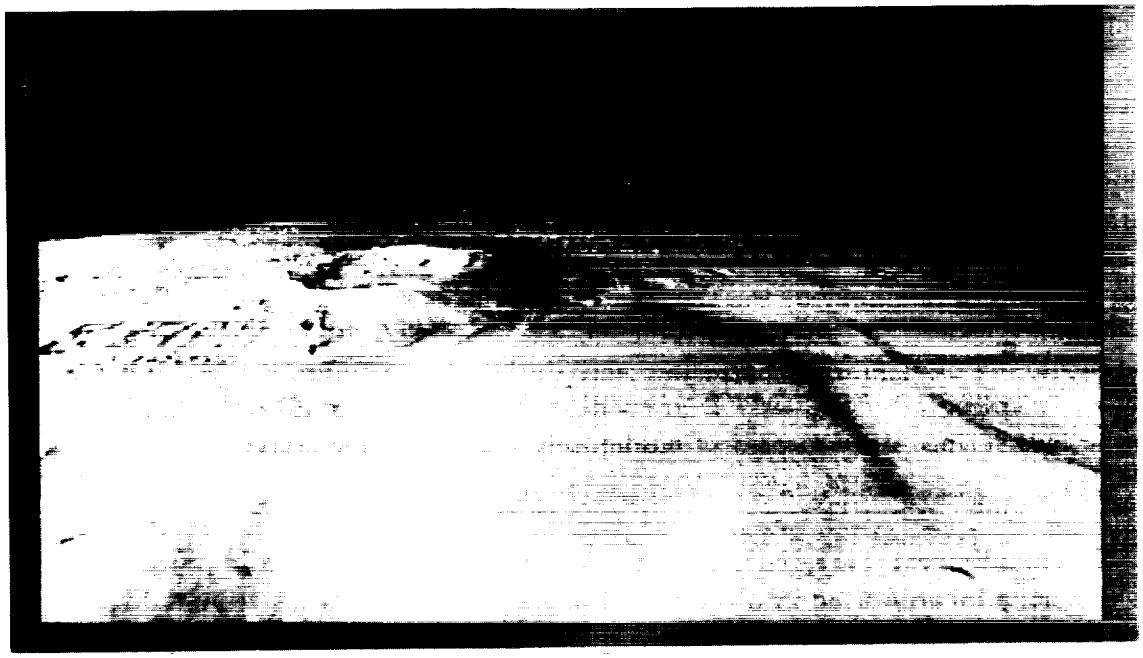

Fig. 1. Perspective view of Apollinaris Patera, looking to the south-east, from a height of approximately 50km. The caldera is 70km across.

TURBULENT SPECTRA, FLUXES, STABILITY AND GROWTH OF THE MIXED LAYER IN THE BOUNDARY LAYER OF MARS; James E. Tillman, Department of Atmospheric Sciences, University of Washington, Seattle, Wa., 98195, Lars Landberg, and Soren E. Larsen, Meteorology Department, Risøe, Danish National Laboratory, Roskilde, DK 4000, Denmark

Spectra of wind and temperature from high frequency measurements in the atmospheric surface layer of Mars are presented for the first time. Heat and momentum fluxes, and stability, are calculated for early spring from estimates of the surface temperature and mean Viking Lander 2 temperatures and winds at 44° N, using similarity theory. The surface temperature estimates are obtained from software developed to improve the temperature measurements and flow distortion by the lander is also taken into account. The spectra are compared with model spectra which have been adjusted to simulate aliasing, and high frequency rolloff, the latter by sensor response, or viscous dissipation. The surface layer parameters are used in the calculation of the model spectra. The model spectra, for three surface roughnesses and two measuring heights, are compared with the calculated spectra producing estimates of z_0. The spectral models depend on the surface parameters and the estimated surface temperature and their agreement with the calculated spectra indicates that the surface layer estimation techniques produce self consistent estimates, both for day and night conditions. The diurnal variation of the mechanically and convectively mixed planetary boundary layer is estimated and the lowest and highest values are presented for the sols analyzed. The results show that similarity theory developed for Earth applies to Mars, the spectral models are universal and that it is possible to estimate the effects of severe aliasing of wind and temperature measurements, and filtering by sensor and atmospheric processes, to produce good parameter dependent model–measured spectra and then in turn estimate the values of parameters.

Lander 2 data were selected for analysis for which 1) the direction of the wind is outside the range of lander interference, 2) the sampling interval is constant during the entire duration of the sample 3) the time series contains no spikes, 4) the sol has a sampling interval of less than 16 seconds and preferably 1.2 seconds with a duration of at least 30 minutes to one hour 5) the selected time series is linearly detrended and 6) the end points are chosen to end with a value close to zero. Sol, 30, is in late summer, before the beginning of significant baroclinic activity later in autumn, sol 447 and 448 are during early spring after the 1977 B great dust storm, Tillman 1988 (1), while sol 554 is during late spring, still a period of moderately low baroclinic activity.

Aliasing and filtering

Since the sampling rates are generally very slow, the effect of aliasing is quite severe and must either be incorporated into the model or corrected for in the estimated spectrum. The spectrum is also distorted by the response time of the wind and temperature sensors and the scale at which molecular dissipation begins, which is approximately 100 times larger than on Earth. The effects of aliasing, sensor response and dissipation are incorporated by correcting the model spectra and comparing them with the calculated spectra. Flow distortion by the lander is also taken into account.

Derivation of stability, z/L, u_* and H

The spectra are scaled to determine if they obey similarity theory which requires calculation of the Monin-Obukhov length, L, the friction velocity, u_*, and the convective heat flux, H. Following Sutton, Leovy and Tillman, 1978 (2) these parameters are estimated from the values of: the mean velocity, U, at height z, the atmospheric temperature at height z, T_{atm}, and the temperature at the surface, T_{surf}, where z is the effective instrument height ($0.93m \leq z < 1.61m$). Sutton et al. calculated surface temperatures with a model for which they point out "ground temperature falls below that predicted by the homogeneous surface model between 1400 and 1900 LT, with a discrepancy of as much as 10° C."

However, the present values of diurnally varying surface temperature are produced by the Viking software and techniques developed by Keith Ronnholm and Conway B. Leovy, (Leovy, private communication) producing downward and upward solar and infrared fluxes at the surface, along with the surface temperature. Optical depth values are obtained from Colburn, Haberle and Pollack (3) and surface albedo, thermal inertia, air density, asymmetry parameter, single scattering albedo of dust and surface albedo are used. Solar geometry and fluxes are calculated using a δ-Eddington 1 layer atmosphere, and sky temperatures, (IR fluxes), are calculated as a function of season. Ground temperature calculations use a single layer thermal conductivity model for a periodic (diurnal) heat source with a Fourier solution.

The height of the convective boundary layer

The correct spectral model for the unstable spectra requires the height of the lowest inversion and two simple models are used. Applying this to the selected sols, mid afternoon convective layer depths range from 3.5 to 9.1 km, using all combinations of 3 values of z_0; 0.3, 1.0, and $3.0cm$ and the two effective instrument heights 0.93 and $1.61m$. (Radiative heating and cooling estimates are not incorporated.) The Martian boundary layer is deeper than Earth's, excluding latent heat dominated convection. An unusual feature of Mars is that since the surface temperatures are mainly determined by radiative balance, the heat fluxes, and ultimately the depth of the convective boundary layer, is determined by the mixing in the lowest layer and therefore by **wind speed**, for the same radiative, mechanical, and topographic conditions.

Terrestrial models of wind and temperature spectra are used, enhanced and adapted for Martian conditions. The model for stable horizontal velocity spectra used in this section was developed by Olesen et al. (4), and further substantiated in Larsen et al.(5). for measurements at 10 m and above; for lower levels a "squeezing" of the length scale has been modelled by a simple exponential form (tested on Earth down to 3m) but extended for Mars down to 0.93 m.

The model developed by Højstrup, Højstrup, et al. (6,7) for unstable horizontal velocity spectra, consists of buoyancy-produced and and shear-produced components, assumed not to interact. The buoyancy-produced component scales with the height of the lowest inversion, z_i, and the shear-produced part with the instrument height.

Comparison between spectra and models

1) **stable velocities.** There is generally good agreement between the measured and the modelled spectra and when the measured spectra diverge from the simple model, then they have the expected n^{-3} behavior. 2) **stable temperatures.** The agreement is fairly good in the low frequency portion of the spectrum while the spectral density is low for the highest measured decade, probably due to the low level of variability during stable conditions coupled with the poor, $\approx 0.8\ K$, resolution of the temperature measuring system. 3) **unstable velocities.** The largest value of the height of the boundary layer gives good agreement between the model and calculated spectrum even though the moderately long sample interval produces large aliasing corrections and confines the measured spectral density to the low-frequency portion of the spectrum. With a scan interval of 1.2 seconds for the v component the high-frequency spectral density agreement between the model and the data is quite good. 4) **unstable temperatures.** The comparison of model with measured spectra again are fairly poor, probably due to excessive noise due to recently identified quantization and sample interval effects compounded by operation of an instrument heater circuit. This effect is sometimes far less important, has been modelled and removed in test cases, and do not affect any other conclusions.

This study provides the first estimates of: 1) the height of the mixed layer, 2) spectra of wind and temperature, 3) the validity of similarity theory on Mars, 4) and bounds of effective measuring height and surface roughness. It confirms and extends the universiality of model wind spectra. Finally and more important, we provide the ability to estimate and determine the self consistiency of Martian atmospheric mixed layer fluxes, stability and heights on a diurnal and annual basis. This can be used to initialize and validate the various models, which previously could only be compared with each other or the efforts of Sutton, Leovy and Tillman (2): these were restricted in season and limited by the results from the surface temperature model available at that time. Analysis of additional data can better estimate z_0 values directly from the measurements and provide the parameters necessary to calculate the vertical profiles of wind and temperature on a daily, seasonal and annual basis.

1. Tillman, James E., (1988) J. Geophys. Res. **93**, D8, pp 9433-9451.
2. Sutton, J. L., C. B. Leovy and J. E. Tillman, (1978) J. Atmos. Sci., **35**, pp P2346-2355.
3. Colburn, D. S., J. B. Pollack, and R. M. Haberle (1989), Icarus **79**, pp 159-189. 4. Olesen, H. R., S. E. Larsen and J. Højstrup, (1984) Boundary-Layer Meteorology. **29**, pp 285-312.
5. Larsen, S. E., H. R. Olesen, and J. Højstrup, (1985) Turbulence and diffusion in stable environments. Edited by J. C. R. Hunt. Oxford University Press. 181-204.
6. Højstrup, J., (1982) J. Atmos. Sci. **39**. pp 2239-2248.
7. Højstrup, J, S. E. Larsen and P. H. Madsen, (1990) Ninth Symposium on turbulence and diffusion (AMS), pp 305-308.
8. Tillman, James E., Lars Landberg, and Søren E. Larsen, Turbulence Spectra from the Boundary Layer of Mars, Manuscript in progress to be published 1991.

AQUEOUS-ALTERATION PRODUCTS IN S-N-C METEORITES AND IMPLICATIONS FOR VOLATILE/REGOLITH INTERACTIONS ON MARS. A. H. Treiman and J. L. Gooding, SN2/Solar System Exploration Division, NASA/Johnson Space Center, Houston, TX 77058.

Introduction. The shergottite, nakhlite, and Chassigny (SNC) meteorites are inferred to be samples from the Martian surface [1,2], and so provide a wealth of information on Martian petrology and geochemistry [3]. Because the SNCs are igneous rocks, it has not been obvious that they could reveal much about low-temperature geochemical processes and atmosphere-surface interactions on Mars. However, five of the eight SNCs are known to contain low-temperature hydrous minerals and related phases of likely Martian origin. Here, we review these Martian weathering and alteration products in SNCs (Table) and outline possible implications for volatile/regolith interactions and regolith sinks for volatiles on Mars.

"Weathering" vs. "Alteration" and Interference of Origin. *Secondary minerals* are those that form by processes other than igneous crystallization, including late-stage cooling, post-emplacement alteration, deuteric alteration, diagenesis, and weathering. Sensu stricto, *weathering* refers only to interactions between rocks and planetary atmospheres, including meteoric water [4]. Secondary minerals of unknown origin should be called *alteration products* until their environments of formation can be specified.

Distinguishing terrestrial from extraterrestrial alteration products in SNCs is a significant task. Proofs that an alteration product is extraterrestrial include: that the product is older than a major shock event [5,6]; that the product is older than the fusion crust (passage through the atmosphere) [6]; and that the product could not form in the terrestrial weathering environment [5,7,8]. The last type of proof can be gained from parallel studies of exterior and interior samples from the same meteorite, and from parallel studies of SNC and other meteorites.

Amphiboles and Biotite. The SNCs are the only achondrites known to contain high-temperature hydrous phases: amphibole in all SNC varieties [9,10,11], and biotite in Chassigny [12]. These minerals occur as inclusions in other igneous phases, implying an extraterrestrial origin. Clearly, hydrous magmas were present on the SNC parent body, and it should not be surprising to find evidence of deuteric and aqueous alteration in the SNCs.

Secondary Minerals. Observed phases fall into two categories: (a) discrete mineral grains, and (b) veinlets and patches of minerals or mineral(oid) mixtures. Most occurrences are in the former category. Ca-carbonate and Ca-sulfate are the most abundant discrete grains in the SNCs, occurring as relict crystals in glassy inclusions in the Elephant Moraine shergottite [5], and isolated grains along fractures in Nakhla and Chassigny [6,13,14]. Other pre-terrestrial salts in the SNCs are listed in the Table.

Veinlets and patches of alteration products are prominent in the nakhlites. They contain rusty iddingsite veinlets [15,16] which are preterrestrial [6,new data]. The veinlets contain smectite clays (mostly Fe-saponite), hematite, and ferrihydrite [17], consistent with earlier work [18]. The bulk compositions of iddingsite veinlets in Nakhla (and Lafayette) are consistent with mixtures of smectite (or chlorite) and iron oxides [6]; these iron oxides may contribute to the ferric iron content of bulk Nakhla [19]. Associated with the iddingsite veinlets are chloride and sulfate salts (Table).

Implications of SNCs for Martian Regolith Volatiles. Given that the SNC meteorites are from Mars, then carbonates, sulfates and hydrous phyllosilicates may be inferred to exist in the Martian regolith. The conditions of their formation are not fully constrained.

Formation of iddingsite from olivine in the nakhlites implies alteration at low T, but not necessarily that of weathering. Hydrous iron oxides and clays do form readily from shergottites under Antarctic conditions [20,21], showing that iddingsite could form under conditions like those of the current Martian surface. Association of sulfates, chlorides, and

carbonates with iddingsite [8] suggests that the altering waters were also saline and oxidizing.

Deposition of salts in other SNCs (Table) is poorly understood. Chassigny contains salts in cracks in olivine and chromite [13,14], no iddingsite is present. EETA79001 contains salts in veins of shock glass, so original textures (and perhaps some minerals) have been lost. The prevalence of carbonate and sulfate phases in these meteorites suggests altering fluids similar to those that acted on the nakhlites. But the absence of iddingsite in Chassigny and the presence of Mg phosphate and other phases in EETA79001 [5] suggest that altering fluids vary.

Altered igneous rocks like the SNCs may constitute a significant reservoir of volatiles on Mars. Abundances of H_2O in the SNC meteorites range up to 0.39% wt, mostly of non-terrestrial origin [22]. Abundances of CO_2 (from carbonate) range up to 0.3%, abundances of SO_2 (from sulfate) range up to 0.27% (although sulfate is more abundant than carbonate in most samples), and abundances of Cl (as Cl+HCl) range up to 0.34% [8]. Most of these SNC volatile inventories are is likely to be of extraterrestrial origin [8]. Accordingly, both the known relict alteration products and the observed terrestrial weathering behavior of SNCs supports the concept that products of rock weathering on Mars should be important sinks for Martian volatiles.

References: [1] Wood C.A. and Ashwal L.D. (1981) Proc. Lunar Planet. Sci., 12B, 1359-1375. [2] Bogard D.D. et al. (1984) Geochim. Cosmochim. Acta, 48, 1723-1739. [3] McSween H.Y. Jr. (1985) Rev. Geophys., 23, 391-416. [4] Gooding J.L. (1986) In M.G. Kivelson (ed.), The Solar System: Observations and Interpretations, Prentice-Hall, 208-229. [5] Gooding J.L. et al. (1988) Geochim. Cosmochim. Acta, 52, 909-915. [6] Gooding J.L. et al. (1991) Meteoritics, 26, 135-143. [7] Gooding J.L. and Muenow D.W. (1986) Geochim. Cosmochim. Acta, 50, 1049-1059. [8] Gooding J.L. et al. (1990) Meteoritics, 25, 281-289. [9] Floran R.J. et al. (1978) Geochim. Cosmochim. Acta, 42, 1213-1229. [10] Treiman A.H. (1985) Meteoritics, 20, 229-243. [11] Johnson M.C. et al. (1991) Geochim. Cosmochim. Acta, 55, 349-366. [12] Harvey R. and McSween H.Y. Jr. (1991) Meteoritics, in press. [13] Wentworth S.J. and Gooding J.L. (1991) Lunar Planet. Sci. XXII, 1489-1490. [14] Wentworth S.J. and Gooding J.L. (1991) Meteoritics, 26, in press. [15] Bunch T.E. and Reid A.M. (1975) Meteoritics, 10, 303-315. [16] Berkley J. et al. (1980) Proc. 11th L.P.S.C., 1089-1102. [17] Treiman A.H. and Gooding J.L. (1991) Meteoritics, 26, in press. [18] Ashworth J.R. and Hutchison R. (1975) Nature, 256, 714-715. [19] Viera V.W.A. et al. (1986) Physica Scripta, 33, 180-186. [20] Gooding J.L. (1986) Geochim. Cosmochim. Acta, 50, 2215-2223. [21] Smith J.V. and Steele I.M. (1984) Meteoritics, 19, 121-133. [22] Karlsson H. et al. (1991) Meteoritics 26, in press. [23] Chatzitheodoridis E. and Turner G. (1990) Meteoritics 25, 354.

TABLE: WELL-CHARACTERIZED ALTERATION PHASES IN SNC METEORITES*#

	EETA79001	Nakhla	Chassigny
$CaCO_3$	(5)	(6,23)	(13,14)
$MgCO_3$			(14)
$(Fe,Mn)CO_3$		(23)	
$CaSO_4 \cdot nH_2O$	(5)	(6,17)	(13,14)
$(Mg)_x(PO_4)_y \cdot nH_2O$	(5)		
$(Mg)_x(SO_4)_y \cdot nH_2O$		(6)	
$(Na,K)Cl$		(6,17)	
S,Cl-Al-silicate	(7)		
Smectites		(6,17)	
$Fe_2O_3 \cdot nH_2O$		(17)	

* number entries refer to literature citations
\# poorly characterized preterrestrial "iddingsite" is present in Lafayette and Governador Valadares (16). Alterations in ALHA77005 are probably terrestrial (21).

PLANET-B : A JAPANESE MARS AERONOMY OBSERVER

K.Tsuruda
Institute of Space and Astronautical Science, Yoshinodai, Sagamihara, Kanagawa 229, JAPAN

This paper introduces a Japanese Mars mission (Planet - B) which is being planned at ISAS (the Institute of Space and Aeronautical Science, Japan). Planet - B aims to study the upper atmosphere of Mars and its interaction with the solar wind. The launch of Planet - B is planned in 1996 by a new launcher M - V which is being developed at ISAS.

The ionosphere of Mars is characterized by its lower pressure compared with the solar wind dynamic pressure. By this reason, penetration of the solar wind deep into the Martian ionosphere is expected as is the case taking place at Venus ionosphere during the period of quiet sun. This may cause erosion of the Martian upper atmosphere and excitation of global motion in the upper atmosphere. As was found by the Soviet Phobos mission, ionized oxygen seems to be accelerated to kev energy in the Martian tail and escape from Mars. In addition to the interaction with the solar wind, the structure of the Martian upper atmosphere is thought to be controlled strongly by the meteorological condition in the lower atmosphere.

The orbit of Planet - B is chosen so that it passes two important regions, the region where the solar wind interact with the Martian upper atmosphere and the tail region where ion acceleration is taking place. Considering the drag due to the Martian atmosphere, the periapsis altitude of 150 km and apoapsis of 10 Martian radii are planned. The orbit plane is nearly parallel to the ecliptic plane. The atitude of the spacecraft is spin stabilized and its spin axis is controlled to point the earth.

The dry weight of the spacecraft is about 250 kg including scientific payload which consists of magnetometer, plasma instruments, HF sounder, UV imaging spectrometer, and monitor of lower atmosphere.

MICROCRATERS ON MARS: EVIDENCE OF PAST CLIMATIC VARIATIONS, A. R. Vasavada, T. J. Milavec and D. A. Paige, Dept. of Earth and Space Sciences, UCLA, Los Angeles, CA 90024.

INTRODUCTION: On Mars, we do not expect to see a full spectrum of impact crater sizes as we do on the Moon because the Martian atmosphere decelerates smaller incoming meteorites. Mars climate models predict thirty-fold variations in Mars' atmospheric pressure due to large amplitude quasi-periodic variations in Mars' obliquity (1,2). More recent studies have shown that uncertainties in Mars' moment of inertia may have resulted in an underestimation of this range (3). In this study, we find that potential variations in the mass of the Martian atmosphere should have dramatic effects on the production rates of centimeter-sized craters on the surface of Mars, and suggest that observations of the densities of Martian microcraters could provide an important validation of the astronomical theory for Martian climate change.

MODEL ATMOSPHERES: The effects of five model atmospheres on a range of micrometeoroid masses were considered. Case one assumes no atmosphere. Case two assumes a 0.14 mb nitrogen-argon atmosphere, which is predicted at high altitude during periods of low obliquity. Case three assumes a 0.3 mb nitrogen-argon atmosphere, which is predicted during periods of low obliquity. Case four assumes a 6.0 mb atmosphere of present composition. Case five assumes a 30 mb CO_2 atmosphere, which is predicted during periods of high obliquity.

PROJECTILE DYNAMICS: All particles were assumed to be normally incident on the Martian atmosphere at an altitude of 200 km. The velocity was assumed to be 8 km/sec, which is an average value for asteroidal and cometary debris at 1.52 AU. We performed trajectory and ablation calculations using models based on data from the Earth and Venus (4,5).

RESULTS: Figure 1 shows calculated surface impact velocities as a function of mass for the five atmospheric cases. The shaded area indicates non hyper-velocity impacts which do not generate sufficient dynamic pressures to fracture or deform the target rock (5,6). Figure 2 shows the dependence of crater diameter on initial projectile mass and impact velocity for the five model atmospheres. We employed Hartung's (7) scaling equation for iron micrometeoroids impacting basaltic rock: $D = 0.00125(\frac{1}{2}mv^2)^{0.37}$ (all in cgs). The darkly shaded area indicates the non hyper-velocity region, while the lightly shaded area indicates the range of crater sizes expected to form only during periods of atmospheric pressures from 0.3 to 6.0 mb. Figure 3 shows differential crater production rates as a function of crater diameter for the five model atmospheres. The rates for the zero atmosphere case are from Grün's estimated flux of interplanetary particles (8). The shaded area again marks crater diameters that are only formed between 0.3 mb and 6.0 mb atmospheric pressure.

DISCUSSION: Microcrater densities can give important clues to Martian climatic history. Figure 3 shows that if Mars has gone through extended periods of low obliquity, then the densities of 1 cm craters on the Martian surface should be significant. Over the course of two major obliquity cycles (2×10^6 years), Ward's polar cap model predicts periods of atmospheric pressures lower than 0.3 mb totalling 100,000 years (2). Figure 3 shows that if this were the case, then approximately five 1 cm craters would be expected to accumulate over every square meter of the Martian surface. It is important to point out that, regardless of uncertainties in the absolute fluxes of interplanetary particles, the production rates of the smallest craters on the surface of Mars should be greatly enhanced during periods of low obliquity.
The return of lunar rock samples during the Apollo era allowed a comprehensive laboratory study of the densities of lunar microcraters. Absolute ages and production rates were able to be determined by radioactive dating methods (6). Studies of microcraters on the Martian surface could be accomplished by returning promising samples, or by *in situ* analysis by mobile robotic devices, which could locate exposed rocks and examine their surfaces in microscopic detail. There is also a distinct possibility that there are sedimentary deposits on Mars that contain "fossil" microcraters, that could extend our record of Mars' atmospheric history far into the past.

(1) Ward, W. R. (1974) J. Geophys. Res. 79, 3375-3386. (2) Ward, W. R. (1974) J. Geophys. Res. 79, 3387-3395. (3) Bills, B.G. (1990) J. Geophys. Res. 95, 14137-14153. (4) Baldwin, B. and Y. Sheaffer (1971) J. Geophys. Res. 76, 4653-4666. (5) Tauber, M.E. and D.B. Kirk (1976) Icarus 28, 351-357. (6) Heiken, G., D. Vaniman and B.M. French (1991) Lunar Sourcebook Cambridge Press, Cambridge, 73-85. (7) Hartung, J.B., F. Horz, F.K. Aitken, D.E. Gault and D.E. Brownlee (1973) Proc. Fourth Lunar Sci. Conf., Geochim. Cosmochim. Acta, Suppl 4, Vol. 3, 3213-3232. MIT Press. (8) Grün, E., H.A. Zook, H. Fechtig and R.H. Giese (1985) Icarus 62, 244-272.

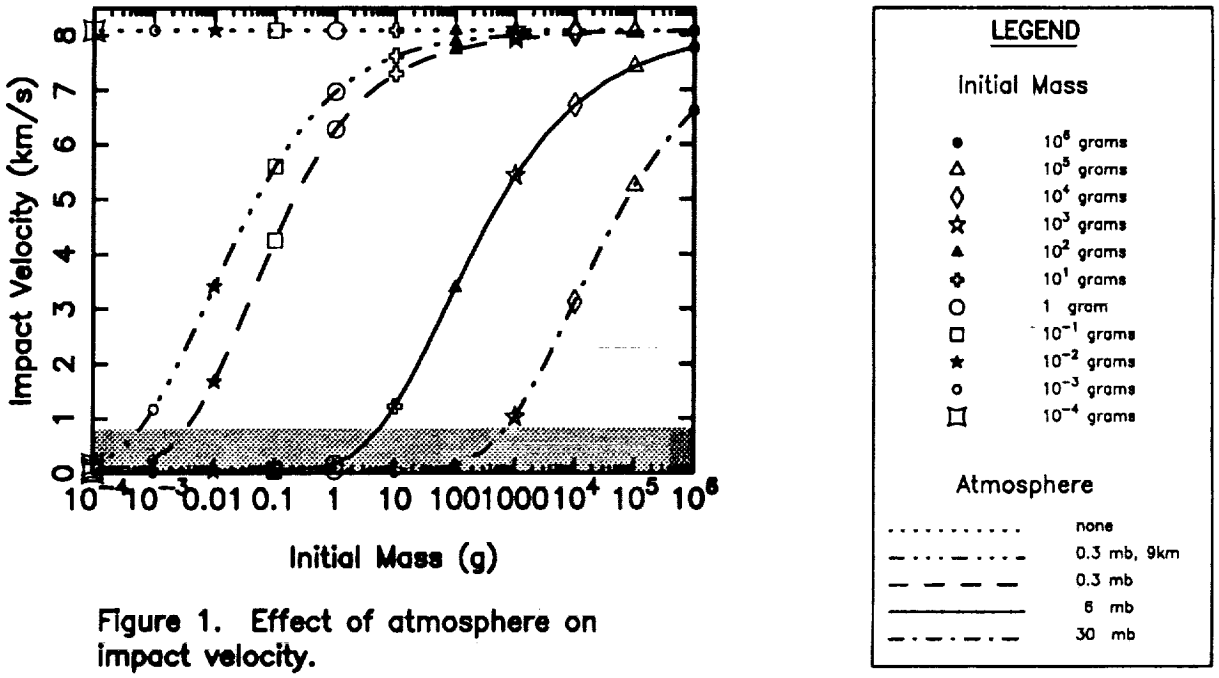

Figure 1. Effect of atmosphere on impact velocity.

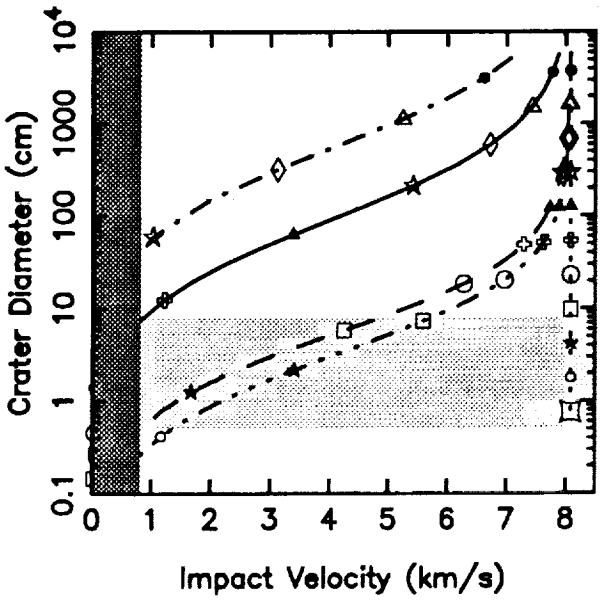

Figure 2. Effect of atmosphere on crater diameter.

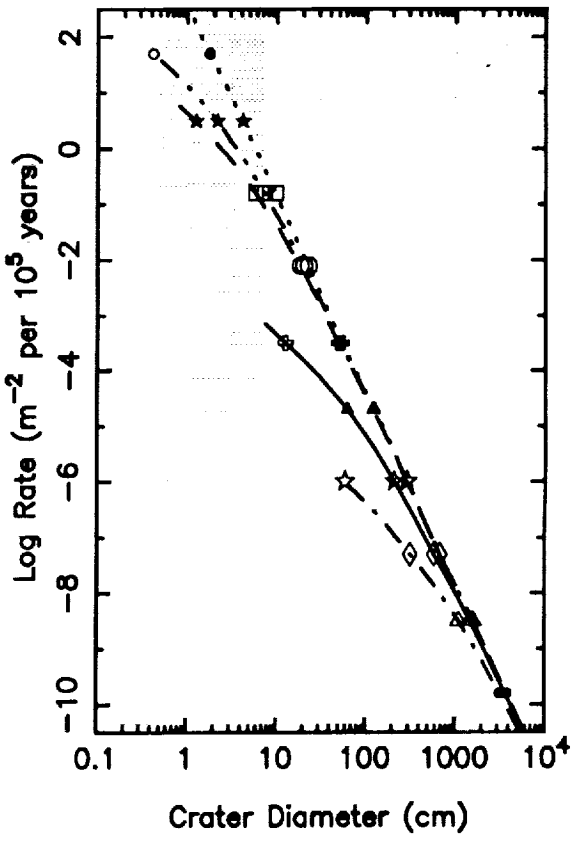

Figure 3. Effect of atmosphere on crater production rate.

THE ULTRAVIOLET ALBEDO OF MARS; R. Wagener, Brookhaven National Laboratory

Ultraviolet observations have been proven successful at studying the composition and structure of the upper atmospheres of the giant planets and Venus. In the case of Mars the analysis of UV data has concentrated on the spatial distribution and temporal behavior of ozone. This paper demonstrates the potential of FUV data (shortward of 200 nm) for measuring the atmospheric structure, in particular the vertical distribution of aerosols.

Between 200 nm and 300 nm the albedo of Mars is dominated by the surface albedo, Rayleigh scattering on CO_2, aerosol scattering and absorption, and some O_3 absorption. Shortward of 200 nm, the main contributions to the albedo come from Rayleigh scattering and absorption by CO_2, and scattering and absorption by aerosol particles, with only minor contributions from other gaseous species like N_2, O_2, H_2O, and CO.

For illustrative purposes, a simple two layer model (atmosphere and surface) is computed using the atmospheric composition measured at the Viking lander sites [1]. This model is then compared to the albedo observed with the International Ultraviolet Explorer (IUE) [2].

This comparison clearly shows that a clear atmosphere with the nominal Viking mixing ratios of CO_2, O_2, and H_2O is incompatible with the IUE data shortward of 200 nm. To obtain a better match between data and model, an aerosol has to be introduced that effectively scatters at these wavelengths. The required reduction in effective CO_2 pathlength is a factor of 5.

The comparison also points out the inadequacy of the IUE data to provide data in the critical wavelength region between 195 nm and 210 nm. Such data will be forthcoming from the Hubble Space Telescope and will provide the opportunity to infer the vertical distribution of aerosols on Mars on a global scale.

The strong sensitivity of the FUV spectrum of Mars to bright aerosols in the upper atmosphere suggests that in conjunction with visible and IR observations it should be possible to segregate dark dust from bright ice particles effectively. Therefore, UV spectroscopic capability should be considered a vital part of any future missions to Mars.

HYDROGEN AND CARBON ISOTOPIC COMPOSITION OF VOLATILES IN NAKHLA: IMPLICATIONS FOR WEATHERING ON MARS; L.L. Watson, S. Epstein and E.M. Stolper, Division of Geological and Planetary Sciences, California Institute of Technology, Pasadena, CA 91125.

Introduction. The nakhlites contain a hydrous alteration product that was originally characterized as "iddingsite" [1] due to its bulk chemical similarities to the terrestrial alteration product of olivine [2]. More recently, this brownish material has been called "rust" since little is known of its mineralogy, although smectite is considered a likely component [3]. The alteration has been speculated to be preterrestrial in origin and recently several pieces of evidence have been reported to support this hypothesis [3,4]. In this abstract, we report results of continuing work utilizing the hydrogen isotopic composition of Nakhla to understand better the alteration event and the fluids that caused it. Since the present martian atmosphere has a D/H ratio 5.15 times SMOW [5] (corresponding to a δD of +4150 ‰; all δD values reported herein are relative to SMOW), measurement of the D/H ratios of the nakhlites could help to determine if the alteration processes that affected these meteorites indeed occurred on their parent planet, presumably Mars [6]. Moreover, if we accept a martian origin for these meteorites and their alteration, measurement of the stable isotope ratios of their alteration phases and comparison to the corresponding atmospheric ratios could provide insights into the nature and origin of fluids interacting with martian igneous rocks. Distinct occurrences of carbonate have also been reported for Nakhla [3]. Although the hydrogen isotopes are the main focus of this work, the results of carbon isotopic measurements are also reported.

Previously reported hydrogen isotope measurements on nakhlites and shergottites have yielded highly variable results. A published δD value for Nakhla is -37‰ with a yield of 2.2 μmoles of H_2 per gram of sample [7], which differs significantly from the reported value of +456‰ measured on 81.6 μmoles of H_2 extracted from 2.8 g of the Lafayette nakhlite [8] . Published values for Shergotty range from -47 [7] to +878‰ [8] with yields of 1-7 μmoles of H_2 per gram of sample [7,8,9]. In all these previous reports, data were obtained after "precombustion" of the sample at temperatures of 350-450°C [7,8,9], which was intended to eliminate terrestrial contamination by organic matter and/or adsorbed water. However, terrestrial iddingsite is typically comprised of a mixture of phases including goethite, smectites, and sometimes carbonates, and it begins to break down at temperatures as low as ~250°C [2]. Thus valuable information on the alteration phases may be lost in the precombustion step employed by previous workers. Our work therefore focuses on isotopic data for gases extracted from Nakhla by stepwise heating at the low temperatures at which iddingsite is expected to break down. By utilizing stepwise heating, it is also possible to more closely monitor the release of volatiles. We have previously measured δD values up to +173‰ in the temperature range where an alteration product of this type should break down [4].

Experimental procedure. For our previous work [4], gases were collected using a vacuum extraction line which was better suited for gas samples larger than the 5-20 μmole aliquots obtained in our procedure. We have spent most of the last six months designing, constructing and testing a new extraction line specifically targeted for our precious, smaller samples. The design has succeeded in reducing blank and memory effects, thus giving more reliable data. Thus far only one ~0.8 gram aliquot of Nakhla specimen USNM-5891 has been run. The sample was coarsely crushed in air and loaded onto the vacuum extraction line in a quartz boat. Stepwise heating was performed with a resistance furnace up to 950°C. The average heating time for each step was 2.5 hours. Condensible gases released from the sample were frozen into a liquid nitrogen trap. Gas that did not freeze was then exposed to hot copper oxide at 675°C to oxidize it to condensible components. The CO_2 and H_2O released by heating were then cryogenically separated. H_2O was reduced to H_2 by passing over hot uranium at 675°C. Yields were measured manometrically. Data are reported without corrections for blanks or memory effects, but based on testing of the new extraction line, we are confident that the effect of these factors is small (the integrated blank over the entire heating range has been measured at ~0.4 μmoles). Isotope ratios were measured mass spectrometrically.

Results and Discussion. Gases were collected at 120, 200, 300, 415 and 600 and 850°C. Hydrogen yields for the 600 and 850°C aliquots were measured separately and then the gases were combined for isotopic analysis. CO_2 samples collected at the two lowest temperature steps amounted to less than 0.5 μmole and were not analyzed isotopically. Excluding the 120°C temperature step,the bulk δD of the sample was +187‰. δD values increase from -91‰ in the 120°C step to +518‰ in the 415-850°C step. The hydrogen content is greatest in the 120°C step and is roughly constant in the 200, 300, and 415°C aliquots. Between 415°C and 850°C the yield drops off considerably. From 850°C to 950°C virtually no H_2 and only minor CO_2 (<1 μmole) were extracted.

Using the isotopic analyses from the 300, 415, 600 and 850°C temperature collections, the bulk $\delta^{13}C_{PDB}$ is 0.0‰. The heaviest component ($\delta^{13}C_{PDB}$ of +29‰) was collected between 300 and 415°C.

The 300-415 and 415-850°C steps in the heating procedure yielded hydrogen with δD values of +296 and +518‰, both of which are heavier than any known terrestrial samples. In general, yields are lower and δD values higher than our previously reported results using the older extraction line set-up [4]. This can be partially explained by reduction of the blank effects with our new apparatus. For hydrogen, the blank contributes gas (thus increasing the yield) with an isotopic composition of ~-140 [10] (thus decreasing the total δD for any temperature step) in the old procedure. However, the blank effects are not thought to be large enough to account for the entire difference. This would be consistent with the heterogeneous distribution of the alteration product in Nakhla [3,4,11] (e.g., samples closer to the fusion crust tend to be more contaminated by terrestrial weathering than those towards the center of a specimen [11]). We thus cannot rule out the possibility that differing degrees of exchange of the alteration product with terrestrial atmospheric water after the meteorite fell are causing the differences between samples. Our latest high temperature results agree well with the +456‰ value reported by Kerridge [5] for Lafayette, but the Lafayette study involved a preheating step to 450°C and thus our bulk δD value is somewhat lower and our yield somewhat higher.

Gooding *et al.* [11] reported that virtually no H_2O was released upon heating of Nakhla, but suggested that hydrogen release was primarily as HCl. We have not reported yields in detail because we are concerned about the possibility of an as yet unidentified gaseous species accompanying hydrogen in our extractions. Thus, hydrogen yields may, in fact, be even lower than we measure. The mass spectrometer allows a crude measurement of the purity of the sample, which leads us to suspect that this is the case. However, the isotopic composition of our samples appears unaffected. We are continuing to consider the question of the hydrogen-carrying species, as well as the possibility of significant release of Cl from our samples.

The release of hydrogen at the low temperatures reported here is consistent with the breakdown of the phases that constitute the alteration product between ~250 and 650°C. Although we must directly confirm that the gases collected in this temperature range are indeed released on breakdown of alteration products in the meteorite and not from some other source within the sample, our tentative identification of these anomalously heavy, low-temperature components with the alteration product supports the hypothesis that the alteration of this meteorite was preterrestrial. The higher yield and lower δD in the lowest temperature fractions are suggestive of a component of terrestrial contamination in the low temperature steps of the extractions. Although there is likely some terrestrial contamination in the fraction extracted at low temperatures, the fact that such high δD values are observed indicates that the low temperature gas should not be discarded in a preheating step as has been done by previous workers. We emphasize, however, that the δD values reported here for the lowest temperature steps, and perhaps for all of the extractions, represent lower limits on the actual values.

Although not as high as the present martian atmosphere, the high δD values are consistent with a martian origin for these meteorites. If, as is often the case for terrestrial occurrences, the "rust" is a product of deuteric alteration, these δD values may reflect the composition of hydrothermal fluids with contributions both from atmospheric (i.e., meteoric) and magmatic sources. If the nakhlites are from Mars, high δD values might be expected due to the known deuterium enrichment in the martian atmosphere. The carbon results are more difficult to assess in these terms. The isotopic composition of carbon (in CO_2) in the martian atmosphere is 0-80‰ enriched relative to the terrestrial mantle [12,13]. Our results are consistent with these data, although this is not significant given the large errors in the measurements of the martian atmosphere. However, the overall $\delta^{13}C$ value we measured for Nakhla is also consistent with terrestrial carbonate formation, which would be expected to produce $\delta^{13}C$ values near 0‰ [14].

REFERENCES: [1] Bunch, T.E. and Reid, A.M. (1975) Meteoritics, *10*, 303-315. [2] Wilshire, H.G. (1958) Am. Min., *43*, 120-147. [3] Gooding, J.C. *et al.* (1991) Meteoritics, *26*, 135-143. [4] Watson, L.L. *et al.* (1991) In *Lunar and Planet. Sci. XXII*, 1473-1474. [5] Bjoraker, G.L. *et al.* (1989) In *Proc. 4th Int. Conf. Mars, Tucson*, 69-70. [6] Bogard, D.D. and Johnson, P. (1983) Science, *221*, 651-654. [7] Fallick, A.E. et al. (1983) In *Lunar and Planet. Sci. XIV*, 183-184. [8] Kerridge, J.F. (1988) In *Lunar and Planet. Sci. XIX*, 599-600. [9] Yang, J. and Epstein, S. (1985) in *Lunar and Planet. Sci. XVI, Suppl. A*, 25-26. [10] Ihinger, P.D. (1991) Ph.D. Thesis, California Institute of Technology, 190pp. [11] Gooding, J.L. *et al.* (1990) Meteoritics, *25*, 281-289. [12] Owen, T. *et al.* (1977) J. Geophys. Res., *82*, 4635-4639. [13] Schrey, U. *et al.* (1986) Astron. Astrophys., *155*, 200-204. [14] Clayton, R.N. and Mayeda, T.K. (1988) Geochim. Cosmochim. Acta, *52*, 925-927.

MODELING THE SEASONAL CYCLE OF CO_2 ON MARS: A FIT TO THE VIKING LANDER PRESSURE CURVES, Wood, S.E. and D.A. Paige, Dept. of Earth and Space Sciences, UCLA, Los Angeles, CA, 90024

Atmospheric surface pressures measured for three years by the Viking landers are extremely valuable for studying Mars' climate. Any realistic model of the Martian seasonal CO_2 cycle should be able to reproduce them. The first serious attempt to match the Viking pressure curves was made by James and North in 1982 (1). Their one-dimensional model of the North-Coakley type solved the heat balance equation at the surface of a one layer planet with flat topography using diurnally and zonally averaged quantities integrated every 1/200 of a Martian year. Their soil layer had a heat capacity of 10^6 J/m^2, but true heat conduction was neglected. Figure 1 shows their best fit to the VL1 pressure curves by varying the seasonal CO_2 frost albedo and emissivity, using the model input parameters shown in Table 1. James and North were unable to match the magnitude of the amplitudes of the Viking curve or the relative depths of the minima using this simple model. They were, however, able to obtain substantially better fits to the Viking data by adding the expected effects of global dust storms and polar hood phenomena in a more complex, two-layer atmospheric model.

We have constructed a more accurate Mars thermal model that is similar to the one used by Leighton and Murray in 1966 (2), which solves radiative, conductive, and latent heat balance at the surface as well as the one-dimensional heat conduction equation for 40 layers to a depth of 15 meters every 1/36 of a Martian day. The planet is divided into 42 latitude bands with a resolution of two degrees near the poles and five degrees at lower latitudes, with elevations relative to the 6.1 mbar reference areoid shown in Fig. 2. This estimate of the Martian zonally averaged topography was derived primarily from radio occultations (3).

To find the best fit to the VL1 pressure data, the thermal inertia of the soil, the frost albedos and emissivities in the northern and southern hemispheres, and the total mass of the cap-atmosphere system were varied over the ranges shown in Table 1. For each simulation, the value of each parameter was kept constant with time. After some initial experimentation, we found very little sensitivity to the albedo and emissivity of the soil, so we fixed at 0.25 and 0.95 respectively. For every combination of parameters, the model was run for 912 sols before results were output. The calculated pressures were scaled to an altitude of -1.5 km, which is the measured altitude of VL1 (4), and compared with the VL1 pressure measurements from July 1976 to July 1978.

Within a reasonable range, the primary effect of changing the total mass of CO_2 was to raise or lower the pressure curve, without much change in shape as long as permanent caps weren't produced. For perfect interannual repeatability, only cases with seasonal caps were considered, despite the fact that there is a residual south polar cap of solid carbon dioxide. Properties of a permanent cap consistent with a convergent model are being investigated. The pressure curve was most sensitive to the combination of frost albedo and emissivity. Although they were each varied independently for the northern and southern caps, their values for the best fits rarely differed by more than 0.02. When one cap had completely sublimated for the summer, the atmospheric pressure was governed chiefly by the frost properties of the other. However, when both caps were nearly the same size, the timing of their exchange of influence was crucial in determining the pressure, and even a slight variation altered the course of the curve for the rest of the year. Our best fit model parameters are shown in Table 1. The best fit pressure curve is shown in Figure 3.

In order to better understand the differences between our results and those of James and North (1), we performed a simulation using their best fit parameters, and included the effects of depth-dependent frost albedo, and flat topography, but neglected the small effects of atmospheric meridional heat flux. Our model produced the dashed curve shown in Fig. 1. It appears that the effect of subsurface heat conduction is to delay and reduce CO_2 condensation during fall and winter. This can be seen in the phase difference between the maxima and minima of the two curves, and as discussed above, this can have effects on pressures for the entire cycle. To compensate for this, James and North had to use an extremely low frost emissivity, whereas we had no problem achieving the observed relative heights of VL1 pressure maxima and minima by taking conduction and topography into account.

We have shown that a realistic one-dimensional thermal model is able to reproduce the VL1 pressure curve reasonably well without having to invoke complicated atmospheric effects such as dust storms and polar hoods. Although these factors may cause our deduced values for each model parameter to differ from its true value, we believe that this simple model can be used as a platform to study many aspects of the Martian CO_2 cycle over seasonal, interannual and long-term climatic timescales.

(1) James, P.B. and G.R. North (1982) JGR 87, 10,271-283. (2) Leighton, R.B. and B.C. Murray (1966) Science 153, 136-153. (3) Kliore, A.J. et al (1973) JGR 78, 4331-4351. (4) Seiff, A. and D.B. Kirk (1977) JGR 82, 4367.

Table 1.

Parameter	Range Investigated	Best Fit Values	James & North Best Fit Values
Soil Thermal Inertia (MKS)	41.86 - 1139.52	83.72	-
Frost Albedo, South	0.50 - 0.85	0.74	0.75
Frost Albedo, North	0.50 - 0.85	0.73	0.75
CO2 Frost Emissivity, South	0.79 - 0.99	0.87	0.57
CO2 frost Emissivity, North	0.79 - 0.99	0.87	0.57
Total mass of CO2 (kg per sq. meter)	130 - 330	230	215

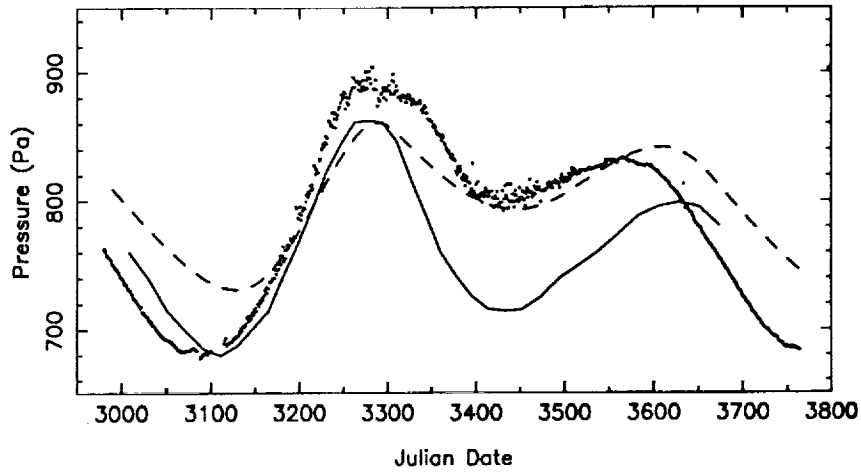

Figure 1. The solid line is James and North's fit to the VL1 daily average surface pressure measurements (dots) using a 1-D model. The dashed line was computed with our more accurate thermal model using James and North's input parameters.

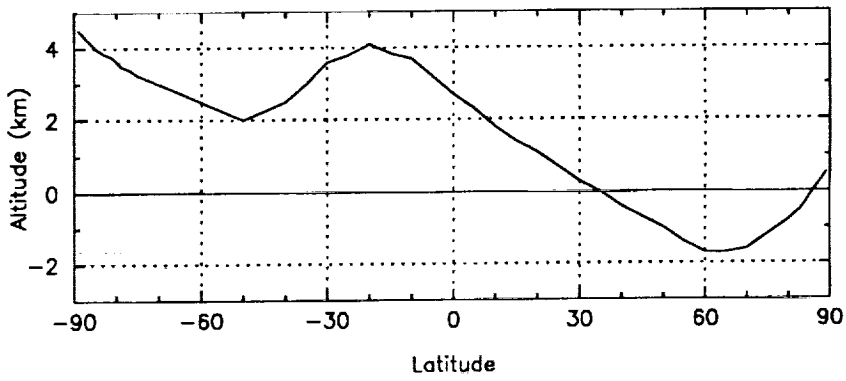

Figure 2. The zonally averaged topography of Mars.

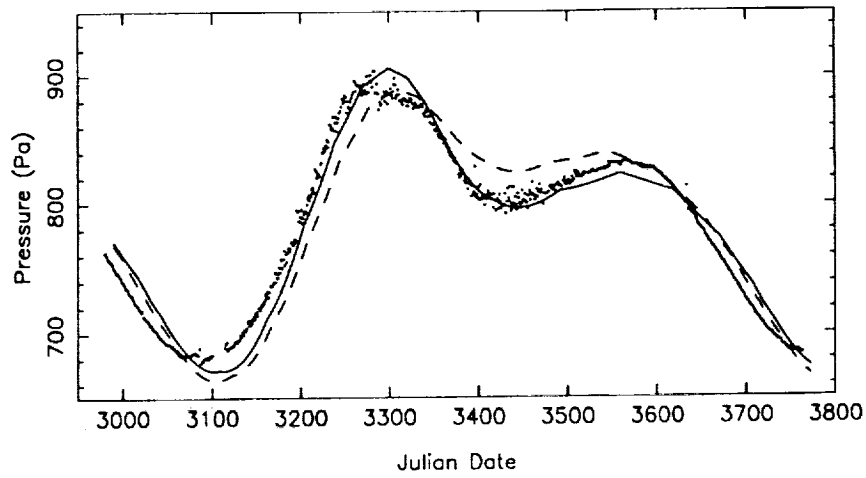

Figure 3. Best fits to the VL1 daily averaged surface pressure measurements (dots) using our thermal model. The solid line assumes the topography in Figure 2. The dashed line uses the same input parameters, but with flat topography.

ON THE ISOTOPIC COMPOSITION OF MAGMATIC CARBON IN SNC METEORITES;

I.P.Wright, M.M.Grady and C.T.Pillinger. Planetary Sciences Unit, Department of Earth Sciences, The Open University, Walton Hall, Milton Keynes, MK7 6AA, England.

SNC Meteorites are thought, from many lines of evidence, to come from Mars (*e.g.* 1,2,3). Thus, samples which during their histories have experienced the martian surface environment in some way, are available for study in the laboratory using the gamut of highly sensitive and precise analytical instrumentation. Although SNC meteorites are relatively fresh igneous rocks of shallow intrusive, or extrusive, origin it transpires that they also contain samples of trapped martian atmospheric gases (*e.g.* 2,4,5), martian weathering products (*e.g.* 5,6,7) and organic materials (8). Since carbon is implicated in some, if not all, of the potential constituents of SNC meteorites, it is clearly an ideal element to study in order to try and constrain the geochemical cycles of volatile elements at the surface of Mars.

A line of investigation which has been pursued in our laboratory over the years involves measurement of the stable isotopic composition of carbon, in its various forms, in SNC meteorites. In order to establish a firm basis for studying the isotopic systematics of carbon in the martian surface environment it is first necessary to try and constrain the $\delta^{13}C$ of bulk Mars. Using SNC meteorites, attempts have been made to assess the $\delta^{13}C$ of the magmatic carbon on Mars; however, since SNC meteorites are somewhat complicated samples, this task is not straightforward. Herein the rather vague qualifier "magmatic" is used to refer to that carbon which was present in the mantle of Mars when the rocks which crystalised to form the SNC meteorites were formed. In this respect the SNC meteorites can be compared with various analogous terrestrial materials which are, by default, better constrained in terms of their formation locale *etc*. Furthermore, on Earth the geodynamic carbon cycle is well understood (*e.g.* 9), although controversy may still surround some of the details! For rocks such as basalts erupted at the Earth's surface, magmatic volatiles are lost to some extent by degassing - it is necessary to resort to experimental studies in order to constrain the solubility of gases under mantle conditions, and thus derive their original concentrations (*e.g.* 10). Degassing results in a small carbon isotopic fractionation between exsolved, and subsequently degassed, CO_2 and carbon dissolved in the magma. Estimates of the magnitude of this isotopic fractionation range from *ca.* 4‰ (11) to 2‰ (12). To a first approximation therefore, analysis of gases exhaled at the Earth's surface during volcanic activity, or gases occluded in glass/minerals *etc*., gives an indication of the carbon isotopic composition of the Earth's mantle. A further control on this value can be gained from analyses of diamonds. Taking all of the available information it would seem that $\delta^{13}C$ of the Earth's mantle lies somewhere in the range -5 to -7‰. Preliminary assessment of magmatic carbon in SNC meteorites, on the other hand, would tend to suggest a $\delta^{13}C$ of -20 to -30‰, which is conspicuously different to that of the terrestrial mantle. It is not obvious why there should be such a difference between the two planets although many explanations are possible.

Firstly, it is possible that the material from which the two planets accreted was different (at least with respect to carbon isotopic composition). Modelling of the formation of the terrestrial planets often advocates heterogeneous accretion with perhaps a late-stage veneer of carbonaceous chondrite-like materials being added to the surface of the planet (*e.g.* 13). In this case it is interesting to compare the $\delta^{13}C$ of terrestrial mantle materials and magmatic carbon from SNC meteorites, with whole-rock $\delta^{13}C$ values obtained from a variety of meteorites. C1 and C2 carbonaceous chondrites generally have $\delta^{13}C$ in the range -5 to -10‰ (*e.g.* 14) whereas C3 carbonaceous chondrites and ordinary chondrites have $\delta^{13}C$ of -15 to -20‰ (14,15). On the basis of carbon isotope measurements, at least, it seems that there could be differences in the constitution of Mars and Earth. However, it should be noted that the $\delta^{13}C$ values for magmatic carbon in SNC meteorites are generally lower than those observed in chondritic meteorites. Secondly, it is possible that $\delta^{13}C$ of the mantles of Earth and Mars are not representative of the respective bulk planets. A process which may have acted to confuse the issue here is core formation. Both Earth and Mars have differentiated to form cores, but the details of these processes may be different for each planet. As such it is possible that in the case of either planet, some carbon has been removed from the mantle, with an accompanying isotopic fractionation. Thirdly, the carbon observed in terrestrial mantle materials may be from a well-mixed upper mantle source. Indeed, mass-balance calculations of carbon at the surface of the Earth (*i.e.* taking the organic and carbonate reservoirs) shows a $\delta^{13}C$ of approximately -5‰. Since the Earth has a dynamic surface environment with the action of plate tectonics *etc.* there exists the possibility of re-cycling carbon from the surface back into the mantle. Obviously re-cycling of carbon cannot be advocated on Mars - the carbon in SNC meteorites could represent a more primitive form of the element than is observed in terrestrial mantle samples.

A final possibility which may explain the apparent difference in the carbon stable isotopic composition of Earth and Mars is that previous $\delta^{13}C$ measurements for magmatic carbon in SNC meteorites are in error to some degree. This possibility is being actively investigated at present (16); the most recent results, which have been obtained using superior instrumentation to that used previously, seem to constrain the $\delta^{13}C$ of magmatic carbon in SNC meteorites to about -20‰, which is not at odds with previous estimates. As such it is considered that detailed investigation of the carbon isotopic systematics of martian surface materials does have the necessary information with which to proceed.

REFERENCES: (1) Wood and Ashwal, 1981, *Proc. 12th Lunar Planet. Sci. Conf.*, **12B**, 1359-1375; (2) Bogard and Johnson, 1983, *Science*, **221**, 651-654; (3) McSween, 1985, *Rev. Geophysics*, **23** 391-416; (4) Becker and Pepin, 1984, *Earth Planet. Sci. Lett.*, **69**, 225-242; (5) Carr *et al.*, 1985, *Nature*, **314**, 248-250; (6) Wright *et al.*, 1988, *Geochim. Cosmochim. Acta*, **52**, 917-924; (7) Gooding *et al.*, *Geochim. Cosmochim. Acta*, **52**, 909-915; (8) Wright *et al.*, 1989, *Nature*, **340**, 220-222; (9) Javoy *et al.*, 1982, *Nature*, **300**, 171-3; (10) Pan *et al.*, 1991, *Geochim. Cosmochim. Acta*, **55**, 1587-1595; (11) Javoy *et al.*, 1978, *Contrib. Mineral. Petrol.*, **67**, 35-39; (12) Mattey *et al.*, 1990, *Contrib. Mineral. Petrol.*, **104**, 492-505; (13) Anders and Owen, 1977, *Science*, **198**, 453-465; (14) Kerridge, 1985, *Geochim. Cosmochim. Acta*, **49**, 1707-1714; (15) Grady *et al.*, 1989, *Meteoritics*, **24**, 147-154; (16) Hartmetz *et al.*, 1991, *This Volume.*

AX64667

N92-29078

85761

P.2

171

COMPARISON OF DRIFT POTENTIAL DERIVED FROM MARS GCM WITH ROCK ABUNDANCE FROM IRTM; ***Pengyang Xu*** and ***Ronald Greeley***, Dept. of Geology, Arizona State University, Tempe, AZ 85287-1404

A General Circulation Model (GCM) for Mars developed at Ames Research Center makes global predictions of wind shear stress as a function of season and dust optical depth [1]. The surface shear stress, pressure, and temperature from the GCM are used here to calculate the *drift potential*, or the amount of sediment that could be moved by the wind. A map of sand roses based on the calculations was generated for comparison with predictions of the distribution of rocks on Mars from Christensen [2], which is derived from IRTM data. The drift potential was defined for Earth as the amount of sand moved at a given place for a stated period of time [3], and was adapted here for Mars. We use $Qj = \sum_{(i,j)} qij\Delta ti$ to calculate the drift potential, where Qj (kg/m) is drift potential at each GCM cell from j bins (12 compass points) for a GCM run period; qij (kg/m/s) is mass flux in i GCM run steps within j bin; Δti = 5400 (sec) is the length of time of i GCM step. The mass flux q may be obtained from a semi-empirical relation described by White [4]: $q = 2.61\rho(U_* - U_{*t})(U_* + U_{*t})^2/g$ (kg/m/s), where U_* is the wind friction velocity; U_{*t} is the saltation threshold friction velocity; g is the gravitational acceleration of Mars; and ρ is the air density. U_* and U_{*t} are related to surface shear stress and air density by $U_* = \sqrt{\tau/\rho}$ and $U_{*t} = \sqrt{\tau t/\rho}$. τ is the surface shear stress which is generated from the GCM; τt = 0.0401kg/m/s^2 saltation threshold shear stress. ρ is derived from the ideal gas law: $\rho = P/RgT$, where pressure (P) and temperature (T) are also output from the GCM; Rg is the gas constant for CO_2. A computer program was developed to do the calculation and produce sand rose diagrams on a Mars base map. The maximum Qj calculated for Mars for each GCM run is averaged to the maximum daily drift potential possible, which is then extrapolated to the whole martian year (Figure 1). The curve can be used to estimate the maximum drift potential per day per j bin per GCM cell on Mars (assuming an unlimited sand supply). Moreover, the maximum possible drift potential for a certain period of time can be estimated by the area under the curve.

Areas shown to have high drift potential are inferred to be aeolian erosional environments which should have relatively high rock abundances (i.e., areas of exposed rock surfaces). Preliminary analysis shows that these areas correlate very well with the moderate to high rock abundance regions. Such areas include Arcadia, northern Acidalia, Utopia, northern areas of Tharsis and Arabia, the area between Chryse and Argyre, the area west of Solis Planum, the northern rim of Hellas, and the area between 30-45°S latitude and 160-220° longitude. However, some areas, such as Chryse/Acidalia, Solis Planum, and Hesperia, show high rock abundance, but no drift potential. These areas may also be erosional surfaces because of relatively high shear stress, although the stress does not exceed threshold. Alternatively, the high rock abundance in Chryse/Acidalia may be attributed to coarse debris derived from outflow channels [2].

REFERENCES CITED

[1] Pollack, J.B., C.B. Leovy, P.W. Greiman, and Y. Mintz, (1981) *J. Atmos. Sci. 38*, p. 3-29.
[2] Christensen, P.R., (1986b) *Icarus, 68*, p. 217-238.
[3] Fryberger, S.G., (1979) A Study of Global Sand Seas, *U.S.Geol. Survey Prof. Paper 1052*, edited by E.D. McKee, p. 137-169.
[4] White, B.R., (1979) *J. Geophys. Res., 84*, p. 4643-4651.

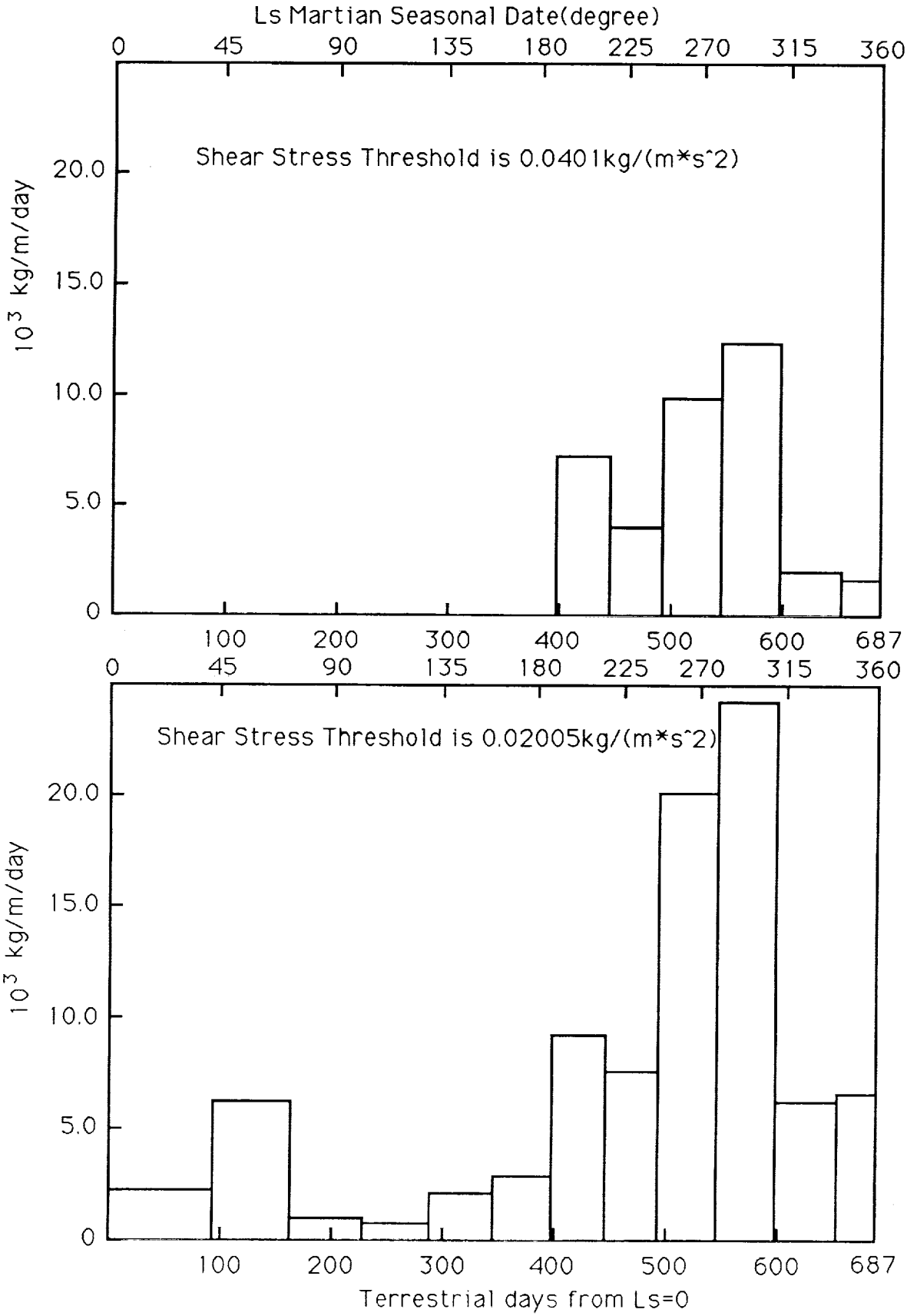

Figure 1. Maximum Daily Drift Potential on Mars

N92-29079
85162
173

CLIMATIC IMPLICATIONS OF THE SIMULTANEOUS PRESENCE OF CO_2 AND H_2O IN THE MARTIAN REGOLITH

A. P. Zent, SETI Institute and NASA Ames Research Center, Moffett Field, Ca 94035.

The current paradigm for quasi-periodic climate change on Mars holds that perhaps a few hundred millibars of CO_2 is available for exchange between the atmosphere and regolith, and that a vast majority of that CO_2 is presently adsorbed onto the regolith. The CO_2 is partitioned between the regolith and atmosphere according to an equilibrium adsorptive relationship. If the atmospheric pressure exceeds the frost point at or near the poles, then quasi-permanent polar caps form and buffer the atmospheric pressure. This model was developed based upon laboratory studies of CO_2 adsorption (1) where no other adsorbates were present.

The possibility that the simultaneous presence of H_2O in the regolith may affect these predictions is examined below. The simultaneous adsorption of H_2O and CO_2 onto commercial molecular sieve was explored during attempts to develop regenerative CO_2 scrubbers for use in humid environments, such as the Apollo command and lunar modules. It was found in room temperature experiments (2,3) that the presence of H_2O in the gas phase depressed the adsorptive capacity of the adsorbent for CO_2 . Unfortunatley there is no data at martian conditions, so extrapolation is necessary, in spite of the uncertainties that are introduced. Carter and Husain (3) derived equations that describe the fractional monolayer coverage (θ) at 273K as a function of pressure (P), based on highly simplified Langmuir adsorption isotherms.

$$\theta_w = \frac{11.1 P_w}{1 + 46.7 P_w} \tag{1}$$

$$\theta_c = \frac{0.4535 P_c}{(1 + 5.48 P_c)(1 + 46.7 P_w)} \tag{2}$$

where pressure must be expressed in mm Hg. By correcting pressures to Mars-like relative humidities, equations (1) and (2) can be used to predict that 10% relative humidity may reduce the adsorbed CO_2 inventory to approximately 4% of its capacity at $R_H = 0$. It is not certain that the same result will persist down to 210 K.

The adsorbed H_2O coverage at martian conditions is probably near a monolayer. In the available laboratory data, there is no record of CO_2 adsorption interfering with H_2O ; the adsorbed H_2O population was approximately the same whether CO_2 was present in the gas phase or not. No H_2O adsorption measurements have ever been made at martian conditions of temperature and partial pressure; it is one goal of this research to make the first measurements of H_2O adsorption at truly Mars-like conditions. The mathematical extrapolation of available laboratory data indicates that adsorptive coverage of H_2O will be on the order of a complete monolayer.

It is very probable that H_2O on Mars will reduce CO_2 adsorption on Mars, relative to the adsorbed population that would exist at $R_H = 0$. This interference arises because the lifetime of adsorbed H_2O is greater than for CO_2 , due to the permanent dipole moment of H_2O , and because the adsorbed lifetime of a molecule is exponentially dependent upon the depth of the potential well in which it sits. Therefore H_2O tends to accumulate in the most stable sites, and CO_2 is preferentially concentrated at sites with weaker bonds. In terrestrial laboratory data, H_2O is observed to reduce the adsorptive coverage of CO_2

when it is present at high relative humidity, and when it is present in coverages approaching a monolyer, and both conditions are expected to obtain on Mars.

If coadsorption severly limits the population of adsorbed CO_2 that is available on the martian regolith, what might be the consequences? The upper limit on the adsorbed CO_2 inventory, based on single adsorbate experiments is around 200 mb (4). If coadsorption limits the adsorbed population to 4% of that value, then perhaps 8 mb of CO_2 is stored in the regolith, an amount comparable to the atmospheric inventory.

If coadsorption actually depresses the population of adsorbed CO_2 , then there would not be a significant increase in atmospheric pressure at high obliquity. A simple plot (Fig. 2) compares the atmospheric pressure as a function of obliquity for inventories of 200 and 8 mb.

We will conduct laboratory measurements of the simultaneous adsorption of H_2O and CO_2 under Mars-like conditions, and develop numerical expressions for use in climate modeling based upon our results.

(1). Fanale, F. P. and Cannon, W. 1971, *Nature* **230** 502 -504.
(2). Dell'Osso, L., J. Winnick, 1969, *Ind. Eng. Chem. Proc. Design and Devel.* **8**, 469 - 476.
(3). Carter, J. W., H. Husain, 1974. *Chem. Eng. Sci.* **29**, 267-273.
(4). Zent, A. P., *et al.* 1987. *Icarus*, **71**, 241 - 249.

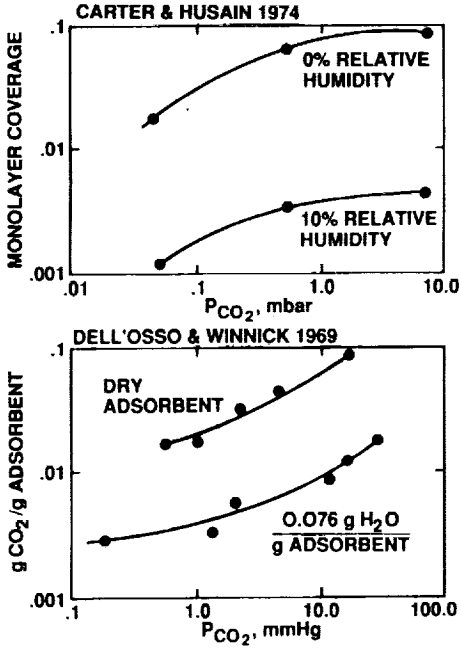

Figure 1. The effect of H_2O adsorption on CO_2 adsorption.

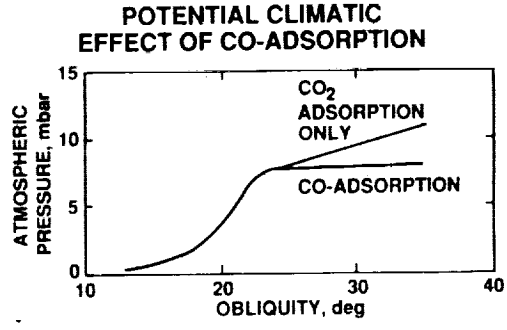

Figure 2. Possible pressure vs. obliquity curves with and without coadsorption effects.

THE ANCIENT OXYGEN EXOSPHERE OF MARS: IMPLICATIONS FOR ATMOSPHERE EVOLUTION; M.H.G. Zhang and J.G. Luhmann, IGPP, UCLA, Los Angeles, CA 90024; A.F. Nagy, Space Physics Research Laboratory, U. of Michigan; S.W. Bougher, Lunar and Planetary Lab., U. of Arizona.

The atmosphere evolution (particularly constituents of water) is influenced by "nonthermal" escape of atoms due to dissociative recombination and by ion pickup by solar wind. Both processes depend on solar EUV, which 1) affects atmosphere temperatures (scale heights) and thereby exosphere and escaping atom density and 2) also affects photoionization rate (which multiplies the greater neutral density to get ion production rate in an "optically thin" atmosphere).

This study involves the calculation (by 2–stream method of Nagy and Cravens (1)) of "hot" oxygen exosphere density profiles for "ancient" atmospheres and ionospheres (e.g., different EUV fluxes) and the associated escaping fluxes. We computed the total production rates above different "nominal" ionopause altitudes (not taking into account the fact that some will reenter the atmosphere). We do not consider the additional neutral escape due to the sputtering process described by Luhmann and Kozyra (2).

The results presented here thus represent conservative estimations of the neutral escape fluxes, but generous estimates of ion loss rates (except that here we do not consider charge exchange and impact ionization ion production processes). Further work along the lines of Luhmann and Kozyra (2) can lead to estimates of sputtering losses over time and the roles played by impact ionization and charge exchange.

References: 1. Nagy, A.F. and T.E. Cravens (1988), Geophys. Res. Lett., 15, 433–435.
2. J.G. Luhmann and J.U. Kozyra (1991), J. Geophys. Res., 96, 5457–5467.

List of Workshop Participants

David Agresti
Physics Department
University of Alabama
Birmingham AL 35294-8042

Warren Akers
1150-D Monroe Drive
Boulder CO 80303-2107

Joan M. Alexander
LASP Campus Box 392
University of Colorado
Boulder CO 80309-0392

S. K. Atreya
Department of Atmosphere and Oceanic Studies
University of Michigan
Ann Arbor MI 48109-2143

Victor R. Baker
Department of Geosciences
University of Arizona
Tucson AZ 85721

Amos Banin
Mail Stop 239-12
NASA Ames Research Center
Moffett Field CA 94035

Nadine G. Barlow
Mail Code SN21
NASA Johnson Space Center
Houston TX 77058

Jeffrey Barnes
Department of Atmospheric Sciences
Oregon State University
St. Ag Hall 326
Corvallis OR 97331-2209

Charles A. Barth
LASP Campus Box 590
University of Colorado
Boulder CO 80309-0590

Jim Bell
Planetary Geoscience Division
PGD/University of Hawaii
2525 Correa Rd.
Honolulu HI 96822

Bruce Betts
Mail Stop 170-25
California Institute of Technology
Pasadena CA 91125

Jean-Pierre Bibring
Institute d'Astrophysique Spatiale
Batiment 120
91405 Orsay-Campus
FRANCE

Diana L. Blaney
Mail Stop 183-501
Jet Propulsion Laboratory
4800 Oak Grove Drive
Pasadena CA 91109

Stephen Bougher
Lunar and Planetary Laboratory
University of Arizona
Space Science Building
Tucson AZ 85721

Alison Bridger
Department of Meteorology
San Jose State University
San Jose CA 95192-0104

Lisa L. Brown
Department of Geosciences
Pennsylvania State University
203 Deike Building
University Park PA 16802

Mark Bullock
c/o David Grinspoon
LASP Campus Box 392
University of Colorado
Boulder CO 80309-0392

Roger G. Burns
Department of Earth, Atmospheric,
and Planetary Sciences
Massachusetts Institute of Technology
Cambridge MA 02139-4307

Michael H. Carr
Mail Stop 946
U.S. Geological Survey
345 Middlefield Road
Menlo Park CA 94025

Augustine Chicarro
ESTEC/Code SI
European Space Agency
2200 AG Noordwijk
THE NETHERLANDS

R. T. Clancy
LASP Campus Box 10
University of Colorado
Boulder CO 80309-0010

Roger N. Clark
Mail Stop 964, Box 25046
U.S. Geological Survey
Denver Federal Center
Denver CO 80225

Steven Clifford
Lunar and Planetary Institute
3600 Bay Area Boulevard
Houston TX 77058-1113

Will Colwell
LASP Campus Box 392
University of Colorado
Boulder CO 80309-0392

David Crisp
Mail Stop 169-237
Jet Propulsion Laboratory
4800 Oak Grove Drive
Pasadena CA 91109

Joy Crisp
Mail Stop 183-501
Jet Propulsion Laboratory
4800 Oak Grove Drive
Pasadena CA 91109

Jeffrey DeBraal
Department of Geology
U.S. Geological Survey
University of Oregon
Eugene OR 974093

James P. Dilly
LASP Campus Box 392
University of Colorado
Boulder CO 80309-0392

Kenneth S. Edgett
Department of Geology
Arizona State University
Tempe AZ 85287-1787

Bruce Fegley
Department of Earth and Planetary Science
Washington University
Campus Box 1169
St. Louis MO 63130

George J. Flynn
Department of Physics
Hudson Hall -223
SUNY at Plattsburgh
Plattsburgh NY 12901

Jane L. Fox
Department of Mechanical Engineering
Institute of Terrestrial and Planetary Atmosphere
State University of New York
Stony Brook NY 11794

Herbert Frey
Mail Code 921
Geophysics Branch
NASA Goddard Space Flight Center
Greenbelt MD 20771

Robert W. Gaskell
Mail Stop 301-125 L
Jet Propulsion Laboratory
4800 Oak Grove Drive
Pasadena CA 91109

D. C. Golden
Mail Code SN14
NASA Johnson Space Center
Houston TX 77058

Ronald Greeley
Department of Geology
Arizona State University
Tempe AZ 85287-1404

David Grinspoon
LASP Campus Box 392
University of Colorado
Boulder CO 80309-0392

Virginia Gulick
Department of Geosciences and Planetary Sciences
University of Arizona
Tucson AZ 85721

Robert M. Haberle
Mail Stop 245-3
Space Science Division
NASA Ames Research Center
Moffett Field CA 94035

W. K. Hartmann
Planetary Science Institute
2421 East Sixth Street
Tucson AZ 85719

Bradley G. Henderson
LASP Campus Box 392
University of Colorado
Boulder CO 80309-0392

Ken Herkenhoff
Mail Stop 183-501
Jet Propulsion Laboratory
4800 Oak Grove Drive
Pasadena CA 91109

David Hinson
Center for Radar Astronomy
Stanford University
219 Durand Building
Stanford CA 94305-4055

Harald Hoffmann
D.L.R. Oberpfaffenhofen
Planetary Remote Sensing
NE-OE-PE D-8031
Oberpfaffenhofen
GERMANY

Robert M. Housley
Science Center
Rockwell International
P.O. Box 1085
Thousand Oaks CA 91360

G. Scott Hubbard
Mail Stop 244-10
Space Projects Division
NASA Ames Research Center
Moffett Field CA 94035-1000

J. D. Iversen
Iowa State University
304 Town Engineering Building
Ames IA 50011

Emil Jagoutz
Max-Planck-Institut fur Chemie
Saarstrasse 23
D-6500 Mainz
GERMANY

Bruce Jakosky
LASP Campus Box 392
University of Colorado
Boulder CO 80309-0392

Bonnie James
NASA Marshall Space Flight Center
Redstone Arsenal
Huntsville AL 35812

P. B. James
Physics and Astronomy Department
University of Toledo
Toledo OH 43606

Jeff Kargel
Lunar and Planetary Laboratory
University of Arizona
Tucson AZ 85721

James F. Kasting
Department of Geosciences
Pennsylvania State University
211 Deike Building
University Park PA 16802

Trude V. V. King
Mail Stop 964
U.S. Geological Survey
P.O. Box 25046
Denver CO 80225

David Knapp
LASP Campus Box 392
University of Colorado
Boulder CO 80309-0392

Hermann Kochan
DLR - RS
P.O. Box 906058
D-5000 Koln 90
GERMANY

Goro Komatsu
Mail Stop 169-237
Department of Planetary Sciences
University of Arizona
Tucson AZ 85721

Leonid Ksanfomality
Academy of Science
Profsyzaya Str. 8432
Space Research Institute
Moscow GSP-1
RUSSIA

Lars Landberg
NCAR MMM
P.O. Box 1000
Boulder CO 80303

S. W. Lee
LASP Campus Box 392
University of Colorado
Boulder CO 80309-0392

B. Lee Lindner
A.E.R., Inc.
840 Memorial Drive
Cambridge MA 02139

Janet Luhmann
Institute of Geophysics
University of California
6877 Slichter Hall
Los Angeles CA 90024-1567

Julio A. Magalhães
Mail Stop 245-3
Space Science Division
NASA Ames Research Center
Moffett Field CA 94035

Paul Mahaffy
Mail Code 915.0
NASA Goddard Space Flight Center
Greenbelt MD 20771

Rocco Mancinelli
Mail Stop 239-12
NASA Ames Research Center
Moffett Field CA 94035

J. P. Manker
Department of Geology and Physics
Georgia Southwestern College
Americus GA 31709

Mark Marley
Mail Stop 245-3
NASA Ames Research Center
Moffett Field CA 94035

Leonard Martin
Lowell Observatory
1400 W. Mars Hill Road
Flagstaff AZ 86001

Terry Z. Martin
Mail Stop 169-237
Jet Propulsion Laboratory
4800 Oak Grove Drive
Pasadena CA 91109

Konrad Mauersberger
School of Physics and Astronomy
University of Minnesota
116 Church Street, S.E.
Minneapolis MN 55455

Alfred S. McEwen
U.S. Geological Survey
2255 N. Gemini Drive
Flagstaff AZ 86001

George E. McGill
Department of Geology and Geography
University of Massachusetts
Amherst MA 01003

Paul Meade
LASP Campus Box 392
University of Colorado
Boulder CO 80309-0392

Mike Mellon
LASP Campus Box 392
University of Colorado
Boulder CO 80309-0392

Jeffrey S. Miller
Lunar and Planetary Laboratory
University of Arizona
Tucson AZ 85712

Douglas W. Ming
Mail Code SN14
NASA Johnson Space Center
Houston TX 77058

Hitoshi Mizutani
Institute of Space Astronomical Science
Yoshinodai Sagamihara
Kanagawaken 229
JAPAN

Jeff M. Moore
Mail Stop 245-3
Space Sciences Division
NASA Ames Research Center
Moffett Field CA 94035

Brian Morrissette
University of Colorado
2915 Baseline Road #234
Boulder CO 80303

Duane Muhleman
Mail Stop 170-25
California Institute of Technology
Pasadena CA 91125

Jim Murphy
Mail Stop 245-3
NASA Ames Research Center
Moffett Field CA 94035

Chan Y. Na
LASP Campus Box 392
University of Colorado
Boulder CO 80302-0392

Adrienne Ono
Department of Earth and Space Science
University of California
Los Angeles CA 90024-1567

David A. Paige
Department of Earth and Space Science
University of California
Los Angeles CA 90024-1567

Thomas Parish
University of Wyoming
Laramie WY 82071

Tim Parker
Department of Geological Sciences
University of Southern California
University Park
Los Angeles CA 90089-0741

Larry J. Paxton
Applied Physics Laboratory
Johns Hopkins University
Johns Hopkins Road
Laurel MD 20723-6099

John Pearl
Mail Code 693-2
NASA Goddard Space Flight Center
Greenbelt MD 20771

J. Plescia
Mail Stop 183-501
Jet Propulsion Laboratory
4800 Oak Grove Drive
Pasadena CA 91109

Robert Plumb
Department of Chemistry
Worcester Polytechnic Institute
Worcester MA 01609

Geoffrey S. Plumlee
Mail Stop 973
U.S. Geological Survey
Denver Federal Center
Denver CO 80225

James B. Pollack
Mail Stop 245-3
Space Science Division
NASA Ames Research Center
Moffett Field CA 94035

Susan Postawko
School of Meteorology
University of Oklahoma
100 East Boyd
Norman OK 73019

David P. Reyes
Department of Geology
Arizona State University
Tempe AZ 85287-1404

Jim Rice
7250 S. Kyrene, Apt. 222
Tempe AZ 85283

Ian Ridley
Mail Stop 973
U.S. Geological Survey
Denver Federal Center
Box 25046
Denver CO 80225

Bashar Rizk
Department of Planetary Sciences
Space Sciences Building
University of Arizona
Tucson AZ 85721

Susan L. Rotto
Astrogeology
U.S. Geological Survey
2255 North Gemini Drive
Flagstaff AZ 86001

Steve Ruff
Planetary Geology
Arizona State University
Tempe AZ 85287-1404

Michelle Santee
Mail Stop 170-25
California Institute of Technology
Pasadena CA 91125

Martha W. Schaefer
Mail Code 921
NASA Goddard Space Flight Center
Greenbelt MD 20771

Ben Schuraytz
Lunar and Planetary Institute
3600 Bay Area Boulevard
Houston TX 77058-1113

Robert B. Singer
Lunar and Planetary Laboratory
University of Arizona
Tucson AZ 85721

Paul P. Sipiera
Schmitt Meteorite Research Group
Harper College
1200 West Algonquin Road
Palatine IL 60067-7387

Martin Slade
Mail Stop 238-420
Jet Propulsion Laboratory
4800 Oak Grove Drive
Pasadena CA 91109-8099

Stan Solomon
Laboratory for Atmospheric Science
University of Colorado
Boulder CO 80309-0392

Stuart K. Stephens
Mail Stop 170-25
Department of Planetary Science
California Institute of Technology
Pasadena CA 91125

Edwin Strickland
Scientific Measurement System, Inc.
2209 Donley Drive
Austin TX 78758

Robert G. Strom
Lunar and Planetary Laboratory
University of Arizona
Tucson AZ 85721

Robert Sullivan
Department of Geology
Arizona State University
Tempe AZ 85287

Kenneth Tanaka
U.S. Geological Survey
2255 N. Gemini Drive
Flagstaff AZ 86001

Gillian Thornhill
Department of Earth Sciences
Walton Hall
Open University
Milton Keynes MK7 6AA
ENGLAND

Allan Treiman
Mail Code SN21
NASA Johnson Space Center
Houston TX 77058

Ashwin Vasavada
4207 Riviera Drive
Stockton CA 95204

Richard Wagener
Environmental Chemistry Division
Building 426
Brookhaven National Laboratory
Upton NY 11973

H. Wänke
Max-Planck-Institut fur Chemie
Abteilung Kosmochemie
Saarstrasse 23
D-6500 Mainz
GERMANY

Laurie Watson
Mail Stop 170-25
California Institute of Technology
Pasadena CA 91125

Paul Wercinski
Mail Stop 244-10
NASA Ames Research Center
Moffett Field CA 94035

Felicity Wong
LASP Campus Box 392
University of Colorado
Boulder CO 80309-0392

Stephen Wood
Department of Earth and Space Science
University of California
Los Angeles CA 90024

Ian Wright
Department of Earth Sciences
Open University
Walton Hall
Milton Keynes MK7 6AA
ENGLAND

Yuk Yung
Mail Stop 170-25
Division of Geology and Planetary Science
California Institute of Technology
Pasadena CA 91125

Lydmila Zasova
Space Research Center
Academy of Science
117810 Moscow GSP-1
RUSSIA

Aaron Zent
Mail Stop 245-3
NASA Ames Research Center
Moffett Field CA 94035

Martina Zhang
Institute for Geophysics and Planetary Physics
University of California
Los Angeles CA 90024

Richard Zurek
Mail Stop 169-237
Jet Propulsion Laboratory
4800 Oak Grove Drive
Pasadena CA 91109